



Aalborg Universitet

AALBORG UNIVERSITY
DENMARK

Indoor Small Cell Deployments: Challenges and Enabling Techniques - With Emphasis on Interference Management

Jørgensen, Niels T.K.

Publication date:
2014

Document Version
Accepted author manuscript, peer reviewed version

[Link to publication from Aalborg University](#)

Citation for published version (APA):
Jørgensen, N. T. K. (2014). *Indoor Small Cell Deployments: Challenges and Enabling Techniques - With Emphasis on Interference Management*. Aalborg University.

General rights

Copyright and moral rights for the publications made accessible in the public portal are retained by the authors and/or other copyright owners and it is a condition of accessing publications that users recognise and abide by the legal requirements associated with these rights.

- Users may download and print one copy of any publication from the public portal for the purpose of private study or research.
- You may not further distribute the material or use it for any profit-making activity or commercial gain
- You may freely distribute the URL identifying the publication in the public portal -

Take down policy

If you believe that this document breaches copyright please contact us at vbn@aub.aau.dk providing details, and we will remove access to the work immediately and investigate your claim.

**Indoor Small Cell Deployments: Challenges and Enabling
Techniques**
- With Emphasis on Interference Management

Ph.D. Dissertation
Niels Terp Kjeldgaard Jørgensen

Aalborg University
Department of Electronic Systems
Fredrik Bajers Vej 7B
DK-9220 Aalborg

NOKIA



Supervisors:

Preben E. Mogensen, PhD
Professor, Aalborg University, Denmark
Principal Engineer, Nokia Networks, Denmark
Klaus I. Pedersen, PhD
Professor, Aalborg University, Denmark
Senior Research Specialist, Nokia Networks, Denmark

Opponents

Gennaro Boggia, PhD
Associate Professor, Politecnico di Bari, Italy
Jarno Niemelä, PhD
Service Manager, Elisa, Finland
Hans-Peter Schwefel, PhD
Professor, Aalborg University, Denmark
Scientific Director, Forschungszentrum Telekommunikation Wien, Austria

List of published papers:

- N. T. K. Jørgensen, T. Isotalo, K. Pedersen, and P. Mogensen, "Joint Macro and Femto Field Performance and Interference Measurements," in *Vehicular Technology Conference (VTC Fall), 2012 IEEE*, September 2012, pp. 1–5
- T. Kolding, P. Ochal, N. T. K. Jørgensen, and K. Pedersen, "QoS Self-Provisioning and Interference Management for Co-Channel Deployed 3G Femtocells," *Future Internet*, vol. 5, no. 2, pp. 168–189, 2013
- I. Rodriguez, H. C. Nguyen, N. T. K. Jørgensen, T. B. Sørensen, J. Elling, M. B. Gentsch, and P. Mogensen, "Path Loss Validation for Urban Micro Cell Scenarios at 3.5 GHz Compared to 1.9 GHz," in *Global Communications Conference (GLOBECOM), 2013 IEEE*, December 2013
- N. T. K. Jørgensen, I. Rodriguez, J. Elling, and P. Mogensen, "3G Femto or 802.11g WiFi: Which is the Best Indoor Data Solution Today?" in *2014 IEEE Vehicular Technology Conference (VTC Fall)*, September 2014
- I. Rodriguez, H. C. Nguyen, N. T. K. Jørgensen, T. B. Sørensen, and P. Mogensen, "Radio Propagation into Modern Buildings: Attenuation Measurements in the Range from 800 MHz to 18 GHz," in *2014 IEEE Vehicular Technology Conference (VTC Fall)*, September 2014
- B. Soret, K. I. Pedersen, N. T. K. Jørgensen, and V. Fernández-López, "Interference Coordination for Dense Wireless Networks," January 2015, accepted for COMMAG - Special Issue: Recent Advances in Technologies for Extremely Dense Wireless Networks

ISBN: 978-87-7152-047-7

Copyright ©2014, Niels Terp Kjeldgaard Jørgensen

This thesis has been submitted for assessment in partial fulfilment of the PhD degree. The thesis is based on the submitted or published scientific papers which are listed above. Parts of the papers are used directly or indirectly in the extended summary of the thesis. As part of the assessment, co-author statements have been made available to the assessment committee and are also available at the Faculty. The thesis is not in its present form acceptable for open publication but only in limited and closed circulation as copyright may not be ensured.

”Get busy living, or get busy dying.”

- Tim Robbins as Andy Dufresne, The Shawshank Redemption 1994

Abstract

Previous years have shown exponential mobile data traffic growth and the traffic growth is expected to persist. Moreover, a significant amount of the traffic is generated in indoor traffic hotspots. In order for network operators to maintain a satisfied user base, comprehensive upgrades of the network are required, thus, Heterogeneous Network (HetNet) deployments are upgrading the traditional macro-only networks. In this thesis, the main scenarios of interest are the co-channel and dedicated channel dense indoor small cell deployments. By means of experimental and theoretical studies the new challenges introduced by these scenarios are addressed.

This thesis contributes with an evolution study in an operator deployed 4G network, and simulations show that indoor small cells are very important in order to reduce the Total Cost of Ownership (TCO) of future cellular networks. Moreover, the indoor small cell solution is also attractive from a user throughput performance point of view. If possible, the network operator should deploy the small cells on a dedicated carrier, thus, reducing the required indoor small cell density.

Given the large potential of indoor small cell deployment, several femto measurement campaigns have been performed. First phase of the measurement campaign verified the indoor propagation models used in the simulation tool. This step is important in order to build confidence in the simulation accuracy. A second femto measurement campaign was performed to fully understand the consequences of uncoordinated indoor small cell deployment and to identify the most critical interference challenges. For uplink the most critical interference issue is increased noise rise at co-channel macro cells. For downlink, closed subscriber group femtos require a dedicated macro carrier to avoid indoor macro coverage holes. These findings were used in the development of an autonomous uplink and downlink femto power control algorithm which protects the co-channel macro users, and at the same time provides femto users with the guaranteed Quality of Service (QoS). Today, WiFi is the de facto indoor small cell technology. Therefore, a combined WiFi and 3G femto measurement campaign is carried out to determine the strong and weak points of each of the competing technologies. The main differentiator, from a user point

of view, between WiFi and 3G femto is shown to be latency and the User Equipment (UE) power consumption; WiFi outperforms the 3G femto in both latency and UE power consumption.

In high traffic scenarios with dedicated channel and dense indoor small cell deployment, intra small cell interference should not be neglected because strong interference coupling between multiple indoor small cells is inevitable. Therefore different Inter-Cell Interference Coordination (ICIC) schemes have been developed, most promising a dynamic Carrier Based Inter-Cell Interference Coordination (CB-ICIC) solution. The proposed CB-ICIC scheme improves the network capacity of up to 60% by means of muting strong small cell interferes, thus protecting low throughput users. Also a low complexity load balancing approach is developed, which delivers a network capacity gain of approximately 10%. In general, it is possible to combine Interference Rejection Combining (IRC) receivers with the developed CB-ICIC scheme or load balancing schemes in order to increase network performance even further. By combining the proposed CB-ICIC framework, IRC receivers, and four transmit antennas, it is shown that the network capacity is increased up to 180%, despite there is no coordination between the network and UE ICIC techniques.

Dansk Resumé

I de foregående år er mobildatatrafikken vokset eksponentielt, og det forventes at væksten fortsætter. Derudover er en betydelig andel af datatrafikken genereret af indendørs mobilbrugere. For at tilfredsstille mobilbrugerne er mobilnetværksoperatører nødsaget til at opgradere deres mobilnetværk. Som en konsekvens heraf, bliver traditionelle netværk som udelukkende består af udendørs macro celler erstattet af heterogene netværk. I denne afhandling er dedikeret og fælles frekvens allokering af indendørs små radioceller det primære netværksscenario. De specifikke udfordringer introduceret i dette scenario er undersøgt ved hjælp af eksperimentelle og teoretiske studier.

Denne afhandling bidrager med et netværksevolutionsstudie i et operatorbaseret 4G netværk. Simuleringsresultater viser at små celler er vigtige i bestræbelserne på at reducere de totale driftsomkostninger i fremtidens mobilnetværk. Baseret på de oplevede datahastigheder, er små celler også en attraktiv løsning. Ydermere, for at reducere det nødvendige antal af indendørs små celler er dedikeret små celle udrulning at foretrække for netværksoperatører.

For at fastslå potentialet af små celler, er det nødvendigt at foretage små celle målekampagner. Første fase er at verificere de indendørs udbredelsesmodeller, som bruges i de forskellige simuleringsværktøjer. Dette er vigtigt for at opbygge troværdighed i simuleringsværktøjernes nøjagtighed. Derefter er en femto celle målekampagne udført for at forstå konsekvenserne af ukoordineret indendørs femto celle netværksudrulning og for at identificere de mest kritiske interferensudfordringer. Øget støjniveau ved macro basestationer er den mest kritiske problemstilling i uplink. I downlink er det påkrævet at have en dedikeret macro celle frekvensallokering for at undgå macro dækningshuller i tilfælde af begrænset-adgangs femto celler. Disse resultater bruges til udviklingen af en automatiseret uplink og downlink femto power kontrol algoritme, der beskytter fælles frekvensblok macro brugere samtidig med at femto brugere er garanteret de aftalte datahastigheder. I dag er WiFi den gængse indendørs små celle teknologi. Derfor er en kombineret WiFi og 3G femto målekampagne udført for at bestemme styrker og svagheder for de før omnævnte teknologier. For en slutbruger er den største forskel latenstid og mobiltelefonens strømfor-

brug, og WiFi leverer de bedste resultater for begge parametre.

I scenarioer med høj datatrafik og høj små celle tæthed på en dedikeret frekvensblok er det nødvendigt at tage højde for intra små celle interferens, da det i disse scenarioer er uundgåeligt med stærk interferens imellem små celler. Af denne grund er to inter-celle interferens koordineringsløsninger udviklet. Den mest lovende løsning er en dynamisk frekvensblok baseret inter-celle interferens koordineringsmetode, denne løsning er i stand til at øge mobilnetværkets kapacitet med op til 60%. Dette opnås ved at mute specifikke frekvensblokke for små celler, der forårsager stærk interferens, således at interferensen mindskes for brugere med lav data hastighed. Derudover er en mobilbrugerbalanceringsalgoritme med lav kompleksitet udviklet, og denne algoritme er i stand til at øge mobilnetværkets kapacitet med 10%. Generelt er det muligt at kombinere de udviklede metoder med interferens afvisende radiomodtagere for at forbedre et mobilnetværks ydeevne yderligere. Ved at kombinere frekvensblok baseret interferens koordinering, interferens afvisende radiomodtagere med fire modtage-antenner er det muligt at øge mobilnetværks kapaciteten med op til 180%. Og det er på trods af at der ingen koordinering er i mellem netværks- og radiomodtagerteknikkerne.

Preface and Acknowledgements

This PhD thesis is the result of a three year research project. The research project has been carried out at the Wireless Communication Networks (WCN) section (former Radio Access Technology (RATE) section), Department of Electronic Systems, Aalborg University under supervision and guidance of Professor Preben E. Mogensen (Aalborg University, Nokia Networks) and Professor Klaus I. Pedersen (Aalborg University, Nokia Networks). In parallel, I have attended the mandatory courses and fulfilled the teaching/working obligations required to obtain the PhD degree. The research project has been co-financed by Vækstforum Danmark, Nokia Networks, and The Faculty of Engineering and Science, Aalborg University.

The main topic of the PhD thesis is indoor small cell deployments. Initially, the small cell deployment was assessed by means of experimental investigations performed at Tampere University of Technology. However, my increasing involvement in Nokia Networks projects meant that my work started focusing on network evolution driven studies and network feature development. Thus, the PhD thesis covers a wide field of academic disciplines. Yet, the recurring motif in the PhD thesis is small cell deployments. The objective of the PhD thesis is to provide guidelines and recommendations on future indoor small cell deployments.

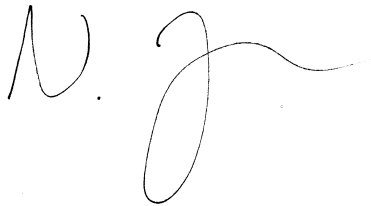
First and foremost, I would like to express my sincere gratitude to my supervisors Professor Preben E. Mogensen and Professor Klaus I. Pedersen. Their continuous guidance, patience, and support throughout my PhD project have been incredible. Preben is (one of) the most enthusiastic, open-minded, and passionate persons I have ever meet in my academic life; not what you would expect from a Professor from Mørke, Djursland. Despite being extremely busy, he always manages to find the time to guide and assist you, whether the purpose is personal or professional. Klaus is the kind of person you can ask anything. He is a great inspiration and always ready to share his technical experience and knowledge. He is extremely talented and his thorough reviews and feedback has helped me improve my work tremendously. Moreover, I am also grateful for the help and guidance provided by Dr. István Z. Kovács during my PhD thesis. It has always been very rewarding to

work with István. I also want to thank Dr. Tero Isotalo who was a great asset to me during my stay in Finland. He was always there to help me and share his knowledge on Finish culture and language. Finally, a thank you to all my co-authors for the invaluable assistance and support during the process of writing papers.

I would also like to thank all my colleagues from Aalborg and Tampere, here I was always surrounded by talented and inspiring people. I will not cite any names; too numerous to mention and the risk of making the inexcusable mistake of leaving someone out. It was the perfect educational environment for a PhD student. Further, I will never forget the passionate and heated football discussions in the office. Finally, being a proud board member and player of our beloved football team *Lokomotiv Limfjorden*, I enjoyed every game we played, the remarkable victories and the fierce defeats.

Last but not least, I am forever grateful for the love and care from my parents and my sister. Even though I have been absent and preoccupied with my thesis, I know I have always had your unqualified support. And to my girlfriend, Anette, I just want to thank you for your love and solicitude to me. And I promise you, that all the challenges of me being distracted and staying up late working on my PhD thesis, is soon over. Finally, I thank my friends for their moral support through my PhD journey, and I hope I can be as good a friend to you, as you have been to me.

Niels Terp Kjeldgaard Jørgensen, Aalborg, September 2014

A handwritten signature in black ink, consisting of a stylized 'N.' followed by a long, flowing, cursive flourish that ends in a small dot.

Contents

Abstract	v
Dansk Resumé	vii
Preface and Acknowledgements	ix
Abbreviations	xv
Nomenclature	xxi
1 Introduction	1
1.1 Mobile Traffic Evolution	1
1.2 Heterogeneous Network Topologies	4
1.3 Mobile Communication System Evolution: From GSM to LTE-A	9
1.4 New Spectrum Opportunities	11
1.5 Scope and Objective of the Thesis	12
1.6 Research Methodology	14
1.7 Publications and Contributions	16
1.8 Thesis Outline	17
2 Experimental Investigations	19
2.1 Small Cell Propagation Characteristics at 3.5 GHz	20
2.2 Indoor Path Loss Investigation	22
2.3 Co-channel Macro and Femto Interference Measurements	25
2.4 QoS Aware Femto Power Control Algorithm	30
2.5 Femto or WiFi as Indoor Data Solution?	35
2.6 Conclusion and Discussion	39

3	Network Evolution Analysis	41
3.1	Prior Art	41
3.2	Network Topology and Traffic Distribution	42
3.3	Network Evolution Options	44
3.4	TCO Assumptions	47
3.5	Result Generation	47
3.6	Performance Evaluation	49
3.7	Conclusion and Discussion	56
4	Dynamic Inter-Cell Interference Coordination	57
4.1	Prior Art	57
4.2	Optimisation Criterion	59
4.3	Small Cell Interference Coordination Framework	60
4.4	Realisation of the Framework	71
4.5	Simulation Scenario	76
4.6	Performance Evaluation	79
4.7	Conclusion and Discussion	87
5	Adaptive Small Cell Load Balancing	89
5.1	Prior Art	89
5.2	Problem Formulation	90
5.3	Developed Load Balancing Framework	91
5.4	Performance Evaluation	96
5.5	Conclusion and Discussion	100
6	Impact of Using Advanced Receivers	101
6.1	Prior Art	101
6.2	System Model	104
6.3	Considered Receiver Structures	105
6.4	Performance Evaluation	106
6.5	Network ICIC Techniques and Advanced UE Receivers	112
6.6	Overview of Network and UE Combinations	113
6.7	Conclusion and Discussion	114
7	Conclusion	117
7.1	Main Findings	117
7.2	Recommendations	119
7.3	Future Work	120
A	Macro and Femto Co-channel Interference	125
B	QoS-Aware Femto Power Control Algorithm	131

C Femto versus WiFi as Indoor Solution	155
D Required Bandwidth	161
E Fixed Frequency Reuse	163
E.1 Evaluation of Fixed Frequency Reuse Schemes	164
F Backhaul Impact	169
F.1 Required Standardisation	170
G Generic MMSE Solution	173
H Reference Signals in LTE and LTE-A	175
H.1 LTE Release 8 Cell Specific Reference Signals	175
H.2 LTE-A UE Specific Reference Signals	177

Abbreviations

$E_C I_0$	Energy per chip over total received power.
3G	3rd Generation.
3GPP	3rd Generation Partnership Project.
ABS	Almost Blank Subframe.
AP	Access Point.
AWGN	Additive White Gaussian Noise.
CA	Carrier Aggregation.
CAC	Composite Available Capacity.
CAGR	Compound Annual Growth Rate.
CAPEX	Capital Expenditure.
CB-ICIC	Carrier Based Inter-Cell Interference Coordination.
CC	Component Carrier.
CDF	Cumulative Distribution Function.
CIO	Cell Individual Offset.
CIR	Carrier to Interference Ratio.
CLTM	Closed Loop Traffic Model.
CoMP	Coordinated Multipoint.
CP	Cyclic Prefix.
CPICH	Common Pilot Channel.
CRS	Cell-specific Reference Signal.
CSG	Closed Subscriber Group.
CSI	Channel State Information.

CSI-RS	Channel State Information Reference Signal.
DC	Dual Carrier.
DI	Dominant Interferer.
DIR	Dominant Interference Ratio.
DL	Downlink.
DMRS	Demodulation Reference Signal.
DSL	Digital Subscriber Line.
ECDF	Empirical Cumulative Density Function.
EDGE	Enhanced Data rate for GSM Evolution.
EE	Energy Efficiency.
eICIC	enhanced Inter-Cell Interference Coordination.
eNB	enhanced Node B.
FDD	Frequency Division Duplex.
FR	Frequency Reuse.
FTP	File Transfer Protocol.
G-ACCS	Generalized Autonomous Component Carrier Selection.
GBR	Guaranteed Bit Rate.
GPRS	General Packet Radio Service.
GPS	Global Positioning System.
GSM	Global System for Mobile Communications.
HARQ	Hybrid Automatic Repeat Request.
HetNet	Heterogeneous Network.
HSDPA	High Speed Downlink Packet Access.
HSDSCH	High Speed Downlink Shared Channel.
HSPA	High Speed Packet Access.
HSUPA	High Speed Uplink Packet Access.
IB	In-Band.
IC	Interference Cancellation.
ICIC	Inter-Cell Interference Coordination.
IEEE	Institute of Electrical and Electronics Engineers.
IMPEX	Implementation Expenditure.

IMT-Advanced	International Mobile Telecommunication-Advanced.
IRC	Interference Rejection Combining.
ISD	Inter-Site Distance.
ISI	Inter-Symbol Interference.
ITU	International Telecommunication Union.
ITU-R	International Telecommunication Union Radiocommunication Sector.
KPI	Key Performance Indicator.
LOS	Line of Sight.
LTE	Long Term Evolution.
LTE-A	Long Term Evolution Advanced.
MAC	Medium Access Control.
MIMO	Multiple Input and Multiple Output.
ML	Maximum Likelihood.
MME	Mobility Management Entity.
MMSE	Minimum Mean Square Error.
MMSE-IRC	Minimum Mean Square Error - Interference Rejection Combining.
MMSE-MRC	Minimum Mean Square Error - Maximum Ratio Combining.
MRC	Maximum Ratio Combining.
MSC	Mobile Switching Center.
MSE	Mean Square Error.
NACK	Negative Acknowledge.
NAICS	Network Assisted Interference Cancellation and Suppression.
NLM	Network Listening Mode.
NLOS	Non Line of Sight.
OB	Out-Band.
OFDM	Orthogonal Frequency Division Multiplexing.
OFDMA	Orthogonal Frequency Division Multiple Access.
OLTM	Open Loop Traffic Model.
OPEX	Operational Expenditure.
OSG	Open Subscriber Group.
PDCCH	Physical Downlink Control Channel.

PDSCH	Physical Downlink Shared Channel.
PMI	Pre-code Matrix Indicator.
PRB	Physical Resource Block.
PSD	Power Spectral Density.
PUSCH	Physical Uplink Shared Channel.
QAM	Quadrature Amplitude Modulation.
QoS	Quality of Service.
QoS-SP-IM	Quality of Service Self Provisioning and Interference Management.
QPSK	Quadrature Phase Shift Keying.
RATE	Radio Access Technology.
RE	Range Extension.
RNC	Radio Network Controller.
RRC	Radio Resource Control.
RRM	Radio Resource Management.
RSCP	Reference Signal Code Power.
RSRP	Reference Signal Received Power.
RSRQ	Reference Signal Received Quality.
RTT	Round Trip Time.
SGSN	Serving GPRS Support Node.
SGW	Serving Gateway.
SINR	Signal to Interference and Noise Ratio.
SNR	Signal to Noise Ratio.
SU	Single User.
SVD	Singular Value Decomposition.
TCO	Total Cost of Ownership.
TDD	Time Division Duplex.
TTI	Transmission Time Interval.
UARFCN	UTRA Absolute Radio Frequency Channel Number.
UE	User Equipment.
UE-RS	User Equipment Specific Reference Signal.
UL	Uplink.
UMTS	Universal Mobile Telecommunications System.

USB	Universal Serial Bus.
VoIP	Voice over Internet Protocol.
WCDMA	Wideband Code Division Multiple Access.
WCN	Wireless Communication Networks.
WiMAX	Worldwide Interoperability for Microwave Access.
WLAN	Wireless Local Area Network.
WSS	Wide Sense Stationary.
ZF	Zero Forcing.

Nomenclature

A_i	Set of active component carriers for small cell i .
B	Transmission bandwidth.
B_i	Set of cell i 's neighbours.
C	Shannon capacity.
C_{OLTM}	Network capacity using OLTM.
G_{Rx}	Receive antenna gain in dB.
G_{Tx}	Transmit antenna gain in dB.
H_n	Set of hypotheses related to UE n .
I_{Total}	Total received wideband power in UL direction.
$I_{n,k}$	Interference experienced by user n on component carrier k .
L	User arrival rate.
L_{LOS}	LOS propagation path loss.
L_{NLOS}	NLOS propagation path loss.
L_{Cable}	Cable loss in dB.
NR	Noise Rise.
NR_{FUE}	The maximum noise rise allowed from each femto UE.
N_{LOS}	LOS distance dependent path loss coefficient.
N_{NLOS}	NLOS distance dependent path loss coefficient.
$N_{B,h}$	Subset of UEs who gain from hypothesis h .
$N_{C,h}$	Subset of UEs who lose from hypothesis h .
N_{CLTM}	Number of UEs per small cell using CLTM.
N_C	Number of component carrier assignment combinations.
$N_{Hypotheses}$	Maximum number of hypotheses in benefit/cost messages.
N_{Rx}	Number of receive antennas.

N_{SC}	Number of small cells.
N_{Tx}	Number of transmit antennas.
N_T	Thermal Noise.
N_b	Is the number of deployed base stations of type b .
O_{LOS}	LOS path loss offset coefficients.
O_{NLOS}	NLOS path loss offset coefficients.
P_{Rx}	Received power in dB.
$P_{Tx,i}(m, l)$	i -th small cell transmission power at sub-carrier m at time l .
P_{Tx}	Transmit power in dB.
P_i	Received power from cell i .
R	Reuse order.
RE_i	Range extension of cell i .
$R_{Message}$	Bit rate of the generated CB-ICIC signalling message.
R_{min}	Minimum guaranteed bit rate.
S	Payload size in bit.
$S_{Hypothesis}$	Size of signalling required per hypothesis in bit.
T_ω	Overload threshold.
T_ψ	Utilised resource threshold.
T_b	Unit TCO for base station of type b .
U_i	Set of connected UEs at small cell i .
$\bar{R}_{n,k}$	Past averaged throughput of user n on component carrier k .
\bar{R}_n	Past averaged throughput of user n .
C_1	Pre-code matrix at serving eNB.
C_i	Pre-code matrix at interfering eNB i .
H_1	Channel matrix between serving cell and UE.
H_i	Channel matrix between interfering eNB i and UE.
\tilde{H}	Effective channel matrix combining channel matrix and precoding.
$\eta_{CB-ICIC-Add}$	Effective CB-ICIC ratio when adding a CC.
$\eta_{CB-ICIC-Mute}$	Effective CB-ICIC ratio when muting a CC.
γ	Signal to Interference and Noise Ratio.
\hat{R}_n	Estimated throughput of user n .
\hat{x}_1	Estimate of desired symbol vector.
ν_T	Minimum net benefit threshold.
ν_h	Net benefit for hypothesis h .
ω_i	Cell load of small cell i .
ψ_i	Long term resource utilisation of cell i .
$\tilde{\nu}_n$	Combined net benefit for UE n .

\vec{n}	AWGN vector.
\vec{x}_1	Desired symbol vector.
\vec{x}_i	Interfering symbol vector from eNB i .
\vec{y}	Received signal vector.
a	Active component carrier index.
b	Is the base station technology.
$f_{Benefit}(\bar{R}_n, \hat{R}_n)$	Benefit function for user n .
$f_{Cost}(\bar{R}_n, \hat{R}_n)$	Cost function for user n .
h	Hypothesis index.
i	Small cell index.
k	Component carrier index.
l	Time index.
m	Sub-carrier index.
n	User index.
r	Reference signal sequence.
t_ψ	Averaging time of the resource utilisation.
$t_{Activate}$	Component carrier activation time.
t_{Add}	Time it take to add a CC.
t_{DSL}	Round trip time for DSL access.
$t_{Deactivate}$	Component carrier deactivation time.
t_{Fiber}	Round trip time for fiber access.
t_{Mute}	Time it take to mute a CC.
t_{Outage}	Time constant for outage UE detection.
t_{RTT}	Round trip time.
$t_{Session}$	UE session time.
t_{avg}	Throughput averaging time.
x	Desired symbol sequence.

Chapter 1

Introduction

This chapter presents the motivation and objectives of the PhD thesis. In Section 1.1 the past, current, and future trends in mobile communication are summarised. It is argued that indoor small cell deployment is an attractive deployment method. However, indoor small cells also pose new challenges which are fundamentally different for network operators compared to typical macro-only networks, as described in Section 1.2. Section 1.3 summarises the mobile communication advances and Section 1.4 recapitulates the new transmission spectrum opportunities and challenges. Naturally, it is not feasible to consider all small cell deployment aspects in this thesis. Therefore, in Section 1.5 objectives are highlighted and equally important the scope of the PhD thesis is defined. Section 1.6 outlines the scientific methodologies applied throughout the PhD study and Section 1.7 lists the contributions during the PhD study. Finally, Section 1.8 contains the thesis outline.

1.1 Mobile Traffic Evolution

In the dawn of the mobile communication age, the all-important technology driver was cellular voice calls. This called for wide area coverage and modest capacity requirements as cellular phones were in the beginning for a selected few. Times are changing, and the mobile communication has evolved dramatically since the beginning. To put numbers in perspective, according to [7] the number of mobile subscribers in the USA in 1985 was 340000, in year 2013 this number was approximately 1000x higher; 336 millions. Nevertheless, voice calls are no longer the mobile adaptation driver.

Before 2011, the main drivers for teenagers to buy a mobile phone in USA were safety and text messaging [8]. And teens in the USA really embraced text messaging, on

average they send or receive more than 3000 text messages per month. However, this significant number of text messages do not explain the immense traffic volume increase, which has been witnessed lately. Today the big thing in the mobile communication world is; broadband data applications or apps. Apps is a general term used for video applications, social-networking applications, and messaging applications to name a few. Today, such applications are the main driver for mobile traffic data, particular video streaming applications. In 2013, the largest mobile traffic data contributor was video services, with 40% of total mobile data traffic. On second and third place you find social-networking and web browsing, respectively [9].

People are not only using their smartphones and tablets when at home. On average each person having a smart phone watch 5 hours of TV on their smart phone per week, 50% of the time the person is not at home [10]. This is caused by the fact that people are always carrying their phone, and they expect to be able to use it where ever they go, e.g. sharing a picture or video with their social circle or being entertained when commuting. This clearly indicates that people expect to be on-line all the time, and it is up to the network operator to provide seamless network coverage and capacity to the ever increasing demands of the end user.

1.1.1 Future Mobile Data Traffic Growth

What are the drivers of tomorrow? Video streaming is not a one-day wonder. In fact, video streaming is expected to increase to more than 50% of the total mobile traffic volume [10], mainly due to larger screens with higher resolutions which require increased video bit rates. Apart from video, it is difficult to predict what are driving mobile traffic data volumes in 10 years. It is important to remember that services such as YouTube, Facebook, and Netflix were basically non-existing 10 years ago, and few could predict the influence they have had on the mobile communication industry today. However, this has not stopped people from trying. Figure 1.1 illustrates the mobile data traffic volumes per month from 2008 to 2013 [11–16]. It is seen that the monthly global traffic volume has increased from 33 PB¹ in 2008 to 1.5 EB² in 2013. Moreover, predictions indicate that the mobile traffic volume is not levelling off. The latest traffic volume reports predict that the mobile traffic growth is continuing [16], in fact, the predicted Compound Annual Growth Rate (CAGR) is 61% from 2013 to 2018. Similar, in [9] a CAGR of 45% from 2013 to 2019 is predicted. Generally speaking, all mobile traffic growth reports agree that mobile data traffic keeps increasing, but there is no consensus on the actual growth rate. Consequently, mobile networks must undergo significant upgrades to keep up with the mobile traffic growth, not only today but also tomorrow.

It is not only the increasing traffic data volumes which are a challenge for network operators. Also the spatio-temporal traffic distribution variations within the network is a

¹1 PB (Petabyte) = 10^{15} B

²1 EB (Exabyte) = 10^{18} B

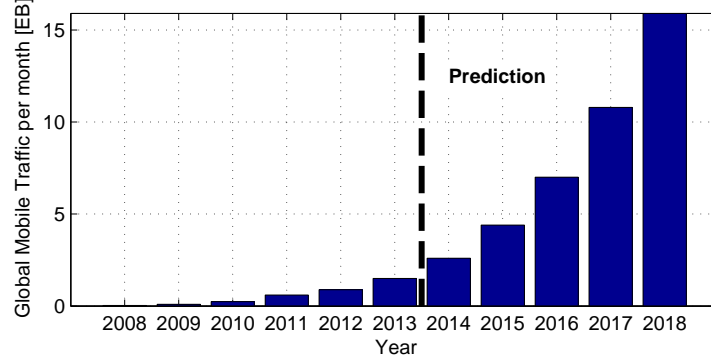


Fig. 1.1: Global mobile traffic per month since 2008 [11–16]. The predictions for 2014 to 2018 are based on [16].

challenge and should not be taken lightly. Today, it is not unlikely to have confined areas generating substantial amount of mobile data traffic, also referred to as traffic hotspots. This scenario is one of the most challenging traffic distribution scenarios, as a massive number of simultaneous user are requesting mobile data services. Realistic examples of such traffic hotspots are transportation hubs or sport venues [17].

1.1.2 Solutions to Increase Network Capacity

In order to keep up with the mobile data traffic growth, network operators generally speaking have three methods to increase the network capacity [18].

- Increase the number of cells
- Improve spectral efficiency
- Use more transmission spectrum

However, network operators can not rely on a single strategy, thus a combination of each of the above methods is the most realistic approach.

By deploying more cells in the network, more radio resources are available, thus, the spatial spectral efficiency is increased and the overall network capacity is improved. New deployment paradigms are developed for future network, which is described further in Section 1.2.

Spectral efficiency is the measure of the received bits per second per Hertz. Methods to improve the spectral efficiency includes transmission techniques such as beamforming, Multiple Input and Multiple Output (MIMO), channel-aware User Equipment (UE) scheduling and interference management. At the receiver side, the spectral efficiency

is improved by increasing the number of receive antennas or by exploiting interference knowledge. With the introduction of more complex mobile communication systems, the spectral efficiency improves. However, the spectral efficiency is bounded by the Shannon capacity [19] and systems such as Long Term Evolution (LTE) are closing this gap [20]. Section 1.3 summarises the mobile communication evolution.

Finally, the available spectrum can be increased to accommodate the future traffic volumes. This might seem as the most simple and promising solution for an operator. However, spectrum is an expensive and sparse resource and allocating additional spectrum is not straightforward. The transmission spectrum topic is further discussed in Section 1.4.

1.2 Heterogeneous Network Topologies

Historically, cellular networks are primarily consisting of wide area macro cells, depicted in Figure 1.2a. This deployment strategy is effective for voice centric networks with more uniform traffic distributions. On the contrary it is not effective for hot spot scenarios, where the main challenge is to increase the spatial spectral efficiency. And this problem becomes more pronounced in the future, where even larger share of the mobile data volume is generated from indoor locations [21] and with an increasing building penetration loss for modern energy efficient buildings [22]. Therefore, network operators must adapt the network to the spatio-temporal traffic distribution in a more efficient manner than wide area macro cells.

A new network deployment paradigm, called HetNet, has been developed to carry the traffic in typical traffic hotspots, see Figure 1.2b. The HetNet deployment scenario is described in [23, 24]. On the contrary to macro-only networks, HetNets consist of an overlay macro network supplemented by small cells. The term small cells covers base station technologies such as micro cells, pico cells, remote radio heads, and femto cells. The differentiator between the small cell technologies are typically the output transmission power, backhaul connectivity, and deployment methodology. HetNet deployment method ensures wide area coverage from the macro cells, and the small cells provide additional network capacity where needed. The open literature contains several HetNet performance studies, and the conclusion is clear; HetNets are capable of boosting the UE throughput performance by offloading hotspot UEs to the small cells.

However, the deployment of outdoor small cell also experiences the problem of increasing building penetration loss, since the signal still has to penetrate the outer building wall. Yet, if the small cells are deployed inside the buildings, the signal only penetrates indoor wall(s) to reach the indoor UEs, as depicted in Figure 1.2c. Hence, in this thesis the indoor femto cell technology is of main interest.

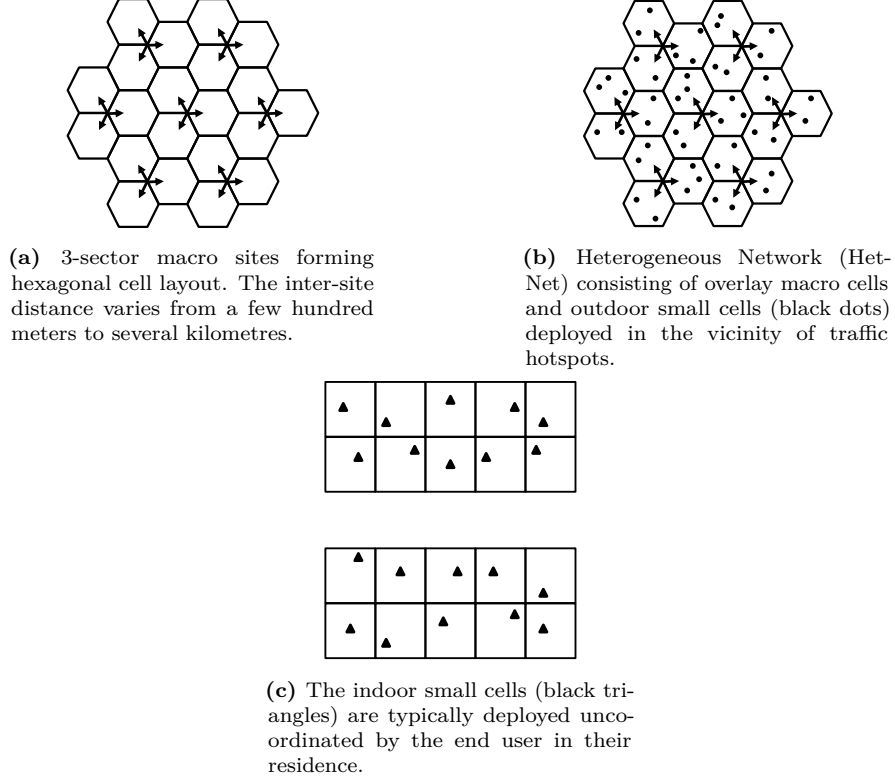


Fig. 1.2: Three examples of network topologies, from the macro-only deployment to dense indoor small cell deployment.

1.2.1 Indoor Femto Cells

Femto cells are low price and low power base stations targeted for indoor deployment scenarios [25], as depicted in Figure 1.2c. The main femto use case is improving indoor voice and data coverage. Opposite the outdoor deployed base station technologies, the femto is deployed indoor close to the indoor users. This reduces the distance dependent path loss and the femto signal does not have to penetrate any outer building walls to reach the femto user. This is an advantage, as the penetration loss of outer building walls can severely reduce the indoor signal strength.

However, the main differentiator between femto cells and other 3rd Generation Partnership Project (3GPP) base stations is the backhaul connection types. For the other base station types the network operator provides a dedicated backhaul connection for the base stations, this could be wired or wireless. On the contrary, the femto backhaul is

potentially via public Internet without any Quality of Service (QoS) requirements. This concept allows the end user to use any existing Internet connection as femto backhaul. Such a solution is motivated by reducing the femto deployment cost and increasing the femto *plug & play* capability. However, this solution implies architectural changes in the operators core network.

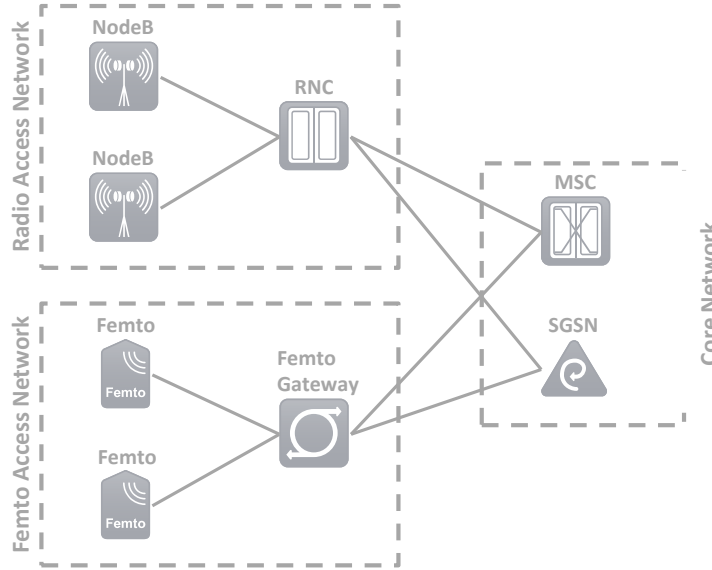


Fig. 1.3: Radio and femto access networks in Universal Mobile Telecommunications System (UMTS)/High Speed Packet Access (HSPA).

Due to the massive number of femto cells, it is necessary to reduce the number of connections towards the core network for scalability reasons. Therefore, in UMTS/HSPA networks, an extra entity is required for femto operation, the *femto gateway*, see Figure 1.3. Apart from aggregating a large number of femto connections towards the core network, the femto gateway also performs femto identification and configuration of operational parameters of the femto access point. The femto gateway connects to the Serving GPRS Support Node (SGSN) and the Mobile Switching Center (MSC) for packet switched and circuit switched communication, respectively [26]. In the femto ecosystem, no dedicated Radio Network Controller (RNC) entity is present. Instead the RNC functionalities are moved either to the femto access point or the femto gateway. E.g. the Radio Resource Management (RRM) functions are moved to the femto access point while the inter-RNC mobility functionality is moved to the femto gateway. More information on UMTS/HSPA femto system architecture is found in [27].

For LTE, two types of femto architectures are specified, see Figure 1.4. The first type

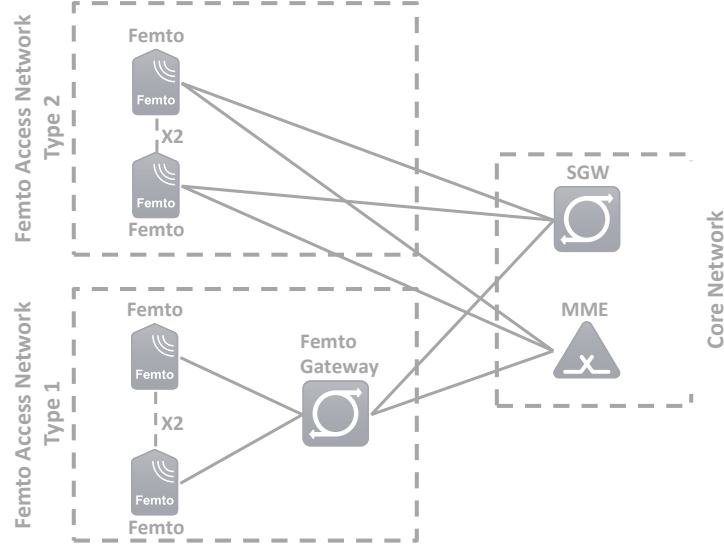


Fig. 1.4: Two types of femto architecture are defined for LTE, with and without a dedicated femto gateway.

is very similar to the UMTS/HSPA approach, where the femto cells connect to a femto gateway, and the femto gateway acts as a femto concentrator towards the core network entities: Mobility Management Entity (MME) and Serving Gateway (SGW). On the contrary, the second femto architecture does not include any femto gateway, here the femto access points connect directly to the MME and the SGW. From LTE Release 10 and onwards, X2 interface between femto cells is defined [28]. If the X2 interface is present, it enables message parsing between the femto cells, which can be exploited for interference management and power control configuration, just to mention a few possibilities.

Further femto deployment savings are achieved by allowing user deployed femto cells. The femto access point is delivered to the end user, and the end user takes care of the deployment of the femto, similar to WiFi access point deployment. Thus, the network operator reduces the femto planning time and cost. The only end user requirements are a power plug and an Internet connection. This deployment method is referred to as uncoordinated deployment. Moreover, if an end user installs a femto access point, it is possible to restrict the access to the femto cell, such that neighbours and other people not belonging to the residence are not allowed femto service. This type of access restrictions are called Closed Subscriber Group (CSG). Furthermore, coordinated femto deployment is also a possibility. Coordinated deployment is typically targeted enterprises or public areas where an operator can access the deployment location. In such a deployment scenario, the access type is typically Open Subscriber Group (OSG) without any access restrictions.

Existing studies have shown that HetNets consisting of macro cells and small cells offer the best compromise in terms Total Cost of Ownership (TCO) [29–31]. The absolute savings varies according to available spectrum, access method, etc. Apart from the TCO aspect of indoor small cell deployment, the experienced user throughput is also of high importance; it must be ensured that the indoor small cells are capable of delivering satisfactory user throughputs, today and in the future. Potentially, indoor small cells deployment reduce the TCO and at the same time significantly improves the UE throughput performance.

1.2.2 Indoor Femto Cell Challenges

Deploying indoor femto cells is not risk free, though. One of the main challenges are related to the interference coupling between the femto and macro cells. Most significant, is the deployment of indoor CSG femto cells. CSG femto cells potentially pose a great threat to the co-channel³ macro performance. When an authorised user is in the vicinity of a CSG femto access point, handover or cell reselection towards the femto cell is performed. The consequence for the authorised user is improved signal power and quality. On the contrary, non-authorised users in the vicinity of a CSG femto access point are not allowed to handover or cell reselect to the CSG femto cell, resulting in worsened received signal quality. Worst case scenario is that the macro service is compromised in case of too severe femto interference. Potential solutions are hybrid access mode and OSG [32, 33] or deployment dedicated carrier [34].

The co-channel deployment of macro cells and CSG femto cells have been studied extensively, thus, the main scenario of interest in this thesis is the uncoordinated deployment of OSG femto cells on a dedicated carrier. Consequently, the macro cell and femto cell interference coupling is not relevant. On the other hand, strong intra-femto layer interference is inevitable. With the increasing traffic volumes the femto density also increases, and in apartment or enterprise environments some femto cells are strongly interference coupled. It might seem thoughtless to allow the end user to decide the deployment location of indoor femto cells. However, this is a viable deployment strategy, if autonomous configuration features are developed to handle the network optimisation. Such configuration features could include femto power control, Range Extension (RE) configuration, carrier assignment, and interference management.

1.2.3 WiFi and Related Challenges

Today, WiFi is the de facto standard for indoor small cells. WiFi access points are plug & play capable and only require a power plug and an Internet connection. Both are typically already available in the residence of the end user. Hence, beside the cost of the electricity

³The term *co-channel* is used when two or more base station technologies are using the same frequency band.

and the Internet backhaul, there is no monthly subscription fee associated with WiFi deployment. And today, WiFi is available in a plethora of personal devices.

The promised peak throughput rates of WiFi are also appealing to end users. The peak throughput performance of WiFi Institute of Electrical and Electronics Engineers (IEEE) 802.11n is 600 Mbps and is enabled by 4×4 MIMO, 40 MHz transmission bandwidth, and 64 Quadrature Amplitude Modulation (QAM). Succeeding WiFi releases, e.g. 802.11ac supports peak throughput data rates up to 866 Mbps per spatial stream, and is achieved by transmission bandwidths up to 160 MHz, 8×8 MIMO, and 256 QAM. Thus, WiFi is a cheap, simple, and high performing solution to facilitate the indoor data capacity requirements. But there are also some WiFi specific disadvantages. The high peak data rates are also a product of the utilised transmission spectrum. In contrast to 3rd Generation (3G) and LTE, WiFi utilise unlicensed spectrum. At 2.4 GHz, 100 MHz of bandwidth is available for WiFi, and at 5 GHz even larger chunks of spectrum is available. However, the exact amount of available spectrum and corresponding regulation is region dependent.

In contrast to schedule based medium access in HSPA and LTE, WiFi medium access is contention based. Consequently, in apartment buildings with no coordination in WiFi deployment and transmission channel selection, the experienced throughput performance is potentially far from the theoretical peak throughput rates [35]. Nevertheless, in large public areas where coordination is possible, improved WiFi performance is expected, but the inherited disadvantages of contention based access is still present. Recent WiFi studies have also focused on autonomous WiFi channel assignment, a comprehensive overview of the techniques are found in [36].

Moreover, compared to the femto technology, WiFi does not feature native voice call support. Obviously, Voice over Internet Protocol (VoIP) applications such as Skype can provide voice support, but WiFi lacks the seamless service provided by macro and femto cells. However, 3GPP is currently investigating how to improve the 3GPP to non-3GPP offloading [37], and thereby improve the end user experience.

1.3 Mobile Communication System Evolution: From GSM to LTE-A

The witnessed mobile data growth rates were not possible without a mobile communication evolution. More than 20 years ago, the first phone call via Global System for Mobile Communications (GSM) was made. The evolution of GSM later included data services such as General Packet Radio Service (GPRS) and Enhanced Data rate for GSM Evolution (EDGE). In terms of data rates, GPRS and EDGE are ancient, however, voice calls are the main use case for GSM.

With the introduction of UMTS and HSPA the first step of the immense traffic data evolution was taken, since the HSPA data user experience is superior to the GSM experience.

And with the introduction of smart phones, with large screens and cameras, applications beside voice calls and text messaging became popular. The data traffic growth has been further propelled by the introduction of LTE. A smart phone usage analysis claims that LTE users consume between 36% to 132% more data than HSPA users, depending on the region [38]. Compared to GSM and HSPA, LTE enables transmission bandwidth of up to 20 MHz, thus, enabling significant higher peak data rates. Apart from the flexible spectrum configuration, other noteworthy LTE features include 4×4 MIMO and Inter-Cell Interference Coordination (ICIC) features.

The latest leap within mobile communication systems was brought to us by International Mobile Telecommunication-Advanced (IMT-Advanced) compliant systems or fourth generation systems. The 3GPP candidate is called Long Term Evolution Advanced (LTE-A) and is also known as LTE Release 10, thus, it is an evolution of LTE Release 8/9 and not a completely new system. The introduction of Carrier Aggregation (CA) marks an important evolution in order to meet, or exceed, the IMT-Advanced peak data rate and spatial efficiency requirements [39]. CA enables aggregation of up to five legacy LTE carriers, hence a maximum system bandwidth of 100 MHz is possible. Hence, CA-enabled UEs can be scheduled on multiple carriers, which enables increased UE peak data rates. LTE-A supports intra-band contiguous/non-contiguous or inter-band non-contiguous CA. This enables network operators to exploit their potentially fragmented spectrum for improving the experienced user peak rates in the network. The interested reader can find more detailed information on LTE-A CA in [40, 41]. Dynamic ICIC techniques which exploit CA have also been developed, such techniques are further discussed in Chapter 4. LTE-A also introduced inter-site CA and Coordinated Multipoint (CoMP) techniques, however these topics are not within the scope of this thesis. For inter-site CA and CoMP studies the interested reader is directed to [42] and [43], respectively.

1.3.1 Interference Challenges and Solutions

Interference related challenges are not a new research topic within wireless communication. However, the type of interference challenge depends on the particular wireless technology. E.g. in GSM macro networks, inter-cell interference is mitigated by applying frequency reuse and frequency hopping schemes [44–46] and advanced receiver technology [47]. In UMTS/HSPA frequency reuse 1 is applied, enabled by the properties of spreading and coding, and this involves new interference challenges. In UMTS, UEs connected to the same cell can be scheduled in the same Transmission Time Interval (TTI) and on the same frequency band due to the properties of Wideband Code Division Multiple Access (WCDMA). UE transmissions are orthogonal in the code-domain. However in frequency selective (multipath environments) transmission channels, the orthogonality properties are not preserved which leads to Inter-Symbol Interference (ISI) and/or intra-cell interference [48]. Therefore, in order to mitigate ISI and intra-cell interference complex receiver types are employed in UMTS/HSPA networks [49, 50].

The introduction of LTE, once again led to new interference challenges. However, careful system design eliminates certain types of interference though. ISI caused by multipath propagation environments is eliminated by applying Cyclic Prefix (CP) prior to each transmitted symbol. Moreover, intra-cell interference is effectively mitigated by the multiple access scheme; Orthogonal Frequency Division Multiple Access (OFDMA) [51]. Remaining is the inter-cell interference which potentially limits the UE throughput performance if not properly accounted for. Especially, UEs located at cell edge may experience strong interference from neighbouring cells. Therefore, proper ICIC can lead to significant improvements in cell edge UE throughput performance.

In LTE Release 8, 3GPP defined a solution to mitigate inter-cell interference called *Release 8 Frequency Domain ICIC* [52, 53]. In Downlink (DL), a framework enables improved cell edge UE performance by coordinating the scheduling process with neighbouring enhanced Node Bs (eNBs). Basically, cell edge UEs are scheduled orthogonal to UEs in neighbouring eNBs. LTE Release 8 also provides ICIC solutions for Uplink (UL). In UL, eNBs can coordinate the scheduling of cell edge UEs and indicate the experienced interference level. However, a major drawback of the Release 8 ICIC solutions is that they only protect the Physical Downlink Shared Channel (PDSCH) and Physical Uplink Shared Channel (PUSCH) (the DL and UL data channels) and not the physical control channels. This means UEs can end up in a control channel coverage hole.

In LTE Release 10, enhanced Inter-Cell Interference Coordination (eICIC) was introduced [54]. eICIC is designed to minimise the macro DL interference towards small cell UEs in HetNets [55]. This is achieved by configuring certain macro subframes as Almost Blank Subframe (ABS), where only control signalling for legacy UEs are transmitted. With eICIC enabled, it is possible to apply an aggressive cell selection bias towards co-channel small cells. In 3GPP terminology, this is known as RE. Thereby, more UEs are offloaded from the macro cells, resulting in improved HetNet throughput performance.

1.4 New Spectrum Opportunities

Equally important, or maybe even more important, is the radio frequency spectrum available for mobile communication. Radio frequency spectrum is a crucial element in modern-day society. Unfortunately, spectrum is a sparse resource and without government regulated spectrum allocations and auctions, a rogue battle for radio frequency spectrum is not unlikely. Fortunately, spectrum use is regulated, not only on country-level but also across national borders, this ensures regional (or even worldwide) operability of personal equipment for end users.

However, as users crave for higher data rates and seamless coverage everywhere, the need for spectrum increases accordingly. And this is not available, at least not in the typical cellular spectrum range from 700 MHz to 2600 MHz, let alone region or worldwide availability. A snapshot of the US spectrum allocation from 700 MHz to 1800 MHz is used as an example, see Figure 1.5. Yellow colour denotes free spectrum, and it is clearly

[illegible]

Alternatively, governments and standardisation bodies can start allocating spectrum at these frequencies. At the World Radio Conference in 2007, the spectrum band covering 1.88 GHz to 3.6 GHz was allocated for terrestrial mobile services [57, 58]. This band is interesting for two reasons mainly; first, it is available in large parts of the world. Second, a considerable amount of contiguous spectrum is available for multiple operators, allowing wider transmission bandwidths supported by mobile communication systems such as 4G-LTE and LTE-A.

Considering the small cell advantages combined with the amount of available spectrum at 3.5 GHz, indoor small cells are believed to play an increasing important role in future indoor deployments [61]. Not only does the signal, between a base station and an end user, not have to penetrate a outer building wall, the outer building wall reduces the interference from outer base stations which are deployed co-channel. This effect is more pronounced for higher frequencies. Therefore, indoor small cell operating at 3.5 GHz is considered a promising solution for boosting indoor capacity in confined areas or to improve deep indoor cellular coverage.

1.5 Scope and Objective of the Thesis

The objective of the PhD thesis is to investigate the potential of indoor small cell deployments. Not all small cell deployments challenges are feasible to cover in this theses, thus,

the scope of the thesis is further defined in this section.

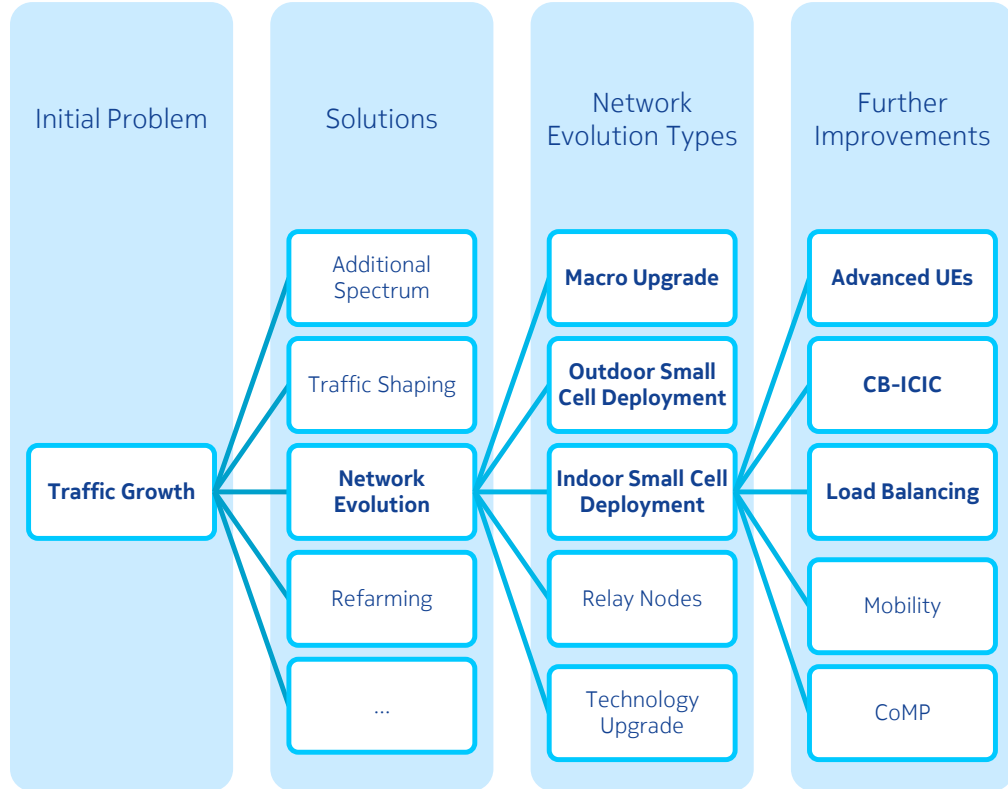


Fig. 1.6: The scope of the thesis is marked with **bold text**.

Figure 1.6 aids the reader to gain an overview of the scope of the thesis. The initial problem is the data traffic growth, as argued in Section 1.1. Several solutions can be applied in order to address the traffic growth. In this thesis the solution of interest is *Network Evolution*. In reality, a network operator would naturally not resort to a single solution only, but rather a combination of several solutions. The third column includes the different network evolution paths. It is decided to focus on the *Indoor Small Cell Deployment* option. The last column includes options for improving the network performance even further. It should be noted these improvement options are not limited to the indoor small cell option. The non-bold options are included in the figure to give a broader overview of the solutions to improve the indoor network capacity.

Network evolution covers a wide variety of deployment scenarios. The focus is narrowed down to *Macro Upgrade*, *Outdoor Pico Deployment*, and *Indoor Femto Cell Deployment*.

Initially, it is necessary to challenge the hypothesis that small cells in general reduce the TCO for network operators compared to macro-only networks and other HetNet deployments. This is important, as reduced TCO is a main driver for the indoor small cell technologies. In the network evolution investigation, the default simulation scenario is a operator deployed network from a European metropolis.

Next part of the PhD thesis is dedicated to investigate techniques for improving the performance of indoor small cell deployments. The focus is on a dense small cell environment, where small cells are the main source of interference, the default simulation scenario is the 3GPP Release 12 Small Cell Scenario 3 [62]. This challenging task is addressed by means of Carrier Based Inter-Cell Interference Coordination (CB-ICIC) and small cell load balancing. Furthermore, a combination of network based techniques and advanced receiver structures are carried out to reveal the performance of uncoordinated ICIC. Is it worthwhile? Or are no further improvement available?

In practice, it is important that ICIC techniques are applied in both DL and UL direction. Nevertheless, this thesis focuses on DL direction; i.e. data is sent at the base station and received at the UE. This is decided since the data traffic volumes are typically DL centric, with a DL to UL ratio in the order of 7:1 [63]. In theory, the proposed technique in Chapter 4 would also be applicable in UL direction. In practice though, the main challenge would be to identify the strongest interfering UEs. Moreover, all simulations assume LTE Frequency Division Duplex (FDD) mode. However, it is important to note, that the proposed techniques are also applicable for Time Division Duplex (TDD) mode networks if the cells coordinate their DL:UL switching point and the network is time synchronised.

The introduction of HetNet imposes great mobility challenges, also for indoor small cells. The interested reader is directed to [64], which contains a comprehensive summary of several state of the art mobility techniques. In this thesis, mobility is not considered. Thus, after the initial cell association the UE do not cell reselect or handover to a new cell.

1.6 Research Methodology

The complexity and dynamic nature of mobile networks makes purely analytical evaluation infeasible. Therefore, it is necessary to resort to other scientific methodology means in order to investigate the mobile network performance. In this PhD thesis, network performance results are based on a combination of experimental results, theoretical models, and system-level simulations. Figure 1.7 illustrates the relation between the applied methodologies. In the following sections, the pros and cons and the applicable scenarios are discussed for each of the scientific methodologies.



Fig. 1.7: Illustration of the applied scientific methodologies in this thesis.

1.6.1 Experimental Analysis

Measurement campaigns are planned and designed to the extent it is practically feasible and makes sense. Obvious, it is not practically possible to organise a measurement campaign including tens of base stations and hundreds or thousands of UEs. The experimental measurement results are used for analytical model extraction, and the proposed models are used in the development of system-level simulators. To the extent it is possible, the experimental results and developed models are compared against existing results and models in open literature, respectively. This step is crucial in order to build confidence and reliability in the experimental results, since the accuracy of system-level simulators is no better than the underlying modelling assumptions. Furthermore, experimental analysis is important as certain real-life performance issues might not be identified or captured due to simplifications of the system-level simulation modelling assumptions.

In the development of empirical models, it is paramount to avoid too case-specific input parameters to the proposed model. The objective is not to develop a model which perfectly describes a site-specific case, as the usage of such is very limited. Instead, a generalised model which describes a more generic scenario is preferred, thus, measurements from several measurement locations are important to satisfy this need.

For the experimental measurements the utilised equipment is either UMTS/HSPA or WiFi compliant or simply continuous wave signal transmissions. This is primarily due to availability constraints, and currently UMTS/HSPA and WiFi are the most widely available. However, model extraction experiments are not necessarily technology specific, thus, the conclusions can be applicable to other technologies as well.

1.6.2 Monte Carlo Simulations

When measurements are not practically feasible, system-level simulations are the preferred methodology, in particular Monte Carlo simulations [65]. Monte Carlo simulations relies on random number generation, and by running simulations repeatedly a distribution of the desired but unknown entity is obtained. Such a simulation approach is effective for communication networks where the overall network performance relies on several complex and inter-dependent processes and models. It is important to obtain enough samples in order to ensure statistical significant results. Moreover, the samples must be acquired when the overall network has reached a steady state, i.e. the average number of user in

the network is constant over a long term scale.

In order to ensure confidence in the system-level simulator tools, the system-level modelling is based on experimental measurement results. Furthermore, it is ensured that the utilised simulation tools are properly calibrated before any simulation studies or feature development are initiated. 3GPP defines a set of simulation scenarios which are suitable for such calibration purposes. These standard scenarios do not necessarily reflect realistic network performance, however, they enable comparison and calibration between simulation results produced by individual parties. Thus, the 3GPP scenarios are ideal for feature oriented development. Obviously, it is not possible to calibrate the operator deployed network from Chapter 3 with 3GPP reference scenarios. In this case, the path loss estimation is based on ray tracing techniques [66] and the ray tracing prediction is calibrated with experimental measurements.

1.7 Publications and Contributions

During the work of this PhD thesis, several publications have been authored or co-authored. A chronological list of the published paper:

- N. T. K. Jørgensen, T. Isotalo, K. Pedersen, and P. Mogensen, “Joint Macro and Femto Field Performance and Interference Measurements,” in *Vehicular Technology Conference (VTC Fall), 2012 IEEE*, September 2012, pp. 1–5.
- T. Kolding, P. Ochal, N. T. K. Jørgensen, and K. Pedersen, “QoS Self-Provisioning and Interference Management for Co-Channel Deployed 3G Femtocells,” *Future Internet*, vol. 5, no. 2, pp. 168–189, 2013.
- I. Rodriguez, H. C. Nguyen, N. T. K. Jørgensen, T. B. Sørensen, J. Elling, M. B. Gentsch, and P. Mogensen, “Path Loss Validation for Urban Micro Cell Scenarios at 3.5 GHz Compared to 1.9 GHz,” in *Global Communications Conference (GLOBECOM), 2013 IEEE*, December 2013.
- N. T. K. Jørgensen, I. Rodriguez, J. Elling, and P. Mogensen, “3G Femto or 802.11g WiFi: Which is the Best Indoor Data Solution Today?” in *2014 IEEE Vehicular Technology Conference (VTC Fall)*, September 2014.
- I. Rodriguez, H. C. Nguyen, N. T. K. Jørgensen, T. B. Sørensen, and P. Mogensen, “Radio Propagation into Modern Buildings: Attenuation Measurements in the Range from 800 MHz to 18 GHz,” in *2014 IEEE Vehicular Technology Conference (VTC Fall)*, September 2014.

Furthermore, a journal paper is accepted for publication in January 2015:

- B. Soret, K. I. Pedersen, N. T. K. Jørgensen, and V. Fernández-López, “Interference Coordination for Dense Wireless Networks,” January 2015, accepted for COMMAG - Special Issue: Recent Advances in Technologies for Extremely Dense Wireless Networks.

The work in the PhD project has also been used in Nokia Networks (formerly Nokia Siemens Networks) customer projects. These joint projects are typically collaborations between Aalborg University, Nokia Networks, and a network operator. The objective is primarily development of network features or network performance evaluations. During the project period, bi-weekly or monthly, meetings are arranged with the involved parties, where the preliminary results are shared and the direction of the project is agreed upon. The projects are typically concluded with a presentation of the project outcome to a broader audience in the customer organisation.

Two patent applications have been filed with colleagues from Nokia (former Nokia Siemens Networks) and Aalborg University. Moreover, a significant time of the PhD project has been dedicated to simulator development. In this thesis, two proprietary system-level simulators are used for the simulation type of studies. Beside the implementation work of the developed features itself, simulation scenario calibration with existing results and bug fixing also required a considerable amount of time and effort. Finally, a 3GPP technical document was submitted [67] based on the experimental measurement results.

1.8 Thesis Outline

This thesis consists of seven chapters and eight appendices. In order to ease the thesis overview for the reader, Figure 1.8 shows the structure of the thesis. The rows show the methodologies from Section 1.6, and the columns depict the topics of the thesis. The figure shows how each topic is treated both by means of measurements and simulations, with the exception of the combined UE and network based ICIC approach. The *Experimental Studies* and *Simulations Studies* naming also covers the analysis and post-processing of the measurement and simulation results.

- Chapter 2: Experimental Analysis - Several measurement campaigns are performed. The main objective of the measurement campaigns is verification or development of simulation models. Measurement campaigns for indoor propagation path loss and outdoor micro cell propagation characterisation have been performed. A measurement campaign is carried out, to quantify the DL and UL femto interference towards co-channel macro UEs and macro cells. Finally, a measurement campaign benchmarking the performance of the indoor femto and indoor WiFi user experience is performed.
- Chapter 3: Network evolution studies - In order to improve the mobile data network capacity, several network evolution paths are available. Three candidate solutions - macro upgrade, outdoor small cell deployment, and indoor small cell deployment -

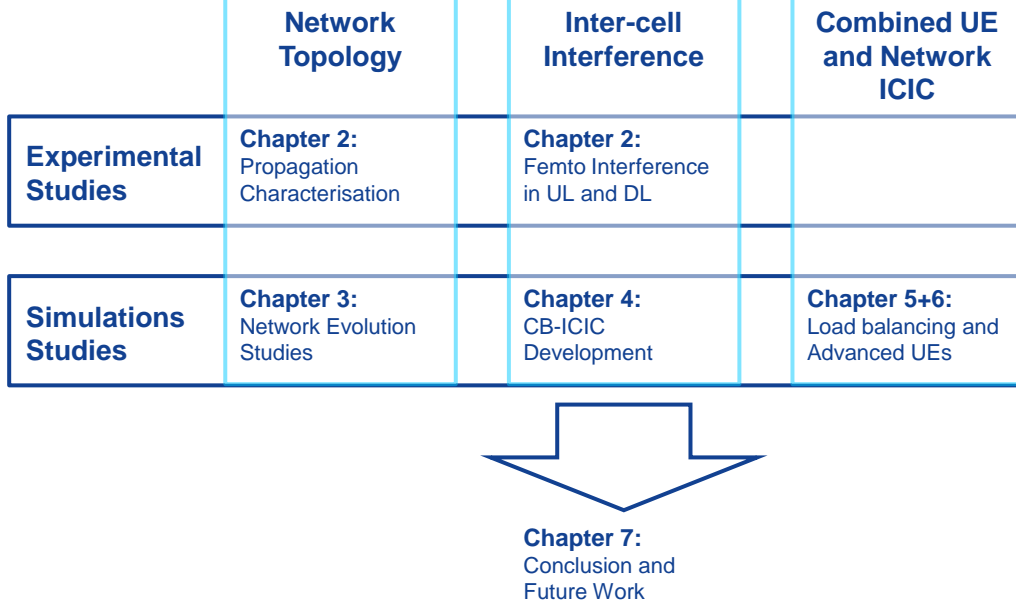


Fig. 1.8: Overview of the thesis structure.

are studied for a operator deployed network. Each solution must be able to provide certain Guaranteed Bit Rate (GBR) performance to the UEs, thus, the best evolution path is found by comparing UE performance and TCO.

- Chapter 4: Novel CB-ICIC framework - To improve the DL UE throughput performance in dense small cell environments, a CB-ICIC framework is developed. The proposed framework is characterised by maximising the network capacity subject to certain GBR. The framework ensures that only carrier changes with a positive net benefit are carried out.
- Chapter 5: Low complexity load balancing algorithm - To balance the user load of the small cells, a low complexity load balancing algorithm is proposed. The algorithm dynamically adjusts the RE value for each small cells according to the instantaneous load conditions.
- Chapter 6: Combining network and UE based ICIC techniques - ICIC techniques are not exclusively targeted the network side. Several ICIC techniques are available at the receiver side, thus, this chapter is dedicated to study the combined effects of network and UE based techniques. Furthermore, a summary of the ICIC techniques are presented to give an overview of the most promising solutions.

Chapter 2

Experimental Investigations

In this chapter the findings from the experimental investigations are presented. Some of the findings are already documented in published papers. Therefore, parts of this chapter are structured as a summary of the published papers. To ease overview of the experimental investigations for the reader, Table 2.1 list the experimental investigation and the outcome objective.

The objective with the experimental investigations is to gain further insight into relevant small cell deployment considerations. First, a measurement campaign concerning micro cell propagation characteristics at 3.5 GHz is described in Section 2.1. The objective is to understand the potential of micro cell deployment as a solution to increasing indoor coverage and capacity. Furthermore, the measurement results are used for propagation model extraction. Next, Section 2.2 presents a validation of a indoor propagation model followed by a co-channel macro and femto interference measurement campaign in Section 2.3. The objective is to identify critical femto to macro co-channel interference issues. This is important to investigate based on experiments, as system-level models might be too simple. Moreover, based on the co-channel macro and femto interference analysis, a self-provisioning and interference aware femto power control algorithm is developed and verified in Section 2.4. Finally, an indoor measurement campaign comparing the performance of High Speed Packet Access (HSPA) femtos and WiFi Institute of Electrical and Electronics Engineers (IEEE) 802.11g is performed. The objective is to shed light on the pros and cons of each of the technologies from an end user point of view.

Table 2.1: Objectives of the experimental investigations.

Experimental Investigations	Objective
Outdoor path loss propagation and outdoor to indoor penetration loss	Extraction or verification of outdoor propagation model and building penetration loss.
Indoor path loss propagation	Extraction or verification of indoor propagation model.
Co-channel macro and femto interference	Identification of critical femto to macro interference issues.
Femto power control algorithm verification	Verification of fundamental parts of a proposed femto power control algorithm.
Femto versus WiFi measurement campaign	Quantification of the end user experience.

2.1 Small Cell Propagation Characteristics at 3.5 GHz

As discussed in Section 1.4, new spectrum at 3.5 GHz is expected to be used for small cell deployment, potentially both outdoor and indoor. Therefore, the objective of the measurement campaign is to model the outdoor 3.5 GHz propagation characteristic in a below roof top small cell environment and compare it to 1.9 GHz propagation. Previously, 3.5G GHz propagation characteristics have been studied for macro cell environments mainly related to Worldwide Interoperability for Microwave Access (WiMAX) deployment studies [59, 60]. But below roof top small cell studies at 3.5 GHz have received less attention.

2.1.1 Measurement Methodology

At the transmitter, two continuous wave signals at 1.9 GHz and 3.5 GHz are combined and transmitted simultaneously. The transmit antenna is deployed at a typical urban micro cell environment below roof top. The location is determined with a Global Positioning System (GPS) receiver. At the receiver side, a network scanner measures the received power at 1.9 GHz and 3.5 GHz. At the same time the measurement position is continuously tracked using a GPS receiver. Measurement routes are planned in the vicinity of the transmitter, such that the measurement routes cover both Line of Sight (LOS) and Non Line of Sight (NLOS) propagation. Furthermore, to measure the building propagation loss, measurement

route are also planned in indoor environments. When measuring indoor, the exact receiver position is determined from building blueprints.

2.1.2 Measurement Analysis

For the full measurement result details, the interested reader is referred to [3]. The following LOS and NLOS path loss models are adopted:

$$L_{\text{LOS}} = O_{\text{LOS}} + 10 \cdot N_{\text{LOS}} \cdot \log_{10}(d) \quad [\text{dB}] \quad (2.1)$$

$$L_{\text{NLOS}} = O_{\text{NLOS}} + 10 \cdot N_{\text{NLOS}} \cdot \log_{10}(d) \quad [\text{dB}] \quad (2.2)$$

where L_{LOS} is the LOS path loss, L_{NLOS} is the NLOS path loss, O_{LOS} is the LOS off set coefficient, O_{NLOS} is the NLOS off set coefficient, N_{LOS} is the LOS distance dependent coefficient, and N_{NLOS} is the NLOS distance dependent coefficient. The O and N coefficients are found by linear regression, the optimisation constraint is to minimise the Mean Square Error (MSE). Measurement results are summarised in Table 2.2. For LOS propagation path loss, the 3.5 GHz carrier frequency increases the path loss roughly 4 dB, whereas the NLOS path loss is increased with almost 6 dB. In practice, the consequence is a reduced effective coverage area of the outdoor small cells.

Table 2.2: Outdoor propagation loss measurement results.

	1.9 GHz		3.5 GHz		Δ path loss [dB]
	O [dB]	N [-]	O [dB]	N [-]	
LOS	39.1	2	42.9	2	3.8
NLOS	27.7	4	33.5	4	5.8

Table 2.3 summarises the outdoor to indoor building penetration loss measurement results. Largest penetration loss is observed for the modern building, due to the construction materials and techniques. It is also for modern buildings the largest difference in building penetration loss is measured, on average the building penetration loss is 5 dB larger for 3.5 GHz. For old building types and shops in a pedestrian street, the difference between 1.9 GHz and 3.5 GHz is smaller. Based on these findings, a 3rd Generation Partnership Project (3GPP) technical document [67] was submitted, and the proposal of increasing the building penetration loss for 3.5 GHz was subsequently adopted in the 3GPP small cell enhancement specification [62].

Furthermore, a measurement campaign focusing specifically on outdoor to indoor building/material penetration loss was also carried out. The objective is to determine the frequency dependant penetration loss for several building materials. The frequency range is from 800 MHz to 18 GHz. The detailed measurement campaign and analysis is found in [5]. The measurement analysis shows irregular frequency dependency for the

Table 2.3: Outdoor to indoor building penetration loss measurement results. Values in dB

	1.9 GHz	3.5 GHz	Δ
Modern building	17.5	22.5	5.0
Old building	7.2	11.5	4.3
Shops	10.0	13.0	3.0

different materials. However, it is evident that the modern building penetration loss is approximately 20 dB higher compared to old building penetration loss. This is explained by the energy efficient construction techniques and the use of energy efficient window glass. The authors of [22] reach a similar conclusion. The consequence from a mobile communication point of view is reduced indoor coverage and capacity from outdoor base stations.

2.2 Indoor Path Loss Investigation

The objective of the indoor propagation investigation is to extract a indoor propagation loss model or verify existing propagation models. The indoor measurement campaign was conducted at the Tampere University of Technology campus. Five femto locations was selected, ranging from a small office (approximately 10 m²) to large open areas. The building structures differs from old concrete buildings to more modern steel and glass based buildings. The diverse locations and building structures ensure that the measurement campaign represent a more generalised indoor environment and not only composed of a single type of indoor environment. In total, the measurement campaign covers more than 40 indoor locations, resulting in more than half a kilometre of indoor measurement routes.

2.2.1 Measurement Methodology

In order to keep track of the positioning on the indoor measurement route, markers are placed on the measurement route for every 2 m in offices and for every 5 m in corridors and large open spaces. In Figure 2.1 a sketch of two measurement routes are illustrated. Based on the building blueprint, the distances from transmitter to the start of the measurement route, to the end of the measurement route, and to the markers on the measurement route are computed. The distance between the transmitter and measurements in between marker are found by interpolation.

A femto of the type Thomson TG870 was used as transmitter and a Rohde & Schwarz TSMU network scanner was used to measure the received signal strength, in Universal Mobile Telecommunications System (UMTS)/HSPA this is known as Reference Signal Code Power (RSCP). The accuracy of the measurement device is ± 1.5 dB. The femto

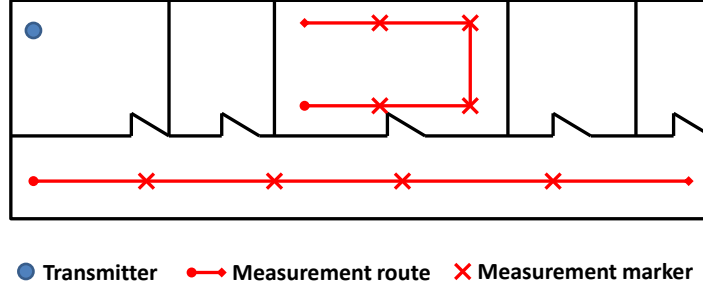


Fig. 2.1: Sketch of two measurement routes in a single measurement location.

carrier frequency is 2.1 GHz (wave length is 0.14 m) and the transmission bandwidth is 5 MHz. The sampling frequency of the network scanner is set to 10 Hz and the walking speed during the measurements is approximately 1 m per seconds, ergo the measurement spacing is roughly 0.1 m. The accuracy of the RSCP measurements is ± 1.5 dB.

In order to filter out fast fading effect, it is decided to apply spatial filtering. For each meter of measurement route, the measurement samples are averaged, see Figure 2.2 for an example. By doing so, the filtered samples are spaced 1 m. It is these filtered samples which are used to calculate the indoor propagation path loss.

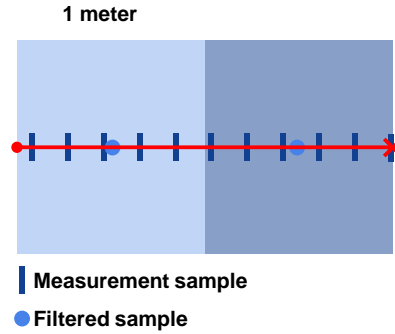


Fig. 2.2: Spatial averaging applied to all measurement samples.

The indoor propagation path loss in dB (L_{Path}) is computed as:

$$L_{Path} = P_{Tx} - P_{Rx} + G_{Tx} + G_{Rx} - L_{Cable} \quad [\text{dB}] \quad (2.3)$$

where P_{Tx} is the transmission power, P_{Rx} is the received power, G_{Tx} is the transmit antenna gain, G_{Rx} is the receive antenna gain, and L_{Cable} is the cable loss. In (2.3), P_{Tx} is known and P_{Rx} is measured by the network scanner, the rest of the parameters are

unknown. Therefore, calibration measurements were performed in an anechoic chamber to determine the unknown parameters.

Some of the measurement are performed during work hours, where it is not ensured that people do not enter or leave the measurement area. Naturally, this could effect the measurement accuracy, however, measurements were repeated if significant variations were observed, e.g. a large group of people enters the room where the measurements are performed and doors or windows being opened or closed.

2.2.2 Measurement Results and Analysis

In order to evaluate the measurement results, the measurements are compared against the International Telecommunication Union Radiocommunication Sector (ITU-R) indoor prediction model [68]:

$$L_{Total} = 20 \cdot \log_{10}(f) + N \cdot \log_{10}(d) + L_f(n) - 28 \quad [\text{dB}] \quad (2.4)$$

where f is the carrier frequency in MHz, N is the distance power loss coefficient, d is the separation distance in meter ($d > 1$ m), L_f is the floor penetration loss factor in dB, and n is the number of floors between transmitter and receiver ($n \geq 1$). For all measurements, the transmitter and receiver is located on the same floor, the carrier frequency is 2.1 GHz and the measurements are performed in office environment. Then, the constants are inserted in (2.4) according to the measurement environment [68, Table 2 and 3]:

$$L_{Total} = 20 \cdot \log_{10}(2100) + 30 \cdot \log_{10}(d) + 15 - 28 \quad [\text{dB}]. \quad (2.5)$$

To ease the comparison of the measurements and the ITU-R prediction model, *least square* curve fitting [69] is applied to the measurement results. The utilised fitting model is:

$$L_{Total} = 20 \cdot \log_{10}(2100) + N_{Fit} \cdot \log_{10}(d) + 15 - d_{fit} \quad [\text{dB}]. \quad (2.6)$$

Figure 2.3 presents the measurement results, the curve fitting, and the ITU-R indoor propagation prediction model. By visual inspection the curve fitting match very well with the ITU-R prediction model. Close to the transmitter the difference is not visible. At larger distances the difference is increased. Table 2.4 summarises the ITU-R prediction model parameters and the curve fitting parameters.

Table 2.4: Comparison of ITU-R prediction model and curving fitting parameters.

	$N[-]$	$d[\text{dB}]$
ITU-R model	30	28
Measurements	31.0	27.7

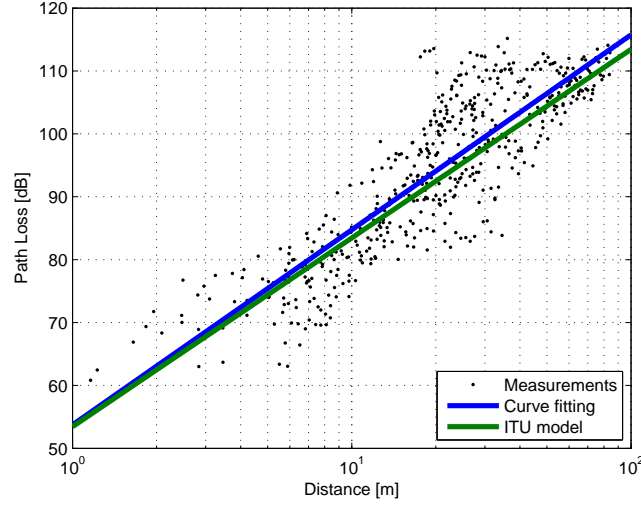


Fig. 2.3: Indoor propagation measurement results compared to the ITU-R indoor propagation prediction model [68].

The quality of the fit is found by computing the standard deviation of the error. The standard deviation of the error between measurement samples and the ITU-R model is 6.3 dB. Considering the measurement equipment accuracy and the shadow fading component defined by ITU-R for the office environment (10 dB), this is found a good match.

2.3 Co-channel Macro and Femto Interference Measurements

Co-channel macro and femto deployments have been studied extensively by means of system level simulations in open literature [34, 70]. In contrast, this investigation contributes with a co-channel macro and femto measurement based analysis. By performing measurements in a live HSPA network, it is possible to reveal any shortcomings in the system-level model assumptions. The object of the measurement campaign is to reveal any potential critical interference issues in a co-channel macro and Closed Subscriber Group (CSG) femto deployment. The focus is on the potential degradation of the macro performance. More users are served by the macro cells and it is important that the performance of the macro users are not compromised by interference from a single or few femto cell deployments.

The Downlink (DL) Key Performance Indicators (KPIs) are macro CPICH $E_c I_0$ ¹ and macro throughput. For Uplink (UL) direction, the KPI is noise rise at the nearest macro base station. Finally, all results and conclusions are documented in [1]. A reprint of this paper is found in Appendix A. However, this section contains a summary of the most important results and conclusions.

2.3.1 Measurement Methodology

The measurement methodology for the DL investigation is similar to the procedure described in Section 2.2.1. A HSPA Universal Serial Bus (USB) data card² is used as measurement device. All measurements are performed during off-hours which means the test network is empty, thus, by using multiple HSPA USB data cards, it is possible to control the interference during the measurements. Figure 2.4 illustrates the macro cell edge measurement environment. The blue \times marks the femto access point location and the dashed red line depicts the outdoor measurement route. The black line corresponds to the outer building wall and the grey lines illustrates the inner walls. Only the window in the femto office is depicted in the figure.

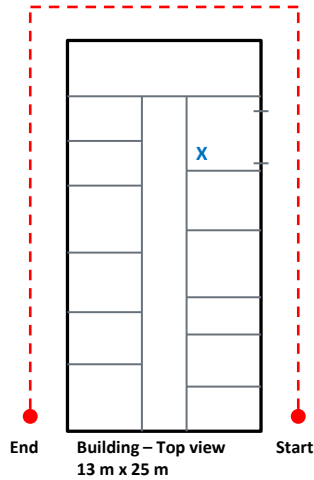


Fig. 2.4: Example of an measurement location. \times marks the femto location, and the dashed red line denotes the measurement route.

In order to measure the femto effect on macro DL performance, four different DL measurements are performed. The four measurements cases are defined as:

¹Common Pilot Channel (CPICH) Energy per chip over total received power ($E_c I_0$)

²Sierra Wireless AirCard USB 309

1. Measure macro CPICH RSCP and macro CPICH $E_C I_0$ ³ when femto is switched OFF.
2. Measure macro CPICH RSCP and macro CPICH $E_C I_0$ when femto is fully loaded.
3. Measure macro High Speed Downlink Packet Access (HSDPA) throughput, CPICH RSCP and macro CPICH $E_C I_0$ when femto is switched OFF.
4. Measure macro HSDPA throughput, CPICH RSCP and macro CPICH $E_C I_0$ when femto is fully loaded.

For the UL measurements, the measurement User Equipment (UE) connects to the indoor femto, and starts a High Speed Uplink Packet Access (HSUPA) transmission. During the data transmission, the measurement UE is moved away from the femto access point. This continues until the UE loses the connection towards the femto cell. Noise rise at the nearest macro base station is the main KPI. From [26, page 179] the definition of noise rise (NR) is:

$$NR = I_{Total} - N_T \quad (2.7)$$

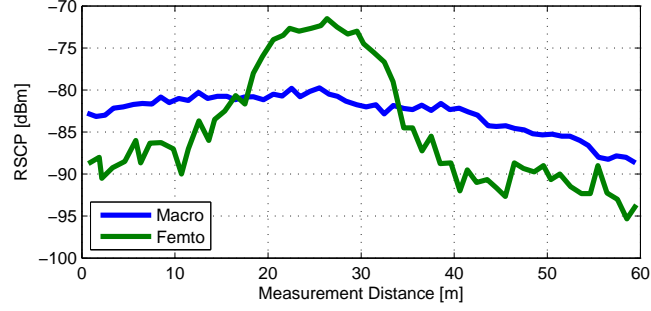
where I_{Total} is the total received wideband power and N_T is the noise power. Thus, during the measurement timespan the macro Radio Network Controller (RNC) logs the required information.

2.3.2 DL Measurement Analysis

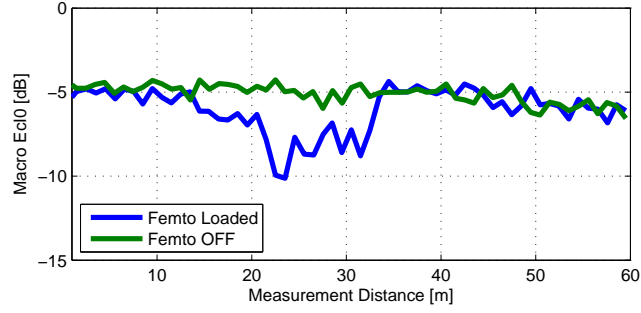
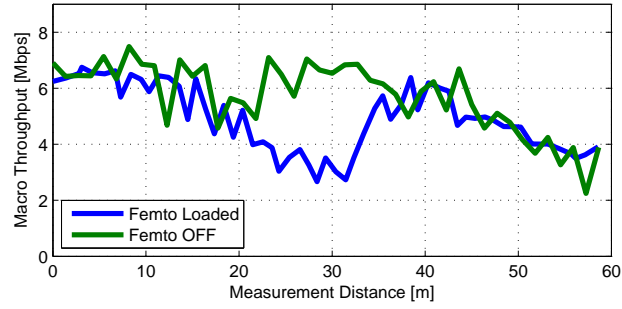
Figure 2.5 depicts the macro and femto RSCP, the macro $E_C I_0$, and the macro Medium Access Control (MAC) throughput, respectively. The location is macro cell edge, as this is the location where the most severe macro performance degradations are recorded. Below the main DL measurement observations are listed.

- Macro RSCP ranges from -90 dBm to -80 dBm, the femto RSCP varies from -95 dBm to -70 dBm. Femto RSCP peaks when measuring just outside the window.
- Without the presence of femto interference, the macro $E_C I_0$ is approximate -5 dB on the entire measurement route.
- A fully loaded femto causes the macro $E_C I_0$ to drop to -10 dB just outside the room where the femto is deployed. The macro $E_C I_0$ remains unchanged on the remainder of the route.

³It is noted that the term $E_C I_0$ includes both interference power and noise power, which is also known as $E_C N_0$.



(a) Macro and femto received signal strength.

(b) Femto interference impact on macro E_{CI0} .

(c) Femto interference impact on macro MAC throughput.

Fig. 2.5: Macro performance degradation due to femto deployment. Measurement location is macro cell edge.

- The macro throughput is degraded when measuring outside the femto room. The throughput drops from 6 Mbps to 3 Mbps. Unaffected on the remainder of the measurement route.
- No outdoor macro coverage holes are detected.

Measurements also showed that a femto which is not serving any users do not cause any macro throughput degradations despite the transmission of CPICH and other mandatory control channels. For sake of simplicity the results are not shown.

If no degradation of macro throughput performance is allowed or a macro user enters the building where the femto is deployed, a potential solution is to deploy a femto-free macro carrier, which is studied in [34]. This solution is also tested, and measurement results confirmed that this is a feasible solution to eliminate the macro throughput degradations caused by femto interference.

2.3.3 UL Measurement Analysis

Figure 2.6 illustrates the UL interference at the macro base station during a measurement at macro cell centre. From the figure, the thermal noise floor is -105.6 dBm, which is observed at the beginning and the end of the measurements. During the measurement, the UL interference peaks at -99.6 dBm. From (2.7) the maximum noise rise is then 6.0 dB. During all the UL measurements, the measured noise rise was in the range from 3 dB to 6 dB.

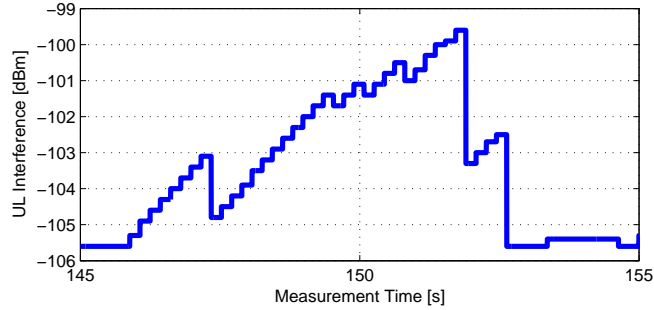


Fig. 2.6: Macro noise rise caused by femto UE. Measurements are performed at macro cell centre.

In network planning, maximum allowed noise rise is an important design parameter when calculating link budgets. Typically, the maximum allowed noise rise is 3 dB [26]. Therefore, an experienced noise rise of 6 dB is clearly too high. In practice, the consequence is a reduced macro coverage area and potentially leave macro cell edge UEs without macro coverage. Potential solutions to reduce the noise rise at the macro cell is to reduce the

femto coverage area (reduce the femto CPICH power) or apply UE power capping. Both solutions are tested, and solves the noise rise problem. However, the downside to both these measures are a reduced femto coverage footprint. Measurements show a femto coverage radius less than 5 m is not uncommon. Thus, co-channel CSG femto and macro deployment at macro cell centre is less attractive due to the relative small femto coverage footprint.

2.4 QoS Aware Femto Power Control Algorithm

Manually configuring the femto power control is time consuming and cumbersome. Alternatively, some global and conservative femto power policies could be applied. This would protect the macro performance but at the same time reduce the femto performance gain. Therefore, a autonomous power control algorithm is proposed in [2]. This section summaries the most notable results of [2]. Moreover, a reprint of the paper is found in Appendix B.

2.4.1 Design Objectives and Concept

The overall design objective is summarised in Figure 2.7 for a simple example with co-channel deployment of macro and femto cells, each serving one user. The objective is to adjust the femto transmit powers of CPICH and High Speed Downlink Shared Channel (HSDSCH), as well as power capping of the femto UE maximum transmit power, subject to the desired design criteria. The assumed design criteria are the following:

1. The femto cell coverage area shall correspond to the residence of the end-user.
2. Femto UEs shall be offered a Guaranteed Bit Rate (GBR) in downlink and uplink in the entire residence of the end-user. The GBRs are planning parameters.
3. The generated uplink noise rise at the nearest macro cell from each femto UE must be limited to NR_{FUE} . NR_{FUE} is a planning parameter that depends on the femto density and the expected offload effect (for instance NR_{FUE} divided by maximum number of simultaneously active femto cells per macro cell area).
4. After fulfilling the above requirements, the generated femto interference towards the macro UEs shall be minimised (save power, improve macro performance).

Summary of Power Control Algorithm

This section gives a short summary of the proposed power control algorithm. For the full details, the interested reader is directed to the paper reprint in Appendix B.

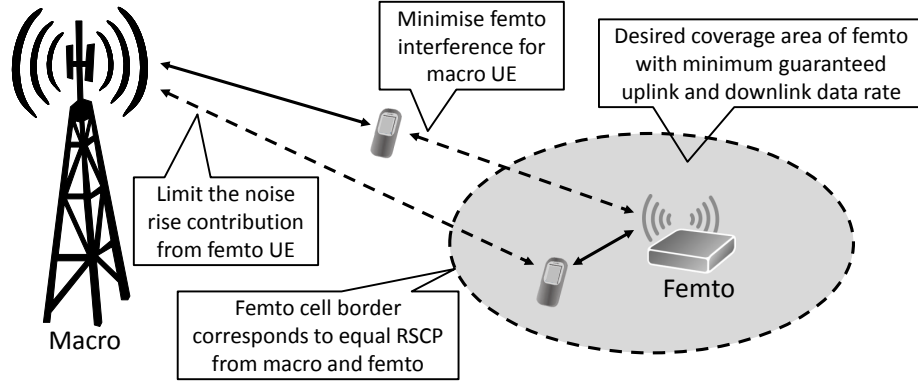


Fig. 2.7: Overview of system model and design objectives.

- The first step in the power control algorithm, is to configure the CPICH power of the femto. This is based on the desired coverage area and the macro signal power measured at the femto utilising Network Listening Mode (NLM) capabilities. The stronger the macro RSCP the higher femto CPICH power. After setting the CPICH power, the femto UE power capping is computed. Here, two aspects are important; first the UE is not allowed to cause a noise rise at the nearest macro exceeding the noise rise constraint. Secondly, the femto UE must be allowed a maximum transmission power which is high enough to overcome the worst case UL interference while being able to send data according to the GBR. If it is not possible to combine both requirements, the femto cell coverage is reduced, and computations start over.
- Next step is to compute the power allocated to HSDSCH. Often the power ratio between HSDSCH and CPICH is fixed, e.g. the CPICH power is typically 10% of the maximum transmission power. A flexible power ratio enables tailored power configurations to the given environment. The HSDSCH is configured such that the femto UE data rate at femto cell edge equals the GBR. Finally, it is ensured that the hardware limited output power of the femto is not exceeded. If it is exceeded, the femto coverage area is reduced and all computations start over.

2.4.2 Concept Verification by Simulation and Measurements

In order to verify the core functionalities of the proposed Quality of Service Self Provisioning and Interference Management (QoS-SP-IM) concept, a measurement campaign is carried out. Verifying the full concept requires extensive measuring trials across a large region. Therefore, the measurement campaign focuses on the prediction of femto coverage area and estimation of uplink noise rise contribution from femto UEs. In order to cover the

extremes in terms femto coverage estimation and noise rise estimation, macro and femto co-channel measurements are performed at macro cell edge and macro cell centre.

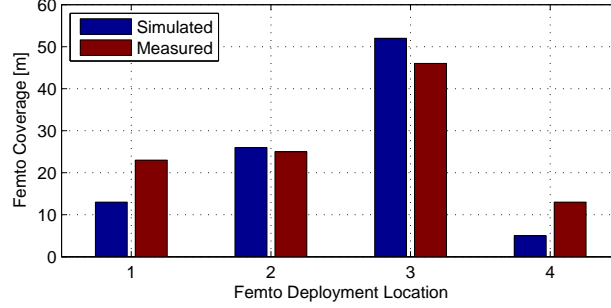
A key element for verification is the ability to predict the femto cell coverage area accurately as a function of the pilot and data power ratios. The CPICH power of the femto cell is set to -10 dBm. Next, the femto indoor coverage is measured at four femto locations with very different macro interference levels. The measurement UE is placed close to the femto and connected to the femto. The femto coverage is measured by walking away from the femto while the UE is kept in connected mode. The distance is measured to the location where the measurement UE lose femto coverage or hands over to the surrounding macro cell. The measurement results are presented in Figure 2.8a. A descent match is obtained, however, it is noted that when the femto is located close to the macro base station, the simulator underestimates the femto coverage compared to the measurement results. Nevertheless, considering the shadowing effects measured in similar environment in Section 2.2, the simulator is considered calibrated.

Next, it is verified whether uplink noise rise from femto UEs is effectively predicted by the algorithm. The uplink noise rise caused by a single femto UE is measured at macro cell edge and macro cell centre. A simulation scenario which corresponds to the measurement environment is configured, and the outcome is presented in Figure 2.8b. It is evident that the difference between the simulated result and the measurement result is insignificant. Further noise rise statistics from the simulations are presented in the paper reprint in Appendix B.

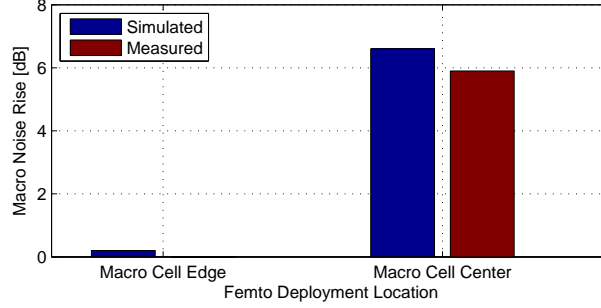
2.4.3 Performance Results

The presented simulation results are for the 3GPP dual stripe model [71]. Two reference power control algorithms are included in the study. First, no power control, which means that all femto cell transmit with 15 dBm, denoted NOPC in the figures. Second, an adaptive solution which has been adopted for 3GPP Long Term Evolution (LTE) femto cells is also included [72], this is denoted 3GPP in the results. For the proposed QoS-SP-IM concept, two GBRs in DL are simulated: 256 kbps and 1 Mbps, denoted QoS-SP-IM (256 kbps) and QoS-SP-IM (1 Mbps), respectively.

In Figure 2.9a the macro UE throughput performance in DL is plotted. This figure exhibits the protection of macro performance properties of the proposed algorithm. With NOPC, 10% of the macro UEs are without service, due to strong femto interference. The 3GPP power control improves the macro performance significantly over NOPC, by reducing the femto transmission power for some femto cells. The performance of the proposed algorithm and a GBR of 1 Mbps is similar to the 3GPP performance. However, best macro 5%-ile UE throughput performance is obtained with the proposed algorithm and a GBR of 256 kbps. E.g. the 5%-ile UE throughput is 0 Mbps, 0.8 Mbps, and 1.2 Mbps for NOPC, 3GPP approach, and proposed algorithm and a GBR of 256 kbps, respectively. This clearly demonstrate the advantage of reducing the HSDSCH power according to the



(a) Comparison of simulated and measured femto coverage.



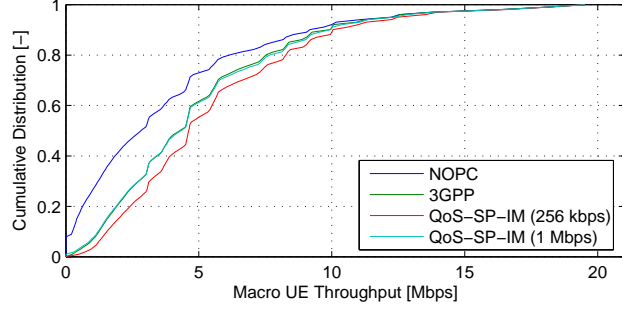
(b) Verification of simulated noise rise.

Fig. 2.8: Simulation and measurement verification.

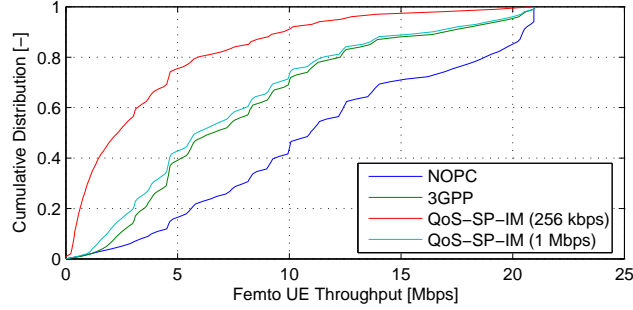
environment.

Figure 2.9b presents the DL throughput performance for femto UEs. Here the results are opposite compared to the macro UE throughput performance. The reason for this, is that the proposed framework reduces the femto power, such that no more than the GBR is provided at femto cell edge. It is noteworthy, that the GBR is fulfilled for at least 95% of the femto UEs by using the proposed power control, however, the average femto user throughput is significant higher than GBR.

Considering both Figure 2.9a and Figure 2.9b, it is concluded that the proposed power control algorithm is capable of protecting the macro DL performance, and at the same time provide the GBR to the femto UEs. Furthermore, the proposed algorithm allows for easy configurable femto performance. However, this involves a trade off between macro and femto performance.



(a) DL throughput for macro UEs in dense femto scenario.



(b) Femto UE throughput in DL for the dense femto scenario.

Fig. 2.9: Macro and femto UE throughput performance in dense scenario.

2.4.4 Summary

A self-provisioning power control algorithm for UMTS/HSPA femto cells is proposed. Femto UEs are guaranteed the agreed Quality of Service (QoS) performance (or better) without compromising the macro UE performance. Femto NLM measurements are used for femto power configuration, this ensures that the femto interference towards the macro cells is minimised. Moreover, a flexible CPICH power to total power ratio assures that the femto coverage is effectively limited to the residence of the end user. Equally important, the proposed power control concept is designed such that the configuration is limited to three intuitive input parameters; DL and UL GBR and femto coverage area in square metres.

Dense femto deployment simulation results show that the proposed power control algorithm effectively eliminates the macro outage in the network. Moreover, at least 95% of the femto UEs are provided with the promised GBR or more. Similar results are obtained for a suburban deployment scenario, thus, the proposed QoS-SP-IM concept

proves versatile and robust against the deployment scenario. In this work the focus is on the most challenging scenario; co-channel macro and femto deployment and CSG. However, the proposed power control algorithm is also applicable in dedicated femto deployment and for Open Subscriber Group (OSG) femto cells. Finally, pivotal elements of the algorithm, such as noise rise estimation and femto coverage area prediction capabilities, are calibrated with measurements which provide confidence in the simulations results.

2.5 Femto or WiFi as Indoor Data Solution?

The objective of the study is to determine the preferred indoor data solution based on the defined end user KPIs. All finding and conclusions are found in Appendix C which contains a reprint of [4]. This section contains a summary of the most notable results and conclusions. In open literature, it is possible to find a vast number of studies related to femto or WiFi performance. Typically, such studies focus on KPIs individually or a single KPI only [73–76]. This study contributes with a study involving multiple end user KPIs, and more importantly, the interdependency between such KPIs. The three end user KPIs investigated in this study are: throughput, latency, and UE power consumption. To ensure realistic performance, this study investigates the femto and WiFi KPIs by means of measurements.

2.5.1 Measurement Methodology

The throughput measurements are performed in office environment and in apartment environment. The femto or WiFi access point is deployed in a room in the office complex or the apartment and measurements are performed in all nearby rooms with coverage. In each room, the DL and UL throughput is measured. During the measurements, the measurement UE is moved around at walking speed.

Latency is measured as the Round Trip Time (RTT) between the measurement phone and a destination server by utilising the *ping* command. Two ping intervals are defined; 2 seconds and 10 seconds. It is noteworthy, that potential Radio Resource Control (RRC) set up time is included in the latency measure.

The UE power consumption is performed by powering the measurement UE with a power meter which logs the power consumption every 1 ms. For the study, realistic usage patterns are investigated, five test cases are defined:

- Idle and screen OFF
- Idle and screen ON
- Web browse, 15 second web page load interval
- Web browse, 45 second web page load interval

- File Transfer Protocol (FTP) file download

It is important to note that during all WiFi test cases the cellular modem is in idle mode, this way cellular voice calls are available via the macro network. In the web browse test cases, 10 different web pages [77] are loaded with intervals of either 15 seconds and 45 seconds.

For all the measurements, identical test procedures are ensured as no user inputs are required during the measurements. Moreover, all measurements are performed with the same measurement phone.

2.5.2 Measurement Equipment and Configuration

The measurement phone used in all the measurements is Samsung Galaxy S III with pre-installed measurement software. For the power consumption measurement, a DC power analyser⁴ is utilised. During all femto measurements, the UTRA Absolute Radio Frequency Channel Number (UARFCN) is 10788 which is also used by as macro carrier. Consequently, all measurements are performed outside office hours or during the night in order to reduce the interference from surrounding users. Further details on the configuration are found in Table 2.5. Since it is not possible to acquire any HSPA Release 7/8 femtos or LTE femtos, it is decided it is not a fair comparison if a IEEE 802.11n/ac WiFi access point is used. Therefore, the IEEE 802.11g WiFi access point is used instead.

Table 2.5: Femto and WiFi capability and configuration.

	Femto	WiFi
Carrier frequency	2 GHz (UARFCN 10788)	2.4 GHz (ISM band)
Bandwidth	5 MHz	20 MHz
Transmission power	+24 dBm	+16 dBm
Version	HSPA Release 6	IEEE 802.11g
Peak DL data rate	14.4 Mbps	54 Mbps
Peak UL data rate	1.45 Mbps	54 Mbps
DL Modulation	Up to 16 QAM	Up to 64 QAM
UL Modulation	Up to QPSK	Up to 64 QAM

2.5.3 Result Analysis

Table 2.6 summaries the spectral efficiency results. The DL spectral efficiency is roughly 0.5 bps per Hz for femto and WiFi at home. WiFi at office location reaches a spectral efficiency of 1.5 bps per Hz. The reason for the increased WiFi performance at the office

⁴Agilent N6705B using Option N6781a

location is a very limited number of interfering WiFi networks, as only single a coordinated WiFi network is deployed. On the contrary, at the home location WiFi networks are available per apartment basis resulting in approximately 10 interfering WiFi networks. In UL direction, the trends are similar. Though, the femto UL modulation limits the femto performance. And at home location, the backhaul limits the WiFi performance in UL.

Table 2.6: Spectral efficiency measurement results. Values in bps per Hz.

	Femto	WiFi
DL - Office	0.43	1.53
DL - Home	0.46	0.50
UL - Office	0.06	1.24
UL - Home	0.13	0.24 ⁵

Table 2.7 presents the latency measurement results. With a ping interval of 2 seconds, the femto latency is up to 5x larger than the WiFi latency, yet, the values are still within the user expectations [78, 79]. If the ping interval is increased to 10 seconds, the WiFi latency remains unchanged. The reason is the contention based medium access method of WiFi. On the contrary, the femto latency is increased significantly, up to more than 3 seconds. From the measurement phone, it is evident that in between the pings, the RRC connection is released. Thus, before sending the next ping, the phone needs to re-establish the RRC connection. This requires intensive signalling between phone and network. In fact, more than 30 control messages need to be communicated [80].

Table 2.7: Latency measurement results.

	Femto	WiFi
2 s ping - Office	99 ms	44 ms
2 s ping - Home	112 ms	23 ms
10 s ping - Office	3.1 s	50 ms
10 s ping - Home	3.3 s	26 ms

In Table 2.8 the power measurement results are summarised. From the table a clear trend is revealed; in idle mode the femto technology shows the lowest UE power consumption, while WiFi performs best when data is transmitted or received. The web browse tests show that the WiFi power consumption is considerably lower than the femto power. The measurement results show that the UE returns much faster to the idle mode power level when connected to WiFi compared to femto. When connected to the femto, the UE is kept in CELL_DCH state despite the web page is already fully loaded. The web browse

⁵This measurement limited by the backhaul performance.

with loading interval of 15 seconds show the highest power consumptions, since the time the UE spends in idle mode is shorter compared to the 45 second load interval.

WiFi also outperforms femto when it comes to the Energy Efficiency (EE) [4, Equation (1)] of a FTP file download. This is explained by the wider transmission bandwidth of WiFi. It is more efficient to transmit with higher throughput for short time than transmit with low throughput for longer time. Similar power results are reported in [81]. Moreover, in [4], results for dual-cell HSDPA are also included which confirms this observation.

Table 2.8: Power measurement results. Best results are in **bold**.

	Femto	WiFi
Power - Idle, screen OFF	77 mW	94 mW
Power - Idle, screen ON	0.8 W	0.9 W
Power, Web browse 15 s	2.0 W	1.3 W
Power, Web browse 45 s	1.8 W	1.2 W
EE, FTP Download	139 kbit/J	1236 kbit/J

2.5.4 Summary

Measurement results showed that the DL spectral efficiency is very similar for femto and WiFi. The only exception is when WiFi is subject to no or very minor interference, in such cases the spectral efficiency of the WiFi is $\sim 3x$ larger than the femto. In UL direction, the trends are the same, however, the femto performance is limited by QPSK modulation. Later releases of HSPA introduces features which improve the DL and UL spectral efficiency.

More severe are the femto latency and femto UE power consumption. For femto UEs these KPIs can not be optimised individually, as they depend on the RRC configuration. High femto latency indicates that the RRC release timer should be increased, such that less signalling is required when the phone needs to transmit data. On the contrary, the web browse power measurements suggest that RRC release timer should be decreased as the femto UE is kept in CELL_DCH mode for excessive amount of time. Therefore, it is impossible to find a trade off which ensures comparable femto latency **and** UE power consumption performance; it is one or the other. Consequently, WiFi offers the best indoor data capacity package.

Nevertheless, recent HSPA releases have introduced a vast amount of improvements [82, see Figure 17.20], e.g. dual cell support, higher modulation, and continuous packet connectivity. Measurements from a HSPA Release 8 macro network in Appendix C, also reveals improved data rates, reduced latency and reduced UE power consumption. Using the measured macro latency as a performance indicator for a Release 8 femto cell, the femto latency is still significantly higher than the WiFi latency, though.

LTE femto cells are expected to further reduce the latency due to flatter system architecture and simpler RRC state design [83]. In addition, enhanced power saving features such as *discontinues reception* and *discontinuous transmission* enables flexible power configurations. E.g. in [84] the authors report power savings up to 95% and less than 20% throughput performance loss, when utilising the enhanced power saving features such as *discontinues reception*. As a result, the performance of LTE femto cells could potentially close the WiFi performance gap, however, it is important to realise that the WiFi technology also evolve. E.g. new transmission spectrum allows for wider transmission bandwidth and increase the end user throughput performance. Further measurement campaigns are required in order to quantify the performance increase of the femto and WiFi evolution and conclude on the outcome.

As a final comment, it is noted that femto cells natively offers cellular voice calls. This could prove a significant advantage if an end user is without macro coverage. In such cases femto cells are the best alternative.

2.6 Conclusion and Discussion

An indoor femto propagation measurement campaign was conducted to investigate typical indoor office environment. A comparison with the ITU-R indoor propagation model shows a good fit. The standard deviation of the error between measurements and the predictions by the ITU-R model is in the order of 6 dB. Such measurement results are valuable in order to calibrate and verify system level simulators as it enhances the confidence of the simulators.

Apart from the indoor propagation validation, also an outdoor micro cellular propagation campaign was performed. The objective was to model the outdoor micro cell propagation at different frequencies. A model for 1.9 GHz and 3.5 GHz was proposed in [3]. Results showed that outdoor micro cellular deployment at 3.5 GHz is less attractive, as additional propagation and building penetration losses of up to 10 dB is not unlikely compared to 1.9 GHz.

Co-channel macro and CSG femto interference measurements were performed with the objective to identify potential indoor femto deployment showstoppers. Results show that the indoor to outdoor femto interference is rather limited in DL and indoor femto deployment does not compromise outdoor macro coverage and performance. Indoor macro coverage holes are inevitable though. Thus, a femto free macro carrier is required for guaranteeing indoor macro coverage. In UL however, femto deployments close to the macro cell centre result in increased noise rise at the macro. Simple UE power capping or reduction of the femto coverage area eliminate this risk with reduced femto coverage area as a consequence.

Furthermore, measurement results and conclusions from the co-channel macro and femto trial were used for development and verification of a QoS aware femto power control algorithm. The design criteria of the algorithm, are to deliver promised QoS in the

residence of the end user while minimising the interference towards the macro layer. This is achieved by exploiting NLM features of the femto cell. The developed power control framework outperforms femto power control methods defined by 3GPP in terms of reducing the macro outage and femto power saving.

Finally, a femto measurement trial is performed which focuses on the end user experience using femto and WiFi indoor data solutions. Both technologies perform similar in terms of spectral efficiency. The real differentiator is latency and UE power consumption. In both disciplines, WiFi outperforms the femto technology. Measurements show that it is impossible to minimise femto latency without increasing the UE power consumption and vice versa. It is only possible to configure the femto such that it is competitive with WiFi in either latency or UE power consumption. The femto technology is HSPA Release 6 and HSPA Release 7/8 or LTE would improve the femto performance. The same is true for WiFi, the tested version is IEEE 802.11g, which has since been succeeded by .11n and .11ac. Therefore, new measurements are required to quantify the performance increase introduced in later versions.

Chapter 3

Network Evolution Analysis

The exponential mobile data traffic growth witnessed the recent years forces the network operators to upgrade their networks. However, it is less obvious how to upgrade the network in practice. Several upgrade options are possible, ranging from macro densification to deployment of small cells, see Section 1.2. Alternatively, it could also involve a technology upgrade, e.g. upgrade all existing High Speed Packet Access (HSPA) sites to Long Term Evolution (LTE) sites etc.

Ideally, the preferred option is the cheapest that performs according to the performance requirements. However, scalability and future-proofing are examples of properties which should not be neglected. It is not sufficient to upgrade the network today, and think it is all good in the future. Consequently, choosing the ideal short-sighted solution might turn out to be less than optimal in the long-term perspective. Thus, it must be ensured that the decision taken today, is part of the long-term strategy.

In this chapter, three network upgrade solutions are investigated. The objective is to determine the best solution in terms of network performance and Total Cost of Ownership (TCO) for future traffic volumes. The optimal solution in urban environment is most likely not the preferred solution in a rural environment. Therefore, the network analysis focuses on the urban scenario. This scenario is selected as it is the most challenging in terms of traffic density. The applied network layout is site-specific, however, the findings can be applied to urban areas with similar network and environment characteristics.

3.1 Prior Art

In [85] the performance of relay nodes in a suburban area is investigated. The relay node deployment is coverage driven. It is shown that the deployment of the outdoor relay nodes

eliminates the coverage problems in the network. Furthermore, the deployments of relay nodes also provides gain in average User Equipment (UE) throughput, in the range from 20% to 55%.

Other network evolution studies focus on the available spectrum utilisation. In [86] the authors conclude that the spectrum is utilised optimally if a dedicated small cell carrier is available. Furthermore, it is shown that a hybrid solution of outdoor pico deployment and indoor femto deployment achieves a good trade off in user performance and small cell density. An indoor network evolution study is presented in [87]. The authors compare the performance of indoor 3rd Generation (3G) HSPA femto cells versus indoor 802.11g WiFi access points. It is concluded that the WiFi deployment is superior, both in terms of network outage and user throughput performance.

Another important parameter, which were not discussed in the previously quoted network evolution studies, is the TCO. This topic has been treated in studies such as [29,31]. Common for the conclusions in those is that indoor small cell deployment is the preferred solution in terms of performance and TCO trade off. However, the conclusion is sensitive to the network topology. The network layouts used in [29,31] are not based on realistic network, hence, it is uncertain how accurate the TCO describes realistic networks.

In this chapter, a realistic network evolution study utilising an operator deployed network is presented. The focus is on small cell deployment. In addition to the network performance, the TCO of the available options is evaluated. Based on the network outage performance and the corresponding TCO, it is possible to conclude on the recommended deployment strategy for future mobile data traffic volumes.

3.2 Network Topology and Traffic Distribution

For the network evolution analysis, an urban area of an European metropolitan area is chosen. All macro cell locations, antenna heights, antenna tilts, and antenna bearings are gathered from an operator deployed Universal Mobile Telecommunications System (UMTS)/HSPA network within the area. The area under investigation is approximately 1.2 km² and consists of four 3-sector macro sites with a macro Inter-Site Distance (ISD) in the range of 300 meter to 400 meter. This is considered the reference network. In order to achieve realistic Signal to Interference and Noise Ratio (SINR) distributions within the investigated area, all surrounding macro sites are considered fully loaded, meaning that they cause interference towards the area of interest.

Apart from the realistic cellular network layout, a digital map of the area is acquired. From the map, building layouts and building heights are available. This enables ray tracing path loss prediction, in particular the dominant path loss model is applied [66]. Only the outdoor path loss is predicted using ray tracing. For indoor path loss, the empirical International Telecommunication Union Radiocommunication Sector (ITU-R) indoor path loss model is applied, this is the model which was verified in Section 2.2. If the base station is outdoor and the UE is indoor, or vice versa, an additional building penetration loss is

applied. The building penetration loss is assumed to equal 20 dB. The UE Downlink (DL) SINR is calculated as the serving Reference Signal Received Power (RSRP) over the total interference plus noise. The total interference includes the signal from macro sites outside the simulation area and the loaded base stations inside the simulation area. No fast fading effects are applied. Moreover, the effects of multi user scheduling, Hybrid Automatic Repeat Request (HARQ), link adaptation, and other Radio Resource Management (RRM) processes are captured by the applied SINR to throughput mapping curves. Users are associated with the cell with highest RSRP + cell Range Extension (RE).

It is necessary to dimension the network with respect to the busy hour traffic volume. Therefore, spatial traffic volume distributions from busy hour are used for the UE traffic generation. Within the area of interest, a single traffic hotspot exists, located at a transportation hub. The total traffic volume¹ in the area is approximately split 80% - 20% between indoor and outdoor. Figure 3.1 illustrates the spatial traffic density and the macro sector positions. Moreover, the traffic hotspot is clearly visible in the area (red coloured area). From the figure, it is also possible to distinguish the building layout and the road system. In multiple-floor buildings, the traffic is assumed to be uniformly distributed among the floors.

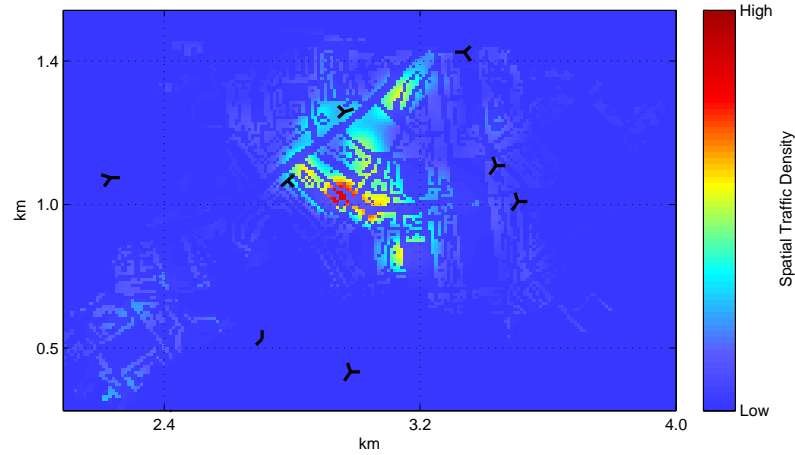


Fig. 3.1: Spatial traffic density. The black lines denote the direction of the macro sectors, and the colours denote the traffic volume. Red colour indicates high UE traffic density.

Within the area of interest, the indoor floors cover approximately 930000 m². E.g. if the ground floor of a three floor building is 200 m², this building contributes with 600 m² of the total indoor square metres. Assuming an average apartment size of 100 m²,

¹Traffic volume is the amount of data generated by all users in the area of interest.

the total number of apartments within the area of interest is 9300, or equivalent 8000 apartments per km². Later in the chapter, the value is used for evaluating the indoor small cell penetration rate.

3.2.1 Traffic Growth Scenarios

The current traffic volume is denoted *Reference*. However, three additional traffic volumes are defined; *Low*, *Medium*, and *High*. These three scenarios cover short-term and long-term traffic growth expectations, but no year is associated with the traffic growth scenarios. It is assumed that the traffic growth factor is the same within the area, i.e. the traffic growth factor in the hotspot equals the traffic growth factor outside the hotspot. Apart from the increasing traffic volumes, the end user expectations regarding data rates are also increasing. Table 3.1 lists data rate requirements for each of the traffic growth scenarios. Consequently, a network evolution step is only valid, if the network provides the Guaranteed Bit Rate (GBR) to at least 95% of the UEs. The percentage of the UEs which are not served with at least GBR is referred to as the network outage. In other words, the network outage must be below 5% for a network evolution step to be valid.

The network evolution study is DL driven. Thus, after deploying the necessary base stations to carry the DL traffic, the Uplink (UL) throughput performance is compared with the UL GBR to verify that the agreed Quality of Service (QoS) is fulfilled. The UL:DL traffic ratio is 1:4.

Table 3.1: Traffic growth scenarios and the corresponding GBRs.

Traffic Growth Scenario	Reference	Low	Medium	High
Traffic Volume	x1 ²	x4	x50	x100
DL GBR	2 Mbps	4 Mbps	4 Mbps	10 Mbps
UL GBR	0.5 Mbps	1 Mbps	1 Mbps	2.5 Mbps

3.3 Network Evolution Options

The utilised network layout is based on data from an operator deployed UMTS/HSPA network. It is assumed that all existing macro sites are upgraded to LTE. Therefore, the reference network is a Frequency Division Duplex (FDD) LTE Release 8/9 network with a carrier frequency of 800 MHz and 10 MHz of FDD DL transmission bandwidth. This is the starting point in the evolution study. Beside the 10 MHz at 800 MHz, two additional chunks of FDD DL spectrum are available; 20 MHz at 2.6 GHz and 20 MHz at 3.5 GHz. The 3.5 GHz band is restricted to outdoor pico or indoor femto use.

²Corresponds to the traffic volume in 2011.

The available base station technologies are limited to: macro base stations, outdoor pico base stations, and indoor femto access points. Table 3.2 lists the properties of each of these technologies.

Table 3.2: Summary of the base station characteristics.

	Macro	Pico	Femto
Location	Outdoor	Outdoor	Indoor
Tx power per 20 MHz	46 dBm	30 dBm	20 dBm
Tx bandwidth (DL)	Up to 2×20 MHz	1×20 MHz	1×20 MHz
Frequency bands	800 MHz and/or 2.6 GHz	2.6 GHz or 3.5 GHz	2.6 GHz or 3.5 GHz
Antenna configuration	2×2	2×2	2×2
Antenna Pattern	According to [71]	Omni-directional v-beam = 90°	Isotropic
Antenna tilt	Coverage optimised	No tilt	No tilt
Transmission scheme	SU-MIMO	SU-MIMO	SU-MIMO
Deployment Strategy	Operator deployed	Outage driven	Outage driven or random with ISD = 25 meter
Access type	Open access	Open access	Open access
Range Extension	0 dB	3 dB	3 dB
Almost Blank Subframes	2/8	-	-

3.3.1 Macro Upgrade

Densification of the existing macro network is not considered an valid evolution option in this area. Thus, allocating additional spectrum is the only available option to improve the macro network performance. Consequently, in addition to the existing 800 MHz carrier an macro carrier at 2600 MHz is deployed at all macro sites. It is noted that Carrier Aggregation (CA) is not assumed, meaning a UE can only be scheduled on either of the macro carriers. Macro carrier load balancing is applied according to [88, Section 3.4.3]. In the remainder of this chapter the macro evolution option is denoted:

D1: Macro Dual Carrier (DC)

3.3.2 Outdoor Small Cell Deployment

In the reference scenario, no outdoor pico cells are present, therefore the location of the outdoor pico cells must be determined. The outdoor pico deployment is outage driven, such that a pico cell is deployed at the location where the network outage is reduced the

most. A more detailed description of the outdoor pico deployment process is available in [85, 89]. The only constraint is that the pico cells should not be deployed in the middle of a road, as this is not a practical feasible. If the outcome of the deployment algorithm is on a road or similar, the pico cell is manually moved to a nearby building or lamppost. The pico antenna height is 5 meter.

Next step is to compute the propagation path loss. Since the pico cells are located outdoor, ray tracing techniques are used to predict the outdoor path loss, similar to the macro cell path loss.

In terms of frequency bands, two options are considered. The pico cells can be deployed co-channel with the macro cells on the 2.6 GHz carrier, or on a dedicated pico carrier (the 3.5 GHz carrier). The first option is referred to as In-Band (IB), and the second option is referred to as Out-Band (OB). Since the pico cells is an addition to the macro network, the two pico evolution options are denoted:

D2: Macro Dual Carrier + In-Band Picos

D3: Macro Dual Carrier + Out-Band Picos

3.3.3 Indoor Small Cell Deployment

Generally, small cells can be deployed in all indoor areas, on all floors. However, in this study two deployment methods are considered; coordinated and uncoordinated. In a coordinated deployment scenario, the indoor small cell deployment is outage driven, similar to the outdoor pico cells. More information on the deployment algorithm in [85, 89, 90]. For uncoordinated indoor small cell deployment, indoor small cells are deployed randomly according to a uniform spatial distribution in the buildings. The only constraint is a minimum small cell ISD of 25 meter, which is applied in the horizontal plane. In multi floor buildings, two small cell are allowed to be deployed closer than the minimum small cell ISD if they are located on different floors. For coordinated deployment, determining the ISD is part of the planning process. Due to the vast amount of indoor small cells, path loss prediction using ray tracing techniques are not feasible; path loss prediction according to [71] is applied.

Similar to the outdoor pico deployment, two carrier configurations are considered; IB and OB. Consequently, four small cell deployment scenarios are available:

D4: Macro Dual Carrier + In-Band Picos + Coordinated In-Band Small Cells

D5: Macro Dual Carrier + In-Band Picos + Uncoordinated In-Band Small Cells

D6: Macro Dual Carrier + In-Band Picos + Coordinated Out-Band Small Cells

D7: Macro Dual Carrier + In-Band Picos + Uncoordinated Out-Band Small Cells

In total, the performance of seven deployment options are compared in Section 3.6.

3.4 TCO Assumptions

The TCO analysis includes Operational Expenditure (OPEX), Capital Expenditure (CAPEX), and Implementation Expenditure (IMPEX) and assumes a three year OPEX period. CAPEX is basically the cost of the used equipment and is a one-time expense. On the other hand, OPEX is an ongoing expense, which relates to the maintenance, electricity, and site rental. Finally, IMPEX is the expense of planning the deployment and the actual deployment of the base stations. This also include the backhaul deployment expenses. Table 3.3 contains the TCO assumptions for each of the base station technologies. It is noted that TCO of the macro network at 800 MHz is not included as this network is assumed to be already deployed. Moreover, note the difference between coordinated and uncoordinated femto access points. Coordinated femto cells are typically installed in public areas or enterprise environments. Thus, a higher quality femto access point supporting more simultaneous users are considered at these locations, hence the higher price mark. Further uncoordinated femto deployment cost reductions are achieved by having the end user do the installation of the femto cells. Finally, note that no backhaul costs are associated with the femto access points, as it is envisioned that existing fixed line Internet connections are used to carry the femto backhaul traffic. The figures used in the TCO analysis are acquired from Nokia colleagues and based on Nokia costumer projects. Additional information on TCO assumptions can be found in two Nokia Siemens Network white papers [91, 92].

The TCO values in Table 3.3 are valid for a single base station unit only. Thus, the TCO for the required network upgrade is computed as:

$$TCO = \sum_b N_b \cdot T_b \quad (3.1)$$

where b is the base station technology, N_b is the number of deployed base stations of type b , and T_b is the 3 year unit TCO for a base station of type b (the last row in Table 3.3).

3.5 Result Generation

The objective of the network evolution study is to compute the required number of macro upgrades and number of small cell to serve at least 95% of the network users with their associated GBR. This is determined for all seven (D1 to D7) evolution paths. Furthermore, the TCO for the seven evolution paths are estimated to complete the network evolution investigation. Based on the network outage performance and the TCO, the recommended evolution option is determined.

Figure 3.2 illustrates the network evolution process. The network evolution is DL driven, this means the network is upgraded to accommodate the DL traffic, and the UL performance is verified afterwards. Thus, this section focus on the DL part of the

Table 3.3: Unit TCO assumptions for each of the base station technologies. Values in €.

	Macro Upgrade	Outdoor pico	Femto Coordinated	Femto Uncoordinated
CAPEX	10100	2330	550	70
Equipment	10100	1800	500	50
Backhaul	0	530	0	0
Femto gateway	0	0	50	20
IMPEX	8500	1850	100	0
Site acquisition	0	350	0	0
Backhaul deployment	0	300	0	0
Installation	8500	300	100	0
Planning	0	400	0	0
Site preparation	0	500	0	0
OPEX (1 year)	1390	1900	50	20
Site Rental	0	600	0	0
Operation	270	840	50	20
Electricity	1120	190	0	0
Backhaul maintenance	0	270	0	0
TCO (3 year OPEX)	22770	9880	800	130

simulation tool. The network simulator is static, meaning there is no moving UEs and mobility issues are not considered. Each simulation run represents a snapshot of UE throughput performance for the given UE distribution in network. The UEs are associated with the cell which maximises the RSRP plus potential RE. Full buffer with GBR traffic is assumed and the scheduler is a minimum bit rate, where UEs are allocated the amount of resources in order to reach the GBR. If all UEs reach the GBR and not all resources are allocated, the remaining resources are distributed equally among the connected UEs. Thus, only empty cells are not transmitting with maximum transmission power, else all cells use maximum transmission power. The number of UEs in the simulation is found from the total data traffic volume during busy hour divided with the data consumption for a single UE.

For the network evolution studies, there are two mandatory inputs to the system simulator;

- Realistic Network Layout which also includes the building layout
- Traffic volume and distribution (named *Traffic Information* in Figure 3.2)

The output of the network evolution simulator is UE throughput performance distributions. If at least 95% of the UEs reach or exceeds the GBR, no further upgrades to the reference

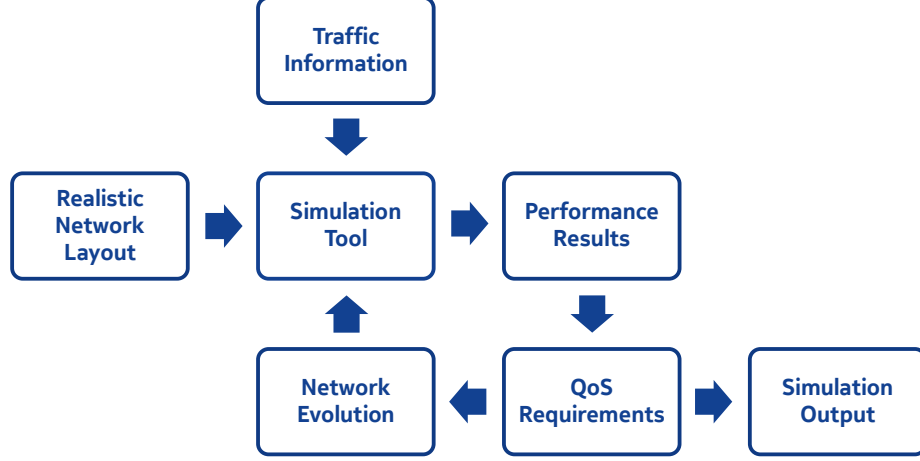


Fig. 3.2: Overview of the network evolution simulation process.

network³ is necessary. However, if less than 95% of the UEs are served with the GBR, further network upgrades are needed. In this work, the seven upgrade options (D1 to D7) listed in Section 3.3 are considered.

The selected network upgrade option is applied and the simulations are rerun. If deployment of additional cells is chosen, the simulation process continues until the maximum number of cells are deployed, or until no further cells can be deployed without violating the minimum ISD constraints. Finally, when the required upgrades are found, it is possible to compute the TCO for the given solution.

3.6 Performance Evaluation

The performance results are divided into three parts, one part for each of the traffic growth scenarios, starting with the low traffic growth scenario.

3.6.1 Traffic Growth Scenario: Low

Figure 3.3 shows the network outage performance in Figure 3.3a and the number of required outdoor pico cells and indoor femto cells in Figure 3.3b. First, focusing on the network outage performance in Figure 3.3a, it is obvious that it is not possible to accommodate the increased traffic load by simply upgrading the macro network to dual carrier as the outage percentage is higher than 40. By deploying additional 30 IB pico

³In these simulations the realistic macro network at the 800 MHz carrier is considered the reference network.

cells, the network drops significantly, however, it is still not possible to fulfil overall outage requirement. Approximately 80% the outage UEs are located indoor and all of the outage UEs are served by macro cells. The minimum pico cell ISD allows deployment of additional 10 pico cells, however, this is still not sufficient to reach the coverage requirement.

On the contrary, if the additional 30 pico cells are deployed OB, the network outage is reduced to 5% and fulfils the requirement. The improved network performance is two-fold: the overall DL transmission bandwidth is increased from 30 MHz to 50 MHz, and compared to the IB pico scenario, no inter-layer interference is present.

Next up is the indoor small cell deployment. All of the four indoor femto deployment strategies are capable of fulfilling the requirements. However, the number of required femto cells per km^2 varies from 90 for coordinated and OB deployment up to almost 600 for uncoordinated and IB deployment. The main reason for the reduced network outage, is the increased macro offloading effect. With indoor femto cells, the macro cells only serve approximately 30% of the UEs.

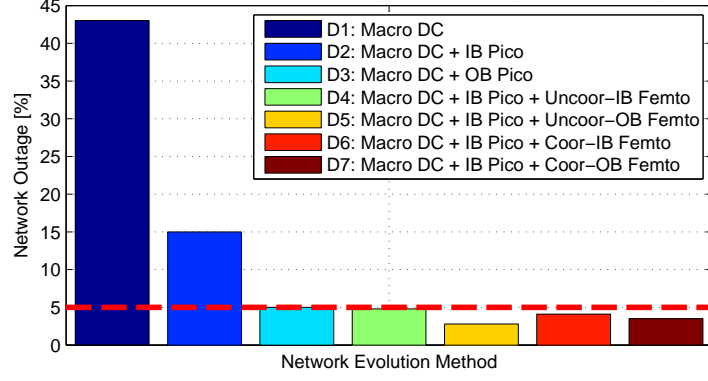
From the network outage requirement, five deployment strategies are valid. Figure 3.3c shows the normalised TCO for the valid deployment options. It is seen that the cheapest solution is deployment of OB pico cells only. This solution reduces the TCO 20% compared to the most expensive, the coordinated deployment of IB femto cells. However, with the very similar TCO reductions, UE throughput performance could also be taken into consideration. Uncoordinated and OB femto cell deployment offers the highest average UE throughput (11.5 Mbps) which is more than double of OB deployment of pico cells only. It is worth noting, that the cost of the additional 3.5 GHz spectrum is not included in the TCO calculations.

3.6.2 Traffic Growth Scenario: Medium

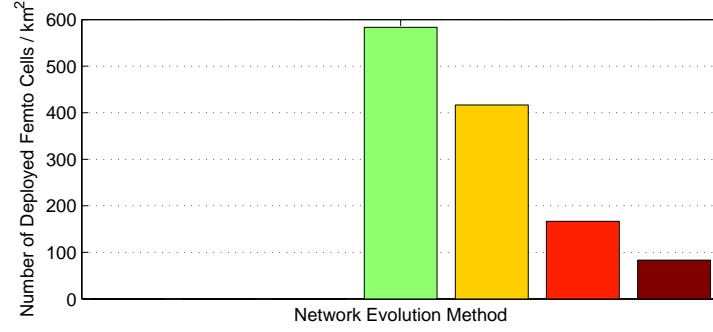
Having narrowed the number of potential network evolution strategies from 7 to 5 for low traffic growth, next step is to study the performance for medium traffic growth scenario. Figure 3.4 shows the combination of network outage in Figure 3.4a and number of new deployed cells per km^2 in Figure 3.4b. Figure 3.4a clearly shows that outdoor-only deployment is simply not suitable for such traffic volumes. The deployment of OB pico cells-only experiences a network outage of more than 30%. Despite the deployment of additional 10 outdoor pico cells, indoor femto cells are required to meet the network outage demands.

All four indoor small cell deployment strategies are able to fulfil the network outage requirements as shown in Figure 3.4a. However, the number of required femto cells varies greatly, from 330 to more than 2000 per km^2 . Generally speaking, IB deployment requires more femto cells than OB due to the mutual macro and pico interference. Next, coordinated deployment requires less femto cells compared to uncoordinated deployment, since the coordinated small cells are deployed in areas with outage UEs in the vicinity.

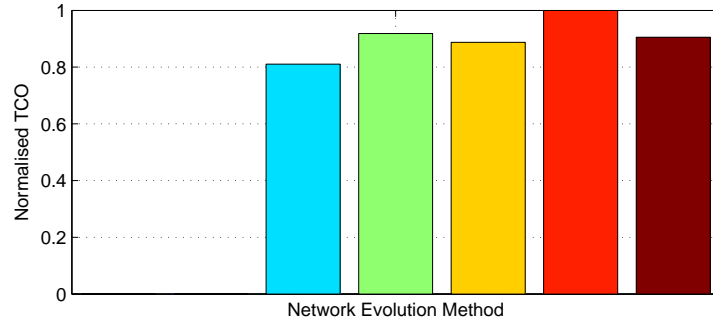
Figure 3.4c shows that the TCO of coordinated IB deployment is approximately twice



(a) Network outage for traffic growth scenario low.

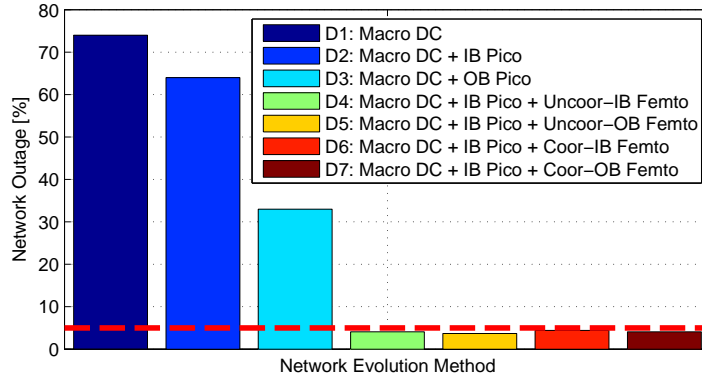


(b) Required femto cells in order to reach the network outage in Figure 3.3a with 25 outdoor pico cells per km².

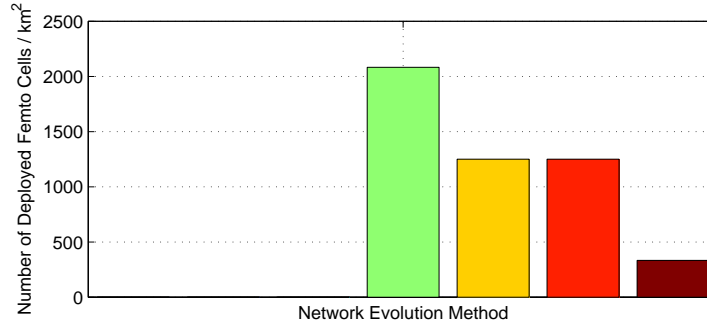
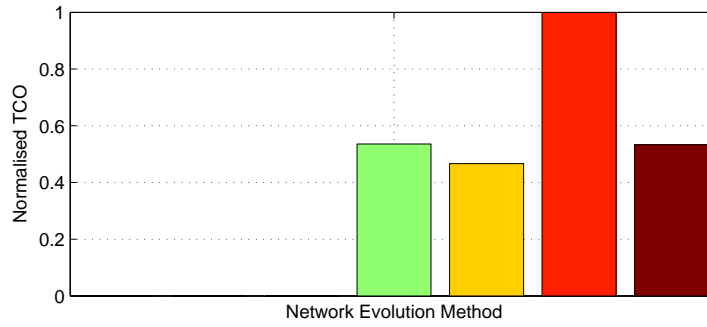


(c) TCO for the valid deployment options in the low traffic growth scenario.

Fig. 3.3: Low traffic growth performance.



(a) Network outage for traffic growth scenario medium.

(b) Required femto cells in order to reach the network outage in Figure 3.4a with 33 outdoor pico cells per km².

(c) TCO for the valid deployment options in the medium traffic growth scenario.

Fig. 3.4: Medium traffic growth performance.

the value of the three remaining strategies. This is a combination of the relative large number of required femto cells and the high TCO per coordinated femto unit. The difference between the remaining three methods is minor and difficult to determine based on network outage and TCO alone.

Regardless of the indoor deployment strategy, the percentage of UEs served by the macro cells is in the range 12% to 18%. On the contrary, more than 70% of the UEs are served by an indoor femto cell, while the remaining UEs are served by outdoor pico cells. This clearly stresses the importance of indoor small cells in future mobile networks.

3.6.3 Traffic Growth Scenario: High

Finally, the high traffic growth scenario, where the traffic volume is increased 100 times compared to the reference traffic volume, is investigated. Figure 3.5a shows the network outage for the seven deployment strategies. At this traffic volume, the most significant change, compared to the medium traffic growth scenario, is that IB and uncoordinated femto deployment is no longer able to meet the traffic demands. It is simply not possible to deploy any further femtos, without violating the minimum femto ISD. The maximum number of indoor femtos in the study area corresponds to approximately 2500 femto per km².

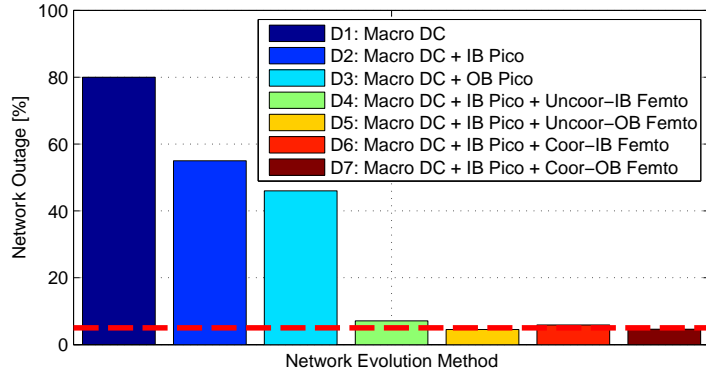
Furthermore, Figure 3.5b also reveals that the number of required coordinated IB femto cells is only 17% lower than the number of required uncoordinated IB femto cells. This indicates that the advantage of coordination is rather limited for the IB scenario. Whether it is coordinated to uncoordinated deployment, a significant number of femto cells is required to offload the large traffic volumes from the macro cell. The exact location is less important.

What is more important is the benefit of deploying OB femto cells. This is visible by the lower number of required femto cells, especially coordinated deployment strategy greatly reduces the number of demanded femto cells. The OB femto cells are capable of offloading more traffic than IB, due to the dedicated femto carrier.

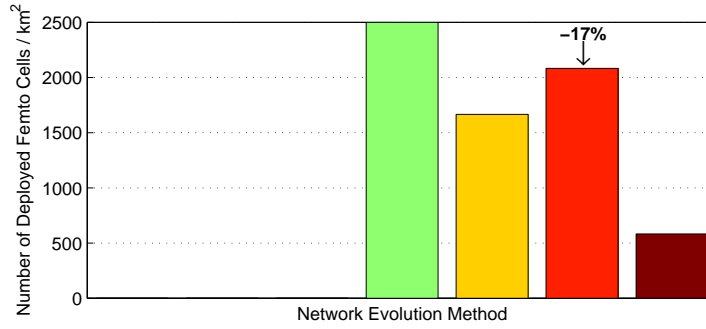
Finally, Figure 3.5c presents the TCO for the high traffic growth scenario. From the figure it is clear that the possibility of OB femto cell deployment is paramount in order to reduce the TCO in the long-term perspective. The OB deployment of femto cells, reduce the TCO with more than 50% compared to IB femto deployment. Both OB solutions are very similar in terms of TCO. The increased unit TCO for a coordinated femto cell is compensated by the low number of required femto cells, as seen in Figure 3.5b.

3.6.4 Recommended Network Evolution

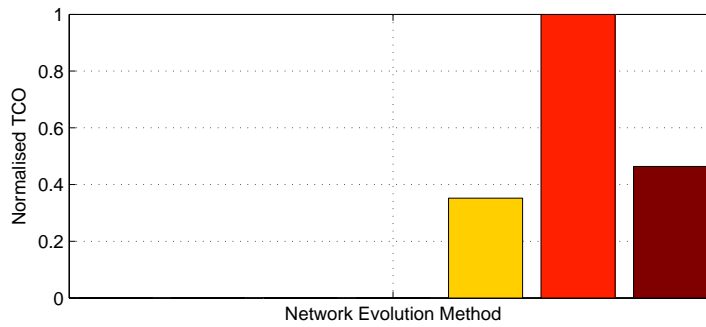
OB pico cell deployment was the preferred deployment strategy in the low traffic growth scenario (Figure 3.3b) but this solution is not scalable, and can not support the traffic volumes in the medium and high traffic growth scenarios. This fact supports the importance of long-term network evolution planning rather than short-sighted planning.



(a) Network outage for traffic growth scenario high.



(b) Required femto cells in order to reach the network outage in Figure 3.5a with 33 outdoor pico cells per km².



(c) TCO for the valid deployment options in the high traffic growth scenario.

Fig. 3.5: High traffic growth performance.

Thus, deployment of IB pico cells accompanied by uncoordinated deployment of OB femto cells provides the best TCO performance, and is the recommended long-term deployment strategy.

Table 3.4: Performance summary of the uncoordinated and OB femto deployment network evolution path.

Traffic Growth Scenario		Low	Medium	High
Traffic volume growth	[-]	x4	x50	x100
Network coverage	[%]	97.2	96.3	95.5
Normalised TCO ⁴	[-]	0.79	0.93	1
Number of pico cells	$[\frac{1}{\text{km}^2}]$	25	33	33
Number of femto cells	$[\frac{1}{\text{km}^2}]$	417	1225	1670
Femto cell penetration	[%]	5	15	21
Femto UE ratio	[%]	44.7	70.4	81.4
Average UE throughput	[Mbps]	11.5	16.7	21.9

Table 3.4 summarises the performance of the OB and uncoordinated femto network evolution strategy. It shows that already at the low traffic growth, the required network upgrades of the macro network, the deployment of the outdoor pico cells, and the 417 femto cells accounts for almost 80% of the TCO in the high traffic growth scenario. This indicates that the additional deployment of the femto cells at medium and high traffic growth significantly reduces the cost per delivered byte. One could erroneously draw the conclusion to omit the macro upgrade and pico deployment to reduce the TCO. However, the macro and pico deployment is important for the end users mobility experience. Furthermore, network operators can not guarantee the uptime of the femto cells deployed in the residence of the end user, and therefore operator controlled base stations are needed to ensure a 24/7 operational network.

In the high load traffic scenario, the required number of femto cells corresponds to a femto cell penetration rate of 21%, meaning on average every 5th apartment should install an indoor femto cell. At this traffic load, the femto cells serves more than 80% of the UE. The remaining 20% is almost equally split between the macro and the pico cells. For low and medium traffic growth, the femto UE ratio is 45% and 70%, respectively. These figures show the importance of macro offloading in future traffic growth scenarios. Apart from the macro offloading effect, the femto cells also guarantee a steady increase in average UE throughput performance, which is significant higher than the GBR in DL.

Regarding the UL performance, simple simulation verifications show that the recommended network evolution path supports UL traffic volumes which are a forth of the DL traffic volume. If this is the case, UL network outage is kept below 2%. More balanced DL:UL traffic ratios were not simulated.

⁴Normalised with respect to the high traffic growth scenario.

In this study one restriction was the combination of several femto deployment strategies. Naturally, a network operator should not rely solely on a single indoor femto deployment strategy. It should be a combination of multiple deployment strategies. E.g. uncoordinated femto deployment makes much sense in residential areas, whereas coordinated femto deployment is a logical method in public buildings, where an operator is granted access to the infrastructure. However, the results from this study are still useful and important in order to understand the strong and the weak points of each of the network evolution strategies in a dense urban environment, which is the most challenging in terms of traffic volumes per km².

3.7 Conclusion and Discussion

In this chapter, a realistic network evolution study has been presented. The area of interest is a dense urban city area of an European metropolis. In order to incorporate both short-term and long-term evolution issues, three traffic growth scenarios are defined; low, medium, and high corresponding to x4, x50, and x100 compared to the reference scenario. Multiple network evolution strategies are defined, covering upgrading the macro network to dual carrier, outdoor pico deployment, and indoor small cell deployment. The three upgrade paths are not mutually exclusive. However, the focus is on the deployment of indoor femto cells. The femto cells can either be deployed uncoordinated or coordinated and in-band or out-band, resulting in four different femto deployment strategies. The Key Performance Indicator (KPI) is the network outage, which must be lower than 5%. Moreover, the TCO of the solution is also taken into consideration.

Simulation results show that either pico cells or femto cells are required in addition to the macro upgrade to handle the traffic in the low traffic growth scenario. The deployment of out-band pico cells achieves the lowest TCO. Unfortunately, the scalability of this solution is not sufficient, and at both medium and high traffic growth scenario, the network outage exceeds the allowed value.

For the medium and high traffic growth scenario, the deployment of uncoordinated out-band femto cells in combination with macro dual carrier upgrades and in-band pico cells is the most promising network evolution path. It is a cost-efficient solution, which offers high flexibility and scalability. Thus, it is the recommended network evolution path for all three traffic growth scenarios. It might not be the cheapest solution in the short-term perspective, however, in the long run it is the cheapest and allows for an easy upgradable network.

Due to the promising potential of the uncoordinated deployment of femto cells on a dedicated carrier, this deployment strategy is adopted in the remainder of the thesis. Especially the dense femto deployment is of interest. The implication of high femto density at high traffic load is increased femto to femto interference. Therefore, interference management for dense indoor femto cells are treated in Chapter 4 through Chapter 6.

Chapter 4

Dynamic Inter-Cell Interference Coordination

In this chapter, the development of a dynamic interference coordination framework is presented. The framework is designed for the dense indoor femto cell (or small cell in general) scenario deployed on a dedicated carrier. In areas with high indoor small cell density, inter-cell interference could potentially limit the overall network performance. Therefore, Inter-Cell Interference Coordination (ICIC) is vital for improving the network performance in future mobile networks with dense small cell deployment.

This chapter is organised as follows: Section 4.1 summarises the related prior art and is followed by a description of the simulation scenario and assumptions in Section 4.5. In Section 4.2 the optimisation criterion is introduced and in Section 4.3 the developed ICIC framework is introduced. A discussion on the impact on the network architecture is found in Section 4.4 followed by a performance evaluation of the framework in Section 4.6. Finally, Section 4.7 concludes the chapter.

4.1 Prior Art

Naturally, the increased interest in small cell deployment and the introduction of Carrier Aggregation (CA) in LTE-A Release 10 has led to more intelligent ICIC schemes. CA allows for reception on multiple Component Carriers (CCs) and thereby enables the possibility of coordinating small cell interference on CC domain level, referred to as Carrier Based Inter-Cell Interference Coordination (CB-ICIC). Hence, the transmission of two strongly interference coupled small cells can be configured on orthogonal sets of

CCs. Compared to 3rd Generation Partnership Project (3GPP) LTE Release 8 ICIC solutions, a significant advantage of CB-ICIC is the additional protection of the Physical Downlink Control Channel (PDCCH) ensuring reliable downlink reception. In [93] a small cell CC selection algorithm is proposed. In a Heterogeneous Network (HetNet) consisting of macro and pico cells, the authors conclude that CB-ICIC ensures high pico cell throughput performance by muting CCs at the macro enhanced Node Bs (eNBs). In [94] the authors compare fixed, random, and autonomous CC selection and the performance of the autonomous CC selection scheme outperforms the other approaches, in both HetNet and dedicated small cell scenarios.

In the 3GPP context, CB-ICIC techniques have also been investigated. Reference [95] reports the User Equipment (UE) throughput performance improvement in the 3GPP Release 12 Scenario 2A described in [62]. Orthogonal primary small cell CC assignment are performed to reduce inter-cell interference. Next, in order to provide high throughput rates for UEs with high channel quality, a secondary small cell CC is assigned if the Reference Signal Received Quality (RSRQ) is higher than a configurable threshold. For low traffic load, CB-ICIC provides significant gain in coverage throughput and moderate gain in peak throughput. On the contrary, at high traffic load the peak throughput is increased significantly using CB-ICIC, and losses are reported for coverage throughput.

Recently, channel assignments has been studied extensively for dense IEEE 802.11 Wireless Local Area Networks (WLANs). The authors of [96] proposes a decentralised algorithm for IEEE 802.11 user deployed networks. The algorithm minimises the network-wide cost, where cost is the sum of all interference caused by the Access Point (AP). Each AP randomly samples a new candidate centre frequency and bandwidth, and compare cost of the candidate cost with the current cost. If the candidate cost is lower, the candidate solution is adopted. If not, the candidate solution is chosen with non-zero probability, which depends on how much worse the candidate solution is. This approach is implemented to prevent the algorithm converges to a local minima. Simulation results and testbed experiments show that the proposed algorithm improves network-wide capacity and the fairness [97] in static and dynamic scenarios. Moreover, reference [36] gives an excellent overview of available WLAN channel assignments schemes.

In [98] graph colouring is applied in order to solve WLAN channel assignment challenges in dense networks such that strongly interference coupled AP are assigned orthogonal channels. Building upon the idea of graph colouring for channel assignment, a CB-ICIC framework is presented in [99]. The framework is denoted Generalized Autonomous Component Carrier Selection (G-ACCS) and is applicable for the 3GPP Release 12 scenario 3. The 3GPP Release 12 Scenario 3 is described in [62, 71]. Initially, all small cells are assigned a base CC, it is coordinated such that the most interference coupled small cells are assigned orthogonal base CCs relying on Network Listening Mode (NLM) [100]. Moreover, each small cell is also able to enable supplementary CCs for transmission. The addition of a supplementary CC is not performed blindly, though. UE measurements assist the small cells in constructing all incoming and outgoing interference relations

between the small cells in the networks. So, before a small cell enables a supplementary CC, it is ensured that Carrier to Interference Ratio (CIR) thresholds are not violated in neighbouring small cells. This is achieved not only by intelligent CC allocation but also by autonomously configuring the Power Spectral Density (PSD) of the potential new supplementary CC. Simulation results show that the main achievement of the G-ACCS is that the coverage throughput is increased significantly without sacrificing the average average UE throughput when compared to static Frequency Reuse (FR) schemes and a NLM based FR-2 scheme.

A more generic ICIC approach is applied in [101]. Here the authors investigate for which scenarios ICIC is beneficial. An opportunistic interference mitigation scheme is adopted from [102] and is compared with an ideal ICIC interference mitigation scheme. Results show that the potential ICIC gain is largest for dense small cell scenarios and low path loss separation. In the investigated scenario, the potential ICIC gain was only moderate when the indoor wall penetration loss was larger than 10 dB. These results support the fact that small cell ICIC solutions must be highly adaptive to the given scenarios.

The proposed ICIC solution presented in this chapter is characterised by being a dynamic Quality of Service (QoS) aware CB-ICIC framework. If a outage user is detected, hypotheses for improving the user throughput are defined. Each hypothesis is evaluated, and the hypothesis resulting in the largest gain is carried out, only if it is positive, though. A hypothesis corresponds to muting a CC at an interfering small cell or activating additional CC(s) at the serving cell.

4.2 Optimisation Criterion

Before introducing the proposed CB-ICIC framework, an optimisation criterion is defined. For network operators, it is important to ensure a certain QoS among users in the network, typically a Guaranteed Bit Rate (GBR). In this work, the GBR is 3 Mbps ($R_{min} = 3$ Mbps). The selection of GBR is based on the simulation results presented in Appendix D. Furthermore, it is paramount to serve as many UEs without the network being overloaded. Thus, the overall optimisation criterion is to maximise the network capacity¹. The network capacity depends on the traffic generating model. Two traffic models are used in this thesis; Open Loop Traffic Model (OLTM) and Closed Loop Traffic Model (CLTM).

4.2.1 Open Loop Traffic Model

Using OLTM, each user is generated according to a Poisson arrival process with average arrival rate L , and each user has a fixed payload of size S . As long as the carried load of

¹Network capacity is defined as the network load where 95% of the UEs are served with at least the GBR.

the network (C_{OLTM}) equals the offered load ($L \cdot S$), the network is non-congested. If the offered load becomes larger than the carried load ($L \cdot S > C_{OLTM}$), the network is considered congested. In simulations where the network is congested the total number of users in the system is steadily increasing, thus, the network never reaches a steady operating point and the simulations results are invalid. Consequently, using the OLTM the optimisation criterion of the small cell interference coordination framework is:

$$\text{Maximise}(L \cdot S) \text{ subject to } R_{min} \leq \bar{R}_n \text{ for all } n \quad (4.1)$$

where n is the user index and \bar{R}_n is the past average throughput for user n . In order not to allocate a vast amount resources to users in cell edge areas or with low SINR the requirement is relaxed to 95% of the user must fulfil $\bar{R}_n \geq R_{min}$.

4.2.2 Closed Loop Traffic Model

Utilising CLTM the number of UEs in the entire network is fixed. At the start of a simulation, a number of UEs are dropped uniformly distributed within the simulation area, the payload size is S . When a UE finishes its session, i.e. when the buffer is empty and all potential Hybrid Automatic Repeat Request (HARQ) processes are completed, the UE is removed from the network and a new UE is dropped with uniform probability in the network. Thus, the load of the network is controlled with the number of UEs per small cell (N_{CLTM}). It is worth noting, that the number of UEs in the network remains constant throughout the simulation. Therefore, using CLTM the network is considered overloaded, if UEs start to pile up in one or few of the small cells. The capacity of the network is defined as the maximum number of UEs per small cell while still fulfilling the GBR constraint. The optimisation criterion for CLTM is expressed as:

$$\text{Maximise}(N_{CLTM}) \text{ subject to } R_{min} \leq \bar{R}_n \text{ for all } n. \quad (4.2)$$

Again, the constraint is relaxed, such that the QoS requirement is lowered to apply to 95% of the UEs only. Another important statistic for CLTM is total number of served UEs, due the inherited feedback in the traffic model. E.g. if the average UE throughput is reduced substantially, the number of served UEs is reduced accordingly, which can result in unfair performance comparison.

4.3 Small Cell Interference Coordination Framework

The developed framework can either be a proactive or a reactive framework. As the names indicate, a proactive framework dynamically adjust the CC selection pro-actively. Basically, a proactive framework is trying to "solve the problems before" they occur. E.g. a proactive framework dynamically adjusts the active CC for the different small cells such that the network is always performing optimal given the optimisation criterion. On the

contrary, a reactive framework only performs changes when a "problem is detected", and the applied changes should solve the detected problem, if possible.

4.3.1 General Description of the Framework

Given the QoS and optimisation criteria, a reactive framework is opted for. The event or problem which triggers the small cell interference coordination framework is when an user is detected to be in outage. Outage is defined as when the past average throughput of a user is lower than the GBR:

$$\bar{R}_n < R_{min} \quad (4.3)$$

where \bar{R}_n is the past averaged throughput for user n and the averaging time period is denoted t_{avg} . Outage UE detection is performed periodic, and the time constant t_{Outage} is 100 ms.

The initial small cell CC assignment corresponds to global FR, where all small cells transmit on all CCs. This assignment is kept as long as no outage UEs are detected. When a user is detected to be in outage, the experience interference must be reduced. This is achieved by muting² CC(s) of the strongest interfering small cell.

After the framework has muted small cells, it is potentially also possible to improve the throughput performance of outage UEs by enabling CC. Thus, in general the throughput of an outage UE can be improved in two ways, as depicted in Figure 4.1. In order to decide between the available changes, denoted hypotheses, the net benefit of each hypothesis is calculated. The net benefit is a measure of the network-wide benefit of the hypothesis and not the benefit for a single outage UE. The hypothesis resulting in the highest net benefit is applied. Though, the hypothesis is only carried out if the net benefit is positive which is not a given.

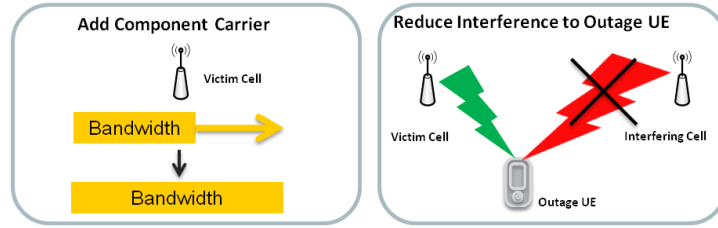


Fig. 4.1: Available options in order to improve throughput of outage users.

In theory, all UEs on non-orthogonal CCs are affected by a hypothesis. Consequently, when calculating the net benefit of a hypothesis, all affected users must be included in the

²The term *mute* refers to a small cell disabling a CC such that no transmission is ongoing on the given CC.

net benefit calculation. E.g. when a small cell is adding a CC, the users served by that small cell are experiencing an increase in throughput performance. In contrast, all users receiving data on the same CC experience a decrease in Signal to Interference and Noise Ratio (SINR) and throughput. Figure 4.2 depicts which users gain and which users lose from the hypothesis of adding a CC. In this example, small cell 1 has the opportunity to add CC 4 in order to increase the throughput for user 1, who is in outage and triggered the CB-ICIC. Consequently, the SINR of user 2 and 3 decrease. Therefore, before small cell 1 is allowed to transmit on CC 4, the benefit and the cost of the decision must be calculated. Hence, the net benefit³ ($\nu_{A,1,4}$) of the decision is calculated as:

$$\nu_{A,1,4} = f_{Benefit}(\bar{R}_1, \hat{R}_1) - f_{Cost}(\bar{R}_2, \hat{R}_2) - f_{Cost}(\bar{R}_3, \hat{R}_3) \quad (4.4)$$

where $f_{Benefit}(\bar{R}_n, \hat{R}_n)$ is the benefit function for user n , $f_{Cost}(\bar{R}_n, \hat{R}_n)$ is the cost function for user n , \bar{R}_n is the past average throughput, and \hat{R}_n is the estimated throughput after the potential change in CC assignment. If $\nu_{A,1,4}$ is positive, then adding CC 4 for small cell 1 is a valid option.

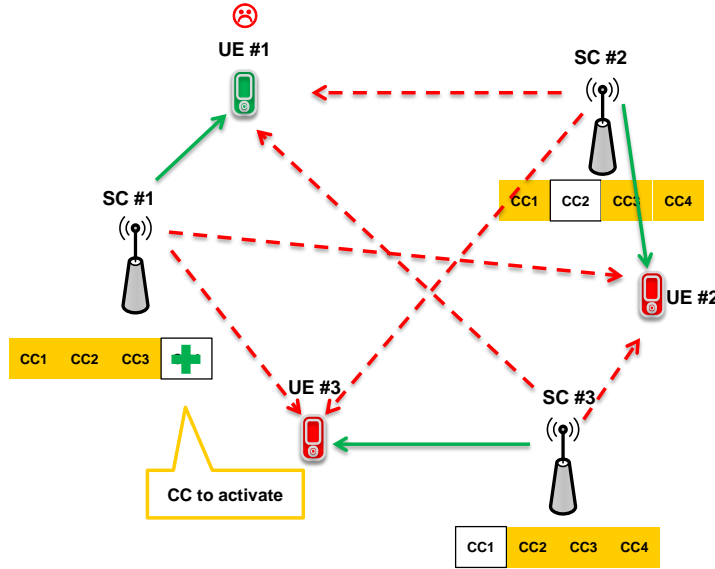


Fig. 4.2: Users affected by adding CC 4 for small cell 1. Green users gain from the decision and red users lose from the decision. A solid green line indicates a desired signal and a dashed red line indicates a interfering signal.

Similarly, the net benefit of muting a CC is computed before the muting of CCs is carried out. When muting CCs, all user served by the muting small cell experience a

³The net benefit of Adding CC 4 at small cell 1 = $\nu_{A,1,4}$.

degradation in throughput. And users scheduled by other small cells on the particular CC are experiencing increased SINR and throughput. In Figure 4.3, it is illustrated which users gain and lose if small cell 3 mutes CC 3. Again, it must be assured that the net benefit of the hypothesis $\nu_{M,3,3}$ is positive. Hence, in this example the benefit and cost of the hypothesis is calculated as:

$$\nu_{M,3,3} = f_{Benefit}(\bar{R}_1, \hat{R}_1) + f_{Benefit}(\bar{R}_2, \hat{R}_2) - f_{Cost}(\bar{R}_3, \hat{R}_3). \quad (4.5)$$

The benefit and cost functions are similar to the benefit and cost functions from (4.4) but the throughput estimation methods differ. Details on the throughput estimation methods are found in Section 4.3.4 through Section 4.3.7.

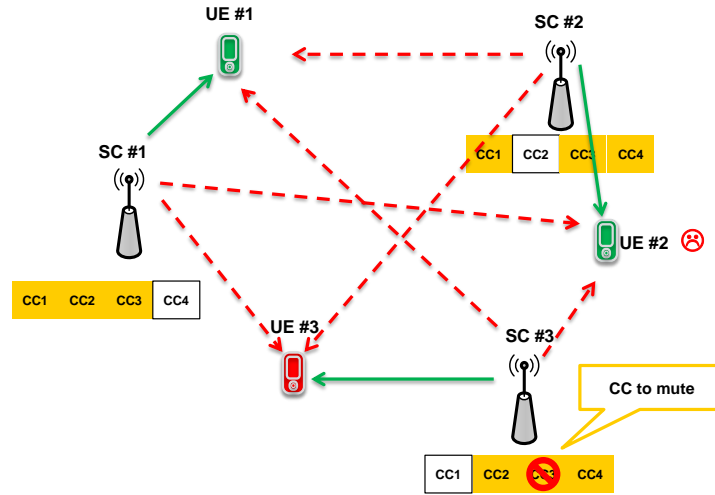


Fig. 4.3: Users who gain from small cell 3 muting CC 3 are marked green, users who lose are marked red. Green lines illustrate desired signals and dashed red lines indicate interfering signals.

In the previous two examples of adding a CC and muting a CC, only a single hypothesis was considered. However, in a practice multiple hypotheses are available. Consider the scenario where user 1 is in outage in Figure 4.2. Table 4.1 summarises the complete set of hypotheses which improves the throughput for user 1 and a corresponding net benefit ν_h is included to complete the example. First step is discard the invalid hypotheses (net benefit is zero or negative). In Table 4.2 all valid hypotheses are sorted according to net benefit ν_h value, which also decides the order in which to perform the different hypotheses. In this example, hypothesis 1 results in the largest net benefit and is carried out.

After performing hypothesis 1, it is estimated if it is required to perform additional hypotheses in order to serve user 1 with at least GBR. If not, no further CC changes are

Table 4.1: Hypotheses and corresponding net benefit (ν_h) for improving the throughput for user 1.

h	Action	Small Cell #	CC #	ν_h
1	Add	1	4	3
2	Mute	2	1	1
3	Mute	2	3	2
4	Mute	3	2	-1
5	Mute	3	3	-2

Table 4.2: Valid hypotheses are sorted according to net benefit ν_h .

$\nu_h \uparrow$	h	Action	Small Cell #	CC #
3	1	Add	1	4
2	3	Mute	2	3
1	2	Mute	2	1

performed. Otherwise, the next hypothesis is carried out, hypothesis 3 in this example. This continues until all valid hypotheses are performed, or the throughput of the victim user reach GBR.

After having presented the net benefit computations for the simple example, the equations are generalised. The net benefit for hypothesis h (ν_h) is computed as:

$$\nu_h = \sum_{l \in N_{B,h}} f_{Benefit}(\bar{R}_l, \hat{R}_l) - \sum_{j \in N_{C,h}} f_{Cost}(\bar{R}_j, \hat{R}_j) \quad (4.6)$$

where $N_{B,h}$ is the subset of users which gain from the hypothesis h and $N_{C,h}$ is the subset of users which lose from hypothesis h . It is noted that a user is not necessarily a part of either $N_{B,h}$ or $N_{C,h}$, and obviously, a UE can not be in both subsets.

4.3.2 Benefit and Cost Functions

A pivotal part of the CB-ICIC framework is the cost and benefit functions. They are paramount for choosing the hypothesis which improves the throughput for the outage UE sufficient and at the same time limits the overall network performance degradation. In practice, the high throughput UEs must sacrifice resources or accept increased interference. However, you do not want to reduce the throughput for the high throughput UEs too much either. It is important to remember, that a reduction in throughput increases the service time⁴ of those UEs. Obviously, if the service time of a UE is increased, the longer

⁴The service time is the time from a user enters the system to all user data is received.

the UE causes interference and is allocated resources. In this work, the benefit and cost functions are realised as:

$$f_{Benefit}(\bar{R}_n, \hat{R}_n) = \log_2 \left(\frac{\hat{R}_n}{R_{min}} \right) - \log_2 \left(\frac{\bar{R}_n}{R_{min}} \right) \quad (4.7)$$

$$f_{Cost}(\bar{R}_n, \hat{R}_n) = \log_2 \left(\frac{\bar{R}_n}{R_{min}} \right) - \log_2 \left(\frac{\hat{R}_n}{R_{min}} \right) \quad (4.8)$$

where \hat{R}_n is the estimated user throughput after performing an action as described in Section 4.3.4 to 4.3.7. It is noted that both the $f_{Benefit}(\bar{R}_n, \hat{R}_n)$ and $f_{Cost}(\bar{R}_n, \hat{R}_n)$ are always positive, since the function \log_2 is a strictly increasing function in the interval $]0, +\infty[$. The net benefit of hypothesis h is computed as:

$$\nu_h = \sum_{l \in N_{B,h}} f_{Benefit}(\bar{R}_l, \hat{R}_l) - \sum_{j \in N_{C,h}} f_{Cost}(\bar{R}_j, \hat{R}_j) \quad (4.9)$$

where $N_{B,h}$ is the subset of users which are positively affected by hypothesis h and $N_{C,h}$ is the subset of users which are negatively affected by hypothesis h , see Table 4.3. Figure 4.4 illustrates the benefit and cost function. The point of interest is where $\frac{\bar{R}_n}{R_{min}} = 1$. This point designates the dividing line of outage UEs and non-outage UEs. Due to the strictly decreasing gradient of \log_2 , improvements or degradation for UEs in outage are weighted higher than for non outage UEs. This ensures that muting is allowed even though the absolute throughput decrease is larger than the absolute throughput improvement.

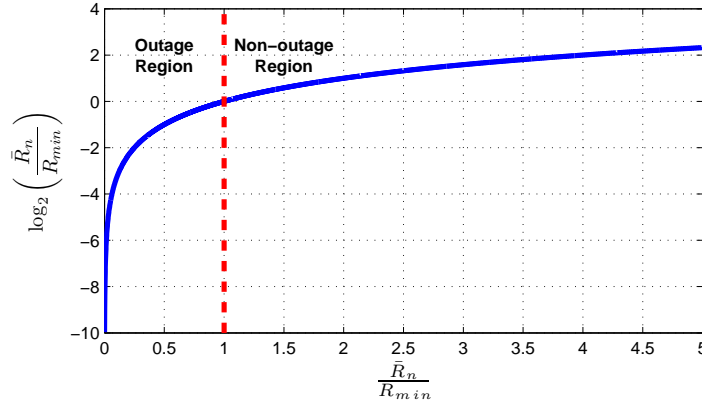


Fig. 4.4: Benefit/cost function. Note that the scaling of x-axis and y-axis differs.

The valid hypotheses ($\nu_h > 0$) are ranked and executed according to their net benefit. This continues until the victim UE is estimated to have reached R_{min} , or there are no

more valid hypotheses to execute. Moreover, if a hypothesis causes another UE to end up in outage, the hypothesis is disregarded.

In case of multiple outage UEs, the framework is limited to execute hypotheses related to a single outage UE only, by design. The reasons for such a limitation are complexity and stability. Calculating benefit and cost for a second UE would require that the framework accounts for the already applied changes. It is stressed, that a second UE would have to wait t_{Outage} (periodicity of the UE outage detection) before the framework is able to change the CC configuration again. In order to decide which UE is prioritised, a combined net benefit for valid hypotheses ($\tilde{\nu}_n$) related to UE n is computed as follows:

$$\tilde{\nu}_n = \sum_{h \in H_n} \nu_h \quad (4.10)$$

where H_n is the set of valid hypotheses related to UE n . Then the prioritised UE n^* is found by:

$$n^* = \arg \max_n \{\tilde{\nu}_n\}. \quad (4.11)$$

Finally, when a UE, which triggered CC muting of a neighbouring eNB, finishes its session, the net benefit of reversing the changes is computed. If the net benefit is positive the changes are reverted.

4.3.3 Reduced Net Benefit Computation

In the example illustrated in Figure 4.2 and Figure 4.3, the complexity of the net benefit computation seems reasonable. However, for the default simulation scenario, the total number of indoor small cells is 20, the number of CCs is four, and baseline results in Appendix E show that it is not unlikely that the instantaneous user load is up to 150 users (7.5 UEs per small cell). Hence, the computation of ν_h is no longer as trivial as in the example. For this scenario and the constraint that each small cell is assigned at least one CC, the number of possible component carrier assignments combinations (potential hypotheses) (N_C) is higher than 7 million:

$$N_C = \sum_{i=0}^{N_{CC}-1} \binom{N_{CC}}{i} \cdot \sum_{j=0}^{N_{SC}-1} \binom{N_{SC}-1}{j} \quad (4.12)$$

$$= \sum_{i=0}^3 \binom{4}{i} \cdot \sum_{j=0}^{19} \binom{19}{j} = 7864320. \quad (4.13)$$

Here, $\binom{\cdot}{\cdot}$ denotes the binomial coefficient. Clearly, it is not feasible to compute and find the optimal component carrier solution for such a large number of potential solutions. Therefore, it is required to reduce the complexity.

In order to reduce the complexity when muting a CC, only UEs which have the candidate CC as the dominant interferer is included in the benefit functions. Similar, when computing the cost of adding a new CC, only users where the new CC is the dominant interferer is included. Computing the cost of muting a CC and computing the benefit of adding a CC always include all user connected to the affected small cell. Table 4.3 gives an overview of which users are included in the cost and benefit computations when adding or muting CCs. In Appendix E more information on the dominant interferer and the Dominant Interference Ratio (DIR) is found. The consequences of applying the restrictions in Table 4.3 are a reduced number of available hypotheses and less UEs to include in the net benefit computations for each hypothesis. In the previous example, it would have the following impact, see Figure 4.5a and Figure 4.5b. UEs not included in the computations are marked in grey, see Figure 4.2 and Figure 4.3 for comparison.

Table 4.3: Users to include in the benefit and cost computations.

	Benefit	Cost
Adding a CC	Users connected to affected small cell	Users where the new CC becomes the dominant interferer
Muting a CC	Users where the muting CC is the dominant interferer	Users connected to affected small cell

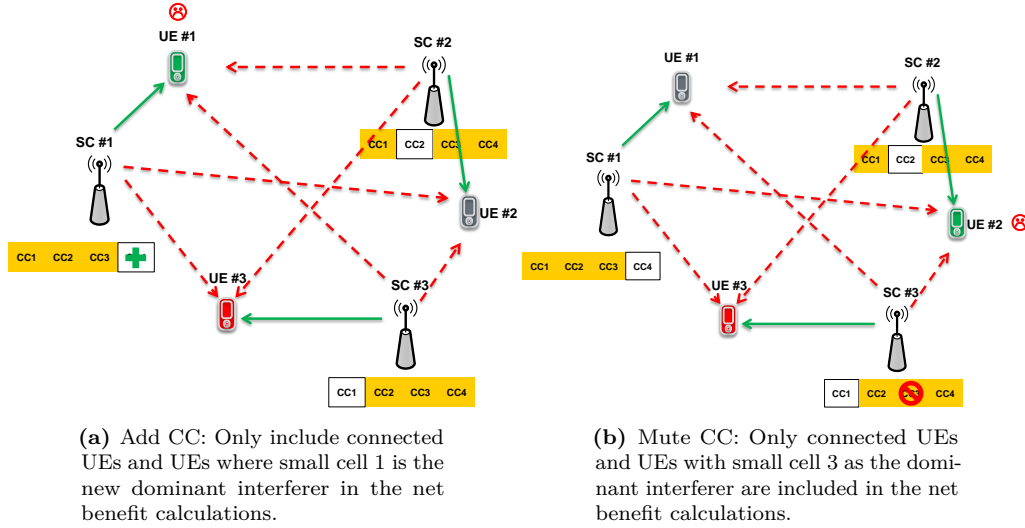


Fig. 4.5: Less UEs are included in the net benefit computations compared to Figure 4.2 and 4.3.

4.3.4 Increased Throughput From Adding a Component Carrier

Assuming the victim cell is not utilising all available CCs, first the SINR is estimated on the potential new CC (k) as:

$$\hat{\gamma}_{n,k} = \frac{\hat{P}_{i^*,n,k}}{I_{n,k} + N_T} \quad (4.14)$$

$$I_{n,k} = \sum_{i \neq i^*} P_{i,n,k} \quad (4.15)$$

where i is the small cell index, i^* denotes the serving cell, $\hat{\gamma}_{n,k}$ is the SINR estimate for user n on component carrier k , $\hat{P}_{i^*,n,k}$ is the estimate of the received power from the serving cell on CC k , N_T is the thermal noise, $I_{n,k}$ is the total interference experienced by user n on component carrier k , and $P_{i,n,k}$ denotes the received power from small cell i . Obviously, a UE is not aware of the received power on an inactive CC. However, similar path loss and transmission power is assumed for all CCs at each small cell. Moreover, it is assumed that the interference from the neighbouring cells is available from UE mobility measurements.

After estimating the user SINR on the potential new CC (k), the active CC (a^*) with most similar SINR is found as:

$$a^* = \arg \min_a (|\gamma_{n,a} - \hat{\gamma}_{n,k}|) \quad (4.16)$$

$$a \in A_{i^*} \quad (4.17)$$

where a is an active CC index, A_i is the set of active CCs at small cell i , and i^* is the serving cell of UE n . The throughput of the most similar CC carrier is known at the small cell, the bandwidth of the all CCs is equal, and given the Shannon capacity theorem, the following assumption is made for computing the throughput of the potential new CC k :

$$\frac{\hat{R}_{n,k}}{\log_2(1 + \hat{\gamma}_{n,k})} = \frac{\bar{R}_{n,a^*}}{\log_2(1 + \gamma_{n,a^*})} \quad (4.18)$$

$$\hat{R}_{n,k} = \frac{\log_2(1 + \hat{\gamma}_{n,k})}{\log_2(1 + \gamma_{n,a^*})} \cdot \bar{R}_{n,a^*} \quad (4.19)$$

where \bar{R}_{n,a^*} is the past average throughput for user n on the active CC a^* . And the resulting throughput estimate for UE n after adding CC k is computed as:

$$\hat{R}_n = \bar{R}_n + \hat{R}_{n,k}. \quad (4.20)$$

This throughput estimate is used as input to the benefit function in (4.7).

4.3.5 Reduced Throughput From Adding a Component Carrier

Adding new carriers increases interference towards other UEs in the network. Nevertheless, as explained in Section 4.3.3 only the cost of the most effected users is calculated. First, the user SINR after adding the new CC is estimated as:

$$\hat{\gamma}_{n,k} = \gamma_{n,k} \cdot \frac{I_{n,k} + N_T}{\hat{I}_{n,k} + N_T} \quad (4.21)$$

where $\hat{I}_{n,k}$ is the interference estimate for user n on component carrier k after adding a new carrier. The total interference estimate after adding a new carrier is computed as:

$$\hat{I}_{n,k} = I_{n,k} + \hat{P}_{i^*,n,k} \quad (4.22)$$

where $\hat{P}_{i^*,n,k}$ is the received power (interference) estimate from the small cell potentially adding a new CC k . Since the CC is not yet activated, the estimate is obtained from one of the active CCs of the candidate small cell. The new reduced throughput on CC k for UE n is:

$$\hat{R}_{n,k} = \frac{\log_2(1 + \hat{\gamma}_{n,k})}{\log_2(1 + \gamma_{n,k})} \cdot \bar{R}_{n,k}. \quad (4.23)$$

Finally, the throughput estimate for UE n is computed as:

$$\hat{R}_n = \bar{R}_n - \bar{R}_{n,k} + \hat{R}_{n,k}. \quad (4.24)$$

This reduced throughput estimate is used in the cost function (4.8) from Section 4.3.2.

4.3.6 Increased Throughput From Muting a Component Carrier

Assume that victim UE n is connected to small cell i^* . First, the Dominant Interferer (DI) on CC k is identified and the DIR is computed.

$$DI_{n,k} = \arg \max_{i \neq i^*} \{P_{i,n,k}\} \quad (4.25)$$

$$I_{n,k}^* = \max_{i \neq i^*} (P_{i,n,k}) \quad (4.26)$$

$$DIR_{n,k} = \frac{I_{n,k}^*}{I_{n,k} + N_T - I_{n,k}^*} \quad (4.27)$$

where $I_{n,k}^*$ is the interference caused by the DI. Then it is possible to estimate the improved SINR after muting as:

$$\hat{\gamma}_{n,k} = \frac{P_{i^*,n,k}}{I_{n,k} + N_T - I_{n,k}^*}. \quad (4.28)$$

Moreover, it is also possible to express the improved SINR as a function of the DIR:

$$\begin{aligned}
\hat{\gamma}_{n,k} &= \frac{P_{i^*,n,k}}{I_{n,k} + N_T - I_{n,k}^*} \\
&= \frac{P_{i^*,n,k}}{I_{n,k} + N_T - I_{n,k}^*} \cdot \frac{I_{n,k} + N_T}{I_{n,k} + N_T} \\
&= \frac{P_{i^*,n,k}}{I_{n,k} + N_T} \cdot \frac{I_{n,k} + N_T}{I_{n,k} + N_T - I_{n,k}^*} \\
&= \gamma_{n,k} \cdot \frac{I_{n,k} + N_T}{I_{n,k} + N_T - I_{n,k}^*} \\
&= \gamma_{n,k} \cdot \frac{I_{n,k} + N_T - I_{n,k}^* + I_{n,k}^*}{I_{n,k} + N_T - I_{n,k}^*} \\
&= \gamma_{n,k} \cdot \left(\frac{I_{n,k} + N_T - I_{n,k}^*}{I_{n,k} + N_T - I_{n,k}^*} + \frac{I_{n,k}^*}{I_{n,k} + N_T - I_{n,k}^*} \right) \\
&= \gamma_{n,k} \cdot (1 + DIR_{n,k}). \tag{4.29}
\end{aligned}$$

This highlights the fact, that a high DIR is advantageous when muting neighbouring small cells. Using the improved SINR estimate from (4.29) the improved throughput after muting on CC k is estimated as:

$$\hat{R}_{n,k} = \frac{\log_2(1 + \hat{\gamma}_{n,k})}{\log_2(1 + \gamma_{n,k})} \cdot \bar{R}_{n,k}. \tag{4.30}$$

Next, the throughput estimate of UE n is computed as:

$$\hat{R}_n = \bar{R}_n - \bar{R}_{n,k} + \hat{R}_{n,k} \tag{4.31}$$

This throughput estimate is used in the benefit function (4.7) in Section 4.3.2.

4.3.7 Reduced Throughput From Muting a Component Carrier

The reduced throughput for user n after the serving cell mutes CC k is computed as:

$$\hat{R}_n = \bar{R}_n - \bar{R}_{n,k} \tag{4.32}$$

where $\bar{R}_{n,k}$ is the past averaged throughput on CC k . The throughput estimate is used in (4.8) when calculating the cost of muting an CC, as explained in Section 4.3.2.

4.3.8 Muting Multiple CCs

It might be beneficial to mute the second strongest interferer on CC k as well. Therefore, if temporary setting

$$P_{DI_{n,k},n,k} = 0 \quad (4.33)$$

and repeat all computations from (4.25) through (4.32) the net benefit of muting the second strongest interferer is obtained, assuming the strongest interferer has already been muted. The procedure of muting multiple neighbouring small cells on CC k is allowed as long as net benefit is larger than ν_T and the victim UE is still in outage. In principle, all interfering small cell could mute on CC k , however, for each CC which is muted the gain of muting additional CCs becomes smaller. At the same time, the cost of muting does not change, whether it is the dominant interferer or a non-dominant interferer that applies muting.

4.3.9 Overview of the Developed CB-ICIC Framework

To ease the overview and workings of the framework, the framework is described in Algorithm 4.1 through Algorithm 4.3. First, in Algorithm 4.1 the more general aspects of the framework is explained. The more detailed net benefit computations when muting one or multiple CC are found in Algorithm 4.2. Last, Algorithm 4.3 describes the net benefit computation when more resources are made available by adding more active CC to the victim small cell.

4.4 Realisation of the Framework

The proposed CB-ICIC framework is implemented as a centralised solution and assuming an ideal backhaul connection with < 1 ms Round Trip Time (RTT) [103]. Furthermore, it is assumed that a central unit collects all relevant information, e.g. UE measurement reports and performance metrics. Based on the available information, the central unit coordinates the small cell CC assignment, whenever a UE is reported in outage. However, a decentralised approach is more suitable in this scenarios. Thus, this section investigates the impact if the proposed framework is to be implemented as a decentralised solution. The decentralised solution requires that UE Channel State Information (CSI) is exchanged between the involved small cells, but in [104] it is proposed to exchange a *per cell* benefit metric between the cells. It is shown that this solution arrives at the same solution as the centralised approach. Thus, a similar concept is envisioned for the developed framework. Moreover, for the decentralised approach a X2 interface between the small cell is assumed. Rather than exchanging UE measurement reports and performance metrics between the small cell, it is decided only to exchange the benefit and cost metrics, from (4.7) and (4.8). This entails several advantages. First of all, the amount of information to share with

Algorithm 4.1 Carrier Based Inter-Cell Interference Coordination Algorithm

```

 $RUN \leftarrow 1$ 
 $h \leftarrow 1$ 
 $\nu_h \leftarrow 0$ 
for  $n \leftarrow 1$  to  $N$  do
  if  $\bar{R}_n \leq R_{min}$  then ▷ Check if UE  $n$  is in outage
    for  $k \leftarrow 1$  to  $K$  do
      if  $k \in A_{i^*}$  then
        Goto Algorithm 4.2 ▷ Calculate net benefit when muting CC
      else
        Goto Algorithm 4.3 ▷ Calculate net benefit when adding CC
      end if
      if  $\nu_h > \nu_T$  then ▷ Check if the last hypothesis is valid
         $h \leftarrow h + 1$ 
      end if
       $\nu_h \leftarrow 0$ 
    end for
     $\tilde{\nu}_n \leftarrow \sum_{h \in H_n} \nu_h$  ▷ Compute the sum of all hypotheses related to user  $n$ 
  end if
end for
if  $h > 1$  then
   $n^* \leftarrow \arg \max_n \{\tilde{\nu}_n\}$  ▷ Find user with largest net benefit
  while  $\sum \tilde{\nu}_{n^*} > \nu_T$  do
     $h^* \leftarrow \arg \max_{h \in H_{n^*}} \{\nu_h\}$  ▷ Find the hypothesis with the largest net benefit
    Perform hypothesis  $h^*$ 
     $\tilde{\nu}_{n^*} \leftarrow \tilde{\nu}_{n^*} - \nu_{h^*}$ 
  end while
end if

```

Algorithm 4.2 Calculate Net Benefit When Muting a Component Carrier

```

while  $RUN$  do                                ▷ Keep muting interferers on CC  $k$  as long as  $\nu_h > \nu_T$ 
  for all users  $l \in N_{B,h}$  do                      ▷ Note that  $n \in N_{B,h}$ 
     $I_{l,k}^* \leftarrow \max_{i \neq i^*} P_{i,l,k}$ 
     $DIR_{l,k} \leftarrow \frac{I_{l,k}^*}{I_{l,k} + N_T - I_{l,k}^*}$ 
     $DI \leftarrow \arg \max_{i \neq i^*} \{P_{i,l,k}\}$ 
     $\hat{\gamma}_{l,k} \leftarrow \gamma_{l,k} \cdot (1 + DIR_{l,k})$ 
     $\hat{R}_{l,k} \leftarrow \frac{\log_2(1 + \hat{\gamma}_{l,k})}{\log_2(1 + \gamma_{l,k})} \cdot \bar{R}_{l,k}$ 
     $\hat{R}_l \leftarrow \bar{R}_l - \bar{R}_{l,k} + \hat{R}_{l,k}$ 
     $\nu_h \leftarrow \nu_h + f_{Benefit}(\bar{R}_l, \hat{R}_l)$ 
     $P_{DI,l,k} \leftarrow 0$                                 ▷ Set DI to 0 in order to find next strongest interferer
  end for
  for all user  $j \in N_{C,h}$  do
     $\hat{R}_j \leftarrow \bar{R}_j - \bar{R}_{j,k}$ 
     $\nu_h \leftarrow \nu_h - f_{Cost}(\bar{R}_j, \hat{R}_j)$ 
  end for
  if  $\nu_h > \nu_T$  &  $R_n < R_{min}$  then
     $h \leftarrow h + 1$ 
  else
     $RUN \leftarrow 0$                                 ▷ Break loop if  $\nu_h < \nu_T$  or user  $n$  has reached  $R_{min}$ 
  end if
end while

```

Algorithm 4.3 Calculate Net Benefit When Adding a Component Carrier

```

for all users  $l \in N_{B,h}$  do
   $I_{l,k} \leftarrow \sum_{i \neq i^*} P_{i,l,k}$ 
   $\hat{\gamma}_{l,k} \leftarrow \frac{\hat{P}_{i^*,l,k}}{I_{l,k} + N_T}$ 
   $a^* \leftarrow \arg \min_a \{|\gamma_{l,a} - \hat{\gamma}_{l,k}|\}$ 
   $\hat{R}_{l,k} \leftarrow \frac{\log_2(1+\hat{\gamma}_{l,k})}{\log_2(1+\gamma_{l,a^*})} \cdot \bar{R}_{l,a^*}$ 
   $\hat{R}_l \leftarrow \bar{R}_l + \hat{R}_{l,k}$ 
   $\nu_h \leftarrow \nu_h + f_{Benefit}(\bar{R}_l, \hat{R}_l)$ 
end for
for all users  $j \in N_{C,h}$  do
   $\hat{I}_{j,k} \leftarrow I_{j,k} + \hat{P}_{i^*,j,k}$ 
   $\hat{\gamma}_{j,k} \leftarrow \gamma_{j,k} \cdot \frac{I_{j,k} + N_T}{\hat{I}_{j,k} + N_T}$ 
   $\hat{R}_{j,k} \leftarrow \frac{\log_2(1+\hat{\gamma}_{j,k})}{\log_2(1+\gamma_{j,k})} \cdot \bar{R}_{j,k}$ 
   $\hat{R}_j \leftarrow \bar{R}_j - \bar{R}_{j,k} + \hat{R}_{j,k}$ 
   $\nu_h \leftarrow \nu_h - f_{Cost}(\bar{R}_j, \hat{R}_j)$ 
end for

```

the neighbouring small cells is greatly reduced. Secondly, each small cell can compute the benefit or cost for each of the potential hypotheses before the information is actually requested.

4.4.1 Required Signalling and Non-Ideal Backhaul Impact

Figure 4.6 illustrates the required signalling for muting CC k at small cell 2. First, the a request for benefit and cost is send to neighbouring small cells. As soon as this request is received, a reply is send back to the victim cell. It is noted that each small cell has already computed benefit and cost for all potential hypotheses, and no additional delay is induced due to benefit or cost computations. At the victim cell, the replies are received after a time which corresponds to the RTT between the small cells. The longest RTT determines the total delay. When all benefit/cost replies are received, the victim cell is able to determine which of the hypotheses to perform, thus, the final signalling event is to inform the involved small cell(s) about the decision. It is important to note that a victim cell requests the net benefit for all potential hypotheses simultaneously, such that only a single message is sent to the involved small cells. For sake of simplicity, only the signalling regarding hypothesis i is included in the figure. Moreover, if the chosen hypothesis requires the victim cell to start transmitting on additional CC(s), one lesser message is required, see Figure 4.7.

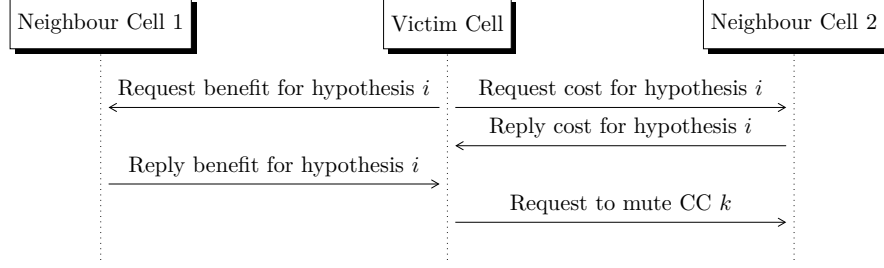


Fig. 4.6: Message flow for muting interfering CC k at neighbour small cell 2. The term *victim cell* is used for the serving cell of a outage UE.

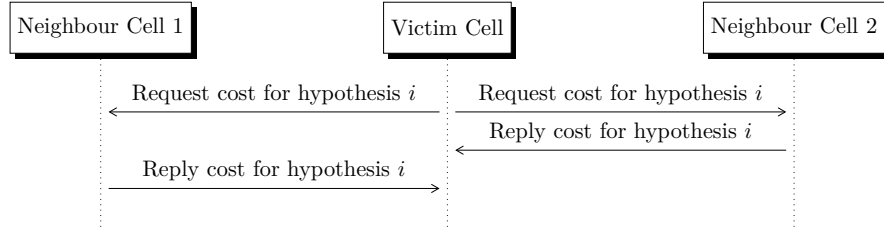


Fig. 4.7: Message flow for adding CC k at victim cell. The term *victim cell* is used for the serving cell of a outage UE.

Appendix F discusses the impact of realistic RTT of the backhaul. The effective CB-ICIC time⁵ is in worst case reduced from 92% to 83% when realistic backhaul is considered. Based on this, a significant gain with realistic backhaul is still assumed. Furthermore, the signalling load of the CB-ICIC framework proves to be insignificant.

4.5 Simulation Scenario

In this section, the default simulation scenario is described and the most important simulation assumptions are discussed. The simulation scenario is used in the remainder of the PhD thesis. It is decided that the indoor small cell simulation scenario should be based on the 3GPP Release 12 Scenario 3 [62, 71]. This ensures that the produced results are comparable with similar interference coordination studies also utilising 3GPP Release 12 Scenario 3. This section is concluded with a comprehensive table with the most notable simulation parameters.

4.5.1 Network Layout

The 3GPP Release 12 Scenario 3 defines two building layouts, yet only the dual stripe layout is utilised in this work. In Scenario 3 all UEs are located inside a dual stripe building, and no wide area macro network is simulated. Consequently, all UEs must be served by an indoor small cell, thus it is decided to deploy a small cell in each apartment in the dual stripe building. The reason for doing so is twofold. First of all, without an overlay macro network available, a small cell in each apartment ensures indoor coverage in the entire building. Secondly, since the objective is investigation of potential ICIC solutions in dense small cell environments, a challenging interference scenario is desired. Furthermore, a X2 interface between the indoor small cells is assumed. Figure 4.8 illustrates the network layout including the dimensions, it is noted that the small cells are dropped with uniform probability inside each apartment. Finally, it should be mentioned that for sake of simplicity the number of floors in this work is limited to 1 floor, resulting in a total of 20 small cells in the default simulation scenario. The outer building penetration loss is 23 dB and the penetration loss of the indoor walls is 5 dB.

4.5.2 Spectrum and Transmission Power

In this study the transmission bandwidth is 20 MHz and the total transmission power is 27 dBm. Furthermore, the available bandwidth is divided into four CCs, each with a bandwidth of 5 MHz. Depending on the interference coordination strategy, the indoor small cells can utilise the entire transmission spectrum (all CCs) or only some of the CCs. In order to keep the PSD constant the total transmission power per CC is 21 dBm,

⁵The percentage of the session time where CB-ICIC improves the throughput for an outage UE.

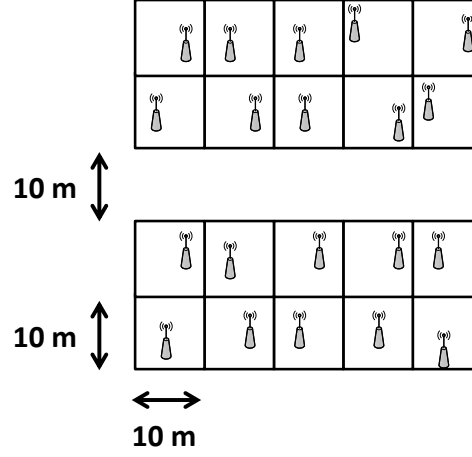


Fig. 4.8: Building layout and small cell density for the considered simulation scenario. Small cells are dropped with uniform distribution in each apartment.

corresponding to 21 dBm per 5 MHz bandwidth. The transmission power and bandwidth relations are shown in Figure 4.9. If a small cell is configured to transmit on multiple CC, contiguous or non-contiguous, intra-cell CA support for all UEs are assumed, i.e. UEs can be scheduled on multiple CCs. Moreover, it is assumed that the distance dependant path loss is independent of the CC, but the fast-fading component is CC dependant. In the simulations, only Frequency Division Duplex (FDD) Downlink (DL) is simulations. However, it is important to note, that the interference challenges are similar for a FDD network and a synchronised Time Division Duplex (TDD) network.

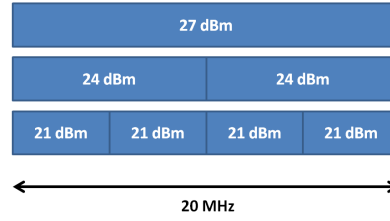


Fig. 4.9: Total transmission power versus transmission bandwidth.

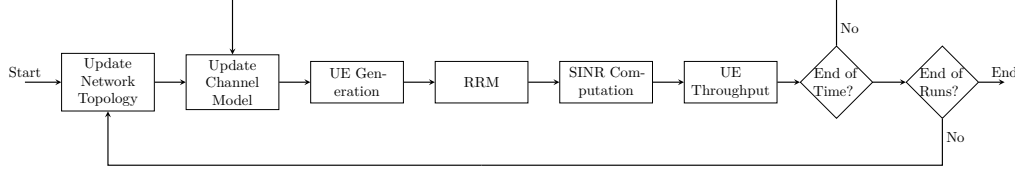


Fig. 4.10: Simulator structure used in Chapter 4 through Chapter 6.

4.5.3 Description of the Simulation Tool

This section describes the simulation tool used for the studies in the remainder of the thesis. The system-level simulator is 3GPP Long Term Evolution (LTE) and Long Term Evolution Advanced (LTE-A) compliant. A block diagram of the system-level simulator is shown in Figure 4.10.

The simulator consists of two main loops; a network topology loop and a time loop. The network topology loop loops over the different network realisations. For each realisation of the network topology, indoor small cells are dropped uniformly in the indoor area in order to model uncoordinated deployment strategy. The time loop loops over the specified simulation time. The simulation time is set, such that the network reach a steady state and the number of UE statistics are significant.

The core of the simulation tool is encapsulated by the two loops. The first block is the UE generation where UEs are created according to the traffic generation model. Next, is the Radio Resource Management (RRM) block. All essential RRM processes are explicit modelled in the simulator. This includes time-domain and frequency-domain UE scheduling and inner- and outer-loop link adaptation. Moreover, HARQ and retransmissions are modelled as well. After the RRM processes, the UE SINR is computed. The SINR is used to compute the specific UE throughput rates. The throughput is calculated from SINR to throughput mapping curves. If the specified simulation time is reached, the simulation statistics are saved and the simulation ends. Otherwise, the user channel model is updated and the process start over. Finally, if the simulation time is reached, new indoor small cell are dropped in the network, and the simulations start all over.

Before any development work is started, proper calibration of the simulation tool is ensured. For this purpose, primarily [105] is used as calibration target. After the calibration process, the simulation results showed a match in path loss distribution and in UE geometry factor⁶.

4.5.4 Simulation Assumptions Summary

Last part of this section is dedicated to the default simulation assumption. Unless otherwise specified, the default simulation parameters are as summarised in Table 4.4. If not included

⁶Also known as the G-factor, see [83, page 228-231]

in the table, the default simulation value is according to [62].

Table 4.4: Default simulation assumptions.

Parameter	Value
System	Downlink LTE-A FDD Release 12
Deployment scenario	3GPP Release 12 Scenario 3 [71, 106]
Network layout	Dual Stripe
Number of floors	1
Number of apartments per floor	20
Indoor small cell density	1.0 (1 per apartment)
Access mode	Open Subscriber Group (OSG)
Carrier frequency	3.5 GHz
Path loss model	InH [71]
Spatial channel model	InH [107]
Transmission bandwidth	20 MHz
Number of CCs	Up to 4
Small cell transmission power	21 dBm per 5 MHz
Error vector magnitude	4%
Time domain scheduler	Proportional fair
Frequency domain scheduler	Proportional fair
Throughput averaging length, t_{avg}	100 ms
Guaranteed bit rate, R_{min}	3 Mbps
Data buffer size (S)	4 Mbit
Traffic model	{Open loop ; Closed loop}
Number of transmit antennas (N_{Tx})	2
Number of receive antennas (N_{Rx})	2
Rank adaptation	Enabled [108]
Transmission mode	4
Receiver type	MMSE-MRC [109]
Cell selection criterion	Best RSRP
UE noise figure	9 dB

4.6 Performance Evaluation

In this section, the performance of the proposed CB-ICIC is compared to global FR. Global FR, where all small cells utilise the entire spectrum, is selected as reference because it provides better performance than fixed FR-2 and fixed FR-4, see Appendix E. In this chapter, global FR is referred to as *Baseline*.

4.6.1 Characteristics of A Congested Network

As mentioned previously, only simulations where the carried load equals the offered load are considered valid, see Section 4.2.1. In Figure 4.11 the offered load versus the carried load is plotted for baseline and CB-ICIC. For low load, it is seen that the carried load equals the offered load. Baseline carried load drops below the offered load at 500 Mbps, thus the network is invalid for 500 Mbps and up. For CB-ICIC the network congests when the offered load is 600 Mbps or more. It is important to note, that this does not correspond to the definition of network capacity.

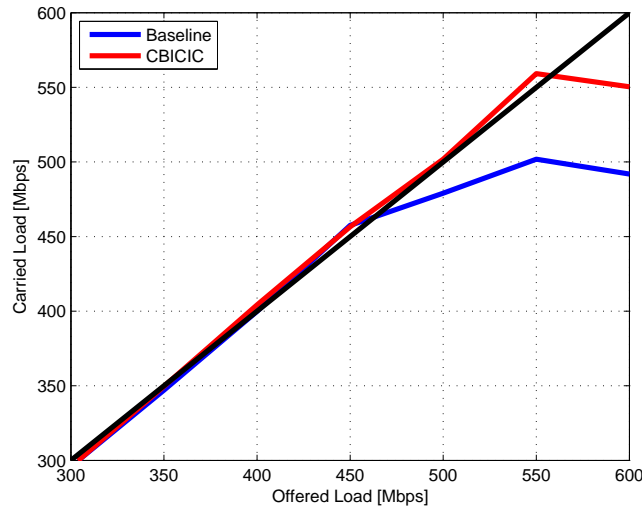


Fig. 4.11: In a congested network, the carried load is lower than the carried load. E.g. the network overloads at 500 Mbps and 600 Mbps for baseline and CB-ICIC, respectively.

Figure 4.12 shows the Empirical Cumulative Density Function (ECDF) of the number of UEs being served by the small cells. For baseline and CB-ICIC, two curves are plotted; one curve for the maximum carried load (dashed) and one curve where the small cell network congests (solid). In each Transmission Time Interval (TTI) the UE-load is sampled in each of the small cells, and presented as an ECDF. For non-congested networks in general, it is seen that $< 5\%$ of the time a small cell is loaded with more than 20 UEs. When the network congests, it is seen that for approximately 5% to 10% of the time a small cell is loaded with more than 40 UEs. This indicates that UEs start to pile up in the network. At the same time, it is noted that the resource utilisation is still not 100%. Thus, the UE load is not distributed evenly between the small cells, leading to a few of the small cells limiting the overall network performance.

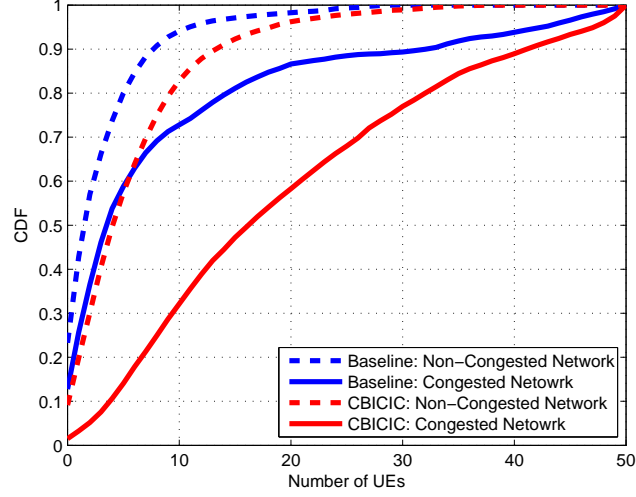


Fig. 4.12: When the network congests, UEs start to pile up in a few of the small cells. It is seen that the user load is not equally balanced between the small cells.

Table 4.5 lists the resource utilisation for baseline and CB-ICIC for various offered loads. In general, the resource utilisation for CB-ICIC is lower than for baseline. The lower resource utilisation for CB-ICIC is two-fold. First, as shown later in Figure 4.14, the UE throughput performance is improved for CB-ICIC. This means, that the UE leaves the network faster, thus using less resources. Second reason is the muting of CC. Consider a small cell where only 3 out of 4 CCs are active. Assuming the bandwidth of the CCs is equal and that the small cell allocates all resources on the 3 active carriers in all TTIs, the resulting resource utilisation would be 75% and not 100%. One could argue which is more correct as it is a matter of definition. However, in this thesis it is decided that the resource utilisation is reported as a percentage of the total amount of resources - active or muted - and not as a percentage of the active resources only.

In the remainder of the thesis, no further results for congested networks are presented. Thus, for *baseline* simulations the offered load is within the range 300 Mbps to 450 Mbps, and for *CB-ICIC* the valid offered load region is 300 Mbps to 550 Mbps.

4.6.2 Network Outage and UE Throughput Performance

In Figure 4.13 the network outage versus the offered traffic load is shown. The used traffic model is the OLTM. At low load, it is seen that the network outage is zero, so all UEs in the network are served with at least R_{min} . With increasing load, not all UEs can be

Table 4.5: Resource utilisation for baseline and CB-ICIC.

Offered Load [Mbps]	Baseline	CB-ICIC	# of active CCs
300	33%	31%	3.9
350	49%	43%	3.9
400	62%	45%	3.3
450	77%	47%	2.8
500	-	51%	2.6
550	-	54%	2.4

served with at least R_{min} , resulting in an increase in network outage. It is seen that the baseline scheme reaches 5% of the UEs in outage for a offered load of 420 Mbps, which defines the network capacity for the baseline scheme. From the figure, it is clear that by enabling CB-ICIC the network capacity increases. In this scenario, the network capacity increases to 510 Mbps, corresponding to an increase of 21%, which clearly demonstrates the advantage of CB-ICIC in a small cell environment.

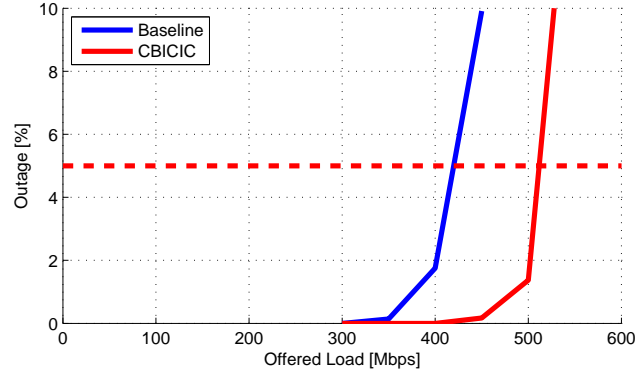


Fig. 4.13: Network outage for baseline scheme and CB-ICIC framework utilising OLTM. The red dashed line denotes the maximum outage allowed in the network.

The 5%-ile and 50%-ile UE throughput performances are plotted in Figure 4.14. The figure shows, that for all traffic loads, the CB-ICIC framework outperforms the baseline UE throughputs. Despite the muted CCs, the 50%-ile UE throughput is not affected negatively. This indicates that the realised benefit/cost functions and net benefit threshold achieves a good trade-off in prioritising the performance of outage UEs versus non-outage UEs. However, for low load, the gains are insignificantly. The reason for this is, that at low load the number of instantaneous UEs in the network is rather low, thus, the interference from neighbouring small cells is relatively small. Furthermore, for low load

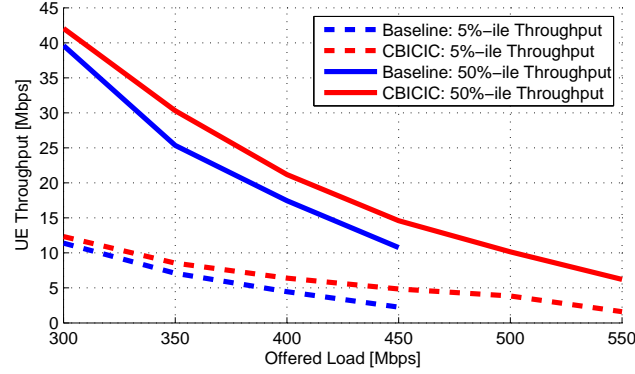


Fig. 4.14: 5%-ile and 50%-ile UE throughput for baseline and CB-ICIC. The small cell network congests at 450 Mbps and 550 Mbps for baseline and CB-ICIC, respectively.

the available resources for each UE is high resulting in high UE throughput. Hence, the CB-ICIC framework is rarely triggered at low load, see Figure 4.15 and Figure 4.16. At high load, the number of instantaneous UEs in the network is higher which means more UEs to share the available resources. Thus, the UE throughput performance is lowered. Consequently, the CB-ICIC framework is triggered more often, leading to higher CB-ICIC gains.

4.6.3 Active Component Carrier Ratio and Update Rate

Figure 4.15 illustrates the probability mass function of active CCs for various loads. For 300 Mbps and 350 Mbps offered load, 4 active CCs is clearly dominant, with a probability of more than 0.9. At these loads, the CC configuration is very similar to baseline, which obviously corresponds to 4 active CCs. The reason that the CB-ICIC framework rarely mutes CCs at low load is that the probability of inter-cell interference is also low. Furthermore, the probability of multiple UEs connected to the same serving cell is low, thus, the resources are not shared with other UEs, this ensures that UEs fulfill their GBR target without triggering the CB-ICIC framework.

At high load, the probability of UEs fulfilling the GBR target is reduced, due to less resources and increased inter cell interference. Consequently, the CB-ICIC framework is triggered more frequently leading to generally more muting being applied to the small cells, which is also evident from the figure. And at offered load = 550 Mbps, it is seen that 2 active CCs is the most probable CC configuration. Generally speaking, at low load the average number of active CCs is 3.9 per small cell and for high load this number is reduced to 2.4, see more details in Table 4.5.

An equally important aspect is the rate of which the CC configuration is updated. As

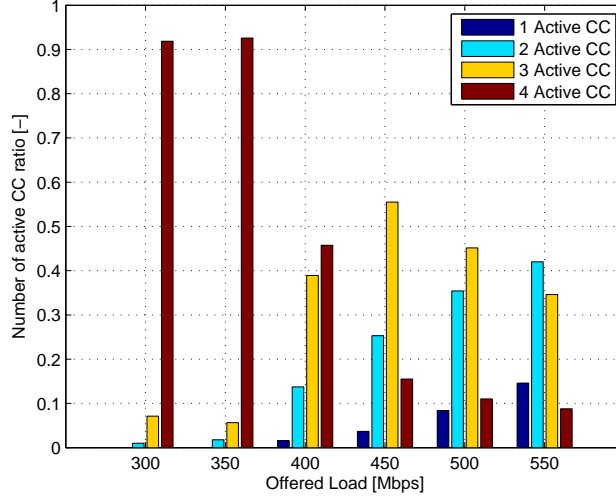


Fig. 4.15: Probability mass function of active CC.

each CC assignment update involves signalling and a transition time between ON/OFF, Figure 4.16 shows the number of CC assignment updates per second per small cell. A update change rate of 1 means that the small cell updates the CC assignment change once every second on average. As expected, and indicated in previous figures, the CC change rate is rather low at low load. On average, a small cell updates its CC assignment once every two minutes. At high load, the small cells update the CC assignment approximately once per second.

4.6.4 Performance Evaluation With Closed Loop Traffic Model

In order to test the sensitivity towards the traffic generation method, also CLTM results are presented. At this point in the PhD thesis, all reported performance results have been for OLTM. However, in order not to replicate all OLTM results, only the most important CLTM results are presented. The network outage versus the number of UEs per small cell in Figure 4.17. First of all it is noted that the traffic load is now expressed as *Number of UEs per Small Cell*. From the figure it is evident, that the CB-ICIC solution significant improves the network outage performance. By applying CB-ICIC, the load where the network fulfils the QoS for 95% of the UEs is increased from 2.5 to 4 UEs per small cell. This corresponds to a network capacity increase of 60%. For OLTM, the network capacity gain was only 21%. This clearly demonstrates the versatility of the CB-ICIC framework towards traffic models.

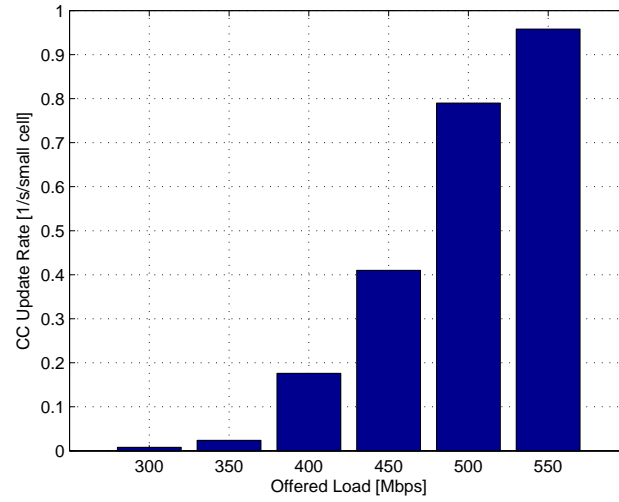


Fig. 4.16: Number of CC assignment changes per second per small cell.

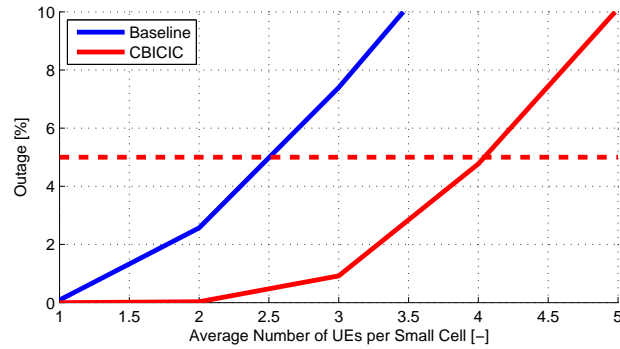


Fig. 4.17: Network outage for baseline and CB-ICIC using CLTM. Red dashed line denotes the maximum allowed network outage.

Beside the importance of the increased network capacity, the total number of served UEs should be emphasised. Due to the feedback in the traffic model, artificial low network outages could be achieved if the number of served UEs is reduced. Therefore, it is important, that this is not the case. Figure 4.18 shows the number of served UEs, including both outage and non-outage UEs. It is clear that for all loads, the proposed CB-ICIC scheme increases the number of served UEs.

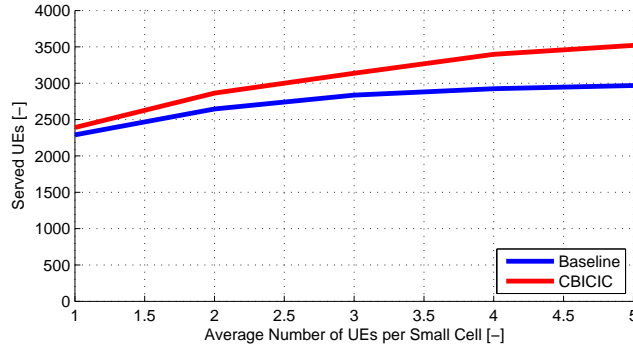


Fig. 4.18: Number of served UEs for CLTM.

The larger CB-ICIC gain for CLTM compared to OLTM is due to increased resource utilisation. The consequence of increased resource utilisation is increased inter-cell interference and more muting options for the CB-ICIC framework. The increased resource utilisation is increased since a new UE is generated whenever a UE finishes their session. Table 4.6 summarises the resource utilisation for the CLTM simulations. Compared to Table 4.5 it is evident that the resource utilisation is higher when using the CLTM. Further, it is also visible that the CB-ICIC applies more muting for the CLTM, hence the larger gain in CLTM.

Table 4.6: Resource utilisation for baseline and CB-ICIC.

# of UEs per cell	Baseline	CB-ICIC	# of active CCs
1	53%	46%	3.9
2	68%	51%	3.3
3	77%	52%	2.9
4	82%	54%	2.7
5	83%	56%	2.6

4.7 Conclusion and Discussion

The poor performance of fixed FR schemes motivates the development of a dynamic CB-ICIC framework which minimise the network outage for a given QoS requirement. The framework works in a reactive manner, which intelligently coordinates the CC assignment, such that outage UEs improve the throughput performance and fulfil the QoS target. Pivotal parts of the framework are the identification of CC assignment hypotheses and the net benefit calculations for each hypothesis. These two steps ensure, that the CC assignment change provides sufficient benefit for the outage UE with minimal impact towards the neighbouring small cells and connected UE. By applying the proposed CB-ICIC framework, the network capacity is increased 20% - 60%, depending on the utilised traffic generation model. This feat is accomplished with control signalling shared between the small cells via ideal backhaul, however with realistic backhaul properties the CB-ICIC is assessed to provide considerable network outage improvements also. Moreover, the amount of control signalling required to support the framework is considered to be minor and is outweighed by the performance gains. Yet, standardisation for sharing the benefit/cost is required by the proposed framework.

Chapter 5

Adaptive Small Cell Load Balancing

Simulation results in Appendix E show that uneven user load in the small cell is the main reason for networks to congest. Typically, a single or a few small cells are limiting the overall network performance, as they are overloaded and User Equipments (UEs) start to pile up in the network. In this chapter, an adaptive small cell load balancing algorithm is developed. The objective is to offload UEs from the high loaded small cells to the less loaded small cells. Moreover, the algorithm must be able to adapt to the instantaneous user load.

The chapter is organised as follows: In Section 5.1 prior art is discussed followed by the problem formulation in Section 5.2. Section 5.3 describes the development of the load balancing algorithm. In Section 5.4 the performance of the developed load balancing algorithm is presented and Section 5.5 concludes the chapter.

5.1 Prior Art

In [110], the authors propose a mobility load balancing algorithm which dynamically adjust the Cell Individual Offset (CIO) via the X2 interface. The proposed algorithm utilises the Composite Available Capacity (CAC) measure defined by 3rd Generation Partnership Project (3GPP) [52]. Based on the CAC measure, the cells negotiate a CIO, i.e. users are offloaded to less loaded cells. The simulation scenario is a Heterogeneous Network (HetNet) with a dedicated macro carrier and a co-channel macro and pico carrier. The objective is to increase the pico utilisation ratio and increase the session satisfaction ratio

by offloading UEs to inactive neighbouring cells. Simulation results show that the proposed algorithm indeed increase the session satisfaction ratio. On the contrary, results also show that the probability of radio link failures increase. Thus, the authors recommend that the load balancing algorithm is service-aware, and is primarily used for video streaming UEs where buffering helps protect against link failure interruptions.

The authors of [111] investigate the performance of several load balancing techniques in HetNets. A network-wide optimisation problem is formulated, and joint user association and resource allocation are performed to find the upper bound performance. Next, a low complexity distributed Range Extension (RE) algorithm is proposed. The algorithm converges to a near optimum solution. A sensitivity study shows that the optimum solution is highly dependent on the transmission power of the different base station technologies. The proposed algorithm improves the throughput for the coverage UEs up to 3x. This emphasises the potential of simple RE biasing. Moreover, in [112] an adaptive RE algorithm is developed for Long Term Evolution (LTE) HetNets - macro and pico cells. The algorithm dynamically adjusts the pico cell RE according to the traffic distribution and the UE performance. Promising simulation results are presented, as the algorithm proves to be versatile and improves the UE throughput performance over static pico cell RE configurations.

The studies in [110–112] focus on the improved user throughput performance or user satisfaction by means of cell range extension adjustments or mobility parameter adjustments in 3GPP compliant network. However, in [113] a more radical and general approach is investigated. The authors formulate the macro and small cell load balancing problem as a bargain problem. For each small cell, a cost and an incentive are defined for offloading macro UEs. Likewise, each macro cell is associated with a cost and incentive to offload UEs to a small cell. In order to improve the small cell pay off, the small cells must form groups, to increase their bargain power towards the overlay macro network. As it is also noted by the authors, their contribution should be used as inspiration in the design of future small cell offloading techniques and solutions.

It is evident from the referenced papers, that recently the primary focus has been on load balancing between a macro layer and a small cell layer. In the co-channel macro and small cell scenario, macro to small cell offloading is the apparent method to improve the overall network throughput performance. However, in this chapter the potential of load balancing between small cell on a dedicated carrier is investigated. This topic has received less attention in open literature.

5.2 Problem Formulation

The scenario of interest is the 3GPP Release 12 Scenario 3, described in Section 4.5. Furthermore, based on the results presented in Section 4.6.1, it is clear that the small cells in the network experience very different instantaneous load conditions. Here load is defined as the number of connected UEs. While some of the small cells are unused, other

small cells serve more than 10 UEs on average. Thus, in order to improve the overall network throughput performance, it is desired to distribute the UEs more equally between the small cells. By doing so, more resources are available for the remaining UEs in the overloaded cell. Moreover, the UEs, which are offloaded to a neighbouring cell, improve their throughput despite the potentially lower Signal to Interference and Noise Ratio (SINR), as more resources are available at the target cell. Consequently, the objective of the load balancing algorithm is:

- Identify overloaded small cell(s) in the network
- Search for one or multiple neighbouring small cells capable of offloading the overloaded small cell(s)
- Apply the necessary load balancing mechanisms

5.3 Developed Load Balancing Framework

First, the means of load balancing must be decided. In this work, the cell association is performed as:

$$i^* = \arg \max_i \{P_i + RE_i\} \quad (5.1)$$

where P_i is the received power from cell i and RE_i is the range extension of cell i . In LTE, P_i is realised as the Reference Signal Received Power (RSRP) measured by the UEs. Thus, two obvious load balancing candidates are the adjustment of the small cell transmission power or individual cell RE bias. Both mechanisms involve inherited pros and cons.

If using the transmission power alternative, the overloaded small cell could increase the transmission power in order to improve the SINR for the connected UEs. However, there are two distinct disadvantages of such an approach; namely the small cell increase the coverage footprint and neighbouring small cell UEs experience increased interference. By increasing the small cell coverage footprint, the probability of new UEs arriving also increase. This is not desired, as the resulting resource-share per UE decreases accordingly. Furthermore, since the surrounding UEs experience a decreased SINR and throughput, the neighbouring small cell(s) would potentially combat this phenomena by also increasing the transmission power. As a result of this side effect, the small cells potentially enter a power race, similar to power race in Uplink (UL) described in [114]. Hence, the end result is that all small cells transmit with the maximum transmission power, which is not the desired outcome.

Alternatively, a small cell could decrease the transmission power in order to shrink the coverage footprint and the probability of new UEs arriving. However, the effect of lower arrival rate is not immediate and does not improve the performance of the already connected UEs. On the contrary, the negative effect of lower transmission power is

immediate, and the consequence is worsened SINR and throughput performance of the connected UEs. Thus, the opposite effect is achieved by lowering the small cell transmission power and is not considered a viable solution.

Cell RE adjustment has been utilised successfully in 3GPP HetNet deployments in combination with network Inter-Cell Interference Coordination (ICIC) features [54]. The RE feature allows manipulation of the small cells coverage area according to the applied cell selection criterion from (5.1). By increasing the RE value, the coverage area of the cell is increased and vice versa. This is possible without effecting the SINR conditions of own cell UEs or neighbour cell UEs. Therefore, individual cell RE is selected as the load balancing mechanism. However, it is important to stress that in this thesis load balancing according to (5.1) is only performed at connection set up. Handover or cell reselection is not used, even though the initial cell selection is no longer optimum.

5.3.1 Load and Overload Criteria

An overloaded small cell is characterised by a large number of connected UEs each being served with a UE throughput significantly lower than the average UE throughput in the network. Hence, the average UE throughput in cell i is defined as the cell specific load parameter:

$$\omega_i = \frac{1}{\#U_i} \sum_{n \in U_i} \bar{R}_n \quad (5.2)$$

where n is the user index, i is the small cell index, U_i is the set of UEs at small cell i , \bar{R}_n is the past average throughput of UE n , ω_i is the cell load of small cell i , and $\#U_i$ denotes the cardinality of the set U_i . It is important to note, that the throughput is based on the throughput of all connected UEs, and not only scheduled UEs. Then, the first criterion for identifying an overloaded cell is:

$$\frac{\omega_i}{\omega_{i^*}} < T_\omega \quad (5.3)$$

where T_ω is the overload threshold, and i^* is a neighbouring small cell. For sake of simplicity, it is decided that a small cell only computes the overload ratio from (5.3) for the small cells in adjacent apartments. In real life scenario this is naturally not an option, as an autonomous solution is preferred. However, realistic neighbour cell pairing can be achieved using UE measurement reports. Yet, this issue is out of the scope of this thesis and is suggested for future studies.

From (5.3) it is clear that the load balancing algorithm does not consider any Quality of Service (QoS) requirements, e.g. a minimum guaranteed bit rate. This is a design choice as it is desirable to adjust the small cell RE before the UEs ends up in outage. Instead, to avoid unnecessary cell RE adjustments a minimum resource utilisation threshold is

defined as a second overload criterion:

$$\psi_i > T_\psi \quad (5.4)$$

where T_ψ is the resource threshold and ψ_i is the average resource utilisation during the last t_ψ seconds. This criteria ensures that the cell RE is only adjusted in the high load scenarios. In low loaded scenarios, it is preferred that UEs connect to the small cell where the maximum RSRP is measured. E.g. if two UEs are connected to a small cell and only one UE is connected to a neighbouring small cell, the intention is not to offload UEs to the small cell with only one connected UE only. Here the desired behaviour is to keep the current RE values.

5.3.2 Description of the Algorithm

The proposed algorithm is designed as a distributed algorithm. This is the preferred choice, as minimal information needs to be shared between a small cell and the neighbouring small cells in adjacent apartments. From (5.3) and (5.4), it is evident, that only the average UE throughput of the connected users are to be shared.

Furthermore, it is decided that the algorithm must be proactive. It is desirable if the users are balanced before the cells are actually overloaded. Thus, each small cell checks periodically (every t_ψ second) if both (5.3) and (5.4) are fulfilled. If both are fulfilled, the small cell must be offloaded. This is either achieved by increasing the cell RE bias in a neighbouring small cell or lower the cell RE bias in own cell. It is important to realise that the absolute value of cell RE is not too interesting in the dedicated small cell scenario. It is the difference in RE bias between cell pairs that is the most interesting value.

Increase Cell RE in Neighbouring Cell

In the dual stripe scenario, a small cell (denoted *victim*) can have up to three adjacent neighbouring small cells, see Figure 4.8 on page 77. Therefore, if the overload criteria is only fulfilled compared to one of the neighbouring small cells (denoted *aggressor*), then the RE of the aggressor is changed by +1 dB. This ensures that the UEs are only offloaded to the aggressor cell. The required cell RE change is signalled from the victim cell towards the aggressor cell. The aggressor cell can either acknowledge the request or Negative Acknowledge (NACK) the request. If a NACK is returned, the victim cell change its own RE bias by -1 dB.

Decrease Cell RE in Own Cell

It is also possible that a small cell is overloaded compared to multiple or all neighbour cells. If more than half of the neighbouring cells are able to offload the victim small cell, then the victim small cell lowers the cell RE value by 1 dB. This ensures that all the neighbouring small cells offload the victim small cell.

The Load Balancing Algorithm

Algorithm 5.1 describes the distributed algorithm which is executed at each small cell with periodicity t_ψ . It is assumed, that load metrics from neighbouring cells are already received. In a realistic implementation, the range of RE is limited. Yet, this is not ensured in Algorithm 5.1, as the algorithm is thought of as a proof of concept.

Algorithm 5.1 Proposed Load Balancing Algorithm

```

for all cells  $i$  do
   $N_O \leftarrow 0$  ▷  $N_O$  is the number of offload candidates
   $\omega_i = \frac{1}{\#U_i} \sum_{n \in U_i} \bar{R}_n$ 
  Forward  $\omega_i$  to neighbouring small cells
  if  $\psi_i > T_\psi$  then
    for all  $i^* \in B_i$  do ▷  $B_i$  is the set of neighbour cells
      if  $\frac{\omega_i}{\omega_{i^*}} < T_\omega$  then
         $N_O \leftarrow N_O + 1$ 
      end if
    end for
    if  $N_O > 0$  then
      if  $\frac{N_O}{\#B_i} \geq 0.5$  then ▷  $\#$  denotes the cardinality of a set
         $RE_i \leftarrow RE_i - 1$ 
      else
        for all  $i^* \in B_i$  do
          if  $\frac{\omega_i}{\omega_{i^*}} < T_\omega$  then
            Request:  $RE_{i^*} \leftarrow RE_{i^*} + 1$ 
            if NACK from  $i^*$  then
               $RE_i \leftarrow RE_i - 1$ 
            end if
          end if
        end for
      end if
    end if
  end if
end for

```

Figure 5.1 shows the involved signalling for the load balancing algorithm with one victim cell and two neighbouring small cells. First the required load information in (5.2) is shared among the small cells. Next, Algorithm 5.1 is executed. Based on the outcome, neighbouring small cells are signalled with the decision. In this example, neighbour cell 2 is requested to increase the RE by 1 dB in order to offload UEs from the victim cell. This request is either acknowledged or not by neighbouring cell 2.

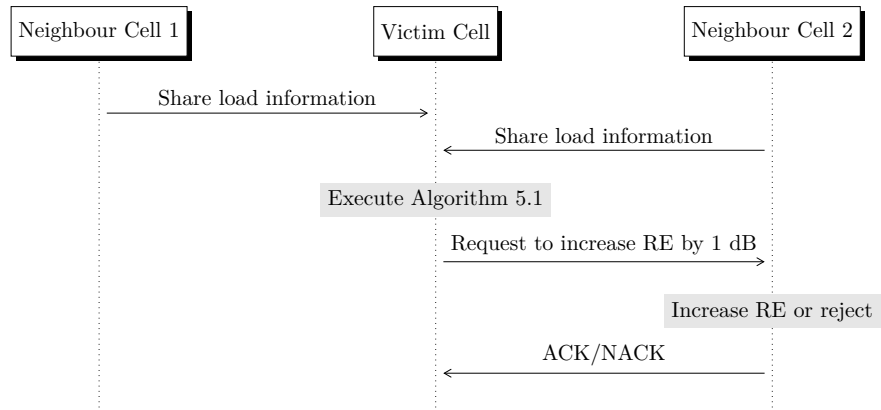


Fig. 5.1: Required signalling for increasing the RE in a single neighbouring small cell.

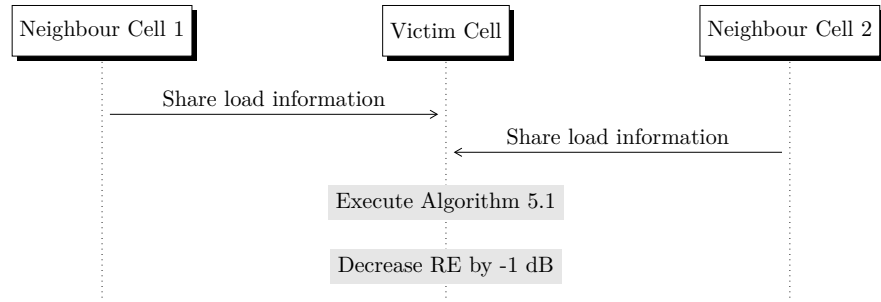


Fig. 5.2: Required signalling if the victim cell offloads UEs to all neighbour cells.

If multiple neighbour cells can accept a higher probability of user arriving, the victim cell decrease the RE by 1 dB, hence no signalling to neighbouring cells area required after Algorithm 5.1 is executed. This scenario is depicted in Figure 5.2.

5.4 Performance Evaluation

Section 5.3 describes three parameters used by the adaptive RE algorithm. Therefore, parameter sweeps are performed in order to maximise the network capacity. The overload threshold (T_ω) was swept from 1.0 to 3.0 with a step size of 0.5, resource threshold (T_ψ) was swept from 0.3 to 0.8 with a step size of 0.1, and the resource averaging time (t_ψ) was swept in the interval 0.5 to 3.0 with a step size of 0.5. Table 5.1 contains the values of the parameters which maximise the network capacity. The remaining results in this section are obtained with the optimum parameters applied.

Table 5.1: Optimum parameter configuration for the load balancing framework.

Parameter	Value	
Overload threshold (T_ω)	[-]	2
Resource threshold (T_ψ)	[-]	0.6
Resource averaging time (t_ψ)	[s]	1

In the following figures, *Baseline* results are compared against the proposed load balancing algorithm results, named *Load Balancing* in the figures. Again, baseline results corresponds to global Frequency Reuse (FR). First, figure 5.3 compares the network outage. Up to offered load of 450 Mbps, no UEs are in outage, neither for baseline nor the adaptive RE algorithm. At 550 Mbps, the baseline results show that the network outage has surpassed the allowed outage requirement, which is 5%. On the contrary, the adaptive RE algorithm reduces the network outage to 3%. Overall, the network capacity is increased approximately 2%. However, it is seen that neither of the methods support a network load larger than 550 Mbps.

Figure 5.4 illustrates the 5%-ile UE throughput performance. It is evident, that only at load 550 Mbps it is possible to distinguish the two curves from each other. The adaptive RE solution improves the 5%-ile UE throughput approximately 37%. The average and 95%-ile UE throughput improvement is not as significant though, thus the results are not included in the thesis.

The general performance improvement is achieved by a more balanced UE distribution between the small cells in the network. Figure 5.5 plots the Empirical Cumulative Density Function (ECDF) of the number of connected users per small cell and the offered load is 550 Mbps. The maximum number of connected UEs are lowered from 27 to 15 by utilising the adaptive RE framework. Moreover, the resource utilisation is increased from 72% to

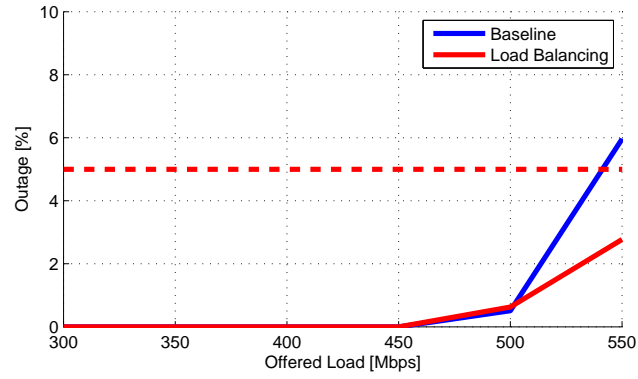


Fig. 5.3: Network outage for adaptive RE algorithm and baseline FR 1 and Open Loop Traffic Model (OLTM).

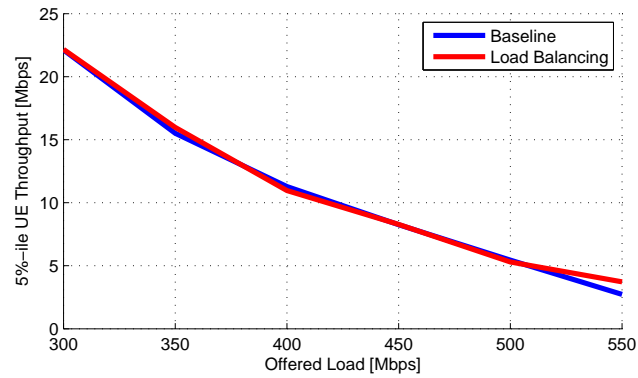


Fig. 5.4: 5%-ile UE throughput for OLTM.

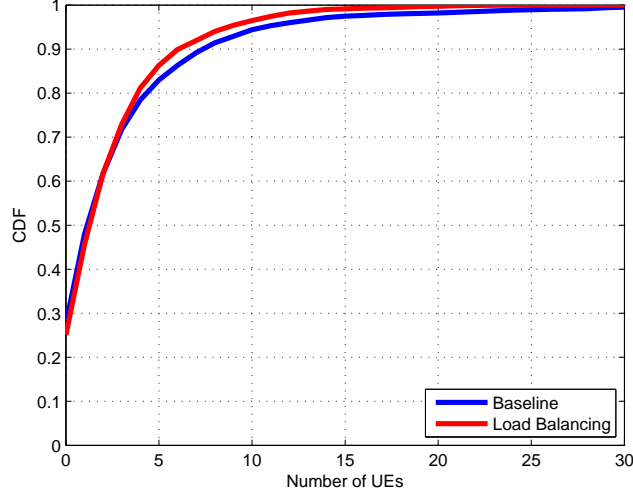


Fig. 5.5: UE distribution for baseline and adaptive RE using OLTM and the offered load is 550 Mbps.

75%, which is observed from the figure.

Figure 5.6 is included to give an overview of the number of cell RE adjustments per small cell per second. At first it is noticed that the number of *Decrease RE* changes is in general larger than the number of *Increase RE* changes. This indicates that a small cell is typically overloaded compared to the majority of its neighbours. And this is in agreement with the characteristics of a congested network. Next, it is noticed that all small cells are at some point overloaded or offloading UEs from a neighbouring small cell during the simulation time. Finally, it is noted that the relative number of changes are much less compared to the relative number of changes for the Carrier Based Inter-Cell Interference Coordination (CB-ICIC) framework presented in Figure 4.16 on page 85. This is by design/parametrisation and is explained by the fact that the load balancing is only performed every second (t_ψ) and the proposed CB-ICIC framework did carrier assignment adjustments every 0.1 second.

Finally, the performance of the load balancing algorithm under CLTM is presented in Figure 5.7. For loads where the average number of UEs per small cell is two or less, the performance of the load balancing algorithm corresponds to the baseline results. However, for increasing load the load balancing algorithm is able to improve the network capacity with approximately 10%, which is larger than the OLTM increase. Yet, the gains are still significantly smaller than the CB-ICIC gains. The UE throughput performance gains for CLTM are in the same order of magnitude as the OLTM gains presented in Figure 5.4,

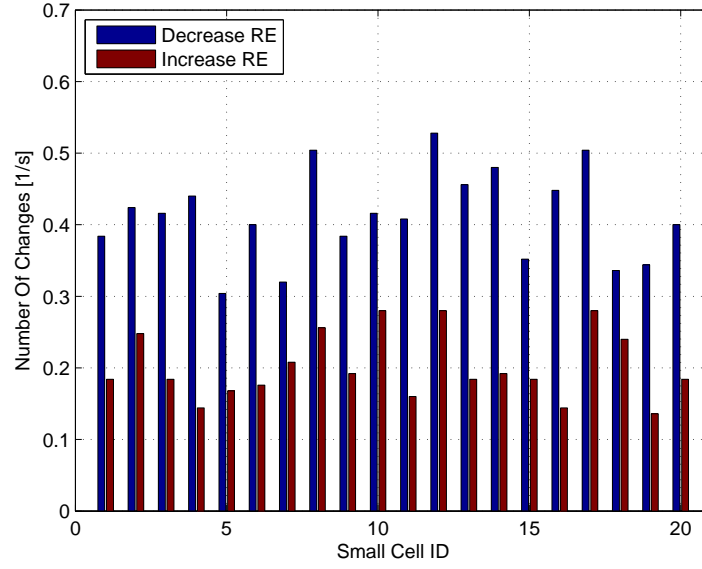


Fig. 5.6: Average small cell RE value after applying the load balancing algorithm at 550 Mbps offered load and OLTM.

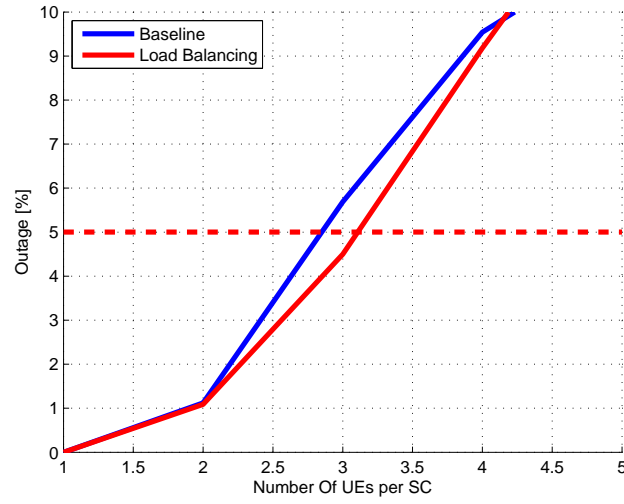


Fig. 5.7: Network outage for adaptive RE algorithm and baseline frequency reuse 1 and Closed Loop Traffic Model (CLTM).

hence they are left out for sake of brevity.

5.5 Conclusion and Discussion

The performance figures in this section have showed that it is possible to offload the most loaded small cells to the less loaded small cells. But it is also clear that the performance gain is at most marginal. Despite the relative low implementation complexity, these results do not justify realisation. However, before the adaptive RE technique is written off, the simulation assumptions and proposal should be discussed.

The current load balancing implementation only performs load balancing during connection establishment immediately after a UE is created in the network. Consequently, an overloaded small cell is not offloaded instantaneously. It is only the probability of new UEs arriving in the overloaded small cell which is reduced. Hence the offloading effect is on a long term scale. Optimally, the algorithm should identify the potential overloaded small cell, before they become overloaded and is a potential subject to further studies.

However, in real network load balancing takes place not only during the connection set up, but also during the active data session, by means of handovers or cell reselections. This is not supported in the simulator, but it is expected that this would improve the load balancing performance as the offloading is immediate. Thus, a load balancing approach should apply extended load balancing both at connection set up and during the data session.

Chapter 6

Impact of Using Advanced Receivers

Until this point in the thesis, only the baseline Minimum Mean Square Error (MMSE) receiver was considered, this is also known as the Minimum Mean Square Error - Maximum Ratio Combining (MMSE-MRC) receiver and is defined in [109]. However, as the computation power of User Equipments (UEs) increases, it enables the implementation of more advanced receiver structures, e.g. inter-cell interference aware receiver types. Consequently, the proposed Carrier Based Inter-Cell Interference Coordination (CB-ICIC) framework and advanced receiver types address the same problem without any coordination. Therefore, it is important to understand the effects of introducing the advanced receivers in networks with network based Inter-Cell Interference Coordination (ICIC) techniques. Can network based and UE based interference techniques compliment each other? Or are no additional gain achieved when combining such? Yet, it is important to note, that the investigated receiver types in this chapter are not novel and have been studied previously, see Section 6.1. But the performance of interference aware receivers and the dense small cell scenario and finite buffer traffic is not previously investigated.

6.1 Prior Art

This section summarises the prior art for UE receivers. The UE prior art is important, since a novel advanced receiver type is not proposed in this chapter. Instead the most suitable prior art receiver type is compared against the baseline receiver.

The Maximum Likelihood (ML) receiver is the optimum receiver as it minimise the

average error probability, however, the receiver complexity is currently too high for practical implementation [115–117]. Thus, a trade off in receiver performance and receiver complexity is sought. A popular approach in wireless communication is linear receiver techniques. Linear receivers estimate the desired symbol vector (\hat{x}_1) by applying an equalisation matrix (\mathbf{W}) to the received signal (\vec{y}).

$$\hat{x}_1 = \mathbf{W}\vec{y}. \quad (6.1)$$

The technique used for computing the equalisation matrix characterises each linear receiver type. One example of a linear receiver is the Zero Forcing (ZF) receiver, also known as *Decorrelator* and *Interference nulling* [116, 118]. The ZF receiver removes the effects of the transmission channel, thus removing the intra-cell interference [118]. This is achieved by applying the inverse¹ of the transmission channel to the received signal. However, the ZF does not take the noise nor inter-cell interference into account, which limits the performance of the ZF since noise and interference are potentially amplified. This is a significant limitation of the ZF receiver, thus, the ZF receiver is desirable in scenarios where the intra-cell interference is dominant over Additive White Gaussian Noise (AWGN) and inter-cell interference.

On the contrary to the ZF receiver, the Maximum Ratio Combining (MRC) receiver preserves the received energy and maximises the Signal to Noise Ratio (SNR) at the cost of potentially high intra-cell interference [116, 118, 120]. In practice, the Hermitian transpose of the channel estimate is applied to the received signal. Consequently, in low SNR region the MRC receiver performance is superior to the ZF receiver, due to the maximisation of the SNR. However, in high SNR region and in the presence of intra-cell interference, the MRC receiver performances worse compared to the ZF receiver [118, Section 8.3.3].

It is clear that MRC and ZF receiver represent two extremes. When noise is dominant over intra-cell interference the MRC receiver is preferred and vice versa. Therefore, the MRC receiver has been defined as a baseline receiver in Long Term Evolution (LTE) [109] for rank 1 transmissions where no intra-cell interference is present. Nevertheless, a more versatile receiver type is preferred.

A popular choice in linear receiver structure is the MMSE receiver [115, 116, 118]. In [118, Figure 8.15] the performance of the ZF, the MRC, and the MMSE receiver is compared. It is clear the MMSE receiver is preferred as it outperforms the other two over the entire SNR range. The generalised MMSE equalisation matrix \mathbf{W}_{MMSE} is expressed as:

$$\mathbf{W}_{MMSE} = \hat{\mathbf{H}}_1^H \mathbf{R}_{MMSE}^{-1} \quad (6.2)$$

where $\hat{\mathbf{H}}_1$ is an estimate of the effective transmission channel, \mathbf{R}_{MMSE} is the MMSE covariance matrix, $(\cdot)^H$ denotes the Hermitian transpose of a matrix, and $(\cdot)^{-1}$ denotes the inverse of a matrix. The interested reader is referred to Appendix G where the generic

¹If $\hat{\mathbf{H}}_1$ is not invertible, the Moore-Penrose inverse is applied instead [118, 119]

MMSE solution is derived, see (G.16).

Typically, the covariance matrix is constructed only using the transmission channel estimate and a noise estimate and the receiver is simply denoted MMSE or MMSE-MRC, see Section 6.3.1. However, if the covariance matrix includes interfering channel estimates, the receiver is capable of suppressing inter-cell interference, see Section 6.3.2. This receiver type is also known as the Interference Rejection Combining (IRC) receiver or Minimum Mean Square Error - Interference Rejection Combining (MMSE-IRC). The terms IRC and MMSE-IRC are used interchangeably in the remainder of this thesis. The concept of the IRC receiver was first proposed in [121] and it is shown that it maximises the Signal to Interference and Noise Ratio (SINR) after combining the received signals. The number of receive antennas is an important factor when it comes to the performance of the MMSE-IRC receiver. If the transmission rank equals the number of receive antennas, no inter-cell interference can be rejected, since all receive antennas are needed for decoding the transmitted symbol stream(s). If the transmission rank is lower than the number of receive antennas, the degree of freedom at the receiver is sufficient for suppression inter-cell interference.

However, the MMSE-IRC receiver introduces the challenge of estimating interfering channels. To ease this task in practice, 3rd Generation Partnership Project (3GPP) introduced User Equipment Specific Reference Signal (UE-RS) - also known as Demodulation Reference Signal (DMRS) - in LTE Release 10. Prior to UE-RS, an UE required knowledge of the interfering channel **and** the UE specific precoding. By utilising UE-RS, UEs are able to estimate the *effective* interfering channel estimate, which includes the precoding effects [122, 123]. The LTE Release 8 and Release 10 signalling concepts are described in Appendix H. Apart from the UE-RS estimation approach, the 3GPP also defines a data based and a Cell-specific Reference Signal (CRS) based approach [109, Section 4.3]. The UE throughput performance of the UE-RS and data based schemes is investigated in [124–126]. The authors conclude that only MMSE-IRC combined with the UE-RS based scheme constantly outperforms the MMSE-MRC. Moreover, [127, Section 12.3] reports up to 2 dB SINR gain utilising the UE-RS based MMSE-IRC receiver over MMSE receiver which is in accordance with the previous reported gains.

Finally, a word on Interference Cancellation (IC) receivers [115, 116, 118]. The approach of the IC receiver is to decode interfering symbols followed by reconstruction of the interfering signal. The reconstructed interference signal is subtracted from the received signal, and thereby obtaining an improved SINR for the desired signal. The process of decoding, reconstructing, and subtracting interfering signals is potentially performed multiple times before the desired symbol is decoded. However, the task of decoding and reconstructing the interfering signals is not trivial, as it requires knowledge of the interfering transmission(s). In fact, 3GPP started work on Network Assisted Interference Cancellation and Suppression (NAICS) [128], however this concept is out of the scope of this thesis.

6.2 System Model

In the Downlink (DL) system model we assume a UE with N_{Rx} receive antennas and N_{BS} enhanced Node Bs (eNBs) with N_{Tx} transmit antennas. Consequently, the number of streams (N_S) supported by the network² is up to $\min(N_{Tx}, N_{Rx})$. In vector form the $N_{Rx} \times 1$ received signal vector ($\vec{y}(m, l)$) for the m -th sub-carrier at time l is described as:

$$\begin{aligned} \vec{y}(m, l) = & \sqrt{P_{Tx,1}(m, l)} \cdot \mathbf{H}_1(m, l) \mathbf{C}_1(m, l) \vec{x}_1(m, l) \\ & + \sum_{i=2}^{N_{BS}} \sqrt{P_{Tx,i}(m, l)} \cdot \mathbf{H}_i(m, l) \mathbf{C}_i(m, l) \vec{x}_i(m, l) + \vec{n}(m, l) \end{aligned} \quad (6.3)$$

where

- $P_{Tx,i}(m, l)$ is the i -th small cell transmission power at sub-carrier m at time l [1×1]
- \mathbf{H}_1 is the channel matrix between the serving eNB and UE [$N_{Rx} \times N_{Tx}$]
- \mathbf{C}_1 is the pre-coding matrix [$N_{Tx} \times N_S$]
- \vec{x}_1 is the desired symbol vector [$N_S \times 1$]
- \mathbf{H}_i is the channel matrix between the interfering eNB i and UE [$N_{Rx} \times N_{Tx}$]
- \mathbf{C}_i is the pre-coding matrix at eNB i [$N_{Tx} \times N_S$]
- \vec{x}_i is the interfering symbol vector from eNB i [$N_S \times 1$]
- \vec{n} is the AWGN vector with variance σ_0^2 [$N_{Rx} \times 1$].

In order to simplify equation (6.3), the $N_{Rx} \times N_S$ effective channel matrix ($\tilde{\mathbf{H}}$) between transmitter and receiver is defined:

$$\tilde{\mathbf{H}} = \mathbf{H}\mathbf{C}. \quad (6.4)$$

Furthermore, the subcarrier index and time index are left out for sake of simplicity. Combining (6.3) and (6.4) yields

$$\vec{y} = \sqrt{P_{Tx,1}} \cdot \tilde{\mathbf{H}}_1 \vec{x}_1 + \sum_{i=2}^{N_{BS}} \sqrt{P_{Tx,i}} \cdot \tilde{\mathbf{H}}_i \vec{x}_i + \vec{n}. \quad (6.5)$$

6.2.1 Precoding In LTE

As expressed in (6.4), the desired data stream is precoded with precode matrix \mathbf{C} . A precode matrix is applied at the transmitter side, in order to improve the channel quality by exploiting Channel State Information (CSI). E.g. if a UE experience low SNR the transmitted signal can be directed in the direction of the UE or in case of multi stream transmission the SINR can be improved by reducing the inter-stream interference. If full

²Known as the system transmission rank.

CSI is known at both transmit and receiver side, the Multiple Input and Multiple Output (MIMO) capacity can be achieved by Singular Value Decomposition (SVD) of the channel matrix and optimal power allocation [129, 130]. However, the requirement of full CSI at the transmitter side is not suitable for a practical communication system, as this requires a vast amount of feedback from the receiver to the transmitter. In LTE, a limited number of known precoder matrices are pre-defined [131]. Based on CSI, the optimum precoder matrix is determined at the receiver side and the Pre-code Matrix Indicator (PMI) is signalled to transmitter. Thereby, the amount of required feedback is reduced to potentially a few bits. Obviously, the quantification of the precoder matrix reduces the channel capacity and depends on the size of the precoding codebook [132]. This process corresponds to LTE transmission mode 4 [131], which is also used in all simulations. Finally, rank adaptation is performed according to the proposed method in [108].

6.3 Considered Receiver Structures

This section describes the receiver structures considered in this PhD thesis. Further information on the MMSE receiver structure is found in Appendix G.

6.3.1 The Baseline MMSE Receiver

The MMSE-MRC receiver type is considered the baseline receiver in this thesis. This receiver is capable of suppressing intra-cell interference while the noise is also taken into account. However, inter-cell interference is treated as noise. The benefit of this solution is simplicity, as no interfering channel estimates are required. The drawback however, is limited performance in case of strong inter-cell interference. The baseline MMSE-MRC receiver is characterised by the $N_S \times N_{Rx}$ equalisation matrix $\mathbf{W}_{MMSE-MRC}$ expressed as:

$$\mathbf{W}_{MMSE-MRC} = \hat{\mathbf{H}}_1^H \mathbf{R}_{MMSE-MRC}^{-1}. \quad (6.6)$$

The $N_{Rx} \times N_{Rx}$ covariance matrix is defined as:

$$\mathbf{R}_{MMSE-MRC} = P_{Tx,1} \cdot \hat{\mathbf{H}}_1 \hat{\mathbf{H}}_1^H + \text{diag} \left(\sum_{i=2}^{N_{BS}} P_{Tx,i} \cdot \hat{\mathbf{H}}_i \hat{\mathbf{H}}_i^H \right) + \sigma_0^2 \mathbf{I}. \quad (6.7)$$

From (6.6) and (6.7) it is noted that the computation of the equalisation matrix only requires estimates of the transmission channel, the power of the noise, and the interference power at each receive antenna.

6.3.2 The Advanced MMSE-IRC Receiver

The MMSE-IRC covariance matrix includes the estimates of the interfering channel matrices, between the UE and interfering eNBs. The result is that the MMSE-IRC receiver

is inter-cell interference aware. For the MMSE-IRC receiver the $N_S \times N_{Rx}$ covariance matrix $\mathbf{R}_{MMSE-IRC}$ is defined as:

$$\mathbf{R}_{MMSE-IRC} = P_{Tx,1} \cdot \hat{\mathbf{H}}_1 \hat{\mathbf{H}}_1^H + \sum_{i=2}^{N_{BS}} P_{Tx,i} \cdot \hat{\mathbf{H}}_i \hat{\mathbf{H}}_i^H + \sigma_0^2 \mathbf{I} \quad (6.8)$$

where the $N_S \times N_{Rx}$ MMSE-IRC equalisation matrix $\mathbf{W}_{MMSE-IRC}$ is computed as:

$$\mathbf{W}_{MMSE-IRC} = \hat{\mathbf{H}}_1^H \mathbf{R}_{MMSE-IRC}^{-1}. \quad (6.9)$$

From (6.8) it is clear that the sum of all interfering effective channel estimates is needed. This challenge is eased by the introduction of UE-RS in LTE Release 10, see Appendix H.

In this thesis, the serving cell transmission channel estimation method is realistic [123], however, for all MMSE-IRC simulations, ideal channel estimation of the effective interfering channels is assumed. Compared to ideal interfering channel estimation, the UE-RS based estimation method is approximately 5% worse according to [125].

6.4 Performance Evaluation

This section presents the different advanced UE simulation cases. The simulations are split into three sections; baseline, four receive antennas, and network ICIC solution in combination with advanced UE receivers. All simulation assumptions are in agreement with Table 4.4 in Section 4.5.4.

6.4.1 Baseline Scenario

In this section, the baseline scenario combined with the MMSE-MRC and the MMSE-IRC receiver is presented. Baseline indicates that global Frequency Reuse (FR) is applied. It is noted that the MMSE-MRC results correspond to the baseline results in Chapter 4 and Chapter 5. To avoid confusion, the MMSE-MRC are also named *Baseline* in this chapter. The MMSE-IRC results are named *Baseline-IRC*.

Figure 6.1 shows the 5%-ile UE throughput performance for the MMSE-MRC and MMSE-IRC. The MMSE-IRC gain is written above the bars for each traffic load. It is clear, that the MMSE-IRC performance is superior. At high load, the gain is 265%, which is considerable higher than the gains reported in [124, 133]. Compared to [133], the increased MMSE-IRC gain is explained by the traffic model. When using the Open Loop Traffic Model (OLTM) the MMSE-IRC gain is two-fold: First of all, the MMSE-IRC improves the spectral efficiency and thereby also the UE throughput by suppressing inter-cell interference. Secondly, the increased UE throughput results in decreased UE session time. Thus, more resources are available for the remaining UEs at the serving cell, or less interference are caused to the surrounding UEs.

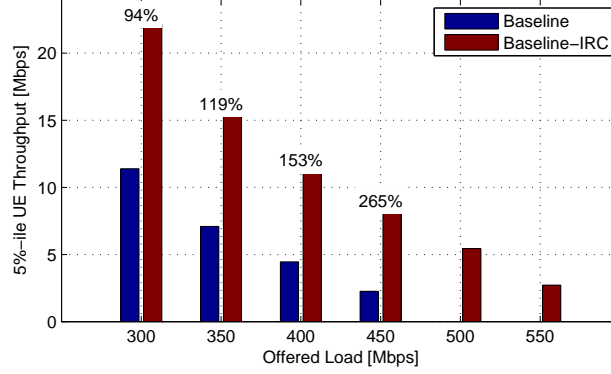


Fig. 6.1: 5%-ile UE throughput performance. The number above the bars denote the MMSE-IRC receiver gain.

Compared to [124] the main difference is the simulation scenario. Based on the performance results, it is implied that the MMSE-IRC potential for dense small cell scenarios is larger than for homogeneous macro-only deployments. The explanation for this is a stronger dominant interferer in the small cell scenario, which is suppressed by the MMSE-IRC receiver. Figure 6.2 compares the Dominant Interference Ratio (DIR) for several 3GPP scenarios and a site specific urban network. It is clear that the DIR is higher for the small cell scenario compared to the other 3GPP scenarios. The DIR in the dense small cell scenario is similar to the DIR experienced in the realistic outdoor small cell network. The SINR improvement after suppressing or muting the Dominant Interferer (DI) was shown in (4.29) on page 70.

Figure 6.3 illustrates the average UE throughput performance. The trends are similar to the 5%-ile UE throughput gain; the MMSE-IRC gain is increasing with the traffic load. Though, the relative MMSE-IRC gains are smaller than the 5%-ile gains. This is expected as the experienced interference for an average UE is smaller than for a 5%-ile UE. However, it is stressed that the mean UE throughput gains are in the range of 27% to 110%, which is still a substantial improvement. Also, the 95%-ile UE throughput is increased, here the MMSE-IRC gain is in the range from 3% to 61%. Though, this is not shown explicit in a figure for sake of brevity. Similar to the 5%-ile case, the mean UE throughput gains are larger than the gains reported in [124].

The general trend, regarding UE throughput performance, is that the MMSE-IRC gain is largest for the 5%-ile UEs since they experience more inter-cell interference from neighbouring small cells. Moreover, the MMSE-IRC gain increases with the traffic load as expected, since the probability of strong inter-cell interference is low at low load. Both of these general observations are expected, and are also in line with previous MMSE-IRC studies.

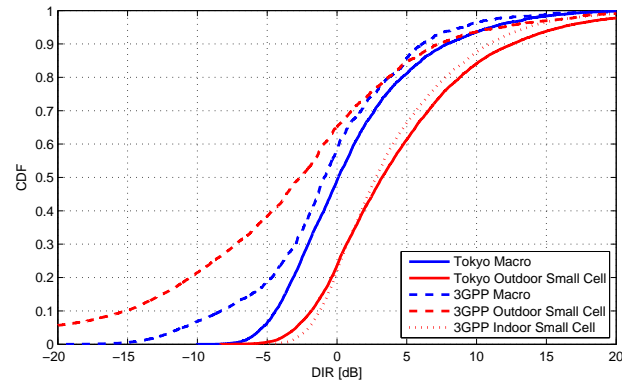


Fig. 6.2: DIR experienced in various 3GPP networks and a site specific network [6].

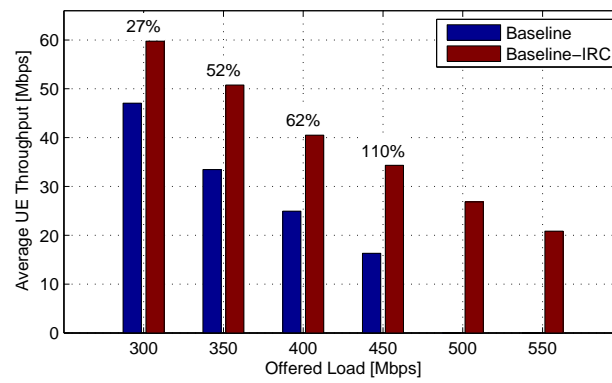


Fig. 6.3: Average UE throughput performance. The MMSE-IRC gain in percent is shown for each of the traffic loads.

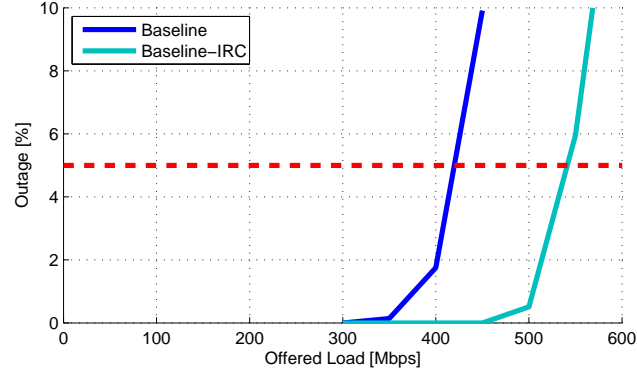


Fig. 6.4: Outage performance of MMSE-MRC receiver and MMSE-IRC receiver. The dashed red line denotes the maximum allowed outage.

Figure 6.4 shows the network outage versus offered load. As expected, the MMSE-IRC receiver is also superior to the MMSE-MRC receiver in terms of network outage. Additionally, the network capacity increases from 420 Mbps to 540 Mbps (+28%). In fact, the achieved gain is larger than the CB-ICIC gain of 21% reported in Figure 4.13 on page 82.

In Figure 6.5, the rank 2 transmission ratio and the SINR improvement for MMSE-MRC and MMSE-IRC receiver at traffic load 450 Mbps is presented. Both metrics are important to understand the full potential of the MMSE-IRC receiver. Figure 6.5a illustrates the Cumulative Distribution Function (CDF) of the rank 2 ratio for each UE. Most remarkable is that all UEs have been scheduled for rank 1 transmission (no vertical line at *Rank 2 Ratio* = 1). In theory, this means that all UEs have gained from the interference rejection capabilities of the MMSE-IRC receiver, also the UEs in high SINR region. Next, it is observed that the rank 2 transmission ratio is increased for the MMSE-IRC receiver compared to the MMSE-MRC receiver, i.e. the MMSE-IRC curve is shifted right. This indicates that the SINR is improved for the MMSE-IRC case.

A similar trend is observed in Figure 6.5b. Here it is seen that the SINR CDF is approximately improved 5 dB due to the MMSE-IRC receiver. This result is remarkable as the MMSE-IRC is capable of increasing both the rank 2 transmission ratio and the SINR per stream. Typically, the SINR for rank 2 transmissions is lower compared to the SINR for rank 1 transmission, as the transmission power is allocated to two streams. However, the gain is not solely a result of the inter-cell interference awareness of the MMSE-IRC receiver. Part of the SINR gain is caused by the fact that the UEs finish their session faster, thus, causing less interference towards neighbouring UEs. E.g. at offered load 450 Mbps, the resource utilisation is reduced from 77% to 51% when the MMSE-IRC receiver is introduced, which clearly indicates that the UEs leave the network faster.

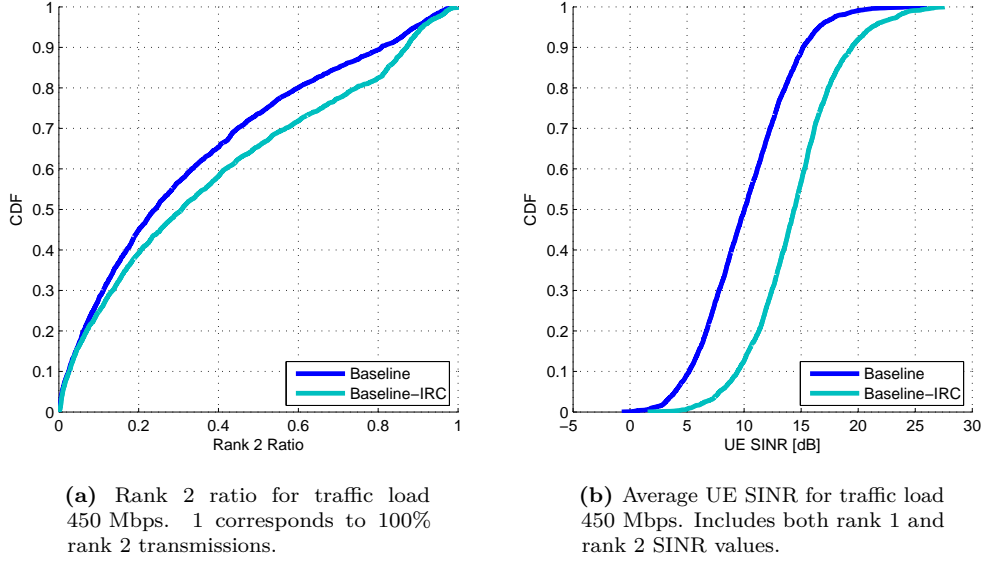


Fig. 6.5: Rank 2 performance and UE SINR for traffic load 450 Mbps.

6.4.2 Four Receive Antenna Scenario

The new spectrum allocations at 3.5 GHz enable the implementation of smaller antennas in the handsets. Therefore, a logical next step from the current 2×2 antenna configuration is 2×4 antenna configurations. Apart from the increased receive diversity, this also enables the MMSE-IRC receiver to reject at least 2 interfering inter-cell interfering streams at all times, since the maximum system rank is 2. Only the number of receive antennas is changed in this section, all other simulation assumptions are according to Table 4.4 in Section 4.5.4. Simulation results for MMSE-MRC receiver and four receive antennas are denoted *Baseline-4Rx* and MMSE-IRC with four receive antennas are denoted *Baseline-4Rx-IRC*.

Figure 6.6 presents the outage performance of the MMSE-MRC and the MMSE-IRC, for two and four receive antennas. The two antenna results were already presented in Figure 6.4 but are included to ease the comparison for the reader. It is seen that four receive antennas improve the network capacity 60% and 75% for the MMSE-MRC receiver and the MMSE-IRC receiver, respectively. The reasons are increased receive diversity and received power. Furthermore, for four receive antennas the MMSE-IRC network capacity gain is 40% (from 675 Mbps to 950 Mbps). For two receive antennas the MMSE-IRC gain was only 28%. This indicates that the advantage of the MMSE-IRC receiver increases with the number of receive antennas, as more interferers can be rejected.

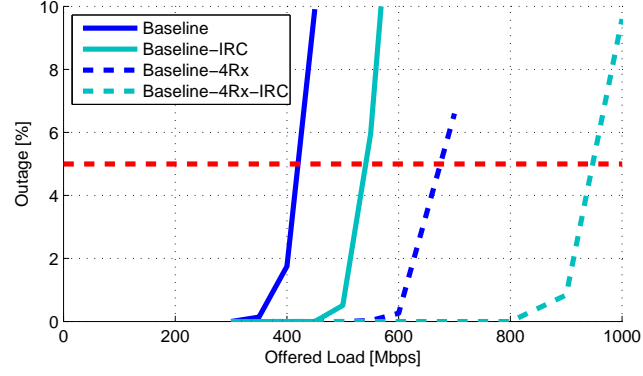


Fig. 6.6: Network outage performance with four receive antennas. The dashed red line denotes the outage requirement. The solid curves are included for comparison purposes and denote the two receive antenna configuration from Figure 6.4.

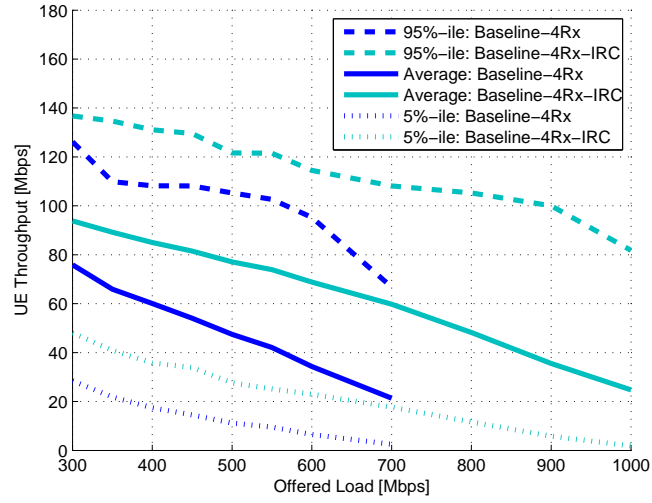


Fig. 6.7: UE throughput performance for MMSE-MRC and MMSE-IRC with four receive antennas.

In Figure 6.7 the 5%-ile, the average, and the 95%-ile UE throughput performance are plotted. It is clear that the MMSE-IRC receiver improves the UE throughput for all UEs. The relative improvement is largest for the 5%-ile UEs and is increasing with the offered traffic. The absolute 5%-ile improvement is approximately 20 Mbps for offered loads in the range from 300 Mbps to 700 Mbps.

6.5 Network ICIC Techniques and Advanced UE Receivers

In this section, the combination of network based and UE based ICIC techniques are studied. This is important as there is no coordination between the two approaches. Thus, one of the techniques could prove redundant. In Figure 6.8 and Figure 6.9, the combination of the proposed CB-ICIC scheme and the MMSE-IRC receiver is named *CBICIC-IRC*. The naming of previously presented results are not changed.

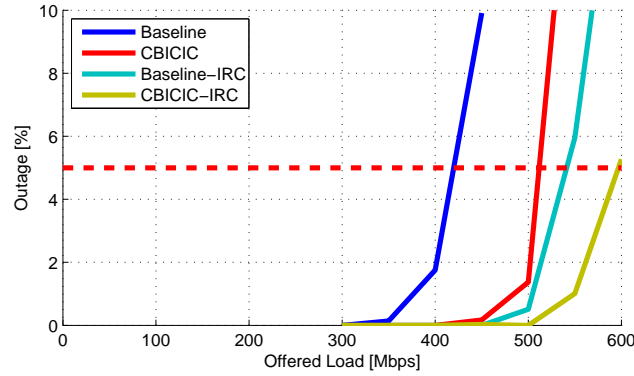


Fig. 6.8: Network outage when combining CB-ICIC and MMSE-IRC receiver for open loop traffic model.

Figure 6.8 shows the network outage for a combination of the proposed CB-ICIC framework and the MMSE-IRC receiver with two receive antennas. The results from Figure 6.4 are included for ease of comparison. First of all, it is clear that a combination of the two approaches further increases the network capacity. The network capacity increases from 540 Mbps to 600 Mbps (11%), which is less than for the MMSE-MRC receiver where a CB-ICIC gain of 21% was observed, see Figure 4.13 on page 82. The main reason for this is that the MMSE-IRC receiver reduce the resource utilisation (load) of the network. Thus, the number of interfering small cell is lowered, and so is the number of valid hypotheses. Furthermore, the MMSE-IRC receiver reduces the impact of the interference, thus, the potential of the CB-ICIC is reduced accordingly.

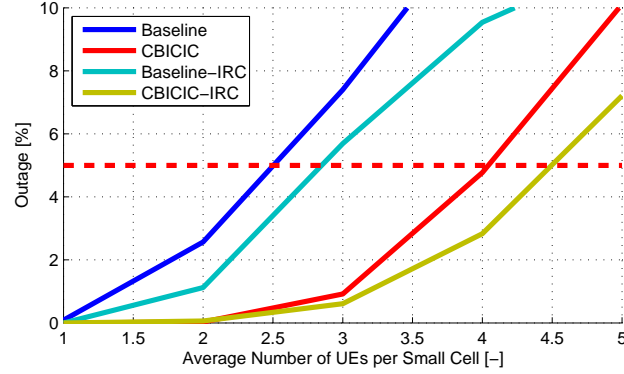


Fig. 6.9: Network outage when combining CB-ICIC and MMSE-IRC receiver and using closed loop traffic model.

A combination of advanced receivers and the CB-ICIC framework is also simulated using the Closed Loop Traffic Model (CLTM), the resulting network outage result is illustrated in Figure 6.9. The CB-ICIC gain for MMSE-IRC is almost as large as the CB-ICIC gain for MMSE-MRC, which is due to the traffic model. Whenever a UE completes a session and is removed from the network, a new UE is generated. This ensures that the resource utilisation is higher compared to the OLTM, and in return the number of valid hypotheses is not effected as much.

6.6 Overview of Network and UE Combinations

This section summarises all the network capacity results presented in Chapter 4, Chapter 5, and this chapter. The objective is to give the reader the opportunity to easily compare the potential of each of the presented ICIC solutions. Figure 6.10 shows the network capacity gain for various combinations of the network and UE based ICIC solutions. Not all the capacity gain numbers are explicitly presented previously. The network capacity gain is shown for both the OLTM and the CLTM, respectively.

In short, the CB-ICIC framework, IRC receivers, four receive antennas, or a combination of these techniques shows great potential for increasing the network capacity. By combining all of the aforementioned techniques and depending on the traffic model the network capacity gain is in the range from 140% to 190%. As mentioned previously, the traffic in a real network is not described entirely by a single traffic model. Consequently, the gains in a real network is expected to be within the gains shown for the OLTM and the CLTM.

Generally speaking, the CB-ICIC solution produces the largest gains for the CLTM. The reason is that the overall network utilisation is larger for the CLTM when the network

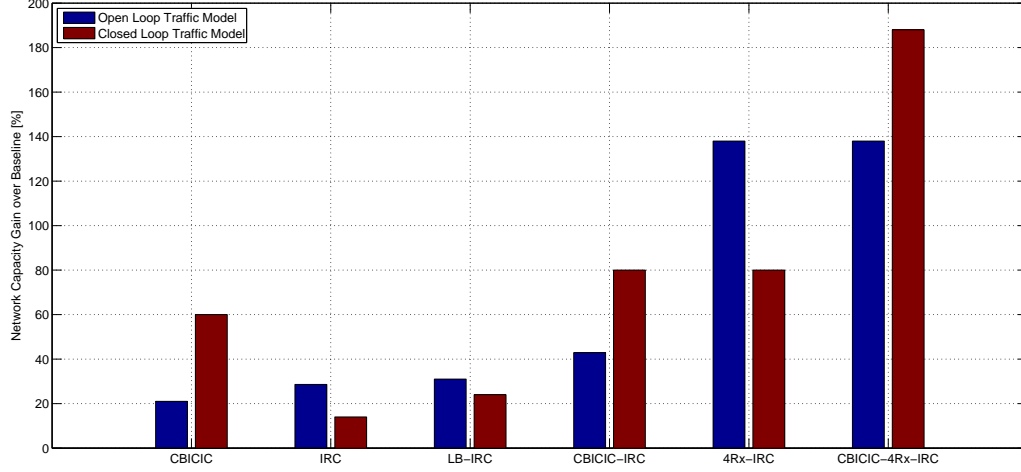


Fig. 6.10: Capacity gain overview of the network and UE based ICIC solutions.

is about to overload. This means the interference is more severe, thus, the gain of coordinating the interference is larger. Moreover, the figure shows that the potential gain of the proposed load balancing algorithm is only marginal.

By combining IRC receivers and the proposed CB-ICIC framework, the outcome is further improvements over the individual solutions, even though there is no coordination of the solutions. Furthermore, the introduction of four receive antennas is shown to significantly improve the network capacity performance for CLTM. On the other hand, the CB-ICIC improvement is neglectable for four receive antennas when the traffic model is OLTM.

6.7 Conclusion and Discussion

In this chapter it has been shown that the MMSE-IRC receiver can significantly improve the UE throughput and decrease network outage. Moreover, the potential of the MMSE-IRC is larger in dense small cell environments compared to the homogeneous macro-only scenario, since the DIR is typically larger in the small cell environment. However, the MMSE-IRC gain requires that the network and UE support UE-RS to exploit the full potential. Finally, it is shown that a combination of the proposed CB-ICIC framework from Chapter 4 and the MMSE-IRC receiver produces promising performance results. Again, it is noted that ideal interfering channel estimation is assumed, and that the overhead of UE-RS is not considered. Thus, the MMSE-IRC performance in this thesis is upper bound.

The combination of UE based and network based ICIC techniques is very interesting and of high importance. It is shown that the advanced UE receiver reduces the network based ICIC gain. Both techniques mitigate the inter-cell interference, without coordinating which interferer to mitigate. The coordination of network based and UE based ICIC techniques is left for future work studies. Recently, coordination between UE and network based ICIC have been addressed by 3GPP and a NAICS work item was approved [134]. The concept is to provide knowledge of the interfering transmissions to the UEs. The specific information required depends on the receiver structure, [128] supplies an overview of the considered receiver structures. The work is still ongoing, and no conclusion has been drawn at this point. However, first results shows promising improvement over the MMSE-IRC receiver [135].

Chapter 7

Conclusion

This PhD project treats the challenges and enabling solutions for indoor small cell deployment. This topic is of high importance as current mobile traffic predictions foresee immense mobile traffic growth in the years to come. Thus, mobile network operators are looking for efficient solutions to cope with future traffic volumes. Deployment of indoor small cells are considered a promising solution to boost indoor coverage and improve the network capacity in confined areas with high traffic load. However, before allowing mass deployment of indoor small cells, potential pitfalls must be analysed thoroughly. This chapter concludes on the main findings in the PhD project and provides recommendations for indoor small cell deployment. Finally, directions for future work in this area are given.

7.1 Main Findings

Comprehensive measurement campaigns are carried out in order to verify and develop simulation models. The indoor ITU-R propagation model is verified and an urban outdoor micro propagation model is proposed. Furthermore, a HSPA co-channel macro and femto measurement campaign is performed to reveal critical femto interference issues. In DL direction the interference issues are modest, as long as the macro users are located outside the femto building. The macro UE only experiences a throughput degradation if located right next to rooms with the indoor femto. The increased building penetration loss of modern buildings helps isolate the femto cells from macro cells and vice versa. However in UL, measurements revealed that without proper femto UE power capping, nearby macro cells could experience significant noise rise, up to 6 dB is measured. Therefore, a self provisioning QoS aware femto power control algorithm is developed to minimise the DL and UL femto interference towards the macro layer. The femto power control algorithm

excels by protecting the surrounding macro cell and nearby macro users, and at the same time the femto users are provided with the agreed QoS. Vital concepts of the femto power control algorithm are verified by measurements.

Measurement results from a IEEE 802.11g WiFi and HSPA femto trial show that WiFi is the preferred technology from an end users point of view. WiFi offers higher DL and UL throughput rates, primarily due to the larger transmission bandwidth. However, the main differentiator is the femto compromise in terms of UE power consumption and latency performance. HSPA femtos can not be competitive in both, due to complex HSPA RRC state processes.

A LTE network evolution study, carried out for a realistic network deployment in a European metropolis, showed that neither coordinated nor uncoordinated femto deployment provided the lowest TCO for short-term network evolution. For short-term traffic growth, deployment of outdoor pico cells on a dedicated carrier is the most TCO efficient. However, this solution is not as scalable as indoor femto deployment. Thus, for medium and long-term traffic growth, the uncoordinated femto deployment performs the best in terms of TCO. Indoor femto cell deployment offers the most efficient indoor macro offloading, this is very important as the indoor UEs are the most challenging. In the high traffic growth scenario, the indoor femto cells serve approximately 80% of the UEs. Simulation results also reveal, that a 50% TCO reduction is achieved if the femto cells are deployed on a dedicated femto carrier. The reason is that the femto coverage area in a co-channel deployment is reduced due to the coexistence with macro and pico cells, thus, co-channel femto deployment requires a considerable higher femto density.

Considering the mobile traffic growth predictions, the conclusion is straightforward; uncoordinated deployment of femto cells on a dedicated carrier is preferred network evolution option. It is scalable, and delivers the lowest TCO and the highest end user throughputs. For a traffic growth of x100 compared to the 2011 traffic volumes, a femto deployment rate of 20% is required, or approximately 1700 femto access point per square kilometre in a dense urban European metropolis environment.

The uncoordinated deployment of OSG LTE femto cells (small cells in general) on a dedicated carrier scenario is investigated further. Typically, the overall network performance is limited by a single or few small cells which are overloaded. Therefore, a novel and QoS aware CB-ICIC framework is proposed. The objective is to maximise the network capacity subject to a certain QoS. The reactive framework is triggered if a user is not fulfilling the QoS. The net benefit of all hypothetical improvements are computed, and the hypothesis with largest net benefit is carried out. The net benefit is computed based on network metrics and UE measurements. For low traffic load scenarios, the framework configures the network as frequency reuse 1. The probability of strong inter-cell interference is low, thus, best network performance is achieved if all small cells utilise the full spectrum. With increasing traffic load, the probability of strong inter-cell interference also increase, thus, users experience reduced throughput rates. If an user experiences throughputs lower than the agreed QoS, then the serving cell can either increase the number of active component

carriers, or neighbouring cells can mute transmission on one or more of the interfering component carriers.

Simulation results show that the developed CB-ICIC framework increases the network capacity between 20% and 60% depending on traffic model assumption. Both the 5%-ile and 50%-ile UE throughput improves by using the CB-ICIC framework. In general, the CB-ICIC gain is largest for high traffic loads, where the inter-cell interference is most severe. At low load, only marginal CB-ICIC gain is observed as the inter-cell interference is low. No simulation results show reduced network performance with the CB-ICIC framework compared to frequency reuse 1.

In the dense small cell environment, large dominant interferer ratios are observed compared to the macro only scenario. Hence, the potential performance gain of the inter-cell interference aware IRC receiver is promising for dense small cell network. Performance results of the IRC receiver show that the network capacity is increased up to 30% compared to the baseline MMSE receiver. More interesting is the combination of CB-ICIC and IRC receivers. Results show that the combined gain is in the range of 40% to 80%. Finally, the number of receive antennas is increased from two to four, and with IRC receiver and CB-ICIC, the overall network capacity increases in the order of 140% to 190%. Overall, the IRC offers considerable performance gain compared to the MMSE receiver in terms of network capacity and UE throughput performance.

A load balancing algorithm is also proposed. The individual cell range extension is adjusted according to the user load in neighbouring cell pairs. When an overloaded cell is detected, the range extension is adjusted, such that the coverage area of the overloaded cell is reduced, and the neighbouring cells are implicit expanding their coverage area. However, the gain of the proposed framework is only marginal. The main reason is that the framework is too slow reacting. The cell range extension is not adjusted until a cell is overloaded, and at this point it is already too late. Only new arriving UEs are offloaded to the neighbouring cells, the already connected UEs keep being connected to the overloaded cell.

7.2 Recommendations

Before providing pointers for future work, small cell deployment recommendations are given in the light of the main findings of the PhD project. The main findings of the project are summarised in these five general small cell deployment recommendations.

Long-Term Network Evolution Strategy - Deployment of indoor small cells proved to be a key in providing a scalable solution to accommodate future traffic volumes.

Dedicated Small Cell Carrier - In general, deployment of small cells on a dedicated carrier is recommended. Dedicated carrier deployment improves the macro offloading significantly and lessen the requirements to small cell deployment densities.

Uncoordinated Indoor Small Cell Deployment - Uncoordinated small cell deployment is generally speaking more efficient in terms of network TCO. Yet, the difference is minor compared to coordinated small cell deployment, and the most suitable option could be dictated by the scenario. E.g. coordinated deployment is most likely the preferred in public areas.

Advanced UEs - Advanced UEs improve the overall network performance significantly, both in terms of experienced UE throughput and reduced network load. Moreover, advanced UEs delay the need for network based ICIC solutions.

Network Based ICIC - Network based ICIC techniques in the carrier domain, such as the proposed CB-ICIC framework, can improve the network capacity substantial. Even with a majority of advanced UEs in the network the potential gain is considerable. At low traffic volumes the gain is marginal, the gain of the CB-ICIC solutions increases with the femto density and the traffic volumes.

7.3 Future Work

This final section, is dedicated to inspire the reader for future indoor small cell work. A non-exhaustive list is provided, it includes work topics which carry on the work presented in this thesis accompanied by topics which are otherwise out of the scope of this thesis.

Measurements showed that WiFi delivers the best end user experience. However, considering that HSPA and IEEE 802.11g both have been superseded by LTE and IEEE 802.11n/ac, new measurements would reveal which of the technologies have improved the most. Especially, the simpler architecture of LTE and reduced complexity of the RRC states and transitions could prove a significant improvement for the femto technology. This is also required to bring the experienced femto performance on par with the experienced WiFi performance.

Even with the small cell deployment advances presented in this thesis, it is possible to improve the indoor small cell performance further. The CB-ICIC framework presented in Chapter 4 is designed for baseline MMSE receivers. If this is compensated, it is expected that the combined performance of CB-ICIC and IRC UEs can be further improved. Furthermore, the typical macro cell and small cell co-channel deployment scenario is deliberately ignored in the design of the CB-ICIC framework because of relative high TCO and existing, dedicated 3GPP techniques such as eICIC. However, the CB-ICIC framework could be extended to this scenario, if network operators do not have dedicated small cell spectrum available.

The proposed load balancing algorithm only showed marginal performance gain. In this thesis the load balancing mechanisms were only applied during establishment of the connection, however, future work must include active mode load balancing, e.g. load

triggered handovers.

The next leap within ICIC could be provided by NAICS receivers, which have experienced an increasing interest in standardisation bodies lately. Hence, the NAICS concept has become part of LTE Release 12. In the NAICS concept the network based and receiver side based ICIC techniques are coordinated, in contrast to the approach applied in Chapter 6. The NAICS framework defines several receiver structures, which have their distinct pros and cons in terms of receiver performance and complexity.

Considering the plethora of expected indoor small cells in future mobile networks, the CoMP reception and transmission feature becomes interesting. Naturally, the CoMP technology potentially impose high demands to the backhaul connection, which might not be available to an average residence today. However, one should keep in mind that the deployment scenarios and traffic volumes are for future growth scenarios, thus, the backhaul has time to mature.

Appendix

Appendix A

Macro and Femto Co-channel Interference

In this appendix a reprint of the paper *Joint Macro and Femto Field Performance and Interference Measurements* is found. This paper aids the discussion and conclusion of Chapter 2.

- N. T. K. Jørgensen, T. Isotalo, K. Pedersen, and P. Mogensen, “Joint Macro and Femto Field Performance and Interference Measurements,” in *Vehicular Technology Conference (VTC Fall), 2012 IEEE*, September 2012, pp. 1–5

Paper Reprint

Joint Macro and Femto Field Performance and Interference Measurements

Niels Terp Kjeldgaard Jørgensen^{#1}, Tero Isotalo^{#2}, Klaus Pedersen^{#3}, and Preben Mogensen^{#1,3}

^{#1} Aalborg University, Denmark, ^{#2} Tampere University of Technology, Finland, and ^{#3} Nokia Siemens Networks
Email: nj@es.aau.dk

Abstract – In this paper macro performance in a co-channel macro and femto setup is studied. Measurements are performed in a live Universal Mobile Telecommunication System (UMTS) network. It is concluded that femto interference does not affect macro downlink (DL) performance as long as the macro Received Signal Code Power (RSCP) is stronger than femto RSCP. We also conclude that a macro escape carrier is a robust DL interference management solution. In uplink (UL) direction it is shown that a single femto UE close to macro cell can potentially cause a noise rise of 6 dB in the surrounding macro cell. In order to limit the noise rise from femto UEs, femto UE power capping and lowering femto common pilot channel (CPICH) power is recommended. The consequence is less uplink interference towards the macro, but also decreased femto coverage. Measurements close to macro cell centre showed femto coverage radius smaller than 5 meter – with realistic power settings. This makes co-channel femto deployment less promising in dense macro environments with good macro RSCP coverage.

I. INTRODUCTION

In the next couple of years mobile data traffic is expected to increase by 92% per year between 2010 and 2015 [1]. To cope with such an increase network operators are required to upgrade the current mobile networks. One potential solution to increase the capacity in existing networks is femto cells. Femto cells are low powered and low priced access points intended for indoor deployment. The low price of femto cell deployment is a consequence of femto cells being self configuring allowing for uncoordinated mass deployment. Furthermore the femto backhaul is expected to be the end user's own fixed internet connection. The fact that femto cells are meant for indoor deployment gives certain advantages over macro cells, namely that the femto cells are inside the same building as the UE being served. This means that there is no additional outdoor to indoor building penetration loss – a factor which could worsen the link budget by some 20 dB or more.

Femto cells can operate in open access or in closed subscriber group (CSG) mode [2]. In CSG mode only a certain group of UEs are allowed to connect to the femto cell. This can potentially limit the performance of macro cell users that do not belong to the CSG list. In this case the femto cell is a severe source of interference – potentially creating a coverage hole in the macro cell. If not dealt with, a dense femto deployment can have a strong impact on macro cell performance. Therefore, interference management schemes are fundamental if femto cells are to become a success in the future.

Today the open literature includes many performance studies for co-channel deployment of macro and femto cells. Various interference management solutions have been extensively studied for such cases for both HSPA and LTE; see [3-6]. However, the majority of these existing performance and interference management studies rely solely on theoretical models and simulations, and therefore the validity of the conclusions depends on the underlying assumptions. Contrary to those previous studies, we here present field measurements for both co-channel deployed macro and femto cells, as well as cases with the availability of a macro escape carrier, free of femto interference.

Our objective is to show representative results from a co-channel macro and femto deployment scenario. As a case study, we present results for HSPA, but many of the results presented can be extended to LTE as well. In this paper, we investigate the interference caused by femtos and femto UEs. Thus, several femto locations are chosen for interference measurements, including femto locations at macro cell edge and macro cell centre, as these locations cover the extremes in terms of path losses to the macro site. It is expected that the interference from femtos in DL is stronger at macro cell edge, whereas interference from femto UEs in UL is worse at macro cell centre, as a consequence of the path loss relations. We also measure the performance of the escape carrier scenario.

The rest of the paper is organised as follows. Section II describes the measurement locations and the macro and femto deployment scenario. In Section III the measurement procedure and equipment are presented. Section IV covers co-channel interference measurement results while Section V includes the escape carrier findings. Finally, Section VI concludes the paper.

II. MEASUREMENT SETUP

The measurement campaign was carried out at the campus area of Tampere University of Technology (TUT). A Nokia Test Network (NTN) macro cell base station provides macro coverage to the entire TUT campus area and has been utilised during the measurements campaign. The sector antenna of macro cell base station was mounted on top of a nearby 4-storey office building. The femto cell was deployed in offices, lecture rooms and hallways at TUT. Basically the only constraint for femto deployment is available power and network plugs. The locations of macro and femto cells together with the measurement routes are shown in Figure 1. There are no buildings between the macro site and location 3

(line of sight propagation conditions), while a single 4-storey building is located between the macro site and both location 1 and 2. The distance between the macro site and the femto cell locations varies between 250 meter (Location 3) and 600 meter (Location 1).

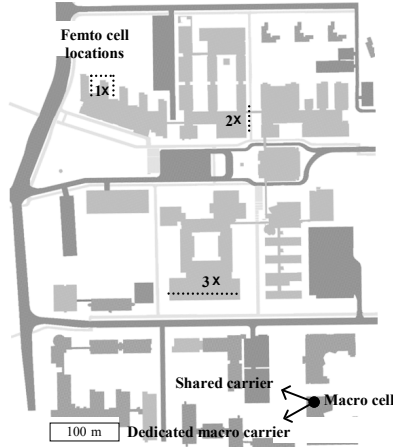


Figure 1 – Femto cell locations and macro cell sector direction. Dashed lines are the DL interference measurement routes.

All 3 femto locations were used for DL interference measurements while only location 1 (macro cell edge) and 3 (macro cell centre) were used for the UL interference measurements. Location 2 was used for the escape carrier scenario [5]. The main parameters of the femto and macro cells are gathered in TABLE I.

TABLE I MAIN PARAMETERS OF FEMTO AND MACRO

Parameter	Unit	Femto	Macro
Total Tx power	dBm	{0; 5; 14; 20}	43
Antenna gain	dBi	0	17
Antenna height	m	–	20
Cable loss	dB	0	3
UARFCN		10662	{10662; 10638}
3GPP Release		8	6
HS-PDSCH codes		max. 15	max. 15
P-CPICH Tx power	dBm	{-10; -5; 5; 10}	33
Max UE Tx power	dBm	{-13; 0}	24

Throughout the measurement campaign a single femto access point [7] was deployed at the measurement location and the femto backhaul was an internet connection at the TUT network. The backhaul capacity was measured to be more than 40 Mbps. Most measurements were performed after office hours to minimise the possibility of having other active UEs in the network and reduce the disturbance from people in the measurement area.

III. MEASUREMENT EQUIPMENT AND PROCEDURES

The DL interference and escape carrier measurements were performed with a UE dongle [8] connected to a laptop

with measurement software [9]. Measurements are performed outdoor while moving along the pre-planned measurement routes outside the femto buildings. Four sets of measurements are conducted:

1. Femto is turned off, and outdoor UE is kept in CELL_DCH state measuring macro RSCP and E_c/I_0 .
2. Femto performing a High-Speed Downlink Packet Access (HSDPA) data transmission and outdoor UE is kept in CELL_DCH state measuring macro RSCP and E_c/I_0 .
3. Femto is turned off, and outdoor macro UE is performing an HSDPA data transmission while measuring macro RSCP, E_c/I_0 and DL throughput.
4. Femto performing HSDPA data transmission and outdoor macro UE is performing an HSDPA data transmission while measuring macro RSCP, E_c/I_0 and DL throughput.

By comparing the different sets of measurements it is possible to determine the interference caused by the femto, as well as the corresponding effect on the macro UE throughput.

For the macro escape carrier measurements a neighbouring macro site sector was configured to a dedicated macro carrier. In an ideal escape carrier scenario both the shared carrier and the dedicated carrier would be configured on all three macro site sectors. In our setup the consequence of using two different sectors is that the dedicated carrier RSCP is 7 dB lower than the shared carrier RSCP. In the ideal escape carrier setup the dedicated and shared carrier RSCPs would be similar assuming similar frequencies. This configuration was chosen because of the required time to configure the macro site. Inter-frequency measurements are triggered when the serving cell E_c/I_0 goes below -15 dB. If a neighbouring inter-frequency cell E_c/I_0 is above -13 dB, an inter-frequency handover is started. Time to trigger is 100 ms [10].

The UL macro interference measurements were conducted at location 1 and 3. During these measurements, the femto UE was performing a High-Speed Uplink Packet Access (HSUPA) transmission while transmitting at maximum transmitting power. In order to cause maximum possible UL noise rise in the macro cell the UE is going to the femto cell edge area, thus increasing the UL transmission power. Macro cell measurements of the uplink noise rise are reported to the Radio Network Controller (RNC). The RNC stores those measurements for later data analysis.

IV. CO-CHANNEL INTERFERENCE MEASUREMENTS

This section covers the co-channel interference measurement results. It is investigated how indoor femto deployment affects macro DL performance and contributes to noise rise in the surrounding macro cell.

A. DL Interference Measurements

For the DL interference measurements one femto cell is deployed in a building at macro cell centre and at macro cell edge. Only the results from macro cell edge are presented

due to page constraints. Macro cell edge results are chosen because of larger path loss from the macro site to cell edge location, and therefore they represent the worst case in terms of propagation. Maximum femto transmission power is 20 dBm, and femto CPICH power is 10 dBm. The measurements were repeated 10 times, and the figures in this section show the average of all measurements.

Figure 2 shows macro RSCP and femto RSCP when measuring at location 1. It is shown that the macro RSCP varies from -90 dBm to -80 dBm.

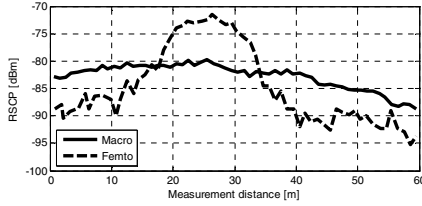


Figure 2 - Macro and femto RSCP measurements, location 1.

More interesting are the femto RSCP measurements. At the first 10 meter and the last 20 meter the femto RSCP is around -90 dBm, thus lower than the macro RSCP. From 18 to 35 meter the femto RSCP is better than macro RSCP. After 25 meter femto RSCP peaks and reaches -73 dBm, 7 dB above the macro RSCP. At this location the femto and measurement UE are only separated by a solid outer wall with metal coated windows.

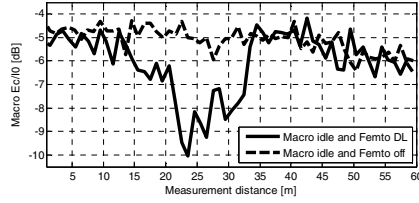


Figure 3 - Femto interference effect on macro E_c/I_0 , location 1.

Figure 3 shows how much the macro E_c/I_0 is affected by a fully loaded femto. At the first 10 meter and last 25 meter the femto has no effect on the macro E_c/I_0 as there is no significant difference in macro E_c/I_0 when the femto is turned on with full load and when the femto is turned off. At the middle part of the measurement route the macro E_c/I_0 drops to -10 dB (5 dB smaller than in non-interfered locations) caused by femto interference. Comparing Figure 2 and Figure 3 reveals that the macro E_c/I_0 is only degraded when the femto RSCP is better than the macro RSCP.

Figure 4 shows how the macro UE throughput in DL is affected by the femto. As expected the only significant difference between the fully loaded femto scenario and femto off scenario is when measuring close to the femto, from 20 to 35 meter. At this part of the measurement route the macro throughput is reduced by more than 2.5 Mbps compared to when the femto is switched off, but still achieved almost 3 Mbps on average. On the remaining part

of the route there is no noticeable difference between the loaded femto and switched off femto measurements.

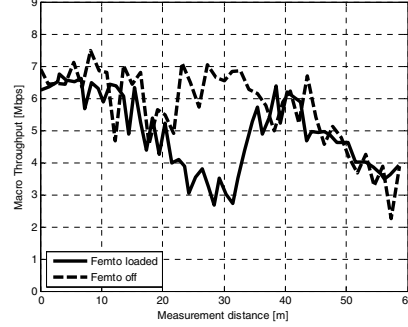


Figure 4 - Macro cell throughput, location 1.

Based on the measurement results from all locations, the general conclusion is that if the macro RSCP is better than femto RSCP, then the macro throughput is not affected by the femto presence, regardless of the femto load. Also, if the macro RSCP and femto RSCP is at the same level or femto RSCP above macro RSCP, then the femto cell makes the macro performance worse. However, in the most interfered locations the outdoor macro throughput keeps staying around 3Mbps on average.

B. UL Interference Measurements

The objective of the UL macro interference measurements is to determine the noise rise from a single femto UE. UL interference measurements were conducted with the femto deployed at macro cell edge and cell centre. At macro cell edge the measured femto UE to macro path loss equals 120 dB and 100 dB for the macro cell centre location. From the RNC recordings the macro cell noise floor is measured to -105.5 dBm. At macro cell edge this implies a noise rise of 0.2 dB, when assuming femto UE transmission power of 0 dBm. At macro cell centre the noise rise contributed by the femto UE is estimated to be 6.6 dB. Measurements confirm the estimated noise rise. TABLE II compares the estimates with the measured noise rise values at macro cell edge and macro cell edge.

TABLE II MACRO NOISE RISE FROM SINGLE FEMTO UE

	Macro cell edge	Macro cell centre
Estimated	0.2 dB	6.6 dB
Measured	0.0 dB	5.9 dB

The small differences between estimated and measured values can result from measurement accuracy, fading channels and the difficulty of forcing the femto UE to constantly transmit at 0 dBm during the measurements.

In network planning a total noise rise in the order of 3 dB is considered [11]. Hence, a 6 dB noise rise from a single femto UE is too large as it would compromise the macro coverage and, in worst case, leave areas without macro coverage. In practice multiple femto UEs would contribute

to macro noise rise and worsen the problem. Therefore, it is paramount that a single femto UE cannot cause a noise rise of 6 dB. Potential solutions to limit the noise rise are power capping the femto UEs lower than 0 dBm, reducing the femto CPICH power, or a combination of both.

Additional measurements with reduced femto CPICH power and power capping the femto UE at -13 dBm were therefore performed. The femto CPICH power was reduced to 5 dBm, -5 dBm, and -10 dBm. When lowering the femto CPICH power the femto coverage shrinks – due to more dominating macro CPICH – and less transmission power is required by the femto UE, thus reducing the contribution to macro noise rise. By applying the new power settings no noise rise contribution from the femto UE was measured at the macro site. Also the femto coverage with the updated power settings was measured. Femto coverage is defined as the area where the femto UE is able to camp on the femto. Measurements were performed by connecting to the femto in CELL_DCH state and then walking away from the femto. Then the distance to the end of the coverage was measured. Femto and femto UE were at all times in the same room/building without any indoor walls in between. This procedure was repeated 3 or more times.

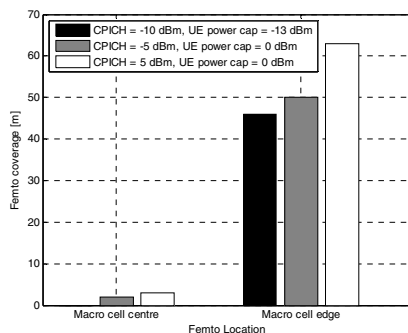


Figure 5 - Femto coverage at macro cell centre and edge for varying CPICH power.

Figure 5 shows the average femto coverage measurement results. At macro cell edge the femto coverage is larger than 45 meter for all CPICH powers. More interesting is the measured femto coverage at macro cell centre. The measurement results show that at macro cell centre the femto coverage is less than 5 meter. The reason for such a small femto coverage is a very good macro coverage. The macro RSCP is -65 dBm at the measurement location. In general it proved very difficult or nearly impossible just connecting to or camping on the femto due to dominating macro CPICH.

These results indicate that femto co-channel deployment close to macro cells becomes less attractive due to the limited effective femto coverage. In dense macro locations the probability of dominant macro RSCP over femto RSCP is high. Therefore, femto deployment is more attractive in areas with less dominant macro RSCP, such as e.g. macro

cell edge, residential, or rural areas. At these locations the femto can provide coverage of up to 60 m depending on power settings.

V. MACRO ESCAPE CARRIER SCENARIO

All previous measurements were performed in a co-channel macro and femto setup. In this section the so-called macro escape carrier scenario is studied. This means that an additional dedicated, femto-free macro carrier is available. The idea is that macro UEs, on the shared carrier, can hand over to the dedicated macro carrier if the macro UE experiences strong interference from a CSG femto, thus avoiding potential macro coverage holes. All escape carrier measurements are performed at least 6 times, and the following figures show the averaged measurement results.

Figure 6 shows the femto RSCP and co-channel macro RSCP on the measurement route. When walking on the measurement route at location 2 you walk towards the femto and away from the macro; see Figure 1. This is also visible as the femto RSCP increases and co-channel macro RSCP decreases.

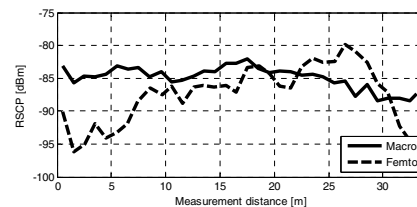


Figure 6 - Co-channel femto and macro RSCP on measurement route.

In Figure 7 the macro E_C/I_0 is shown. We measured back-and-forth on the measurement route, thus “Start of route” is shown twice. Both a femto UE and a macro UE are performing a HSPDA download during the measurements.

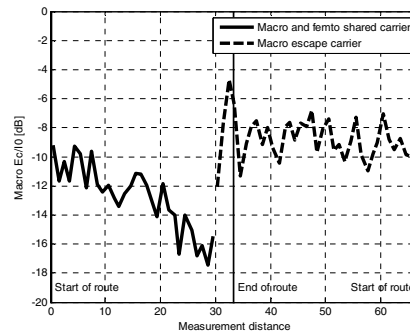


Figure 7 - Macro E_C/I_0 on co-channel carrier and on dedicated carrier.

At the start of the measurement route the macro E_C/I_0 is -11 dB on the co-channel carrier. As the macro UE gets closer to the femto, the macro E_C/I_0 deteriorates because of femto interference. Right before the end of the measurement route

an inter-frequency handover to the dedicated carrier is completed. After the handover the macro E_c/I_0 is -9 dB. Close to the femto, the measured E_c/I_0 decreases by almost 8 dB with reference to the level at the start of the route, but the macro UE is able to recover from the femto interference by handing over to the macro escape carrier. During the measurements the HSDPA session always continued on the escape carrier, except for a HSDPA transmission break for a couple of seconds during the inter-frequency handover, as illustrated in Figure 8.

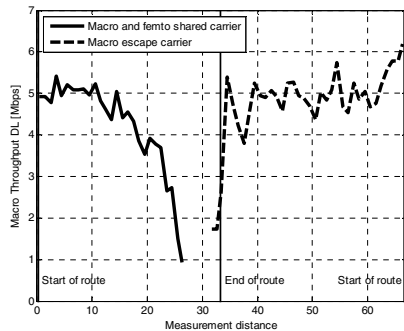


Figure 8 - Macro throughput on co-channel and on dedicated carrier.

Prior to the measurements, no inter-frequency mobility optimisation was performed. Macro UE throughput dropped to 1 Mbps before the handover was triggered. With optimised mobility parameters the handover might be triggered earlier. However, handover optimisation is out of the scope of this paper, and the default mobility parameters are considered reasonable.

Based on the measurement results the macro escape carrier scenario proved a good, robust interference management solution in DL direction. The main drawback of the solution is the obvious requirement of two carriers. Also, the escape carrier scenario only resolves femto interference in DL. For additional UL interference management solutions, see Section IV.B.

VI. CONCLUSION

This paper studied the consequences of co-channel macro and femto deployment from an interference point of view and also suggests potential solutions in case of strong femto interference.

Based on our results we conclude that as long as the macro RSCP is better than femto RSCP, the macro UE DL performance is most likely not being degraded. Basically this means that as long as the femto is deployed indoor, and macro UEs are located outdoor, an acceptable macro performance is guaranteed. Our worst case result showed that an outdoor macro UE was still served with almost 3 Mbps in DL.

In situations where strong femto interference is inevitable, e.g. macro UE entering buildings with one or more femtos

deployed, the macro escape carrier proved a good interference management solution. Whenever the serving macro E_c/I_0 dropped below the threshold for inter-frequency handovers, due to femto interference, an inter-frequency handover was triggered and executed. And we never experienced any dropped connections. The drawback of this interference management solution is the need of two or more available UMTS carriers.

What is more critical is the UL noise rise towards the macro when the femto is deployed at macro cell centre. A UL noise rise of 6 dB was measured. This is clearly unacceptable. Reduced femto CPICH power and femto UE power capping was investigated, but the outcome was very small femto coverage area. The consequence is that co-channel femto deployment is only an option in locations with no dominant macro, e.g. rural areas.

Considering both the DL and UL findings the concluding femto co-channel deployment guidelines are: indoor co-channel femto deployment is most useful at macro cell edge, and furthermore, a network operator should always deploy a femto-free macro escape carrier in order to guarantee reliable macro coverage.

ACKNOWLEDGMENT

We would like to thank Jarno Niemelä for fruitful discussions and troubleshooting of the femto setup, Jari Kossila for macro network configuration, NSN Femto Support in Wrocław, Rajadurai Subramaniam and Rohit Ahuja for helping out with femto measurements, and Anite for providing the necessary measurement equipment.

REFERENCES

- [1] Cisco, "Cisco Visual Networking Index: Global Mobile Data Traffic Forecast Update, 2010 - 2015", February 2011.
- [2] 3GPP: TS 25.467, "Universal Telecommunications Systems (UMTS); UTRAN architecture for 3G Home Node B (HNB); Stage 2", April 2011, Version 10.1.0.
- [3] M. Yavuz et al, "Interference management and performance analysis of UMTS/HSPA+ femtocells", Communications Magazine, IEEE, vol.47, no.9, pp. 102-109, September 2009.
- [4] A. Szufarska et al, "Interference Mitigation Methods for LTE-Advanced Networks with Macro and HeNB Deployments," *Vehicle Technology Conference (VTC Fall), 2011 IEEE*, vol., no., pp.1-5, 5-8 Sept. 2011.
- [5] Femto Forum, "Interference Management in UMTS Femtocells", December 2008.
- [6] J. Gora et al, "Deployment aspects of 3G femtocells," *Personal, Indoor and Mobile Radio Communications, 2009 IEEE 20th International Symposium on*, vol., no., pp.1507-1511, 13-16 Sept. 2009.
- [7] Arcadyan Femtocell Access Point MAF9001A, <http://www.arcadyan.com>.
- [8] Sierra Wireless AirCard USB 309, <http://www.sierrawireless.com/>.
- [9] Anite, Nemo Outdoor, <http://www.anite.com>.
- [10] 3GPP: TS 25.331, "Radio Resource Control (RRC); Protocol Specification", September 2011, Version 10.5.0.
- [11] H. Holma et al, *WCDMA for UMTS: HSPA evolution and LTE*, 5th edition, John Wiley & Sons, Ltd, Chichester, UK, 2010.

Appendix B

QoS-Aware Femto Power Control Algorithm

The paper reprint in this appendix complements the discussion and conclusions of Chapter 2.

- T. Kolding, P. Ochal, N. T. K. Jørgensen, and K. Pedersen, “QoS Self-Provisioning and Interference Management for Co-Channel Deployed 3G Femtocells,” *Future Internet*, vol. 5, no. 2, pp. 168–189, 2013

Paper Reprint

Future Internet **2013**, *5*, 168–189; doi:10.3390/fi5020168

OPEN ACCESS

future internet

ISSN 1999-5903

www.mdpi.com/journal/futureinternet

Article

QoS Self-Provisioning and Interference Management for Co-Channel Deployed 3G Femtocells

Troels Kolding ¹, Pawel Ochal ¹, Niels Terp Kjeldgaard Jørgensen ^{2,*} and Klaus Pedersen ^{1,2}

¹ Nokia Siemens Networks, Research Center Aalborg, Niels Jernes Vej 10, 9220 Aalborg, Denmark; E-Mails: troels.kolding@nsn.com (T.K.); pawel.ochal@yahoo.com (P.O.); klaus.pedersen@nsn.com (K.P.)

² Radio Access Technology, Department of Electronic Systems, Aalborg University, Niels Jernes Vej 12 A6-1, 9220 Aalborg, Denmark

* Author to whom correspondence should be addressed; E-Mail: nj@es.aau.dk; Tel.: +45-9940-8645.

Received: 21 February 2013; in revised form: 7 March 2013 / Accepted: 22 April 2013 /

Published: 2 May 2013

Abstract: A highly efficient self-provisioning interference management scheme is derived for 3G Home Node-Bs (HNB). The proposed scheme comprises self-adjustment of the HNB transmission parameters to meet the targeted QoS (quality of service) requirements in terms of downlink and uplink guaranteed minimum throughput and coverage. This objective is achieved by means of an autonomous HNB solution, where the transmit power of pilot and data are adjusted separately, while also controlling the uplink interference pollution towards the macro-layer. The proposed scheme is evaluated by means of extensive system level simulations and the results show significant performance improvements in terms of user throughput outage probability, power efficiency, femtocell coverage, and impact on macro-layer performance as compared to prior art baseline techniques. The paper is concluded by also showing corresponding measurements from live 3G high-speed packet access (HSPA) HNB field-trials, confirming the validity of major simulation results and assumptions.

Keywords: 3G and/or WCDMA; femtocell and/or home NodeB; QoS provisioning; interference management; network listen mode

1. Introduction

In certain scenarios, a 3G femtocell, Home Node-B (HNB) in 3GPP terminology, is a cost-effective alternative to providing indoor coverage compared to outdoor high power base stations [1]. Furthermore, for incumbent operators with very limited spectrum resources and a great amount of fixed network installations, HNBs may be used to roll out significant cellular capacity. For such deployments, HNBs and wide area macro Node-Bs (MNB) often will need to co-exist in the same frequency band. This is the most challenging deployment scenario and therefore the one considered in this paper. For the co-channel case, a tradeoff among protecting macro users and boosting femto performance must be found, see e.g., [1–4] and embedded references. However, the proposed scheme also offers benefits for HNBs deployed on a dedicated carrier.

We consider both cases when the HNB is configured for open or closed subscriber access (OSG and CSG). While provisioning is equally important, some interference aspects are relaxed in the OSG case. However, even when HNBs are configured for open access by all macro users, their potential configuration and density can still pose a risk to e.g., macro uplink. For other considerations related to mobility performance and the recommended use of reserved macro-only carrier, the reader is referred to [1].

Besides the physical deployment aspects, operators that deploy HNBs also have a sales and provisioning strategy that is based around the service level agreement defined with the end-customer. As examples, 3G HNB may be deployed as a voice coverage solution which supplements a parallel Wi-Fi solution for data, or it may be provisioned as a stand-alone mobile broadband solution. Any provisioned solution must fulfill end-customer requirements and at the same time meet operator requirements related to wide area performance, including robustness and data offload effect.

In this paper, our ultimate goal is to explore the extent possible for autonomous QoS (quality of service) self-provisioning and interference management. A key aspect which will receive continued growing research interest to drive down deployment cost of dense small cell networks in the future. Specifically, and from an operator's viewpoint, we want to clarify if it is possible to control deployment by means of distributing only intuitive deployment parameters such as guaranteed coverage (in meters or dB) and downlink and uplink data rates for anyone connected to the 3G HNB. To do so, we make use of a light-cognitive element of the 3G HNB; e.g., the simple built-in user equipment (UE) receiver module that can be used to sense the surrounding network. This module enables what is known as network listen mode (NLM) [1]. We want to see if by conducting advanced processing enabled by NLM we can ensure that deployed and uncoordinated HNB can fulfill the service level agreement while at the same time self-minimizing dead zones and remaining within an allowed interference budget to protect the wide area uplink performance.

For 3G HNBs, 3GPP does not specify interference management and provisioning techniques and these are left for proprietary implementation and thus an object for extensive research. Most common reference assumptions, also applied as references throughout this paper, is a full-power transmit mode as well as an interference management solution standardized for LTE but adapted for 3G here [1]. Other research has pursued similar goals and considered interference management tradeoffs in co-channel deployments, ranging from general analysis in e.g., [2,5] to practical schemes that utilize NLM measurements combined with UE measurements in e.g., [6] and uplink measurements in e.g., [7]

Future Internet **2013**, *5*

170

to gain more knowledge of the local deployment conditions prior to optimization. Closed-loop methods between macro and small cell layer have been considered to adapt uplink power control settings [8,9]. As such, the method in [9] uses micro economic techniques to distribute feasible signal to interference and noise ratio (SINR) targets to femtocell optimizing overall network utility. However, in our work we focus on autonomous self-provisioning to avoid fast feedback mechanisms between the layers that can track the variations in user load as this is typical assumption to lower overall deployment costs. Furthermore, we are concerned with absolute QoS targets as this relates closely to end-user perception as well as agreements made between operator and said end-user. In addition, the method documented in this paper differentiates itself by (1) joint optimization of downlink and uplink interference parameters; and by (2) enabling an operator-controlled tradeoff among absolute setting for coverage and capacity in the femtocell according to service level agreement with end-users. Here we focus on the initialization of the HNB parameters but the approach can be combined effectively with e.g., time variant learning methods employing e.g., measurements from user devices similar to e.g., [2,6].

The paper begins with a description of the system model after which the autonomous QoS self-provisioning and interference management concept is introduced. Next, simulations are used to prove the validity of the concept and understand sensitivity to key system parameters. A key challenge surrounding any theoretical or analytical work regarding small cells are the uncertainties related to propagation and interference paths in indoor/outdoor co-channel deployments. Hence, we next show a partial verification of the noise rise estimation and femto coverage estimation of our concept obtained through practical field trials after which conclusions are drawn.

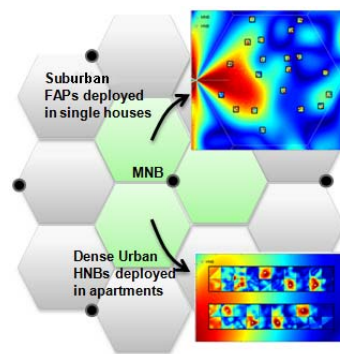
2. System Model and Design Objective

The assumed system model is based on the 3GPP defined High Speed Packet Access (HSPA) system [1,10], assuming co-channel deployment of all cells on a single carrier of 5 MHz bandwidth. A regular hexagonal grid of three sector macro base station sites is assumed as shown in Figure 1, each having a downlink transmission power of 43 dBm per cell and a 14 dBi antenna gain. For the sake of simplicity, the MNBs are assumed to always transmit at their maximum power level with a constant transmit power for the primary common pilot channel (P-CPICH). In addition to the macro-layer, HNBs are deployed across the network area according to two basic deployment strategies: either in houses (suburban) or in apartments (dense urban). This system model provides some variability due to its indoor propagation model (based on indoor distance and internal walls). Moreover, the shadowing model ensures that there is variance between the effective propagation loss a femtocell connected user experiences to the nearest macro base station and the estimated propagation loss using the NLM method at the HNB.

Each HNB is serving a single cell with two 0 dBi omni directional antennas. The maximum HNB transmission power is assumed to be 15 dBm. Via NLM operation, the HNB is able to perform measurements in the downlink transmission band, including (i) received signal strength indicator (RSSI); and (ii) received signal pilot code power (CPICH RSCP) from other transmitting cells in the vicinity [11]. Serving cell selection for each UE is based on UE measurements of RSCP, *i.e.*, the UE connects to the cell with strongest RSCP. A UE connected to an HNB is denoted an HUE and a UE connected to a MNB is denoted an MUE. When simulating with CSG HNBs, only UEs with matching

CSG identity are allowed to connect. In this context, we consider any UE within an apartment or a house with an HNB to be part of the CSG, whereas any user outside of this space is unable to access the HNB. In the OSG case, there are no restrictions.

Figure 1. Basic simulation model with hexagonal macro area and HNBs deployed in either single houses (suburban) or in apartments of three-floor buildings (dense urban).



We include common channels such as the P-CPICH, the high speed shared control channel (HS-SCCH), as well as the high speed downlink shared channel (HS-DSCH) in our modeling. The HS-DSCH is a time-domain shared channel with hybrid automatic repeat request (H-ARQ) and fast modulation coding, ranging from QPSK with high effective coding rate to 64QAM with low effective coding rate. Assuming up to 15 high speed physical downlink shared channel (HS-PDSCH) codes, the maximum downlink data rate equals 21.1 Mbps [1]. Each UE is assumed to be equipped with two uncorrelated receive antennas, using a standard linear minimum mean square error (MMSE) receiver. The packet scheduling is round robin type. For more information on downlink fast link adaptation and packet scheduling, the reader is referred to [1,12,13].

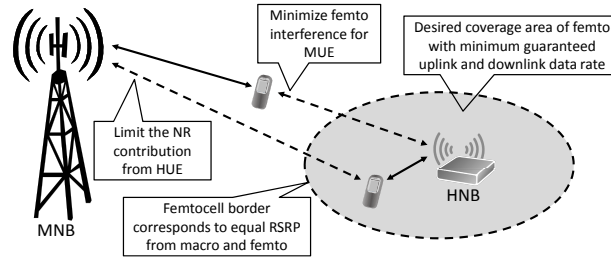
Contrary to the downlink, the uplink uses dedicated channel transmission for each UE with fast closed loop power control with a 1.5 kHz command rate. The maximum UE transmission power equals 24 dBm, with the possibility for the network to configure lower maximum output power for some UE (also known as configuration of UE power capping) e.g., HUEs. Uplink reception is based on two receiver antennas with MMSE. The uplink packet scheduler is a standard best effort [1]. For the MNB, the scheduling is furthermore subject to a maximum uplink noise rise (NR) target, as well as minimum data rate per user. The NR is defined as the total received power divided by the thermal noise power [1], assuming a NR target of 6 dB for the MNB.

The overall design objective is summarized in Figure 2. for a simple example with co-channel deployment of MNBs and HNBs, each serving one user. The objective is to adjust the HNB transmit powers of P-CPICH and HS-DSCH, as well as the HUE maximum transmit power, subject to the desired design criteria. The assumed design criteria in this study are the following:

- (i) The femtocell coverage area shall correspond to PL_{femto} ;

- (ii) HUEs shall be offered a minimum data rate of ReqThp_{DL} and ReqThp_{UL} for the downlink and uplink, respectively, in the entire home/apartment of the end-user. ReqThp_{DL} and ReqThp_{UL} are planning parameters;
- (iii) The generated uplink NR at the nearest MNB from each HUE must be limited to NR_{HUE} . NR_{HUE} is a planning parameter that depends on the HNB density and the expected offload effect (for instance NR_{HNB} divided by maximum number of simultaneously active HNBs per macrocell area);
- (iv) After fulfilling the above requirements, the generated HNB interference towards the macro UEs shall be minimized (save power, improve macro performance).

Figure 2. Overview of system model and design objectives.



In this paper, the femtocell coverage area is defined as the area where the RSCP of the specific femtocell is higher than the RSCP for all other cells. Even though only a single HNB is shown in the above figure, our proposed algorithm is not limited to the single HNB case. It is an advantageous design choice not to consider inter-HNB interference when calculating the HNB powers, as this prevents HNBs from entering a transmit power race where strongly coupled HNBs keep increasing the total transmit power. Such an event would not improve the target performance indicators in the region between the competing femtocells, but would in turn result in increased interference towards the macro network and, thus, lower the overall utility of the network.

Depending on the radio and interference conditions, it may be impossible to fulfill all of the listed design criteria. As an example, if the HNB coverage area is close to the MNB, fulfilling both the requirement on HUE uplink data rate and maximum generated NR towards the macro may be conflicting. In case of such conflicting requirements, it is considered most important to protect the macro performance. The interference management algorithm for dealing with these issues is derived in Section 3. Table 1 lists the parameters used in the derivation of the interference management algorithm in Section 3.

Given the outlined design objectives, the key performance indicators (KPI) considered in this study are user experienced throughput in uplink and downlink, as well as the corresponding outage probabilities for experiencing data rates below certain targets. Such information is extracted from an empirical cumulative distribution function (cdf) of user data rates, obtained from extensive Monte-Carlo simulations. We also consider the transmission power aspects, both in terms of downlink transmission powers from the HNBs, as well as HUE uplink transmission powers.

Table 1. List of used notation in the derivation of the proposed algorithm.

Name	Description	Default value
$\eta_{Total/CPICH}$	Total transmit power to CPICH power ratio.	10 dB
F_{load}	Average load of the MNBs surrounding the HNB.	-
F_{Margin}	Fading margin.	-
I_{HNB}	Interference measured at the HNB.	-
$I_{HNB_estimated}$	Estimated interference measured at the HNB.	-
iF	Other macrocell to own macrocell interference ratio.	-
L_p	External wall penetration loss.	20 dB
NR_{HUE}	Allowed noise rise contribution from HUEs.	-
NR_{macro}	Noise rise at the MNB.	-
$NR_{MNB-HUE}$	Noise rise at the MNB caused by HUEs in HNB under test.	-
$P_{common-CH}$	Transmit power of the common channel.	-
P_{CPICH}^{opt}	HNB optimal P-CPICH transmit power.	-
P_{CPICH_macro}	Common pilot channel transmit power of the MNBs.	33 dBm
$P_{HNB-IoOther}^{RX}$	Total received power at HNB from MUEs in the non-overlapping macrocells.	-
$P_{HNB-MaxTx}$	Maximum HNB transmission power.	-
$P_{HNB-MUE}^{RX}$	Received power at HNB from virtual MUE in the overlapping macrocell.	-
$P_{HNB-TOTAL}^{RX}$	Total received power at HNB.	-
P_{HSDSCH}^{opt}	HNB optimal HS-DSCH transmit power.	-
P_{HUE}^{TX}	Transmission power of the HUEs.	-
P_{HUE_max}	Maximum available HUE transmission power.	23 dBm
$P_{MNB-HUE}^{RX}$	Received power at MNB from HUE.	-
$P_{MNB-MUE}^{RX}$	Received power at MNB from MUE.	-
P_{MUE}^{TX}	Transmission power of the MUEs.	-
P_{Noise}	Thermal noise power measured at the MNBs	-102.7 dBm
PL_{femto}	Desired femtocell coverage range. Design parameter.	56 dB or 62 dB
$PL_{MUE-MNB}$	Path loss between MUE and MNB.	-
$ReqThp_{DL}$	Required HUE downlink throughput. Design parameter.	256 kbps or 1 Mbps
$ReqThp_{UL}$	Required HUE uplink throughput. Design parameter.	256 kbps
$RSCP_{macro}^{CPICH}$	Strongest co-channel macro RSCP measured at the HNB.	-
SF	HS-DSCH spreading factor.	16

It is noted that the setting of the parameters depends on the deployment conditions and the provisioning strategy of the operator. We provide some examples in Table 2 of how the algorithm can be configured for various deployment use-cases.

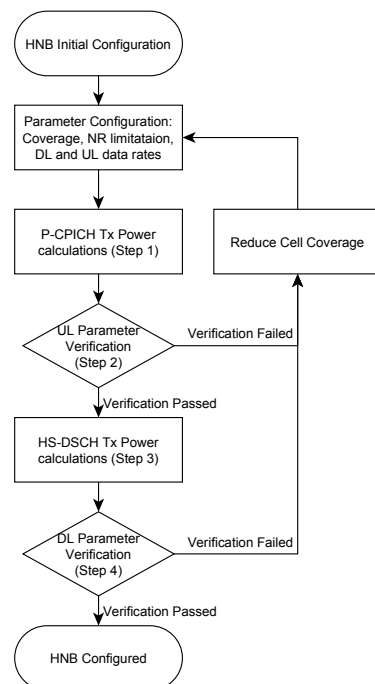
Table 2. Hypothetical deployment scenarios and how they are controlled by algorithm parameters.

Deployment goal	Access	PL_{femto}	$ReqThp_{DL}$	$ReqThp_{UL}$
Rural voice service (safety)	OSG	Infinite	Mainly voice, e.g., 256 kbps	Mainly voice, e.g., 256 kbps
Rural voice service (safety)	CSG	According to SLA, building/area know-how	Mainly voice, e.g., 256 kbps	Mainly voice, e.g., 256 kbps
Urban voice service	CSG	According to SLA, building know-how	Mainly voice, e.g., 256 kbps	Mainly voice, e.g., 256 kbps
Data service	CSG	According to SLA, building know-how	According to SLA, e.g., 1 Mbps	According to SLA, e.g., 512 kbps

3. QoS Self-Provisioning and Interference Management Concept

The high level diagram and algorithm flow of the proposed quality of service self-provisioning and interference management (QoS-SP-IM) concept is presented in Figure 3.

Figure 3. High level overview of the QoS self-provisioning and interference managing algorithm.



The overall solution design includes four execution steps in order to configure the HNB. First of all, the P-CPICH is calculated with respect to the coverage requirements and the surrounding macrocell radio frequency (RF) environment in *Step 1*. In *Step 2*, the HUE power calculations are performed. All UL traffic in the overlaying macrocell is assumed at the femtocell edge and the corresponding interference towards the HNB can be computed. From this it is possible to configure the HUE power to meet the UL required throughput target. Moreover, it is checked if the NR from HUE exceeds the limit. If the NR limit is exceeded, the femtocell coverage area is reduced and the CPICH calculations in *Step 1* are reiterated. If uplink verification is passed, the HS-DSCH transmit power is configured in *Step 3*. The HS-DSCH is configured such that end-users get the targeted downlink data rate, without exceeding it at the femtocell edge. Thus, the leakage to other base stations is effectively controlled. Finally, downlink requirement verification is performed in *Step 4*. Both the HUE coverage area and the

HUE downlink data rates are checked. If not passed the HNB coverage area must be reduced and the CPICH power calculations in Step 1 are reiterated.

If the target requirements cannot be fulfilled in a real life deployment (e.g., the femtocell coverage is smaller than desired or target throughput rate not met), a warning report is generated and transferred to the operation and the maintenance system. Further development of the algorithm include dynamic power control based on UE feedback, however, the aim of this paper is the initialization of HNB power parameters.

3.1. Step 1—The P-CPICH Power Calculations

In order to determine the optimal P-CPICH transmit power, P_{CPICH}^{opt} , both the RSCP measurements at the HNB towards the strongest co-channel MNB, $RSCP_{CPICH}^{macro}$, and the desired femtocell coverage range, PL_{femto} , are used. Optimal P-CPICH transmit power means configuration of pilot channel power in order to be able to obtain the required femtocell range. This range is defined where the users exactly sees the same RSCP from the target femtocell and from the nearest undesired cell (macrocell). We therefore estimate the required P-CPICH transmit power as

$$P_{CPICH}^{opt} = RSCP_{CPICH}^{macro} \cdot PL_{femto}. \quad (1)$$

3.2. Step 2—Uplink Parameter Verification

Next, it is assumed that a single virtual MUE representing all uplink traffic generated towards the overlaying macrocell is located just outside the femtocell coverage. Such a case corresponds to the situation where the HNB is exposed to the highest possible uplink interference from overlaying MUEs, hence it is the worst-case scenario. This step is necessary to properly evaluate the dependencies between pilot channel configuration and uplink QoS agreed between end-user and an operator. Secondly, it is assumed that the femtocell boundary is a single apartment or house. The path loss from MNB to HNB can be computed from the known macro CPICH power and the measured macro RSCP at the HNB. Therefore, in order to estimate the path loss from MNB to MUE, and according to the assumptions the virtual MUE is located at femto cell edge and outside the building, the path loss from MNB to MUE, $PL_{MUE-MNB}$, is described as

$$PL_{MUE-MNB} = \frac{P_{CPICH_macro}}{RSCP_{CPICH}^{macro}} \cdot \frac{1}{PL_{femto} \cdot L_p} = \frac{P_{CPICH_macro}}{P_{CPICH}^{opt} \cdot L_p} \quad (2)$$

where L_p is the external wall penetration loss and P_{CPICH_macro} is the common pilot channel transmit power of the surrounding macro. The external wall penetration loss is included here since we assume that the desired femtocell coverage area is confined to the indoor space. If the femtocells are installed outdoor with a certain desired coverage area, the value of L_p should be set to 0 dB.

This virtual MUE is having a transmission power in the way that it contributes to the full macro-layer noise rise within its own macrocell. The total power from this virtual MUE received at the nearest macro is thus calculated taking into account the allowed NR and the NR consumed from othercell interference, which is not mapped into the virtual MUE. The received power at the nearest macro from the virtual MUE can thus be estimated as

Future Internet **2013**, *5*

176

$$P_{MNB-MUE}^{RX} = P_{Noise} \cdot \left(\frac{NR_{macro} - 1}{1 + iF} \right) \quad (3)$$

where the constant P_{Noise} is the thermal noise power measured at the MNB which equals -102.7 dBm. The parameter iF represents the other macrocells interference to own macrocell interference ratio and is further described in [1]. Knowing the path loss from the virtual MUE to the MNB as well as an assumed fading margin, F_{Margin} , needed to accommodate the expected fading observed by the MUE, we get to the final expression for virtual MUE transmit power as

$$P_{MUE}^{TX} = P_{MNB-MUE}^{RX} \cdot PL_{MUE-MNB} \cdot F_{Margin} \quad (4)$$

The transmission power of the virtual MUE has a significant impact on the interference reception at the HNB and has an influence on the transmission power of the HUE in order to guarantee a certain femto uplink performance. Still assuming the virtual MUE being located just outside the femto house/apartment received power from the virtual MUE at the target HNB, $P_{HNB-MUE}^{RX}$, is computed as

$$P_{HNB-MUE}^{RX} = \frac{P_{MUE}^{TX}}{PL_{femto} \cdot L_p} \quad (5)$$

Not only does the virtual MUE cause interference at the HNB, also MUEs connected to other macrocells create interference to the HNB as the virtual MUE only represents the UL traffic for the overlaying macrocell. Therefore, the received power at the HNB from other MUEs is also calculated, $P_{HNB-Iother}^{RX}$. Knowing the other to own macrocell interference ratio, the thermal noise power and the allowed noise rise for macrocells, $P_{HNB-Iother}^{RX}$ is calculated as

$$P_{HNB-Iother}^{RX} = \frac{P_{Noise}}{L_p} \left((NR_{macro} - 1) \cdot \frac{iF}{iF + 1} \right) \quad (6)$$

In addition, the total received power at the HNB, $P_{HNB-TOTAL}^{RX}$, is a sum of all observed interferer and noise powers, *i.e.*,

$$P_{HNB-TOTAL}^{RX} = P_{Noise} + P_{HNB-MUE}^{RX} + P_{HNB-Iother}^{RX} \quad (7)$$

Knowing the total received interference and noise power at the HNB it is possible to calculate the required transmission power of the HUE, P_{HUE}^{TX} , to satisfy the required uplink data rate at the cell border:

$$P_{HUE}^{TX} = \text{sinr}(\text{ReqThp}_{UL}) \cdot PL_{femto} \cdot P_{HNB-TOTAL}^{RX} \quad (8)$$

where $\text{sinr}(\dots)$ is a mapping function from required uplink data rate to required SINR.

Next, the NR generated by the HUE towards the nearest MNB is checked. Based on the assumption that the path loss from the MNB to any location inside the femtocell equals the path loss from MNB to HNB, the HUE generated noise rise, $NR_{MNB-HUE}$, is calculated as:

$$P_{MNB-HUE}^{RX} = \frac{P_{HUE}^{TX} \cdot RSCP_{macro}^{CPICH}}{P_{CPICH_macro}} \quad NR_{MNB-HUE} = \frac{P_{MNB-HUE}^{RX} + P_{Noise}}{P_{Noise}} \quad (9)$$

where $P_{MNB-HUE}^{RX}$ is the received power from HUEs at the strongest MNB and $NR_{MNB-HUE}$ is the NR contribution from HUEs transmitting with required minimum uplink data rate. Moreover, it is checked whether the generated NR is within the allowed target

$$NR_{MNB-HUE} < NR_{HUE} \quad (10)$$

If the NR from HUEs exceeds the NR target, the femtocell range is reduced according to the following iterative expression

$$PL_{femto} = \frac{PL_{femto}^*}{\Delta_{step}} \quad (11)$$

where Δ_{step} is the reduction of the desired femto path loss and PL_{femto}^* is the previously assumed value of the femto path loss. After reduction of the desired femto path loss according to Equation (11), the calculations from Equation (1) and onwards are repeated. Finally, when Equation (10) is fulfilled it is ensured that the computed HUE transmission power does not exceed the HUE power capping constraint

$$P_{HUE}^{TX} \leq P_{HUEmax} \quad (12)$$

If the HUE power capped constraint is violated, the desired femto path loss has to be reduced according to Equation (11) and the algorithm has to be re-calculated from Equation (1). If both the NR and HUE power capping constraints are fulfilled the next step is the HS-DSCH power calculation.

3.3. Step 3—The HS-DSCH Power Calculations

The data channels power of the HNB has direct impact on the data rate available for HUE connected to the HNB. Thus, calibration is based on agreed requirements, e.g., data rates expected at the femtocell edge. The transmission power of the data channels, P_{HSDSCH}^{opt} , to reach the required downlink throughput at the cell edge is calculated as

$$P_{HSDSCH}^{opt} = \text{sinr}(\text{ReqThp}_{DL}) \cdot \frac{PL_{femto} \cdot I_{HNB}}{SF} \quad (13)$$

where I_{HNB} is the interference measured by the HNB and SF is the spreading factor and equals 16 for the HS-DSCH. It is assumed that the interference level from the surrounding network is the same in the whole femtocell area, which is only an estimate since it depends especially on whether interference from other femtocells is strongly present.

Estimating this interference is rather complicated as it depends on the active load. We therefore base the estimation on the RSCP CPICH NLM measurements of all macrocells in the vicinity: $RSCP_{CPICH_k}$. We only consider macrocells not to put neighboring femtocells into a race condition where they keep increasing their power to fulfill cell edge rates. This would only lead to worse network performance and similar cell edge data rates for the competing femtocells. Utilization of RSCP makes the approach independent on network load during NLM measurements and we can then apply modification afterwards. The interference at the HNB, $I_{HNB_estimated}$, is estimated as

$$I_{HNB_estimated} = \eta_{Total/CPICH} \cdot F_{load} \cdot \sum_{k=1}^K RSCP_{CPICH_k} \quad (14)$$

where F_{load} is the assumed average load of the surrounding cells and $\eta_{Total/CPICH}$ is the assumed ratio between the average total transmit power of a base station and its pilot power. We assume $\eta_{Total/CPICH} = 10$ for the simulations but it is a parameter that is set by the operator depending on the macro network configuration.

3.4. Step 4—Downlink Parameter Verification

Finally, the total transmit power configuration of the HNB must satisfy the following inequality

$$P_{HSDSCH}^{opt} + P_{CPICH}^{opt} + P_{common-CH} \leq P_{HNB-MaxTX} \quad (15)$$

where $P_{common-CH}$ is the power of the common control channels and $P_{HNB-MaxTX}$ is the hardware limitation on maximum HNB transmission power. If Equation (16) is not satisfied the femtocell coverage is reduced according to Equation (11). The new configuration requires execution of algorithm with new configuration parameters from Equation (1).

The end-user required uplink or downlink throughput is not guaranteed in the entire apartment/house if Equations (10), (12) and (15) are not all fulfilled in the first iteration of the proposed QoS-SP-IM algorithm. If Equations (10), (12) and (15) are not fulfilled the femtocell range was reduced during the execution of the algorithm. However, from an operator's point of view, the macro performance in the surrounding macrocells is preserved and is not degraded due to dense HNB deployment but at the cost of higher outage in femtocell performance. Tradeoffs are shown in the next section.

3.5. A Note on Parameter Initialization versus Adaptation

As mentioned earlier, we are focused in this paper on the initialization on the HNB parameters. The above method will typically be repeated when the HNB is idle or every time interval which commonly is configured by the HNB vendor or its management system (could be e.g., every few hours). It should be noted that the initialization will be the best network configuration possible given information we have at the HNB location. However, as users connect to the system, the imperfections of the modeling will become visible. For instance, while an HNB may see good isolation to a macrocell, a connected HNB user may be standing in a window opening with different coupling to the nearest macrocell. Also, load conditions which are assumed for the provided algorithm will vary over time which may lead to HUEs getting excessive or inadequate throughput compared to the targets.

Hence, a method as devised here will be combined with adaptation, e.g., using observed throughput levels for its connected users as well as collecting neighbor interference reports (e.g., handover triggered measurements) to fine-tune the parameters compared to the initial settings. In this paper, we focus only on the initialization but we are to some extent including dynamic imperfections as we add users to the system. We have e.g., shadowing models as well as indoor modeling with wall counts which mimic the situation that some HNB users have a different path loss to its neighbors compared to the value predicted by the NLM method. Given our user distribution method, we also have varying network load conditions. As shall be seen by the simulation results, our method is robust against these variations. Further work will integrate and clarify the value of further dynamic adaptation.

4. Simulation Results

Extensive quasi-static system level simulations are conducted in order to assess the performance of the proposed scheme. The basic simulation methodology is in coherence with the 3GPP guidance for HetNet simulations [14], including simulation of both downlink and uplink and the major RRM

algorithms such as packet scheduling, power control (PC), link adaptation, *etc.* [13]. Cases with co-channel deployment of OSG and CSG HNBs in line with assumptions outlined in Section 2 are simulated. We primarily focus on dense urban environments with 500 meters macro inter-site distance, and the case with CSG HNBs deployed inside multi-floor buildings. The so-called dual-stripe 3GPP model is adopted, simulating two adjacent three-floor building blocks, each consisting of 2×10 apartments of 10×10 meters per floor [14].

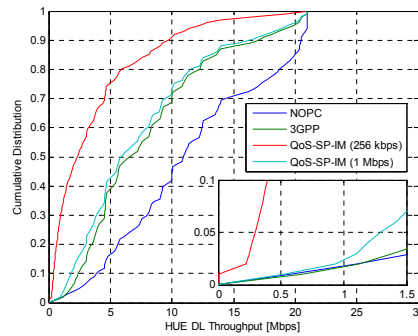
It is assumed that 30 HNBs with different CSGs are randomly placed inside those two building blocks, one HNB per four apartments, with the constraint of a maximum of one CSG HNB per apartment. Each apartment with a CSG HNB also has at least one HUE with matching CSG identity. In addition, MUEs are randomly placed, assuming that 80% of those are located inside the building blocks. If an MUE is dropped inside an apartment with an HNB, the MUE is considered an HUE with CSG identity matching the HNB. Except for the former constraints, serving cell selection corresponds to the cell with strongest RSCP for the UE. Thus, a UE with configured CSG identity may also connect to the macro-layer if it is subject to higher RSCP from that layer as compared to the HNB with matching CSG identity. In order to further evaluate the scalability of the proposed QoS-SP-IM algorithm, we also present example performance results from a suburban residential scenario. The suburban environment is characterized by a larger macro inter-site distance of 1732 meters and CSG HNBs placed inside separate single-floor residential family homes. More information on the simulation assumptions for both the dense urban and suburban scenario is available in [15,16].

In addition to simulation of the derived QoS-SP-IM algorithm in Section 3, two simpler cases are also simulated in order to have baseline results to compare against. The baseline cases include: (i) no power control (NOPC), where the HNBs simply transmit at their maximum power of 15 dBm; and (ii) an adaptive HNB PC scheme where the HNB Tx power is adjusted depending on RSCP from the strongest macro-cell. The latter method is referred to as “3GPP,” as this solution has recently been adopted by 3GPP for the LTE femtocells [15]. To be more specific, the 3GPP solution for the HNB transmission power expressed in dBm equals $\min\{RSCP_{CPICH}^{macro} + 55\text{dB}; P_{max}\}$, where $RSCP_{CPICH}^{macro}$ is the RSCP from the strongest received macro at the HNB (measured using NLM) and P_{max} equals the maximum HNB transmission power. For both NOPC and 3GPP cases, it is assumed that the CPICH to total transmit power equals -10 dB. Recall from Section 3 that with QoS-SP-IM, the CPICH power is adjusted dynamically. For the simulations, we assume that the desired HNB coverage in terms of equivalent path loss equals 56 dB and 62 dB for the dense and suburban environments, respectively. These values can be estimated based on typical size of apartment/homes as, building types, and maximum separation between HUE and HNB.

Figure 4 shows the cumulative distribution function (cdf) of the experienced downlink end-user throughput for HUEs. As expected, the best HUE performance is observed for the NOPC case, *i.e.*, HNB transmitting at its maximum power. The results for the QoS-SP-IM algorithm with a desired throughput guarantee of 256 kbps and 1 Mbps shows accurate adjustment according to those targets. It is observed that the outage probability only equals 3%–4% for the QoS-SP-IM algorithm, *i.e.*, first evidence of the QoS-SP-IM algorithm’s ability to self-adjust the HNB transmission power to fulfill the minimum QoS target. For the considered case, the scheme with 3GPP HNB PC seems to result in performance close to that of the QoS-SP-IM algorithm with 1 Mbps downlink target. Looking at the

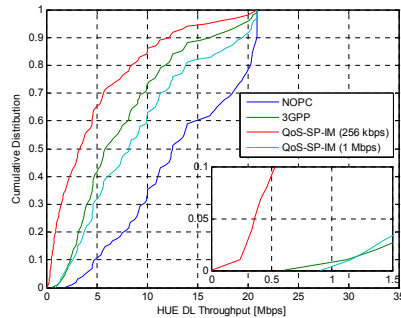
50th percentile or 90th percentile throughput, it is observed that HUEs often experience much higher end-user throughputs as compared to their minimum guaranteed throughput in the service level agreement.

Figure 4. Cumulative distribution function of experienced HUE downlink throughput in dense urban for different HNB Tx power configuration schemes.



In order to demonstrate the scalability of the proposed QoS-SP-IM algorithm to self-adjust for different environments, similar results as in Figure 4 are pictured in Figure 5 for the suburban scenario. Again it is observed that the QoS-SP-IM algorithm efficiently self-adjusts so the outage probability for the desired throughput targets of 256 kbps and 1 Mbps equals only on the order of 1%. Despite the many differences between the dense and suburban environments, it is interesting to note that the experienced HUE throughput in Figures 4 and 5 is actually fairly close.

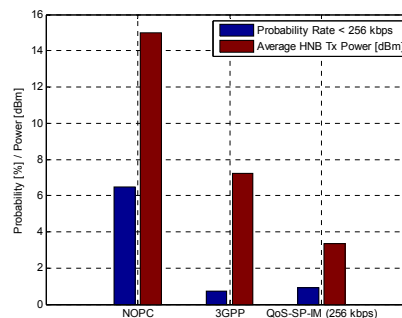
Figure 5. Cumulative distribution function of experienced HUE downlink throughput in suburban for different HNB Tx power configuration schemes.



Next, we look in more detail towards outage defined inside the home or the apartment. We extend our outage definition considering that any user in an HNB home/apartment would be interested to connect to the HNB (e.g., for the case with different charging policies) or that the operator wants to offload the user from the macro network. We therefore look across the whole area of the apartment or

home where an HNB is installed and we report the outage defined as where the user is unable to get a minimum throughput of 256 kbps from neither the MNB nor the HNB. This outage probability for the dense urban scenario is reported in Figure 6. Also the average HNB Tx power resulting from each scheme is reported in Figure 6. The QoS-SP-IM algorithm displays very high performance, with only ~1% probability of not connecting to the HNB or experiencing too low a throughput. The former is achieved with less than 4 dBm HNB Tx power. The higher performance of the QoS-SP-IM algorithm is obtained by adjusting CPICH power to desired coverage, while afterwards setting the HS-DSCH power to meet the minimum throughput requirement. The NOPC case naturally uses 15 dBm Tx power, but despite the relative high power, there is 6% probability of experiencing too low a throughput. The latter comes from not having all UEs connecting to their own HNB, but instead connecting to the outside macro-layer not being able to offer the desired throughput. This behavior is observed because the HNB CPICH Tx power is too low (−10 dB compared to the total HNB Tx power), thus leading to less coverage but higher cell throughput performance. The 3GPP HNB PC solution shows comparable performance to the QoS-SP-IM algorithm in terms of outage probability, but at the expense of using 4 dB higher transmit power.

Figure 6. Displayed key performance metrics for the three considered HNB Tx power setting methods in the dense urban scenario: **(a)** Probability that a UE with matching CSG identity inside the same apartments as its own HeNB experience a downlink throughput lower than 256 kbps; **(b)** average HNB transmit power.



As commented earlier, one of the merits of the derived QoS-SP-IM algorithm is its ability to dynamically adjust the CPICH and data channel HNB Tx power to achieve the desired objectives in terms of coverage and minimum target data rate. Thus, while the CPICH to total HNB Tx power is fixed at −10 dB for cases with NOPC and 3GPP PC, the QoS-SP-IM algorithm computes these power settings for each HNB. The cdf of the CPICH to total HNB TX power for the QoS-SP-IM algorithms is reported in Figure 7 for the dense urban scenario. Here it is, among others, visible how the HNB decreases the data channel power as the minimum target bit rate is decreased from 1 Mbps to 256 kbps.

The impact on MUE performance is shown in Figure 8. Here, it is clearly demonstrated that the use of NOPC for CSG HNBs have significant influence on MUE performance, showing that 8% of the MUE gets no service (zero throughput). The latter is naturally a result of experiencing too high

interference from nearby CSG HNB(s), causing macro-layer coverage holes, or dead-zones as it is also sometimes called. The best MUE performance is clearly observed for QoS-SP-IM algorithm. Here it is also visible that the cost of increasing the minimum target throughput inside their home with an accessible HNB comes at a cost of lower throughput for MUEs.

Figure 7. Cumulative distribution function of HNB CPICH to total Tx power for the dense urban scenario.

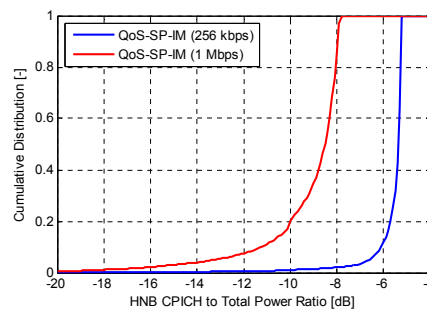
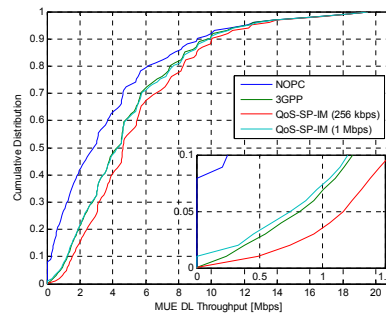


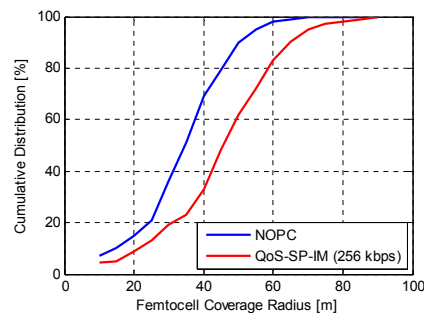
Figure 8. Dense urban downlink performance of macro users versus algorithm for setting transmission powers (CSG case).



As discussed earlier, a key benefit of our proposed algorithm is the dynamic adaptation of the CPICH and the HS-DSCH powers to reach optimal tradeoff among coverage and capacity. Figure 9 illustrates the potential of our proposed algorithm in the suburban case when compared to NOPC. In the method here, the target coverage of the algorithm is set to infinite which automatically instructs the algorithm to maximize the cell coverage to the point where target QoS in both downlink and uplink can still be maintained and ensuring that NR conditions are still met (see e.g., Table 2). Compared to the NOPC algorithm, we now also accept the use of maximum transmit power in the femtocell but we redistribute it optimally to the control and data channels to get the right balance. The result is clear: A net

coverage gain of 10–15 meters is obtained in most cases. This is a clearly perceived advantage for remote buildings where femtocells are deployed mainly for coverage and safety (e.g., for emergency calls).

Figure 9. Effective femtocell coverage *versus* algorithm (coverage target of QoS-SP-IM set to ∞).



As stated earlier, the joint optimization of downlink and uplink is important in order to scale the capacity and coverage of the cell (downlink parameters) while ensuring that the allowed budget for NR contribution as well as uplink performance of the femtocell is critically met. To simulate the different approaches, we deploy a large set of uplink users and they attempt to get a 3.8 Mbps uplink service (to test high noise rise risks). If a user gets reliable connection but less SINR, it is allocated the possible maximum uplink data rate. The NR statistics at the MNB is compiled and results are shown in Table 3.

Table 3. Uplink simulation results in a dense urban scenario.

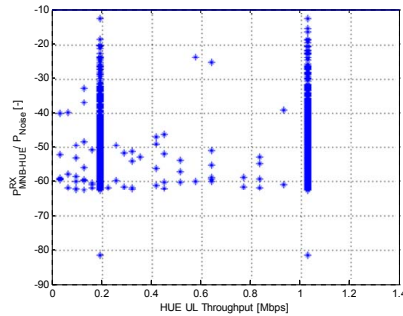
Uplink Interference Metrics	No power control, HUE allowed to transmit up to 24 dBm	No power control, HUE power capping of −20 dBm	QoS-SP-IM (256 kbps), Adaptive uplink power capping
Noise rise from worst-case HUE, found across all simulated cells	23.95 dB	0.21 dB	0.14 dB
Mean noise rise from worst-case HUE found in each simulated cell	8.48 dB	0.02 dB	0.02 dB
Mean per HNB NR contribution across all HUE in all cells	4.82 dB	0.01 dB	0.01 dB

It is seen that without any uplink protection, the macro network is severely impacted by the presence of the HUE population. Across all simulations and cell locations, a NR of nearly 24 dB was experienced by a single HUE at the nearby MNB. Numbers are smaller on average but still significantly high to pose a threat to the macro-layer. With a fixed power capping of −20 dBm, the noise rise contribution is effectively controlled, *i.e.*, contributions in the 0.01 dB range. It is seen that the dynamic method of our solution, although it provides higher HUE transmit powers and performance when conditions are right, still effectively controls the NR contribution from the HNBs.

The difference is that it still allows the uplink QoS to be part of the dimensioning process and thus guaranteed.

When exploring in more detail the uplink performance *versus* the QoS target, we need to compare uplink throughput available to UE *versus* what NR that UE produces towards the overlay macro. For the settings here, we have allocated to each HNB an own interference contribution to nearest MNB of -11.7 dB compared to the noise floor. We achieve this value by reserving 3dB noise rise for MUEs and then divide the remaining noise rise contribution (3 dB) to 30 simultaneously active HNBs per macro site. We combine simulations for 200 kbps and 1 Mbps QoS target respectively and the per-HUE interference at MNB is plotted in Figure 10.

Figure 10. HUE interference at nearest macro site *versus* achieved uplink throughput.



Investigating the user statistics, the outage for the 200 kbps case is 3.8%, thereby indicating good accuracy of the algorithm. As we are achieving a compromise between desired downlink coverage and desired uplink rate in the algorithm, we are slightly sacrificing the uplink performance when setting the QoS target to high values. For the 1 Mbps case, we observe that 76% of users are able to achieve the uplink throughput. 90% of users exceed 500 kbps and 95% of users achieve 256 kbps. The reported HUE UL performance is found reasonable, considering that the proposed QoS-SP-IM algorithm preserves the MUE UL performance, see Table 2. For both scenarios we can see from Figure 10 that no HUE exceeds the set NR limit.

5. Verification by Field Measurements

In order to verify the core functionality of the proposed QoS-SP-IM concept, a measurement campaign was carried out. Verifying the full concept requires extensive measuring trials across a large region so our measurement results focus on the femto coverage area and uplink noise rise contribution from HUEs *versus* power settings, as well as interference scenario. We have performed co-channel measurements with a femtocell and a macrocell in the same frequency band (2132.4 MHz) and have ensured a very wide dynamic range of interference level from macro in our measurements, by performing the measurements at macrocell edge and macrocell center. The measurement campaign was carried out at the campus area of Tampere University of Technology (TUT). A Nokia Test Network (NTN) macrocell base station (3GPP Release 6) provided macro coverage to the entire TUT

campus area. As the NTN is only used for test purposes, the network is considered empty after office hours and is ideal for simulation verification. The sector antenna of the macrocell base station was mounted on top of a nearby four-storey office building. For the measurement campaign, the HNB was deployed in offices, lecture rooms, or hallways at TUT and the chosen locations of the MNB and the HNB are shown in Figure 11.

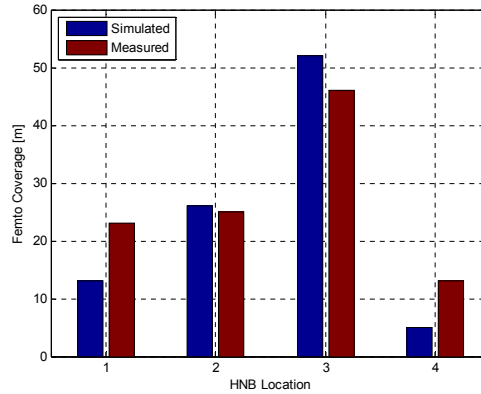
Figure 11. HNB locations and MNB sector direction.



There are no buildings between the MNB and HNB location 4, hence LOS propagation, while a four-storey building is located in between the macro site and femto location 1, 2, and 3. Moreover, the distance between the MNB and the HNB locations varies between 250 m (Location 4) and 600 m (Location 1), while the MNB to HNB path loss was measured to 120 dB and 100 dB, for HNB location 1 and 4, respectively.

Throughout the measurement campaign, a single HNB was deployed at the measurement location and the backhaul was public internet via TUT network. Most measurements were performed after office hours to minimize the possibility of having other active UEs in the network, *i.e.*, minimize the uplink noise rise error. The HNBs, measurement UEs, and the measurement software were all 3GPP Release 8 compliant [17–20].

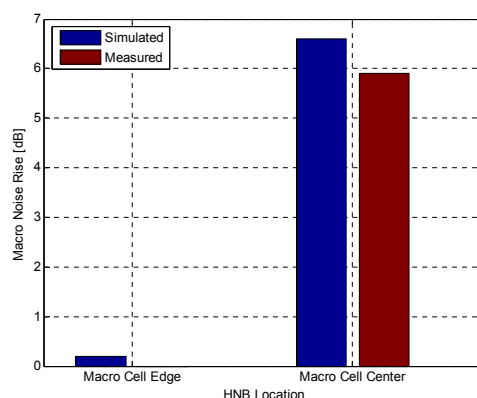
A key element for verification is the ability to predict the femtocell coverage zone accurately as function of set pilot and data power ratios. The CPICH power of the HNB was set to -10 dBm. Next, the femto indoor coverage was measured at all four HNB locations with very different macro interference levels. The measurement UE was placed close to the HNB and connected to the HNB. The femto coverage was measured by walking away from the HNB while the UE was kept in connected mode. The distance was measured to the location where the measurement UE lost femto coverage or handed over to the surrounding macrocell. This procedure was repeated three times and the femto coverage was determined by averaging the three measurements. Figure 12 shows the measured femto coverage and the simulated femto coverage for similar RF conditions.

Figure 12. Measured and simulated femto coverage.

Despite the small differences the simulation results are considered verified by the measurement results. For example, in the simulations, the femto antenna patterns are assumed to be omnidirectional, though, in reality, this is not true. Due to practical implementation imperfections, the actual antenna pattern varied up to ± 10 dB when measured in an anechoic radio chamber—the antenna pattern measurements are not presented in the paper. Consequently, the femto coverage area varies accordingly to the actual rotation of the HNB. Therefore, from Figure 12, the measurement and simulation results show a good match given the expected accuracy, with some underestimation happening when HNB is near to the macro center.

Next, it was verified whether uplink noise rise from HUE is effectively predicted by the algorithm (9). The uplink noise rise caused by a single HUE was measured at locations 1 and 4. These locations were selected as they represent the extremes in terms of HNB to MNB path loss, as location 1 is located at macrocell edge and location 4 is located at the macrocell center with LOS propagation conditions. The measurements were performed by starting a HSUPA data session while the measurement UE was connected to the HNB and then forcing the HUE to transmit at the maximum allowed transmission level (0 dBm during the measurements), by walking away from the HNB, before leaving the femto building, still connected to the HNB, and causing the HUE to generate maximum possible uplink interference in the surrounding macrocell. By accessing radio network controller (RNC) data from the measurement time span, the potential uplink noise rise is found. The femto CPICH transmit power was 10 dBm during the measurements (e.g., case with rather aggressive coverage enhancement for the femtocell). The uplink noise rise measurements were performed at macrocell edge and at macrocell center. Figure 13 shows the measured noise rise and the simulated noise rise.

The measurement and simulation results show a good match. The small differences between measured and simulated values are within the measurement accuracy and can be explained by the varying UE transmit power during the measurements due to the fading characteristics of the transmission channel between the HUE and the MNB and between the HUE and the HNB.

Figure 13. Measured and simulated noise rise in the macrocell.

6. Conclusions

In this paper, we provided a framework for QoS self-provisioning for 3G small cells based on a lightly cognitive approach—the network listen mode. The QoS self-provisioning and interference management method utilizes network measurements to optimally configure power configuration of its different downlink channels, as well as the suitable uplink transmit power limits for connected users. The method works for both dedicated and shared carrier deployment of femtocells as well as for both open and closed subscriber group modes. However, in this paper, we have chiefly focused our attention on the most challenging shared channel and restricted access modes.

It is shown that our algorithm controls the target data rates with high accuracy and good robustness against the modeled dynamic effects which cannot be predicted by the HNB-only based method. Examples have shown only few percent outages of up to 1 Mbps downlink throughput and additionally guaranteed across the whole intended femtocell coverage zone. In uplink, fair rates around 256–512 kbps can be guaranteed, but beyond these rates, tradeoffs need be established. Besides controlling the desired femtocell service levels to tight margins, the solution offers additional benefits in terms of required downlink transmit power. Compared to not using power control and a fixed data to pilot power ratio, the proposed method provides 9 dB transmission power saving and better outage performance. Compared to a 3GPP reference method, the outage is very similar, but a power saving close to 4 dB is still achieved. By a simple parameter setting (coverage target set to infinity), the method automatically boosts the femtocell range while maintaining the QoS requirements at the cell edge. For the case where a 256 kbps service is sufficient, the method offers approximately 15-meter coverage radius increase compared to a no power control reference with a fixed and typical transmit power ratio.

The framework was partially verified by field measurements in an existing network deployment with femtocell deployed on same carrier as macro. The results show a good match between predicted and offered coverage in real network with test equipment for macrocell edge deployment of small cell.

Future Internet **2013**, *5*

188

Furthermore, the assumptions related to uplink noise rise dimensioning were verified. The predicted NR contribution from a single user connected to the small cell was checked depending on the small cell geographical position during extensive measurement campaign. While not being a full verification of the proposed method, it verifies the main assumptions behind the algorithms. Future work will focus on moving beyond the initial parameter initialization to further enhancements that could be made possible by collecting measurements of end-users session throughputs and measurement reports from connected devices.

Acknowledgements

The authors appreciate the strong support from colleagues at Nokia Siemens Networks Kalle Jokio, Srinivasan Selvaganapathy, as well as Tero Isotalo and Rajadurai Subramaniam from the Tampere University of Technology for measurement campaign support.

References

1. Holma, H.; Toskala, A. *WCDMA for UMTS-HSPA Evolution and LTE*, 5th ed.; John Wiley & Sons Ltd.: Hoboken, NJ, USA, 2010.
2. Mahmoud, H.; Guvenc, I. A Comparative Study of Different Deployment Modes for Femtocell Networks. In Proceedings of 2009 IEEE 20th International Symposium on the Personal, Indoor and Mobile Radio Communications, Tokyo, Japan, 13–16 September 2009.
3. Kolding, T.E.; Ochal, P.; Czerepiński, P.; Pedersen, K.I. Impact of Carrier Configuration and Allocation Scheme on 3G Femtocell Offload Effect. In Proceedings of the IEEE Vehicular Technology (VTC-Spring), Yokohama, Japan, 15–18 May 2011.
4. Calin, D.; Claussen, H.; Uzunalioglu, H. On femto deployment architectures and macrocell offloading benefits in joint macro-femto deployments. *Commun. Mag.* **2010**, *48*, 26–32.
5. Han, K.; Choi, Y.; Kim, D.; Na, M.; Choi, S.; Han, K. Optimization of Femtocell Network Configuration under Interference Constraints. In Proceedings of 7th International Symposium on the Modeling and Optimization in Mobile, Ad Hoc, and Wireless Networks WiOPT 2009, Seoul, Korean, 23–27 June 2009.
6. Nagaraja, S.; Chande, V.; Goel, S.; Meshkati, F.; Yavuz, M. Transmit Power Self-Calibration for Residential UMTS/HSPA + Femtocells. In Proceedings of the 2011 International Symposium on Modeling and Optimization in Mobile, Ad Hoc and Wireless Networks (WiOpt), Princeton, NJ, USA, 9–13 May 2011.
7. Morita, M.; Matsunaga, Y.; Hamabe, K. Adaptive Power Level Setting of Femtocell Base Stations for Mitigating Interference with Macrocells. In Proceedings of the 2010 IEEE 72nd Vehicular Technology Conference Fall (VTC 2010-Fall), Ottawa, ON, USA, 6–9 September 2010.
8. Jo, H.-S.; Mun, C.; Moon, J.; Yook, J.-G. Interference mitigation using uplink power control for two-tier femtocell networks. *Wirel. Commun. IEEE Trans.* **2009**, *8*, 4906–4910.
9. Chandrasekhar, V.; Andrews, J.G.; Muharemovict, T.; Shen, Z.; Alan, G. Power control in two-tier femtocell networks. *IEEE Trans. Wirel. Commun.* **2009**, *8*, 4316–4328.
10. Parkvall, S.; Englund, E.; Lundevall, M.; Torsner, J. Evolving 3G mobile systems: Broadband and broadcast services in WCDMA. *IEEE Commun. Mag.* **2006**, *44*, 68–74.

11. 3GPP Technical Specification 25.214. Physical Layer Procedures (FDD) Version 9.7.0. Available online: <http://www.3gpp.org> (accessed on 23 April 2013).
12. Pedersen, K.I.; Frederiksen, F.; Kolding, T.E.; Lootsma, T.F.; Mogensen, P.E. Performance of high speed downlink packet access in co-existence with dedicated channels. *IEEE Trans. Veh. Technol.* **2007**, *56*, 1261–1271.
13. Pedersen, K.I.; Mogensen, P.E.; Kolding, T.E. Overview of QoS options for HSDPA. *IEEE Commun. Mag.* **2006**, *44*, 100–105.
14. 3GPP Technical Specification 36.814. Evolved Universal Terrestrial Radio Access (E-UTRA); Further Advancements for E-UTRA Physical Layer Aspects. Version 9.0.0. Available online: <http://www.3gpp.org> (accessed on 23 April 2013).
15. Szufarska, A.; Safjan, K.; Strzyz, S.; Pedersen, K.I.; Frederiksen, F. Interference Mitigation Methods for LTE-Advanced Networks with Macro and HeNB Deployments. In Proceedings of the 2011 IEEE Vehicular Technology Conference (VTC Fall), San Francisco, CA, USA, 8 September 2011; pp.1–5.
16. Gora, J.; Kolding, T.E. Deployment Aspects of 3G Femtocells. In Proceedings of the 2009 IEEE 20th International Symposium on Personal, Indoor and Mobile Radio Communications, Tokyo, Japan, 13–16 September 2009; pp. 1507–1511.
17. Arcadyan Femtocell Access Point MAF9001A. Available online: <http://www.arcadyan.com> (accessed on 23 April 2013).
18. Thomson TG870, Residential Gateway with Integrated 3G Femtocell. Available online: <http://www.technicolorbroadbandpartner.com> (accessed on 23 April 2013).
19. Sierra Wireless AirCard USB 309. Available online: <http://www.sierrawireless.com/> (accessed on 23 April 2013).
20. Anite, Nemo Outdoor. Available online: <http://www.anite.com> (accessed on 23 April 2013).

© 2013 by the authors; licensee MDPI, Basel, Switzerland. This article is an open access article distributed under the terms and conditions of the Creative Commons Attribution license (<http://creativecommons.org/licenses/by/3.0/>).

Appendix C

Femto versus WiFi as Indoor Solution

This appendix contains a paper reprint of the paper *3G Femto or 802.11g WiFi: Which is the Best Indoor Data Solution Today?* This paper supports the discussion and conclusion of Chapter 2.

- N. T. K. Jørgensen, I. Rodriguez, J. Elling, and P. Mogensen, “3G Femto or 802.11g WiFi: Which is the Best Indoor Data Solution Today?” in *2014 IEEE Vehicular Technology Conference (VTC Fall)*, September 2014

Paper Reprint

3G Femto or 802.11g WiFi: Which is the Best Indoor Data Solution Today?

Niels T. K. Jørgensen *, Ignacio Rodriguez *, Jan Elling † and Preben Mogensen *‡

*Department of Electronic Systems, Aalborg University, Aalborg, Denmark. Email: {nj, irl, pm}@es.aau.dk

†Telenor A/S, Aalborg, Denmark. Email: jae@telenor.dk

‡Nokia Solutions and Networks, Research Center Aalborg, Denmark. Email: preben.mogensen@nsn.com

Abstract—In this paper HSPA Release 6 femto and IEEE 802.11g WiFi indoor data solutions are investigated from an end user perspective. Femto and WiFi access points are deployed at typical locations in an urban environment and end user performance is measured. Three key performance indicators (KPI) were defined - downlink and uplink user data rates, latency and mobile power consumption. These three KPIs are of high importance when choosing an indoor data solution. Our measurements show that the downlink and uplink data rates of the WiFi solution are significantly higher than femto data rates. Similarly, latency results show that WiFi outperforms the femto solution. Especially, the radio resource control (RRC) connection set-up time increases the latency for the femto. In terms of idle power consumption the best results are obtained when the mobile camps on the femto. Whereas, WiFi performs best in all active mode power consumption measurements. Based on our KPIs, the preferred indoor data solution today is WiFi. The deciding factor is the combined latency and power performance of the WiFi, where WiFi outperforms the femto.

I. INTRODUCTION

In 2012 mobile data traffic grew 70 % and 33 % of the traffic was offloaded onto fixed networks through WiFi or femto cells [1]. These numbers show that indoor networks already play an important role in the wireless communication world today. In addition the share of mobile data traffic offloaded by WiFi or femto cells is expected to increase even further, up to 46 % in 2017. Consequently, indoor small cells have received plenty of attention in academia and open literature [2] [3]. Both technologies are low cost solutions to improve indoor data capacity, usually deployed by the end user, and connected to public Internet. Despite the similarities there are also some fundamental differences. Whereas, the WiFi access point is a standalone device, the 3G femto access point connects to a femto gateway. The femto gateway acts as a femto concentrator towards the cellular core network and for configuration of femto access points. Hence, the femto solution is more complex than the plug and play WiFi solution. Though, for an end user the femto and WiFi installation procedure is identical. In terms of spectrum, the femto solution requires licensed spectrum where the WiFi solution utilizes unlicensed spectrum.

Achievable downlink and uplink user data rates are important in marketing and adaptation of wireless communication technologies, and user data rates have also been studied in several papers, both in terms of system simulations and measurement campaigns. For example, the measurements in [4] concludes that femto HSDPA data rates are up to five times higher than macro HSDPA data rates.

The importance of low latency should not be neglected. In [5] it is studied how increased website loading delays affect the users experience. Delay is the time from the user is clicking on a hyperlink to the time the web page is loaded. The authors conclude that website delays should be kept under 4 seconds. Otherwise, users tend to stop using the website. The authors of [6] conclude that for simple tasks on the internet, the delay should be less than 2 seconds. None of the delay studies specify any access technology, but they clearly indicate the maximum expected delay when dealing with internet services and applications. In [7], 3G femto round trip time is measured to approximately 130 ms. But it is not measured how the RRC connection set-up procedure effects the overall femto latency.

Mobile power consumption has also been studied extensively as it is part of the overall user experience. In [8], the power consumption when connected to 3G macro and WiFi is measured. It is concluded that the tail energy overhead is significant in 3G, because the mobile is kept in high power states after data transfers are completed. A similar conclusion is reached in [9].

This paper contributes with an indoor 3GPP Release 6 femto and 802.11g WiFi measurement campaign performed in realistic environments and for applicable use cases. Our objective is to determine which is the ultimate indoor data solution today from an end user perspective. For an end user the important key performance indicators (KPI) are: user data rates, latency, and mobile power consumption. Previous studies have mainly focussed on the KPIs independently or for a single technology only. We are measuring all KPIs for both femto and WiFi, including the interaction between the different KPIs. And based on the outcome, we conclude which is the best indoor data solution today.

Section II introduces the measurement scenarios and measurement equipment, followed by measurement methodology in Section III. In Section IV, the measurement results are presented, and finally, Section V concludes the paper.

II. MEASUREMENT SCENARIO AND EQUIPMENT

Two measurement scenarios are chosen; a typical enterprise scenario and a typical apartment scenario. Common for both measurement locations is an overlay live macro network with inter-site distances of a few 100 meters. At both locations the macro network supports HSDPA dual cell, resulting in a DL bandwidth of 10 MHz. The surroundings are characterized by typical urban building constructions. At both measurement locations, indoor macro coverage is sufficient for both voice and data services, so an indoor data solution should provide

higher data rates and increase the network capacity.

A. Enterprise Environment

The first measurement location is a 3-floor office building with a ground area of approximately 15 m x 45 m. Inside, 20 offices and meeting rooms are connected by a single corridor. During the measurement campaign, a WiFi or a femto access point is deployed in an office in the middle of the corridor at ground floor. Hence, the femto and WiFi access points provide indoor coverage to offices 25 meters away. Measurements are performed in all the accessible offices and meeting rooms at ground floor. Outside the building, the serving 3-sector macro site is located approximately 150 meters away. In previous measurement campaigns, the building penetration loss has been measured to approximately 20 dB at 2 GHz [10] and the indoor macro received signal code power (RSCP) is ranging from -90 dBm to -65 dBm. Finally, it is noted that a planned indoor WiFi network is already deployed in the building and is active during all measurements. Therefore, it is not possible to select a non-interfered WiFi channel for the measurements. This location is referred to as *Enterprise* location.

B. Home Environment

The second measurement location is in a residential area with surrounding apartment building blocks of up to 5 floors. The area of the apartment is 60 m² and consist of 5 rooms and is located at the third floor in a 5-floor building. Due to installation constraints, the femto and WiFi access points are deployed in the corner of the apartment and the coverage radius is up to 10 meter. During the measurement campaign, indoor cellular service was provided by an outdoor 3-sector macro site located approximately 150 meters away from the apartment. The indoor RSCP is in the range -80 dBm to -70 dBm. Since it is a residential area, there is no coordination of the WiFi access points deployment. Consequently, the number of visible WiFi networks is approximately 10, and depends on the exact location in the apartment. For the measurement campaign the WiFi channel with the best quality is chosen, which is the channel with the lowest interfering RSSI level. This location is referred to as *Home* location.

C. Measurement Equipment

The femto access point is an IP Access E16 and is UMTS/HSPA 3GPP Release 6 compliant. During measurements, the total wideband transmission power of the femto access point was manually configured to +24 dBm and the common pilot channel (CPICH) power to +14 dBm. HSDPA dual cell is not supported by the femto. The femto is co-channel deployed with the existing macro network and connects to a femto gateway in the cellular core network. Two different WiFi access points were used at the two locations. Both are IEEE 802.11g compliant. The WiFi total transmit power is set to +16 dBm. Table I lists the femto and WiFi specifications.

At both locations, the same backhaul is used for the femto and WiFi access points. The backhaul performance was measured, and the results are presented in Table III in Section IV.

TABLE I. MEASUREMENT SET-UP.

	Femto	WiFi
Carrier frequency	2.0 GHz (UARFCN 10788)	2.4 GHz (ISM band)
Bandwidth	5 MHz	20 MHz
Transmission power	+24 dBm	+16 dBm
CPICH Power	+14 dBm	-
Version	HSPA Release 6	IEEE 802.11g
Peak DL data rate	14.4 Mbps	54 Mbps
Peak UL data rate	1.45 Mbps	54 Mbps
DL Modulation	Up to 16 QAM	Up to 64 QAM
UL Modulation	Up to QPSK	Up to 64 QAM

III. MEASUREMENT METHODOLOGY

For the user data rates and the latency measurements a Samsung Galaxy S III device was used. The measurement software of the mobile is QualiPoc¹, which enables logging of phone and network data. HSDPA dual cell is supported by the mobile, and is utilized for the macro DL measurements. All measurements are also performed for macro, and the macro results are mainly included as reference results.

A. User Data Rates

All data rate measurements were performed during off peak hour in order to minimize interference from other users of the network and other WiFi access points. Consequently, the measurements were performed during the evening at Enterprise and during the night at Home. In practice, it is impossible to avoid interfering users completely, hence the measurements results are considered the best achievable performance in the given environments.

In all available rooms, DL and UL file transfers are performed. The file transfers are performed via the file transfer protocol (FTP), and the average FTP DL or UL throughput is computed per file transfer. It is ensured that each file transfer lasts at least 1 minute. During the file transfer, the measurement mobile is moved around inside the room at walking pace. When measuring the femto data rates, a measurement is considered invalid if the mobile is handed over to a macro cell before the file transfer is complete and left out of the comparison. Measurements are performed in 15 offices at Enterprise and 5 rooms at Home and the measurements are performed twice in each office/room.

B. Latency

In this work, the latency is measured as the round trip time (RTT) plus potential RRC set-up time for femto [11]. By utilizing the Internet Control Message Protocol (ICMP) *ping* command it is possible to time the latency. Table II lists the latency test parameters. In our set-up, the radio resource control (RRC) connection release timer is shorter than 10 seconds. Therefore, with a ping interval of 2 seconds, the measured latency includes only the RTT. However, for a ping interval of 10 seconds, the measured latency includes both the RTT and the RRC set-up time. The latency measurements are performed in the same room where the femto or WiFi access point is deployed.

C. Mobile Power Consumption

For the power measurements an Agilent N6705B (using Option N6781a) DC power analyzer is used. The power analyzer measures and logs the instantaneous power consumption of the mobile. During power measurements the battery of

¹©SwissQual AG

TABLE II. LATENCY TEST PARAMETERS.

Parameter	Value
Destination	http://www.google.com (212.10.212.30)
Number of packets	25
Packet size	32 bytes
Ping interval #1	2 seconds
Ping interval #2	10 seconds

the mobile is removed, and the mobile is powered by the DC power analyzer. The sampling period is 1 ms and the measurement duration is 30 seconds, except for the FTP download case. In the FTP download case the measurement duration depends on the achievable user data rate. For practical reasons, the power measurements are only performed at the Enterprise location.

We are performing five power measurements for macro, femto, and WiFi:

- Idle mode - screen OFF
- Idle mode - screen ON
- Load a new web page every 15 seconds - screen ON
- Load a new web page every 45 seconds - screen ON
- 20 MB FTP download - screen ON

For the two web browse test cases, a total of 10 web pages are loaded with intervals of 15 and 45 seconds. The 10 web pages are the top 10 most popular web pages according to [12]. In test cases where the screen is ON, the brightness is set to MAXIMUM. For the WiFi idle mode test case and screen OFF, WiFi connectivity is kept enabled. And during all WiFi measurements the cellular modem is not disabled, it is in idle mode. This way, cellular voice service is always available via the macro network. No user inputs are required for the measurements which ensures identical test procedures.

Comparison of the FTP test case is not straightforward. In this case the measurement duration depends on the achievable DL data rate. Instead of comparing the average power, the energy efficiency (EE) is computed as:

$$EE = \frac{R_{avg}}{P_{FTP} - P_{idle, ScreenON}} \quad [\text{bit/J}] \quad (1)$$

where R_{avg} is the average downlink data rate, P_{FTP} is the average power during the FTP test, and $P_{idle, ScreenON}$ is the average power in idle mode and screen ON.

IV. MEASUREMENT RESULTS

Before presenting the data rate, latency, and power measurements, the backhaul quality measurement results are presented in Table III. It is seen that the Enterprise data rates are significant higher than the Home data rates. Though, it is important to note that the data rates are on par with the median data rates in Denmark. In first half of 2013 the median DL and UL data rates in Denmark were 20.4 Mbps and 1.9 Mbps, respectively [13]. Therefore, similar results are to be expected in an average Danish household.

TABLE III. BACKHAUL PERFORMANCE AT ENTERPRISE AND HOME. MEASURED VIA WWW.SPEEDTEST.NET.

	DL	UL	RTT
Enterprise	61 Mbps	33 Mbps	13 ms
Home	16 Mbps	2.8 Mbps	23 ms

A. User Data Rates

Figure 1 shows the measured DL data rates at Enterprise and Home. It is seen that the WiFi at Enterprise performs

best by a large margin. Even at the offices at the ends of the corridor (more than 20 meter away from the WiFi access point) the DL throughput is 5 Mbps. Despite the coverage area of WiFi at Home is smaller, the achievable data rates are lower due to increased number of interfering WiFi networks. The maximum femto DL throughput measured is approximately 4 Mbps. Based solely on achievable user data rates, WiFi is the preferred solution. However, the comparison is not fair. First of all, the DL transmission bandwidth of the femto is only 5 MHz, whereas for macro the DL transmission bandwidth is 10 MHz due to the HSDPA dual cell. For WiFi the transmission bandwidth is 20 MHz, shared between DL and UL. The spectral efficiency (SE) for macro, femto and WiFi is close to 0.5 bps/Hz, except WiFi at Enterprise where WiFi differs from the others with a SE of 1.53 bps/Hz. This is due to less interfering WiFi networks and is in general accordance with the conclusion from [14]. Therefore, when comparing the DL spectral efficiency, WiFi performs best if only single user and a few interfering WiFi networks are present, e.g. in a planned WiFi network environment. Otherwise, there is no particular difference between the achievable femto and WiFi user SE. Despite the higher femto RSCP the macro and femto SE are similar because femto only supports 16 quadrature amplitude modulation (QAM).

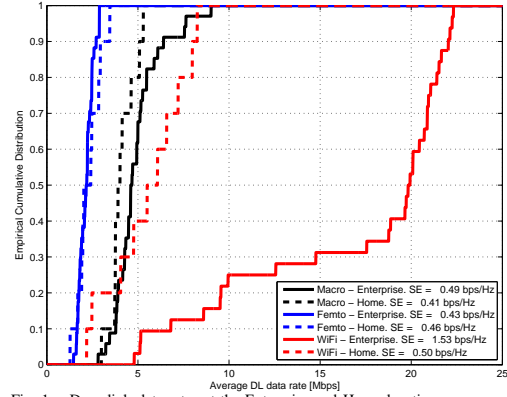


Fig. 1. Downlink data rates at the Enterprise and Home locations.

The measured UL throughput is shown in Fig. 2. Again, it is seen that the WiFi performance is significantly higher at Enterprise than the rest. It is also seen that the WiFi throughput at Home is limited by the backhaul throughput (2.8 Mbps). The femto UL throughputs are practically independent of the location. Similar to the DL, an end user would prefer the WiFi solution due to the experienced data rates. Also, when comparing the UL SE WiFi performs best with a SE of more than 0.24 bps/Hz compared to less than 0.13 bps/Hz for femto. This number might seem low, but one should keep the maximum theoretical SE in mind, as this is only 0.29 bps/Hz due to the quadrature phase shift keying (QPSK) modulation limitations.

B. Latency

Next, the femto and WiFi latency is compared. Table IV shows the latency for the Enterprise location with a ping interval of 2 seconds. Backhaul performance is included as upper bound reference with an average latency of 24 ms. The

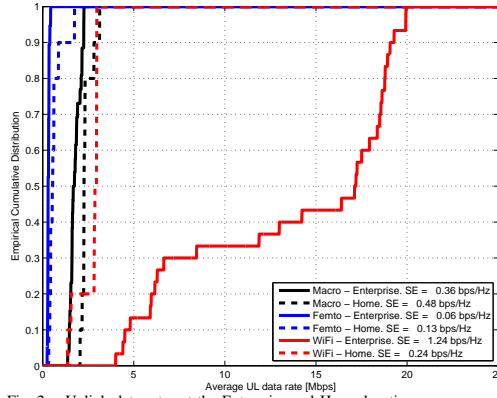


Fig. 2. Uplink data rates at the Enterprise and Home locations.

WiFi latency is the best with an average of 44 ms, and is quite consistent with a minimum measured latency of 36 ms and a maximum of 47 ms. Whereas, the average latency of the macro and the femto solution is approximately the double of the WiFi and just below the 100 ms mark. The maximum latency of the macro and the femto is 119 ms and 112 ms, respectively. These results are similar to those reported in [7].

TABLE IV. MEASURED LATENCY WITH A PING INTERVAL OF 2 SECONDS AT ENTERPRISE.

	Backhaul	Macro	Femto	WiFi
Average	24 ms	83 ms	99 ms	44 ms
Minimum	22 ms	53 ms	92 ms	36 ms
Maximum	35 ms	119 ms	112 ms	47 ms

At Home, the WiFi and macro latencies are reduced while the femto latency is increased, see Table V. Still, the latency is not a big differentiator between the wireless solutions, and well below the acceptable limits from [5] and [6].

TABLE V. MEASURED LATENCY WITH A PING INTERVAL OF 2 SECONDS AT HOME.

	Wired	Macro	Femto	WiFi
Average	18 ms	71 ms	112 ms	23 ms
Minimum	14 ms	53 ms	105 ms	12 ms
Maximum	31 ms	105 ms	131 ms	46 ms

Table VI lists the latency results for ping intervals of 10 seconds at Enterprise and Home, respectively. It is noted that the measured values include both the RTT and the RRC set-up time for macro and femto. As expected, the WiFi latency does not change when the ping interval is increased to 10 seconds as there is no need for control signalling in contention based medium access systems. On the contrary, the macro and femto average latency has increased significantly due to the RRC set-up time. With a interval of 10 seconds the average macro latency increases to almost 1.5 seconds.

The latency of the femto is affected even worse, it is increased to more than 3 seconds, approximately 60 times longer than the average WiFi latency. The increased latency is definitely noticed when using the femto for Internet browsing and also longer than the acceptable 2 seconds from [6]. When the ping interval is 10 seconds, the mobile leaves the

TABLE VI. MEASURED LATENCY WITH A PING INTERVAL OF 10 SECONDS.

	Enterprise			Home		
	Macro	Femto	WiFi	Macro	Femto	WiFi
Average	1.4 s	3.1 s	50 ms	1.2 s	3.3 s	26 ms
Minimum	126 ms	99 ms	37 ms	66 ms	101 ms	12 ms
Maximum	3.3 s	4.6 s	189 ms	3.1 s	4.6 s	46 ms

CELL_DCH state [11] during the ping intervals. Therefore, the mobile needs to come back to CELL_DCH before it is possible to use the data connection again. The required signalling is sent via the femto to the femto gateway via public Internet. The connection via public internet is best effort without any quality of service (QoS) requirements [15]. A few times during the measurements the phone was kept in CELL_DCH due to background signalling, resulting in minimum latency significantly lower than the average.

Measurements show that WiFi achieves the lowest latency for all the tested scenarios. From a user point of view, the increased femto latency is definitely noticeable during web browsing. The main problem arises when the mobile is not in CELL_DCH state when traffic is about to be sent and the mobile therefore needs to go to CELL_DCH state before the data connection is available for the user. A potential solution to the problem is to increase the inactivity timer such that the mobile is kept in CELL_DCH while the user is reading a web page.

C. Mobile Power Consumption

Table VII presents the power measurement results. In idle and screen OFF, the WiFi power consumption is approximately 22 % higher than the femto power. With the screen ON, WiFi power is only 7 % higher than femto, since the screen/CPU is now the major contributor in terms of power consumption. In theory, with screen OFF and in idle mode, the battery would last 4 days and 7 hours with femto, and 3 days and 12 hours with WiFi. Battery capacity is 7.8 Wh.

TABLE VII. POWER MEASUREMENT RESULTS.

	Macro	Femto	WiFi
Power - Idle, screen OFF	85 mW	77 mW	94 mW
Power - Idle, screen ON	0.9 W	0.8 W	0.9 W
Power, Web browse 15 sec	2.1 W	2.0 W	1.3 W
Power, Web browse 45 sec	1.8 W	1.8 W	1.2 W
EE, FTP Download	222 kbit/J	139 kbit/J	1236 kbit/J

Comparing the web browse test cases show that WiFi performs best. The web browse 15 second test case show that the femto power is approximately 45 % higher than WiFi and 51 % higher in the web browse 45 second test case. The reason for the high femto power is that the mobile is kept in RRC_connected mode (CELL_DCH, CELL_PCH, or CELL_FACH) after the web pages are loaded, whereas the mobile returns faster to the idle power level when connected to WiFi. Also, WiFi is almost 10 times more energy efficient compared to femto in the FTP DL test.

In idle mode the power consumption is lowest when the mobile is camping on the femto, otherwise WiFi performs best. For an end user this means, that WiFi delivers the best power performance if the specific mobile is used more than approximately 30 minutes per day. Using a femto and considering the web browse model where a website is loaded every 45 seconds the mobile battery lasts for 4 hours and 30 minutes. Using WiFi, the battery lasts almost 7 hours.

D. Result Discussion

Based on the DL and UL experienced data rates, WiFi is the preferred indoor solution from an end user point of view. This is mainly due to the wider transmission bandwidth of the WiFi system and support of higher modulation. However, even when comparing the spectral efficiency, WiFi performs best. Especially, if the WiFi network is not interfered by other WiFi networks. The experienced data rates would be higher, if the tested WiFi equipment was IEEE 802.11n/ac compliant. Similar, a HSPA Release 7 compliant femto could also improve the experienced femto data rates and spectral efficiency as HSPA Release 7 supports higher modulation than HSPA Release 6.

Our latency measurements showed that this is the main disadvantage of the femto solution. The measured femto average latency was longer than 3 seconds if the mobile was not kept in CELL_DCH state during ping intervals. Such latency is simply too long compared to end user expectations, and considerably shorter latencies are expected in wireless communications systems today. For comparison, the WiFi latency was below 50 ms. If the mobile was kept in CELL_DCH mode, the femto latency is approximately 100 ms. However, the power consumption in CELL_DCH is higher than in idle [8]. Therefore, configuring the inactivity timers is a trade-off between perceived user performance and mobile power consumption. Potentially, 3GPP LTE femto cells could improve the femto latency [16]. Field trials have shown that latency for macro LTE networks are lower compared to macro HSPA networks [17][18].

The lowest idle mode power consumption was achieved when the mobile was camping on the femto, WiFi power consumption was 22 % higher. During the web browse sessions the mobile's average power was lowest for WiFi. In femto and macro networks the mobile stays in the high power RRC states after the data transmission is completed. For end users, this means that if the mobile is used for web browsing more than 30 minutes per day, WiFi is the best solution in terms of power consumption. WiFi also showed the best power efficiency in the FTP file download test.

Basically, our measurements show that WiFi provides better latency and active mode power consumption than the femto, regardless of the femto RRC configuration. Increasing the RRC inactivity timers would reduce the femto latency at the expense of increased mobile power consumption. Decreasing the RRC inactivity timers reduces the power consumption but increases latency.

V. CONCLUSION

Increasing mobile data volumes and user expectations encourage the deployment of indoor small cell networks. Femto and WiFi solutions are two strong candidates for present and future indoor data networks. An indoor femto (3GPP Release 6) and WiFi (IEEE 802.11g) measurement campaign was carried out to conclude which solution is the preferred indoor data solution today for an end user.

Three key performance indicators were identified: user data rate, latency, and mobile power consumption. Based on our key performance indicators, WiFi is the best indoor data solution. WiFi offers higher data rates, lower latency and lower active mode power only at the cost of a slightly higher idle power compared to femto. The major femto disadvantage was high

latency due to required RRC state transitions. Our measurement results also showed that the femto RRC set-up has a huge impact on both latency and power consumption. It was not possible to find a compromise where femto outperforms WiFi in latency and power consumption.

In the future, WiFi 802.11ac and 3GPP LTE will be the de facto WiFi and cellular standards. Further research is necessary to determine the performance improvements introduced in the aforementioned standards.

ACKNOWLEDGMENT

The authors would like to thank Mads Lauridsen (AAU) for his assistance during the power consumption measurements and Per Andresen (Telenor) for macro and femto configuration. The project is partly funded by The European Regional Development Fund.

REFERENCES

- [1] Cisco, "Cisco Visual Networking Index: Global Mobile Data Traffic Forecast Update, 2012–2017," White Paper, February 2013.
- [2] V. Chandrasekhar, J. Andrews, and A. Gatherer, "Femtocell Networks: A Survey," *Communications Magazine, IEEE*, vol. 46, no. 9, 2008.
- [3] S. Hasan, N. Siddique, and S. Chakraborty, "Femtocell versus WiFi - A Survey and Comparison of Architecture and Performance," in *Wireless VITAE. 1st International Conference on*, 2009.
- [4] J. Weitzen and T. Grosch, "Measuring coverage quality for femtocell and macrocell broadband data services," in *COMCAS. IEEE International Conference on*, 2009, pp. 1–4.
- [5] D. F. Galletta, R. Henry, S. McCoy, and P. Polak, "Web Site Delays: How Tolerant Are Users?" *JAIS*, vol. 5, pp. 1–28, 2003.
- [6] F. F. Nah, "A Study on Tolerable Waiting Time: How Long are Web Users Willing to Wait?" *Behaviour & Information Technology*, vol. 23, no. 3, pp. 153–163, May 2004.
- [7] M. Kankare, A. Asp, Y. Sydorov, J. Niemelä, and M. Valkama, "Large-Scale Femtocell Network Deployment and Measurements," in *Multiple Access Communications*, ser. Lecture Notes in Computer Science, M. Jonsson, A. Vinel, B. Bellalta, N. Marina, D. Dimitrova, and D. Fiems, Eds. Springer International Publishing, 2013, vol. 8310.
- [8] N. Balasubramanian, A. Balasubramanian, and A. Venkataramani, "Energy Consumption in Mobile Phones: A Measurement Study and Implications for Network Applications," in *Proceedings of the 9th ACM SIGCOMM Conference on IMC*. New York, NY, USA: ACM, 2009.
- [9] L. Wang and J. Manner, "Energy Consumption Analysis of WLAN, 2G and 3G interfaces," in *GreenCom, IEEE/ACM Int'l Conference on Int'l Conference on CPSCom*, 2010, pp. 300–307.
- [10] I. Rodriguez, H. C. Nguyen, N. T. Jørgensen, T. B. Sørensen, J. Elling, M. B. Gentsch, and P. Mogensen, "Path Loss Validation for Urban Micro Cell Scenarios at 3.5 GHz Compared to 1.9 GHz," *GlobeCom. IEEE Conference and Exhibition*, 2013.
- [11] 3GPP, "Technical Specification Group Radio Access Network; Radio Resource Control (RRC); Protocol specification (Release 11)," 3rd Generation Partnership Project (3GPP), TS 25.331 V11.7.0, sep 2013.
- [12] eBizMBA. (2014, Jan.) Top 15 Most Popular Websites. [Online]. Available: <http://www.ebizmba.com/articles/most-popular-websites>
- [13] Erhvervsstyrelsen, "Telestatistik Første halvår 2013," Tech. Rep. ISSN: 1903-3753, 2013.
- [14] L. G. Garcia, I. Rodriguez, D. Catania, and P. Mogensen, "IEEE 802.11 Networks: A Simple Model Geared Towards Offloading Studies and Considerations on Future Small Cells," in *VTC Fall, IEEE 78th*, 2013.
- [15] 3GPP, "Technical Specification Group Radio Access Network; UTRAN architecture for 3G Home Node B (HNB); Stage 2 (Release 12)," 3rd Generation Partnership Project (3GPP), TS 25.467 V12.0.0, dec 2013.
- [16] J. Andrews, H. Claussen, M. Dohler, S. Rangan, and M. Reed, "Femtocells: Past, Present, and Future," *Selected Areas in Communications, IEEE Journal on*, vol. 30, no. 3, pp. 497–508, 2012.
- [17] M. Laner, P. Svoboda, P. Romirer-Maierhofer, N. Nikaen, F. Ricciato, and M. Rupp, "A Comparison Between One-Way Delays in Operating HSPA and LTE Networks," in *WiOpt, 10th International Symposium on*, 2012.
- [18] B. McWilliams, Y. Le Pezennec, and G. Collins, "HSPA+ (2100 MHz) vs LTE (2600 MHz) Spectral Efficiency and Latency Comparison," in *NETWORKS, XVth International*, 2012, pp. 1–6.

Appendix D

Required Bandwidth

For the performance evaluation, the transmission bandwidth parameter is paramount for the simulated throughput performance. Hence, the selection of transmission bandwidth and Guaranteed Bit Rate (GBR) constraint is strongly correlated. If the GBR is set too high compared to the transmission bandwidth, the system becomes capacity limited rather than interference limited. In a capacity limited scenario, Inter-Cell Interference Coordination (ICIC) techniques are not likely to improve the overall network performance. Lowering the GBR, the resource utilisation increase, and the system becomes interference limited. Based on [23, 95] a resource utilisation operation point of approximately 70% is targeted.

Assuming the default simulation parameters (no ICIC techniques employed), listed in Table 4.4 on page 79, and a transmission bandwidth ranging from 20 MHz to 60 MHz, the supported GBR is presented in Figure D.1. The supported GBR is defined as the 5%-ile UE throughput, meaning that at least 95% of the User Equipments (UEs) are served with at least GBR. The figure includes two curves, for resource utilisation of 60% and approximately 70%. As expected, if the network is less loaded, the supported GBR is higher and vice versa. For the simulated transmission bandwidth range, there is almost a linear dependency between transmission bandwidth and supported GBR. For sake of simplicity, a GBR of 3 Mbps is selected. The implication of this, is that the total transmission bandwidth is set to 20 MHz. If a larger transmission bandwidth (and GBR) is selected, the consequence is a significant increase in simulation time, however, the conclusions for larger bandwidths are expected to be similar to the 20 MHz bandwidth simulation conclusions.

Generally speaking, Long Term Evolution Advanced (LTE-A) supports carrier aggregation of up to 5 Component Carriers (CCs), the supported bandwidth for each CC ranges

from 1.4 MHz to 20 MHz [136, 137]. Each CC is backward compatible with Release 8/9 UEs. Furthermore, in [138] it is shown that the number of CCs should approximately be half of the maximum number of neighbours. Therefore, in this work the number of CCs is set to four. This implies that the bandwidth of each CC is 5 MHz, which ensures 3GPP compliance in terms of CC configuration.

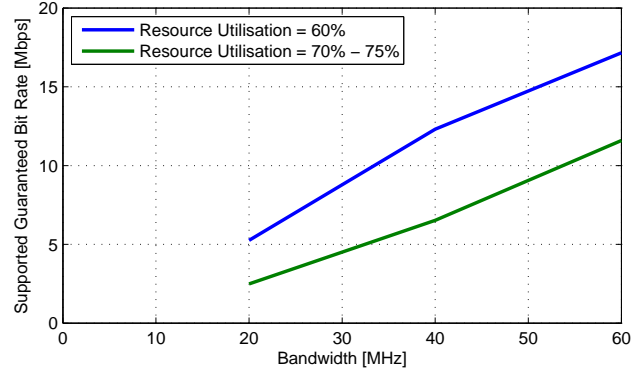


Fig. D.1: Supported Guaranteed Bit Rate versus transmission bandwidth.

Appendix E

Fixed Frequency Reuse

The simplest form of Frequency Reuse (FR) is FR-1, also known as global FR which simply means that all small cells utilise the entire spectrum for transmission. This also implies that a user in a FR-1 network potentially experiences strong interference from a neighbouring small cell in the close vicinity. To protect users from such situations, FR-2 or FR-4 can be applied. In a FR-2 deployment the transmission bandwidth is divided into two transmission bands, from now on referred to as Component Carriers (CCs). Half of the small cells transmit on the first CC and the other half of the small cell transmit on the second CC. The advantage of FR-2 is that users only experience interference from half of the small cells, thus the users experience greater Signal to Interference and Noise Ratio (SINR) than in an FR-1 deployment. Ideally, the FR-2 pattern is designed such that small cells close to each other (in terms of path loss) are utilising different CC for optimum user SINR improvement.

Naturally, the downside of applying FR is the reduced transmission bandwidth. For FR-2 the bandwidth is halved and for FR-4 only one forth of the original bandwidth is utilised. Therefore, the capacity gain of the SINR improvement must be larger than the capacity loss due reduced bandwidth before FR larger than one makes any sense:

$$C_1 = B \cdot \log_2 (1 + \gamma_1) \quad (\text{E.1})$$

$$C_R = \frac{B}{R} \cdot \log_2 (1 + \gamma_R) \quad (\text{E.2})$$

$$C_R > C_1 \quad (\text{E.3})$$

where B is the FR-1 transmission bandwidth, γ is the user SINR, R is the reuse order, and C is the Shannon capacity [19]. From (E.1) to (E.3) the required FR SINR improvement is calculated. Figure E.1 illustrates the required gain for different frequency reuses. For low

SINR users the required FR SINR gain is below 10 dB for all the illustrated FR schemes. However, for high SINR user the required FR-2 SINR gain is 30 dB and for FR-4 the required SINR gain is 90 dB. Consequently, frequency reuse is mainly advantageous for low SINR users. For high SINR users the required SINR improvement is unrealistic high, thus high SINR user throughput performance is expected to degraded.

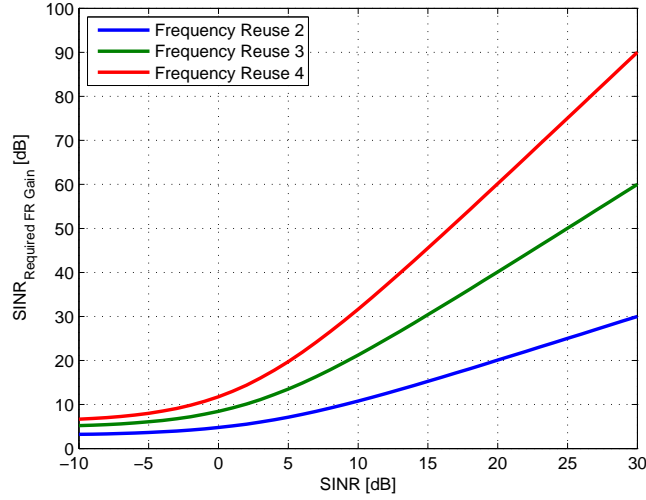


Fig. E.1: Required SINR gain for different frequency reuses.

E.1 Evaluation of Fixed Frequency Reuse Schemes

FR-1, FR-2, and FR-4 pattern is applied according to Figure E.2, the simulation scenario is described in Section 4.5. By applying the above FR-2 pattern it is ensured that no small cells in adjacent apartments transmit on the same CC. Two small cells transmitting on the same CC is always separated by at least 2 indoor (or outdoor) walls. In the case of FR-4 small cells transmitting on the same CC is always separated by at least 3 indoor (or outdoor) walls.

Figure E.3 shows the 50%-ile UE throughput for FR-1, FR-2, and FR-4 versus the offered load. The figure clearly shows that the 50%-ile UE throughput for FR-1 is superior to FR-2 and FR-4. Especially at low load, the performance drop of FR-2 and FR-4 is significant. As the offered load is increased, the relative gain of FR-1 decreases as expected. At higher load, the UEs experience an increased interference and the gain of FR-2 and FR-4 increases, and at maximum load the performance of FR-2 equals the performance of

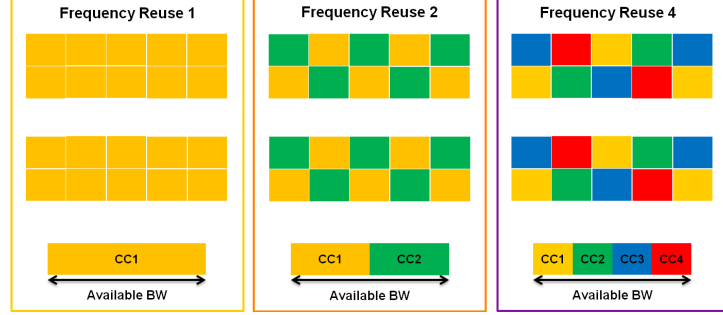


Fig. E.2: Frequency reuse 1, 2, and 4 pattern in the simulated scenario.

FR-1. This implies that the SINR gain of FR-2 is never larger than the reduced bandwidth penalty. The figure also reveals that for FR-2 and FR-4 the network overloads already at offered load of 400 Mbps.

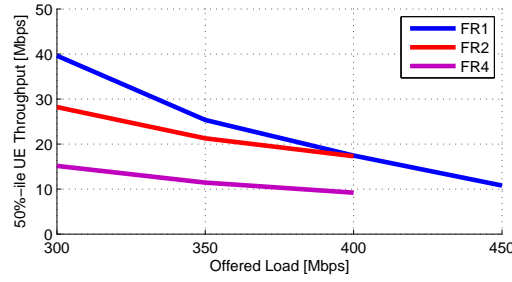


Fig. E.3: 50%-ile User Equipment (UE) throughput for FR-1, FR-2, and FR-4.

In Figure E.4, the 5%-ile UE throughput performance is presented. The trends are similar to the trends from Figure E.3. From a coverage throughput point of view, FR-1 is the best performing solution. Even at high load, the gain of reduced interference is smaller than the loss of transmission bandwidth. Therefore, the conclusion is clear, FR-2 and FR-4 are not suitable in a dense small cell environment. It is important to stress, that this conclusion is only valid when the small cells are Open Subscriber Group (OSG). Frequency reuse only improves the UE throughput performance if the small cells are Closed Subscriber Group (CSG) as reported in [133, 139, 140]. In CSG scenarios, the UEs might not connect to cell with the strongest received power, since the UEs are only allowed to connect to the small cell located in the same room or apartment. And this leads to low SINR areas inside the building. For UEs located in these low SINR UEs, frequency reuse improves the throughput significantly.

In order to understand the limiting factor of the fixed FR schemes Figure E.5 depicts

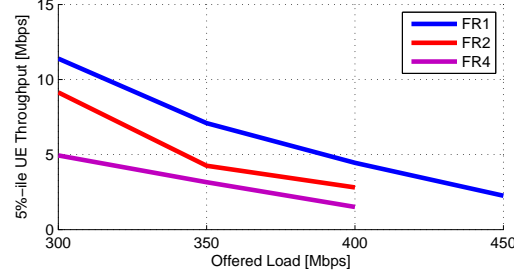


Fig. E.4: 5%-ile UE throughput for FR-1, FR-2, and FR-4.

the number of UE arrivals per second for each of the small cells in the scenario. The number of UE arrivals varies between 4 and 9. The large variation in number of UE arrivals is due to the actual locations of the small cells. E.g. if a small cell is deployed close to an indoor wall, the coverage area of the small potentially extends deep into the neighbouring apartment. Thus, the number of UE arrivals reflects the size of the small cell coverage area. Small cells with a high number of UE arrivals are more prone to overload than small cells with a low number of UE arrivals.

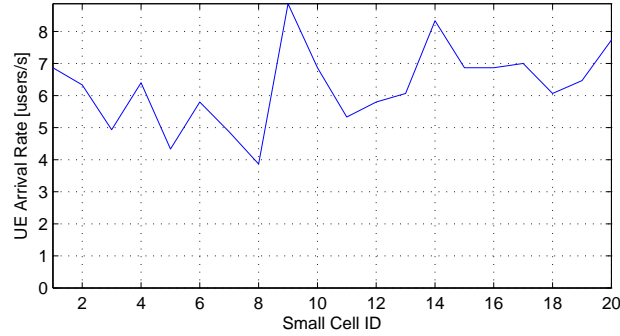


Fig. E.5: Number of UE arrivals per second. Offered load is 500 Mbps which corresponds to an average UE arrival rate of 6.25 UEs/s per small cell.

Figure E.6 illustrates the outage contribution from each of the small cells. It is remarkable, that one small cell (number 14) accounts for almost 30% of the outage, meaning that 30% of the UEs in outage were served by small cell 14. Comparing with Figure E.5 it is seen that small cell 14 has the second highest UEs arrival of all the small cells. Figure E.6 also reveals that the outage contribution varies significantly between the small cells. And three small cell serves all their UEs with the Guaranteed Bit Rate (GBR). Thus, the figure indicates that the overall network outage performance is limited

by small cell 14.

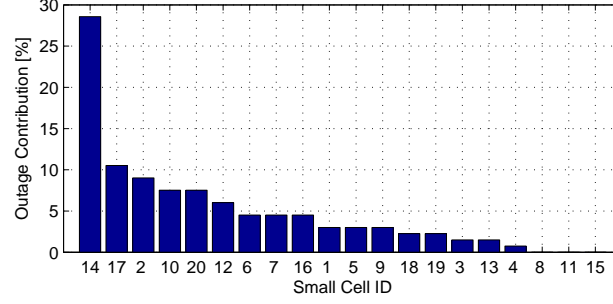


Fig. E.6: Outage contribution from each of the small cells.

Figure E.7 shows the Dominant Interference Ratio (DIR) Cumulative Distribution Function (CDF) utilising FR-1 and assuming Open Loop Traffic Model (OLTM). It is seen that UEs experience the highest DIR values for low load. This is explained by the fact, that only a few UEs are active simultaneously, thus, only few of the neighbouring small cells are causing the non-dominant interference part. By increasing the network load, the number of interfering small cells also increases. Consequently, the non-dominant part of the interference increase more than the dominant interferer. However, it worth noting that the total interference increase for higher network loads. More importantly, the figure also tells, that the DIR is larger than 0 dB in approximately 85% of the time, or in other words, the dominant interferer is as strong as the non-dominant interferers combined. In [6] the DIR for different 3rd Generation Partnership Project (3GPP) network topologies are compared. The DIR of the dense small cell environment is larger than the other network topologies, which means that the potential of muting only the dominant interferer is larger for the dense small cell scenario.

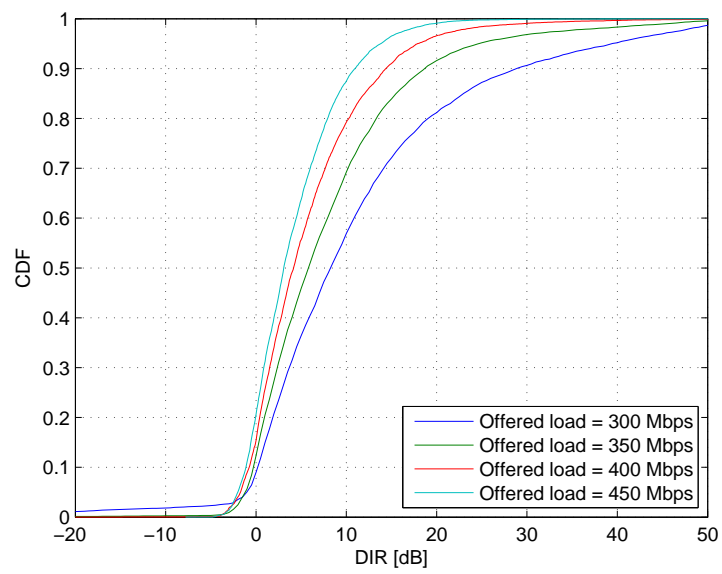


Fig. E.7: DIR for FR-1 and OLTM.

Appendix F

Backhaul Impact

Based on the message sequence charts presented in Section 4.4.1, it is clear, that the time from a outage User Equipment (UE) triggers the framework to the time the action is completed equals:

$$t_{Add} = t_{RTT} + t_{Activate} \quad (F.1)$$

$$t_{Mute} = 1.5 \cdot t_{RTT} + t_{Deactivate} \quad (F.2)$$

where t_{Add} is the time from a UE triggers the framework to a Component Carrier (CC) is added, t_{Mute} is the time from a outage UE triggers the framework to a CC is muted, t_{RTT} is the round trip time, $t_{Activate}$ is the CC activation time, and $t_{Deactivate}$ is the CC deactivation time. Reference [141] specifies the requirements for $t_{Activate}$ and $t_{Deactivate}$ which is 34 ms and 9 ms, respectively.

In [103], different backhaul technologies/classes and their properties are defined based on operator input. The average carried load per small cell is up to 27.5 Mbps (550 Mbps/20) in the results presented in Section 4.6. Thus, the required backhaul throughput is 50 Mbps¹. Considering, the possibility of end user provided backhaul, two backhaul technologies from [103, Table 6.1-1] are considered; *Fiber Access 1* and *Digital Subscriber Line (DSL) Access*. The one way latency for those technologies are specified as 10-30 ms and 15-60 ms, respectively. Using the average value, the Round Trip Time (RTT) for Fiber Access 1 (t_{Fiber}) is 40 ms and 75 ms for DSL Access (t_{DSL}). From these values, it is possible to calculate the effective Carrier Based Inter-Cell Interference Coordination (CB-ICIC) ratio

¹This requirement is valid for transmission spectrum of 20 MHz only.

for an UE being served with exactly R_{min} as:

$$\eta_{CB-ICIC-Add} = \frac{t_{Session} - t_{Add} - t_{avg}}{t_{Session}} \quad (F.3)$$

$$\eta_{CB-ICIC-Mute} = \frac{t_{Session} - t_{Mute} - t_{avg}}{t_{Session}} \quad (F.4)$$

$$t_{Session} = \frac{S}{R_{min}} \quad (F.5)$$

where $t_{Session}$ is the UE session time, $\eta_{CB-ICIC-Add}$ is the effective CB-ICIC time when a CC is added, $\eta_{CB-ICIC-Mute}$ is the effective CB-ICIC time when a CC is muted, S is the payload size, and t_{avg} is the throughput averaging time. Table F.1 summarises the values used for calculating the effective CB-ICIC ratio.

Table F.1: Values used for calculating the effective CB-ICIC ratio.

	Ideal Backhaul	Fiber Access 1	DSL Access
t_{RTT}	0 ms	40 ms	75 ms
$t_{Activate}$	0 ms	34 ms	34 ms
$t_{Deactivate}$	0 ms	9 ms	9 ms
t_{avg}	100 ms	100 ms	100 ms
S	4 Mbit	4 Mbit	4 Mbit
R_{min}	3 Mbps	3 Mbps	3 Mbps

By using the values from Table F.1 in (F.1) through (F.4) the effective CB-ICIC ratio is computed, and presented in Figure F.1. The effective CB-ICIC ratio for ideal backhaul is 92%, whether a CC is muted or added. It is only during t_{avg} that the UEs are not gaining from CB-ICIC. For non-ideal backhaul, it is seen that the effective CB-ICIC ratio lies in the interval from 83% to 87%. For this example the decrease in effective CB-ICIC ratio due to non-ideal backhaul is rather limited. Obviously, this also implies a decrease in CB-ICIC gain, however it is assessed that a significant CB-ICIC is still achievable with non-ideal backhaul. Basically, if $t_{Session} \gg (t_{RTT} + t_{avg})$ it is evaluated that CB-ICIC is able to deliver significant gains compared to ideal backhaul.

F.1 Required Standardisation

The proposed CB-ICIC framework is not 3GPP Long Term Evolution Advanced (LTE-A) Release 12 compliant. More specifically, there is not support for the benefit/cost signalling and muting request. To give an estimate of the benefit/cost message size, the size of a single benefit/cost hypothesis messages, is listed below:

- Add or mute: 1 bit

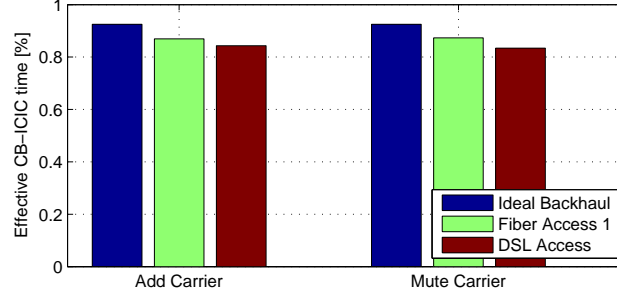


Fig. F.1: Effective CB-ICIC ratio for different backhaul technologies.

- Acting cell: 9 bit (size of physical cell identity [131,142])
- CC identity: 2 bit

In total, the signalling size of each hypothesis ($S_{Hypothesis}$) requires 12 bit. Yet, multiple hypotheses are typically available. Furthermore, from simulation results it is evident that up to 8 hypotheses were executed as the consequence of a single outage UE. To be on the safe side, up to 10 hypotheses should be supported in the benefit/cost messages ($N_{Hypotheses}$). Considering the worst case scenario, where a single small cell constantly serves at least one outage UE, the bit rate of the generated signalling messages ($R_{Message}$) is 24 kbps per outage UE, and is calculated as:

$$R_{Message} = \frac{S_{Hypothesis} \cdot N_{Hypotheses} \cdot N_{SC}}{t_{Outage}} \quad (F.6)$$

where N_{SC} is the number of small cells and t_{Outage} is the outage identification periodicity. This bit rate is upper bound and typically a much lower signalling bit rate is required. This amount of required signalling is considered tolerable given the network performance increase provided by the CB-ICIC framework.

Appendix G

Generic MMSE Solution

In this section the general *minimum mean square error* solution is derived. Consider the filtering system depicted in Figure G.1. The inputs $x[n]$ and $d[n]$ are generated from a jointly Wide Sense Stationary (WSS) source.

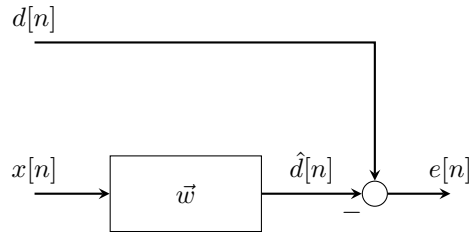


Fig. G.1: Block diagram of filtering system.

An estimate of the desired signal \hat{d} is obtained by applying the filter \vec{w} to the observed signal vector $x[n]$:

$$\hat{d}[n] = \vec{w}^H \vec{x}[n]. \quad (\text{G.1})$$

Then, the quality of the estimation is given as:

$$e[n] = d[n] - \hat{d}[n] \quad (\text{G.2})$$

A commonly used optimisation criterion is the Mean Square Error (MSE) [143, page 419], and the objective is to choose the equalisation vector \vec{w} such that the MSE is minimised.

The equalisation vector which minimises the MSE is denoted \vec{w}_{opt} :

$$J_{MSE} = E[|e[n]|^2] \quad (\text{G.3})$$

$$\vec{w}_{opt} = \arg \min_{\vec{w}} J_{MSE} \quad (\text{G.4})$$

Vector \vec{w}_{opt} is found when the derivative of the cost function (with respect to \vec{w}) equals 0:

$$\frac{J_{MSE}}{\partial \vec{w}} = 0 \quad (\text{G.5})$$

The left side of (G.5) is rewritten by inserting (G.1) and (G.2).

$$\frac{J_{MSE}}{\partial \vec{w}} = \frac{E[|e[n]|^2]}{\partial \vec{w}} = \frac{E[|d[n] - \hat{d}[n]|^2]}{\partial \vec{w}} = \frac{E[|d[n] - \vec{w}^H \vec{x}[n]|^2]}{\partial \vec{w}} \quad (\text{G.6})$$

The derivative of this expression is computed by using the chain rule method [144, page 444]:

$$\frac{J_{MSE}}{\partial \vec{w}} = E \left[2 \cdot e[n] \frac{d[n] - \vec{w}^H \vec{x}[n]}{\partial \vec{w}} \right] = E[2 \cdot e[n] \cdot (-\vec{x}[n])] \quad (\text{G.7})$$

$$\frac{J_{MSE}}{\partial \vec{w}} = -2E[e[n]\vec{x}[n]]. \quad (\text{G.8})$$

By combining (G.1), (G.2), (G.5), and (G.8), the expression is rewritten as follows:

$$E[e_{min}[n]\vec{x}[n]] = 0 \quad (\text{G.9})$$

$$E[(d[n] - \vec{w}_{opt}^H \vec{x}[n]) \vec{x}[n]] = 0 \quad (\text{G.10})$$

$$E[\vec{x}[n]d[n] - \vec{x}[n]\vec{x}[n]^H \vec{w}_{opt}] = 0 \quad (\text{G.11})$$

$$E[\vec{x}[n]\vec{x}[n]^H] \vec{w}_{opt} = E[\vec{x}[n]d[n]]. \quad (\text{G.12})$$

Next, the autocorrelation matrix and the cross-correlation vector is defined as:

$$\mathbf{R}_{xx} = E[\vec{x}[n]\vec{x}[n]^H] \quad (\text{G.13})$$

$$\vec{r}_{xd} = E[\vec{x}[n]d[n]]. \quad (\text{G.14})$$

Now optimal equalisation vector \vec{w}_{opt} is found by combining (G.12), (G.13), and (G.14):

$$\mathbf{R}_{xx} \vec{w}_{opt} = \vec{r}_{xd} \quad (\text{G.15})$$

$$\vec{w}_{opt} = \mathbf{R}_{xx}^{-1} \vec{r}_{xd}. \quad (\text{G.16})$$

From (G.16) it is clear that the auto correlation matrix must be invertible. This is ensured, since autocorrelation matrices are positive definite, and one property of a positive definite matrix is that it is invertible [145].

Appendix H

Reference Signals in LTE and LTE-A

With the introduction of Minimum Mean Square Error - Interference Rejection Combining (MMSE-IRC) receivers, which potentially are inter-cell interference aware, the requirement of a practical estimating method for the transmission channel between User Equipments (UEs) and interfering enhanced Node Bs (eNBs) has followed. In Long Term Evolution Advanced (LTE-A) Release 10, a new reference signalling concept is introduced. However, first Long Term Evolution (LTE) Release 8 Cell-specific Reference Signals (CRSs) are described.

H.1 LTE Release 8 Cell Specific Reference Signals

In LTE Release 8, Channel State Information (CSI) and channel estimation is aided by known pilot signals, called CRS. The CRS are transmitted across the entire transmission bandwidth in order to enable channel estimation and detailed sub-carrier CSI estimation. From the received pilot signals and the known pilot signals the influence of the transmission channel is calculated. Due to overhead considerations, CRS are not transmitted in all sub-carriers. Using interpolation, channel estimates are obtained for sub-carriers where no CRS is transmitted. For in-depth details of LTE Downlink (DL) channel estimations the interested reader is referred to [123].

Figure H.1 shows a simplified illustrations of the pre-coding and addition of CRS process for LTE Release 8, x and r denotes the desired data symbol sequence and reference signal sequence, respectively. From the figure it is clear the CRS are cell-specific and

depends on the number of transmit antennas. Furthermore, it also shows that in order for advanced UEs to estimate the effective channel estimate, the pre-coding must be known in advance.

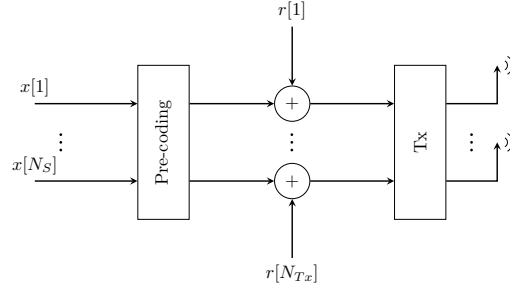


Fig. H.1: Simplified legacy reference symbol encoding process.

In LTE Release 8, the CRS is defined for up to 4 antenna ports. Naturally, the more transmit antennas, the more CRSs need to be transmitted, thus, the overhead also increase. Consider one subframe consisting of 14 Orthogonal Frequency Division Multiplexing (OFDM) symbols and 12 sub-carriers resulting in a total of 168 resource elements. In Table H.1 the number of transmitted CRS and the corresponding CRS overhead is summarised for transmission with normal Cyclic Prefix (CP). It is worth noting, that for four transmit antennas, the CRS overhead is more than 14% of the resource elements. Furthermore, the overhead is independent on the transmission rank, and depends only on the number of transmit antennas.

Table H.1: CRS overhead in LTE Release 8 for normal CP [131].

Number of Tx Antennas	Number of Transmitted CRS	CRS Overhead [%]
1	8	4.8
2	16	9.5
4	24	14.3

In order to meet the requirements of International Mobile Telecommunication-Advanced (IMT-Advanced), as specified by the International Telecommunication Union (ITU) [39], multiple antenna systems are considered an important feature [146,147]. However, antenna systems with four antenna elements are not considered sufficient. Considering, that the CRS overhead for four antenna elements are already more than 14%, a new reference signalling concept with higher multiple antenna efficiency was introduced in LTE-A Release 10.

H.2 LTE-A UE Specific Reference Signals

In LTE Release 8, the CRS are primarily used for transmit antenna identification and serving cell transmit channel estimation. However, in LTE-A Release 10, new reference signals are introduced to more efficiently support multiple transmit antennas and ease the task of practically estimate the interfering transmission channels [122]. This is achieved by introducing so-called Channel State Information Reference Signal (CSI-RS) and User Equipment Specific Reference Signal (UE-RS). As indicated by the name, the purpose of the CSI-RS are for the UEs to obtain the CSI of the serving cell, very similar to the purpose of the legacy CRS. More interesting is the UE-RS. The UE-RSs are pre-coded with the specific UE pre-coding matrix, thereby the name UE-RS. Consequently, the UE data and the UE-RS are multiplexed before the pre-coding process as illustrated in Figure H.2.

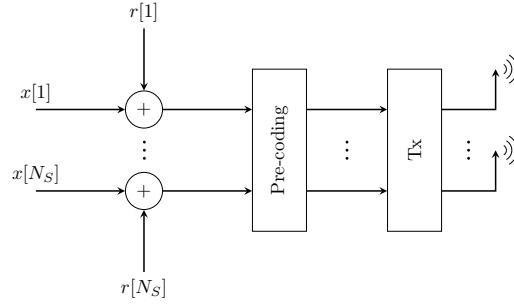


Fig. H.2: Simplified LTE-A UE-RS encoding process.

One of the arguments for introducing UE-RS where the lower overhead for multiple antenna systems. From Figure H.2 it is clear that the number of UE-RS are rank dependent. This means, that the UE-RS overhead for a rank 2 transmission is the same for a 2×2 and a 4×4 antenna configuration. Table H.2 contains the UE-RS overhead for normal CP as specified in [131]. Comparing Table H.1 and Table H.2 it is evident that the overhead of UE-RS is comparable to CRS, despite the fact, UE-RS is defined for up to eight transmit antennas.

Table H.2: UE-RS overhead in LTE-A Release 10 for normal CP [131].

UE transmission rank	Number of Transmitted UE-RS	UE-RS Overhead [%]
≤ 2	12	7.1
> 2	24	14.3

Naturally, UE-RS are only available for UEs which are scheduled. Therefore, CSI-RS

are needed for unscheduled UEs to obtain initial CSI. However, UE-RS diminishes the requirement of CSI-RS compared to legacy CRS. Consequently, the density of CSI-RS is considerably lower than the CRS density. The CSI-RS density is in fact configurable, and according to [82, 148], the density of CSI-RS is typically 1 resource element per antenna port per Physical Resource Block (PRB) and the periodicity is 10 ms. Worst case scenario, i.e. 8 transmit antennas, this corresponds to an overhead of less than 0.5%.

Other important topics related to the introduction of UE-RS and CSI-RS are the support of legacy UEs and codebook design, however, both of these topics are out of scope of this thesis. The performance degradation of legacy UEs due to the introduction of CSI-RS is investigated in [148–150].

Bibliography

- [1] N. T. K. Jørgensen, T. Isotalo, K. Pedersen, and P. Mogensen, “Joint Macro and Femto Field Performance and Interference Measurements,” in *Vehicular Technology Conference (VTC Fall), 2012 IEEE*, September 2012, pp. 1–5.
- [2] T. Kolding, P. Ochal, N. T. K. Jørgensen, and K. Pedersen, “QoS Self-Provisioning and Interference Management for Co-Channel Deployed 3G Femtocells,” *Future Internet*, vol. 5, no. 2, pp. 168–189, 2013.
- [3] I. Rodriguez, H. C. Nguyen, N. T. K. Jørgensen, T. B. Sørensen, J. Elling, M. B. Gentsch, and P. Mogensen, “Path Loss Validation for Urban Micro Cell Scenarios at 3.5 GHz Compared to 1.9 GHz,” in *Global Communications Conference (GLOBECOM), 2013 IEEE*, December 2013.
- [4] N. T. K. Jørgensen, I. Rodriguez, J. Elling, and P. Mogensen, “3G Femto or 802.11g WiFi: Which is the Best Indoor Data Solution Today?” in *2014 IEEE Vehicular Technology Conference (VTC Fall)*, September 2014.
- [5] I. Rodriguez, H. C. Nguyen, N. T. K. Jørgensen, T. B. Sørensen, and P. Mogensen, “Radio Propagation into Modern Buildings: Attenuation Measurements in the Range from 800 MHz to 18 GHz,” in *2014 IEEE Vehicular Technology Conference (VTC Fall)*, September 2014.
- [6] B. Soret, K. I. Pedersen, N. T. K. Jørgensen, and V. Fernández-López, “Interference Coordination for Dense Wireless Networks,” January 2015, accepted for COMMAG - Special Issue: Recent Advances in Technologies for Extremely Dense Wireless Networks.
- [7] CTIA Research, “Wireless Industry Indices Report: 2013,” CTIA - The Wireless Association, Annual Report, 2014.
- [8] The Nielsen Company, “Mobile Youth Around the World,” December 2010.
- [9] Ericsson, “Ericsson Mobility Report,” June 2014.
- [10] Ericsson Consumerlab, “TV and Media,” August 2013.
- [11] Cisco, “Cisco Visual Networking Index: Global Mobile Data Traffic Forecast Update,” January 2009.

- [12] —, “Cisco Visual Networking Index: Global Mobile Data Traffic Forecast Update, 2009-2014,” February 2010.
- [13] —, “Cisco Visual Networking Index: Global Mobile Data Traffic Forecast Update, 2010 - 2015,” February 2011.
- [14] —, “Cisco Visual Networking Index: Global Mobile Data Traffic Forecast Update, 2011 - 2016,” February 2012.
- [15] —, “Cisco Visual Networking Index: Global Mobile Data Traffic Forecast Update, 2012 - 2017,” February 2013.
- [16] —, “Cisco Visual Networking Index: Global Mobile Data Traffic Forecast Update, 2013 - 2018,” February 2014.
- [17] J. Erman and K. K. Ramakrishnan, “Understanding the Super-sized Traffic of the Super Bowl,” in *Proceedings of the 2013 Conference on Internet Measurement Conference*, ser. IMC '13. New York, NY, USA: ACM, 2013, pp. 353–360.
- [18] Nokia Siemens Networks, “LTE Release 12 and Beyond,” 2012.
- [19] C. E. Shannon, “Communication in the Presence of Noise,” *Proceedings of the IRE*, vol. 37, no. 1, pp. 10–21, 1949.
- [20] P. Mogensen, W. Na, I. Kovacs, F. Frederiksen, A. Pokhariyal, K. Pedersen, T. Kolding, K. Hugl, and M. Kuusela, “LTE Capacity Compared to the Shannon Bound,” in *Vehicular Technology Conference, 2007. VTC2007-Spring. IEEE 65th*, April 2007, pp. 1234–1238.
- [21] Cisco, “Cisco Service Provider Wi-Fi: A Platform for Business Innovation and Revenue Generation ,” 2012.
- [22] A. Asp, Y. Sydorov, M. Valkama, and J. Niemela, “Radio Signal Propagation and Attenuation Measurements for Modern Residential Buildings,” in *Globecom Workshops (GC Wkshps), 2012 IEEE*, December 2012, pp. 580–584.
- [23] A. Damnjanovic, J. Montojo, Y. Wei, T. Ji, T. Luo, M. Vajapeyam, T. Yoo, O. Song, and D. Malladi, “A Survey on 3GPP Heterogeneous Networks,” *Wireless Communications, IEEE*, vol. 18, no. 3, pp. 10–21, June 2011.
- [24] A. Ghosh, N. Mangalvedhe, R. Ratasuk, B. Mondal, M. Cudak, E. Visotsky, T. A. Thomas, J. G. Andrews, P. Xia, H. S. Jo, H. S. Dhillon, and T. D. Novlan, “Heterogeneous Cellular Networks: From Theory to Practice,” *Communications Magazine, IEEE*, vol. 50, no. 6, pp. 54–64, June 2012.
- [25] J. G. Andrews, H. Claussen, M. Dohler, S. Rangan, and M. C. Reed, “Femtocells: Past, Present, and Future,” *Selected Areas in Communications, IEEE Journal on*, vol. 30, no. 3, pp. 497–508, April 2012.
- [26] H. Holma and A. Toskala, *WCDMA for UMTS: HSPA Evolution and LTE*. New York, NY, USA: John Wiley & Sons, Inc., 2007.
- [27] 3GPP, “Technical Specification Group Radio Access Network; UTRAN architecture for 3G Home Node B (HNB); Stage 2 (Release 12),” 3rd Generation Partnership Project, Technical Specification 25.467 V12.0.0, December 2012.

- [28] —, “Technical Specification Group Radio Access Network; Evolved Universal Terrestrial Radio Access (E-UTRA) and Evolved Universal Terrestrial Radio Access Network (E-UTRAN); Overall description; Stage 2 (Release 12),” 3rd Generation Partnership Project, Technical Specification 36.300 V12.1.0, March 2014.
- [29] A. A. Widaa, J. Markendahl, and A. Ghanbari, “Toward Capacity-Efficient, Cost-Efficient and Power-Efficient Deployment Strategy for Indoor Mobile Broadband,” in *24th European Regional Conference of the International Telecommunication Society, Florence, Italy, 20-23 October 2013*. Florence: ITS, 2013.
- [30] P. Grønsund, O. Grøndalen, and M. Lähteenoja, “Business Case Evaluations for LTE Network Offloading with Cognitive Femtocells,” *Telecommun. Policy*, vol. 37, no. 2-3, pp. 140–153, March 2013.
- [31] Z. Frias and J. Pérez, “Techno-economic analysis of femtocell deployment in long-term evolution networks,” *EURASIP Journal on Wireless Communications and Networking*, vol. 2012, no. 1, pp. 1–15, 2012.
- [32] H.-S. Jo, P. Xia, and J. Andrews, “Open, closed, and shared access femtocells in the downlink,” *EURASIP Journal on Wireless Communications and Networking*, vol. 2012, no. 1, p. 363, 2012.
- [33] G. de la Roche, A. Valcarce, D. Lopez-Perez, and J. Zhang, “Access Control Mechanisms for Femtocells,” *Communications Magazine, IEEE*, vol. 48, no. 1, pp. 33–39, January 2010.
- [34] J. Gora and T. E. Kolding, “Deployment Aspects of 3G Femtocells,” in *Personal, Indoor and Mobile Radio Communications, 2009 IEEE 20th International Symposium on*, September 2009, pp. 1507–1511.
- [35] L. Garcia, I. Rodriguez, D. Catania, and P. Mogensen, “IEEE 802.11 Networks: A Simple Model Geared Towards Offloading Studies and Considerations on Future Small Cells,” in *Vehicular Technology Conference (VTC Fall), 2013 IEEE 78th*, September 2013, pp. 1–6.
- [36] S. Chiochan, E. Hossain, and J. Diamond, “Channel Assignment Schemes for Infrastructure-Based 802.11 WLANs: A Survey,” *Communications Surveys Tutorials, IEEE*, vol. 12, no. 1, pp. 124–136, First Quarter 2010.
- [37] 3GPP, “Technical Specification Group Core Network and Terminals; Access Network Discovery and Selection Function (ANDSF) Management Object (MO) (Release 12),” 3rd Generation Partnership Project, Technical Specification 24.312 V12.5.0, June 2014.
- [38] Informa Telecoms & Media, “Understanding today’s smartphone user - An analysis of data-usage patterns in the world’s most advanced 4G LTE markets,” 2013.
- [39] ITU-R, “Requirements related to technical performance for IMT-Advanced radio interface(s),” International Telecommunication Union, Report M.2134, 2008.
- [40] M. Iwamura, K. Etemad, M.-H. Fong, R. Nory, and R. Love, “Carrier Aggregation Framework in 3GPP LTE-Advanced,” *Communications Magazine, IEEE*, vol. 48, no. 8, pp. 60–67, August 2010.
- [41] R. Ratasuk, D. Tölö, and A. Ghosh, “Carrier Aggregation in LTE-Advanced,” in *Vehicular Technology Conference (VTC 2010-Spring), 2010 IEEE 71st*, May 2010, pp. 1–5.

- [42] H. Wang, C. Rosa, and K. I. Pedersen, "Dedicated Carrier Deployment in Heterogeneous Networks with Inter-site Carrier Aggregation," in *Wireless Communications and Networking Conference (WCNC), 2013 IEEE*, April 2013, pp. 756–760.
- [43] D. Lee, H. Seo, B. Clerckx, E. Hardouin, D. Mazzaresse, S. Nagata, and K. Sayana, "Coordinated Multipoint Transmission and Reception in LTE-Advanced: Deployment Scenarios and Operational Challenges," *Communications Magazine, IEEE*, vol. 50, no. 2, pp. 148–155, February 2012.
- [44] M. Rahnema, "Overview of the GSM System and Protocol Architecture," *Communications Magazine, IEEE*, vol. 31, no. 4, pp. 92–100, April 1993.
- [45] M. Mouly and M.-B. Pautet, *The GSM System for Mobile Communications*. Palaiseau, France: Cell and Sys, 1992.
- [46] T. Halonen, J. Romero, and J. Melero, *GSM, GPRS and EDGE Performance : Evolution Towards 3G/UMTS*. Chichester: Wiley, 2002.
- [47] R. Meyer, W. Gerstacker, R. Schober, and J. Huber, "A Single Antenna Interference Cancellation Algorithm for Increased GSM Capacity," *Wireless Communications, IEEE Transactions on*, vol. 5, no. 7, pp. 1616–1621, July 2006.
- [48] K. Hooli, M. Juntti, and M. Latva-aho, "Inter-path Interference Suppression in WCDMA Systems with Low Spreading Factors," in *Vehicular Technology Conference, 1999. VTC 1999 - Fall. IEEE VTS 50th*, vol. 1, 1999, pp. 421–425 vol.1.
- [49] I. Ghauri and D. T. M. Slock, "Linear Receivers for the DS-CDMA Downlink Exploiting Orthogonality of Spreading Sequences," in *Signals, Systems and Computers, 1998. Conference Record of the Thirty-Second Asilomar Conference on*, vol. 1, November 1998, pp. 650–654 vol.1.
- [50] C. D. Frank, E. Visotsky, and U. Madhow, "Adaptive Interference Suppression for the Downlink of a Direct Sequence CDMA System with Long Spreading Sequences," *Journal of VLSI signal processing systems for signal, image and video technology*, vol. 30, no. 1-3, pp. 273–291, 2002.
- [51] S. Sesia, I. Toufik, and M. Baker, *LTE, the UMTS Long Term Evolution from Theory to Practice*. Chichester, U.K: Wiley, 2009.
- [52] 3GPP, "Technical Specification Group Radio Access Network; Evolved Universal Terrestrial Radio Access Network (E-UTRAN); X2 application protocol (X2AP) (Release 12)," 3rd Generation Partnership Project, Technical Specification 36.423 V12.1.0, March 2014.
- [53] D. Astely, E. Dahlman, A. Furuskar, Y. Jading, M. Lindstrom, and S. Parkvall, "LTE: the Evolution of Mobile Broadband," *Communications Magazine, IEEE*, vol. 47, no. 4, pp. 44–51, April 2009.
- [54] K. I. Pedersen, Y. Wang, S. Strzyz, and F. Frederiksen, "Enhanced Inter-Cell Interference Coordination in Co-Channel Multi-Layer LTE-Advanced Networks," *Wireless Communications, IEEE*, vol. 20, no. 3, pp. 120–127, June 2013.
- [55] D. Lopez-Perez, I. Guvenc, G. de la Roche, M. Kountouris, T. Q. S. Quek, and J. Zhang, "Enhanced Intercell Interference Coordination Challenges in Heterogeneous Networks," *Wireless Communications, IEEE*, vol. 18, no. 3, pp. 22–30, June 2011.

- [56] Federal Communications Commission. (2014, July) Spectrum Dashboard. [Online]. Available: <http://reboot.fcc.gov/spectrumdashboard/searchSpectrum.seam>
- [57] 3GPP, "Technical Specification Group Radio Access Network; UMTS-LTE 3500 MHz Work Item Technical Report (Release 10)," 3rd Generation Partnership Project, Technical Report 37.801 V10.0.0, October 2011.
- [58] Ericsson, "Regional 3500 MHz band arrangements and use," 3rd Generation Partnership Project, Technical Document RP-080133, March 2008.
- [59] S. Kun, W. Ping, and L. Yingze, "Path Loss Models for Suburban Scenario at 2.3GHz, 2.6GHz and 3.5GHz," in *Antennas, Propagation and EM Theory, 2008. ISAPE 2008. 8th International Symposium on*, November 2008, pp. 438–441.
- [60] G. L. Siqueira, G. L. Ramos, and R. D. Vieira, "Propagation Measurements of a 3.5 GHz Signal: Path-Loss and Variability Studies," in *Microwave and Optoelectronics Conference, 2001. IMOC 2001. Proceedings of the 2001 SBMO/IEEE MTT-S International*, vol. 1, 2001, pp. 209–212 vol.1.
- [61] FCC, "Amendment of the Commission's Rules with Regard to Commercial Operations in the 3550-3650 MHz Band," Federal Communications Commission, Notice 12-148, December 2012.
- [62] 3GPP, "Technical Specification Group Radio Access Network; Small cell enhancements for E-UTRA and E-UTRAN - Physical layer aspects (Release 12)," 3rd Generation Partnership Project, Technical Report 36.872 V12.1.0, December 2013.
- [63] Red Mobile Consulting, "Study of Future Demand for Radio Spectrum in Canada 2011-2015," June 2012.
- [64] D. Xenakis, N. Passas, L. Merakos, and C. Verikoukis, "Mobility Management for Femtocells in LTE-Advanced: Key Aspects and Survey of Handover Decision Algorithms," *Communications Surveys Tutorials, IEEE*, vol. 16, no. 1, pp. 64–91, First Quarter 2014.
- [65] R. F. W. Coates, G. J. Janacek, and K. V. Lever, "Monte Carlo Simulation and Random Number Generation," *Selected Areas in Communications, IEEE Journal on*, vol. 6, no. 1, pp. 58–66, January 1988.
- [66] R. Wahl, G. Woelfle, P. Wertz, and P. Wildbolz, "Dominant Path Prediction Model for Urban Scenarios," in *14th IST Mobile and Wireless Communications Summit*, June 2005.
- [67] Nokia Siemens Networks, Nokia, "Field Measurement Results at 1.9 GHz and 3.5 GHz," 3rd Generation Partnership Project (3GPP), Technical Document R1-131233, April 2013.
- [68] ITU-R, "Propagation data and prediction methods for the planning of indoor radiocommunication systems and radio local area networks in the frequency range 900 MHz to 100 GHz," International Telecommunication Union, Recommendation P.1238-7, February 2012.
- [69] J. Moré and D. Sorensen, "Computing a Trust Region Step," *SIAM Journal on Scientific and Statistical Computing*, vol. 4, no. 3, pp. 553–572, 1983.
- [70] M. Yavuz, F. Meshkati, S. Nanda, A. Pokhariyal, N. Johnson, B. Raghothaman, and A. Richardson, "Interference Management and Performance Analysis of UMTS/HSPA+ Femtocells," *Communications Magazine, IEEE*, vol. 47, no. 9, pp. 102–109, September 2009.

- [71] 3GPP, "Technical Specification Group Radio Access Network; Evolved Universal Terrestrial Radio Access (E-UTRA); Further advancements for E-UTRA physical layer aspects," 3rd Generation Partnership Project, Technical Report 36.814, March 2010.
- [72] A. Szufarska, K. Safjan, S. Strzyz, K. I. Pedersen, and F. Frederiksen, "Interference Mitigation Methods for LTE-Advanced Networks with Macro and HeNB Deployments," in *Vehicular Technology Conference (VTC Fall), 2011 IEEE*, September 2011, pp. 1–5.
- [73] M. Kankare, A. Asp, Y. Sydorov, J. Niemelä, and M. Valkama, "Large-Scale Femtocell Network Deployment and Measurements," in *Multiple Access Communications*, ser. Lecture Notes in Computer Science, M. Jonsson, A. Vinel, B. Bellalta, N. Marina, D. Dimitrova, and D. Fiems, Eds. Springer International Publishing, 2013, vol. 8310, pp. 100–112.
- [74] J. A. Weitzen and T. Grosch, "Measuring Coverage Quality for Femtocell and Macrocell Broadband Data Services," in *COMCAS. IEEE International Conference on*, 2009, pp. 1–4.
- [75] H. Claussen, "Performance of Macro- and Co-Channel Femtocells in a Hierarchical Cell Structure," in *Personal, Indoor and Mobile Radio Communications, 2007. PIMRC 2007. IEEE 18th International Symposium on*, 2007, pp. 1–5.
- [76] S. F. Hasan, N. H. Siddique, and S. Chakraborty, "Femtocell versus WiFi - A Survey and Comparison of Architecture and Performance," in *Wireless VITAE. 1st International Conference on*, 2009, pp. 916–920.
- [77] eBizMBA. (2014, January) Top 15 Most Popular Websites. [Online]. Available: <http://www.ebizmba.com/articles/most-popular-websites>
- [78] D. F. Galletta, R. Henry, S. McCoy, and P. Polak, "Web Site Delays: How Tolerant Are Users?" *JAIS*, vol. 5, pp. 1–28, 2003.
- [79] F. F.-H. Nah, "A Study on Tolerable Waiting Time: How Long are Web Users Willing to Wait?" *Behaviour & Information Technology*, vol. 23, no. 3, pp. 153–163, May 2004.
- [80] GSM Association, "Fast Dormancy Best Practises," GSM Association, Official Dpcomment TS.18 V 1.0, July 2011.
- [81] M. Lauridsen, H. Wang, and P. Mogensen, "LTE UE Energy Saving by Applying Carrier Aggregation in a HetNet Scenario," in *Vehicular Technology Conference (VTC Spring), 2013 IEEE 77th*, June 2013, pp. 1–5.
- [82] H. Holma and A. Toskala, *LTE for UMTS: Evolution to LTE-Advanced*. Wiley, 2010.
- [83] —, *LTE for UMTS - OFDMA and SC-FDMA Based Radio Access*. Wiley Publishing, 2009.
- [84] T. Kolding, J. Wigard, and L. Dalsgaard, "Balancing Power Saving and Single User Experience with Discontinuous Reception in LTE," in *Wireless Communication Systems. 2008. ISWCS '08. IEEE International Symposium on*, October 2008, pp. 713–717.
- [85] C. Coletti, P. Mogensen, and R. Irmer, "Performance Analysis of Relays in LTE for a Realistic Suburban Deployment Scenario," in *Vehicular Technology Conference (VTC Spring), 2011 IEEE 73rd*, May 2011, pp. 1–5.
- [86] C. Coletti, L. Hu, N. Huan, I. Z. Kovács, B. Vejlgaard, R. Irmer, and N. Scully, "Heterogeneous Deployment to Meet Traffic Demand in a Realistic LTE Urban Scenario," in *Vehicular Technology Conference (VTC Fall), 2012 IEEE*, September 2012, pp. 1–5.

- [87] L. Hu, C. Coletti, N. Huan, P. Mogensen, and J. Elling, "How Much Can Wi-Fi Offload? A Large-Scale Dense-Urban Indoor Deployment Study," in *Vehicular Technology Conference (VTC Spring), 2012 IEEE 75th*, May 2012, pp. 1–6.
- [88] C. Coletti, "Heterogeneous Deployment Analysis for Cost-Effective Mobile Network Evolution - An LTE Operator Case Study," Ph.D. dissertation, Aalborg University, 2012.
- [89] C. Coletti, P. Mogensen, and R. Irmer, "Deployment of LTE In-Band Relay and Micro Base Stations in a Realistic Metropolitan Scenario," in *Vehicular Technology Conference (VTC Fall), 2011 IEEE*, September 2011, pp. 1–5.
- [90] L. Hu, C. Coletti, H. Nguyen, I. Z. Kovács, B. Vejlgaard, R. Irmer, and N. Scully, "Realistic Indoor Wi-Fi and Femto Deployment Study as the Offloading Solution to LTE Macro Networks," in *Vehicular Technology Conference (VTC Fall), 2012 IEEE*, September 2012, pp. 1–6.
- [91] Nokia Siemens Networks, "Deployment strategies for Heterogeneous Networks," 2012.
- [92] —, "Technology Vision for the Gigabit Experience," June 2013.
- [93] C. Sun, L. Huang, J. Jiang, and G. Lu, "Interference Management by Component Carrier Selection for Carrier Aggregation System in Heterogeneous Networks," in *Proceedings of the 2012 International Conference on Information Technology and Software Engineering*, ser. Lecture Notes in Electrical Engineering, W. Lu, G. Cai, W. Liu, and W. Xing, Eds. Springer Berlin Heidelberg, 2013, vol. 210, pp. 969–977.
- [94] J. Li, Y. Liu, J. Duan, and X. Liang, "Flexible Carrier Aggregation for Home Base Station in IMT-Advanced System," in *Wireless Communications, Networking and Mobile Computing, 2009. WiCom '09. 5th International Conference on*, September 2009, pp. 1–4.
- [95] NTT DOCOMO, "Performance Evaluation of ICIC for SCE," 3rd Generation Partnership Project (3GPP), Technical Document R1-133459, August 2013.
- [96] J. Herzen, R. Merz, and P. Thiran, "Distributed Spectrum Assignment for Home WLANs," in *INFOCOM, 2013 Proceedings IEEE*, April 2013, pp. 1573–1581.
- [97] R. K. Jain, D.-M. W. Chiu, and W. R. Hawe, "A Quantitative Measure Of Fairness And Discrimination For Resource Allocation In Shared Computer Systems," Digital Equipment Corporation, Tech. Rep., September 1984.
- [98] J. Riihijarvi, M. Petrova, P. Mahonen, and J. A. Barbosa, "Performance Evaluation of Automatic Channel Assignment Mechanism for IEEE 802.11 Based on Graph Colouring," in *Personal, Indoor and Mobile Radio Communications, 2006 IEEE 17th International Symposium on*, September 2006, pp. 1–5.
- [99] L. G. U. Garcia, I. Z. Kovács, K. I. Pedersen, G. W. O. Costa, and P. E. Mogensen, "Autonomous Component Carrier Selection for 4G Femtocells - A Fresh Look at an Old Problem," *Selected Areas in Communications, IEEE Journal on*, vol. 30, no. 3, pp. 525–537, April 2012.
- [100] 3GPP, "Technical Specification Group Radio Access Network; Evolved Universal Terrestrial Radio Access (E-UTRA); FDD Home eNode B (HeNB) Radio Frequency (RF) requirements analysis (Release 11)," 3rd Generation Partnership Project, Technical Report 36.921 V11.0.0, September 2012.

- [101] D. H. Kang, K. W. Sung, and J. Zander, "Is Multicell Interference Coordination Worthwhile in Indoor Wireless Broadband Systems?" in *Global Communications Conference (GLOBECOM), 2012 IEEE*, December 2012, pp. 4255–4260.
- [102] V. Chandrasekhar and J. G. Andrews, "Spectrum Allocation in Tiered Cellular Networks," *Communications, IEEE Transactions on*, vol. 57, no. 10, pp. 3059–3068, October 2009.
- [103] 3GPP, "Technical Specification Group Radio Access Network; Scenarios and requirements for small cell enhancements for E-UTRA and E-UTRAN (Release 12)," 3rd Generation Partnership Project, Technical Report 36.932 V12.1.0, March 2013.
- [104] R. Agrawal, A. Bedekar, S. Kalyanasundaram, N. Arulselman, T. Kolding, and H. Kroener, "Centralized and Decentralized Coordinated Scheduling with Muting," in *Vehicular Technology Conference, 2014. VTC Spring 2014. IEEE 79th*, May 2014.
- [105] Qualcomm Incorporated, "Dual-strip Small Cell Calibration Statistics for Scenario 2b and 3," 3rd Generation Partnership Project (3GPP), Technical Document R1-132496, May 2013.
- [106] Alcatel-Lucent, "Simulation assumptions and parameters for FDD HeNB RF requirements," 3rd Generation Partnership Project (3GPP), Technical Document R4-091422, March 2009.
- [107] ITU-R, "Guidelines For Evaluation Of Radio Transmission Technologies For IMT-2000," International Telecommunication Union, Recommendation P.1225-0, February 1997.
- [108] I. Z. Kovács, M. Kuusela, E. Virte, and K. I. Pedersen, "Performance of MIMO Aware RRM in Downlink OFDMA," in *Vehicular Technology Conference, 2008. VTC Spring 2008. IEEE*, May 2008, pp. 1171–1175.
- [109] 3GPP, "Technical Specification Group Radio Access Network; Enhanced performance requirement for LTE User Equipment (UE) (Release 11)," 3rd Generation Partnership Project, Technical Report 36.829 V11.1.0, December 2012.
- [110] P. Fotiadis, M. Polignano, D. Laselva, B. Vejlgaard, P. Mogensen, R. Irmer, and N. Scully, "Multi-Layer Mobility Load Balancing in a Heterogeneous LTE Network," in *Vehicular Technology Conference (VTC Fall), 2012 IEEE*, September 2012, pp. 1–5.
- [111] Q. Ye, B. Rong, Y. Chen, M. Al-Shalash, C. Caramanis, and J. G. Andrews, "User Association for Load Balancing in Heterogeneous Cellular Networks," *ArXiv e-prints*, May 2012.
- [112] P. Tian, H. Tian, J. Zhu, L. Chen, and X. She, "An Adaptive Bias Configuration Strategy for Range Extension in LTE-Advanced Heterogeneous Networks," in *Communication Technology and Application (ICCTA 2011), IET International Conference on*, October 2011, pp. 336–340.
- [113] L. Gao, G. Iosifidis, J. Huang, L. Tassiulas, and D. Li, "Bargaining-Based Mobile Data Offloading," *Selected Areas in Communications, IEEE Journal on*, vol. 32, no. 6, pp. 1114–1125, June 2014.
- [114] Y. Jiang, Y. Zhou, M. Anand, F. Meshkati, V. Chande, N. Ko, and M. Yavuz, "Benefits of Transmit and Receive Diversity in Enterprise Femtocell Deployments," in *Modeling and Optimization in Mobile, Ad Hoc and Wireless Networks (WiOpt), 2011 International Symposium on*, May 2011, pp. 456–460.

- [115] A. J. Paulraj, D. A. Gore, R. U. Nabar, and H. Bolcskei, "An Overview of MIMO Communications - A Key to Gigabit Wireless," *Proceedings of the IEEE*, vol. 92, no. 2, pp. 198–218, February 2004.
- [116] J. Proakis, *Digital Communications*, 4th ed. McGraw-Hill Science/Engineering/Math, August 2000.
- [117] M.-O. Damen, H. El-Gamal, and G. Caire, "On Maximum-Likelihood Detection and the Search for the Closest Lattice Point," *Information Theory, IEEE Transactions on*, vol. 49, no. 10, pp. 2389–2402, October 2003.
- [118] D. Tse and P. Viswanath, *Fundamentals of Wireless Communication*. New York, NY, USA: Cambridge University Press, 2005.
- [119] R. Penrose, "A generalized inverse for matrices," *Mathematical Proceedings of the Cambridge Philosophical Society*, vol. 51, no. 03, pp. 406–413, 1955.
- [120] D. G. Brennan, "Linear Diversity Combining Techniques," *Proceedings of the IRE*, vol. 47, no. 6, pp. 1075–1102, June 1959.
- [121] J. H. Winters, "Optimum Combining in Digital Mobile Radio with Cochannel Interference," *Selected Areas in Communications, IEEE Journal on*, vol. 2, no. 4, pp. 528–539, July 1984.
- [122] Y.-H. Nam, Y. Akimoto, Y. Kim, M. il Lee, K. Bhattad, and A. Ekpenyong, "Evolution of Reference Signals for LTE-Advanced Systems," *Communications Magazine, IEEE*, vol. 50, no. 2, pp. 132–138, February 2012.
- [123] F. Weng, C. Yin, and T. Luo, "Channel Estimation for the Downlink of 3GPP-LTE Systems," in *Network Infrastructure and Digital Content, 2010 2nd IEEE International Conference on*, September 2010, pp. 1042–1046.
- [124] M. Lampinen, F. Del Carpio, T. Kuosmanen, T. Koivisto, and M. Enescu, "System-Level Modeling and Evaluation of Interference Suppression Receivers in LTE System," in *Vehicular Technology Conference (VTC Spring), 2012 IEEE 75th*, May 2012.
- [125] K. Pietikainen, F. Del Carpio, H. Maattanen, M. Lampinen, T. Koivisto, and M. Enescu, "System-Level Performance of Interference Suppression Receivers in LTE System," in *Vehicular Technology Conference (VTC Spring), 2012 IEEE 75th*, May 2012.
- [126] NTT DOCOMO, "Performance of Interference Rejection Combining Receiver for LTE," 3rd Generation Partnership Project, Technical Document R4-113528, July 2011.
- [127] H. Holma and A. Toskala, *LTE Advanced: 3GPP Solution for IMT-Advanced*. Wiley, 2012.
- [128] 3GPP, "Technical Specification Group Radio Access Network; Study on Network-Assisted Interference Cancellation and Suppression (NAIC) for LTE (Release 12)," 3rd Generation Partnership Project, Technical Report 36.866 V12.0.1, March 2014.
- [129] I. E. Telatar, "Capacity of Multi-antenna Gaussian Channels," *European Transactions on Telecommunications*, vol. 10, pp. 585–595, 1999.
- [130] C.-N. Chuah, D. N. C. Tse, J. M. Kahn, and R. A. Valenzuela, "Capacity Scaling in MIMO Wireless Systems Under Correlated Fading," *Information Theory, IEEE Transactions on*, vol. 48, no. 3, pp. 637–650, March 2002.

- [131] 3GPP, “Technical Specification Group Radio Access Network; Evolved Universal Terrestrial Radio Access (E-UTRA); Physical channels and modulation (Release 12),” 3rd Generation Partnership Project, Technical Specification 36.211 V12.0.0, December 2013.
- [132] D. J. Love, R. W. Heath, and T. Strohmer, “Grassmannian Beamforming for Multiple-Input Multiple-Output Wireless Systems,” *Information Theory, IEEE Transactions on*, vol. 49, no. 10, pp. 2735–2747, October 2003.
- [133] F. M. L. Tavares, G. Berardinelli, N. H. Mahmood, T. B. Sorensen, and P. Mogensen, “On the Potential of Interference Rejection Combining in B4G Networks,” in *Vehicular Technology Conference (VTC Fall), 2013 IEEE 78th*, September 2013, pp. 1–5.
- [134] MediaTek, Renesas Mobile Europe, Broadcom Corporation, “Study on Network-Assisted Interference Cancellation and Suppression for LTE,” 3rd Generation Partnership Project, Technical Document RP-130404, March 2013.
- [135] Intel Corporation, “System-level evaluation of NAICS receivers,” 3rd Generation Partnership Project, Technical Document R1-134126, October 2013.
- [136] 3GPP, “Technical Specification Group Radio Access Network; Evolved Universal Terrestrial Radio Access (E-UTRA); Base Station (BS) radio transmission and reception (Release 10),” 3rd Generation Partnership Project, Technical Specification 36.104 V10.5.0, December 2011.
- [137] —, “Technical Specification Group Radio Access Network; Evolved Universal Terrestrial Radio Access (E-UTRA); Carrier Aggregation; Base Station (BS) radio transmission and reception (Release 10),” 3rd Generation Partnership Project, Technical Report 36.808, July 2013.
- [138] F. Ahmed, O. Tirkkonen, M. Peltomäki, J.-M. Koljonen, C.-H. Yu, and M. Alava, “Distributed Graph Coloring for Self-organization in LTE Networks,” *JECE*, vol. 2010, pp. 5:1–5:10, January 2010.
- [139] Y. Wang, S. Kumar, L. Garcia, K. I. Pedersen, I. Z. Kovács, S. Frattasi, N. Marchetti, and P. E. Mogensen, “Fixed Frequency Reuse for LTE-Advanced Systems in Local Area Scenarios,” in *Vehicular Technology Conference, 2009. VTC Spring 2009. IEEE 69th*, April 2009, pp. 1–5.
- [140] L. G. U. Garcia, K. I. Pedersen, and P. E. Mogensen, “On Open versus Closed LTE-Advanced Femtocells and Dynamic Interference Coordination,” in *Wireless Communications and Networking Conference (WCNC), 2010 IEEE*, April 2010, pp. 1–6.
- [141] 3GPP, “Technical Specification Group Radio Access Network; Evolved Universal Terrestrial Radio Access (E-UTRA); Requirements for support of radio resource management (Release 12),” 3rd Generation Partnership Project, Technical Specification 36.133 V12.3.0, March 2014.
- [142] —, “Technical Specification Group Radio Access Network; Evolved Universal Terrestrial Radio Access (E-UTRA); Radio Resource Control (RRC); Protocol specification (Release 12),” 3rd Generation Partnership Project, Technical Specification 36.331 V12.1.0, March 2014.
- [143] T. Rappaport, *Wireless Communications: Principles and Practice*, 2nd ed. Upper Saddle River, NJ, USA: Prentice Hall PTR, 2001.

- [144] E. Kreyszig, *Advanced Engineering Mathematics: Maple Computer Guide*, 8th ed. New York, NY, USA: John Wiley & Sons, Inc., 2000.
- [145] K. B. Petersen and M. S. Pedersen, "The Matrix Cookbook," November 2012, version 20121115. [Online]. Available: <http://www2.imm.dtu.dk/pubdb/p.php?3274>
- [146] S. Parkvall, E. Dahlman, A. Furuskar, Y. Jading, M. Olsson, S. Wanstedt, and K. Zangi, "LTE-Advanced - Evolving LTE towards IMT-Advanced," in *Vehicular Technology Conference, 2008. VTC 2008-Fall. IEEE 68th*, September 2008, pp. 1–5.
- [147] Y. Kishiyama, A. Benjebbour, T. Nakamura, and H. Ishii, "Future Steps of LTE-A: Evolution toward Integration of Local Area and Wide Area Systems," *Wireless Communications, IEEE*, vol. 20, no. 1, pp. 12–18, February 2013.
- [148] Nokia, Nokia Siemens Networks, "Intra-cell CSI-RS densities: Rel'10 performance and Rel'8 legacy impact," 3rd Generation Partnership Project, Technical Document R1-100326, January 2010.
- [149] Samsung, "Performance evaluation for CSI-RS design," 3rd Generation Partnership Project, Technical Document R1-100106, January 2009.
- [150] LG Electronics, "Investigation on the Number of RE for CSI-RS," 3rd Generation Partnership Project, Technical Document R1-100647, January 2010.